THE FRACTURE OF EPOXY RESINS AND THE EFFECTS OF RUBBER INCLUSIONS

by

Stephen James Shaw

A thesis submitted for the degree of

Doctor of Philosophy of The

City University, London

August 1984

CONTENTS

ACKNOWLEDGEMENTS

The author would like to express gratitude to Dr A J Kinloch (PERME) and Mr K W Allen (City University) for guidance and supervision throughout the course of this study.

The author would also like to thank Mr P McKee (MQAD, Woolwich) for assistance with the electron microscopy studies and Mr A G Daniel (PERME) for processing the various micrographs and photographs. Also Dr D Tod (PERME) for assistance with Dynamic Mechanical studies.

Thanks are also due to the Ministry of Defence for assistance with the compilation of this thesis.

Last, but by no means least, sincere thanks are due to Mrs M Corthine (PERME) for invaluable assistance with various experimental procedures and Miss R Channon and staff for typing the thesis.

ABSTRACT

The deformation and fracture behaviour of a rubber-modified epoxy, and that of its unmodified counterpart has been studied. The materials have been examined both in 'bulk' and when used as a thin adhesive layer for bonding steel adherends.

Bulk Behaviour

Values of fracture toughness, the type of crack growth and the resultant fracture surfaces have been studied over a wide range of temperatures, displacement rates and specimen thicknesses. Both systems exhibit essentially the same types of crack growth behaviour. However, the values of fracture toughness for the rubber-modified epoxy were almost always significantly higher than those for the unmodified epoxy. A mechanism based on cavitation of the rubber particles and shear yielding of the matrix is proposed. This accounts for the increased fracture toughness and other alterations in property in the rubber-modified material.

The deformation and fracture data are used to calculate values of the crack opening displacement. The rate/temperature dependence of this, together with other correlations, indicate that the extent of blunting at the crack tip governs the toughness of the epoxy materials and controls the type of crack propagation observed. A quantitative expression is presented which describes the variation of fracture toughness with both temperature and rate. Two parameters from this expression are shown to be material constants and to provide a unique failure criterion.

Adhesive Joint Behaviour

The fracture behaviour of the rubber-modified epoxy as an adhesive between mild-steel adherends has also been examined. Values of adhesive fracture energy, type of crack growth and resultant fracture surface appearance have been studied as a function of adhesive bond thickness, joint width and displacement rate. The bond thickness particularly is shown to have a pronounced effect on adhesive fracture energy with a maximum occurring at a specific bond thickness. This relationship is discussed in terms of a plastic zone restriction/adhesive layer constraint model. This enables the bulk properties of the adhesive to be used to semi-quantitatively explain the dependence of G_{Ic} upon bond thickness.

LIST OF MAIN SYMBOLS AND ABBREVIATIONS

a	crack length
b	three-point-bend specimen width
c	critical distance ahead of crack tip
d	three-point-bend specimen depth
e	strain
$\dot{e}$	strain rate
e_y	yield strain
h	specimen height
mg	cantilever beam geometry factor
m	gradient of three-point-bend load-displacement curve
r	distance (polar co-ordinate)
r_y	plastic zone radius
r_{y1}	plane strain plastic zone radius
r_{y2}	plane stress plastic zone radius
t	thickness of adhesive layer
t_m	bond thickness at maximum adhesive fracture energy, G_{Icm}
v_p	volume fraction of particles
w	specimen width
$\dot{y}$	crosshead displacement rate
A_o	initial cross-sectional area
C	compliance
E	Young's modulus
E_a	Young's modulus of adhesive
E_s	Young's modulus of substrate
F	work done
G_c	fracture energy
G_{Ic}	mode I fracture energy

G_{Icm}	maximum adhesive fracture energy
G_{Ice}	fracture energy of epoxy matrix
G'	storage dynamic shear modulus
G''	loss dynamic shear modulus
H	bulk specimen thickness/adhesive joint width
K	stress-intensity factor
K_c	stress intensity factor at fracture (fracture toughness)
K_{Ic}	mode I fracture toughness
K_{Ics}	K_{Ic} for sharp crack
K_{c1}	plane strain fracture toughness
K_{c2}	plane stress fracture toughness
K_{Ic}'	fracture toughness at thickness H_1
K_{Ic}''	fracture toughness at thickness H_2
L	three-point-bend support span
P	applied load
P_c	applied load at onset of crack growth
P_y	applied load at yield
Q	geometry factor
T	temperature
Tg	glass transition temperature
Tg R	glass transition temperature of rubber particles
Tg E	glass transition temperature of epoxy matrix
T_β E	β relaxation of epoxy matrix
U	stored elastic energy
β	secondary molecular relaxation
γ	surface free energy
δ	crack opening displacement
δ_{tc}	crack opening displacement at crack growth

θ	angle (polar co-ordinate)
λ_t	extension ratio at failure of rubber particles
ν	Poissons ratio
ρ	crack tip radius
σ_c	applied stress at crack growth
σ_{tc}	critical stress at crack tip
σ_y	yield stress
σ_{yc}	uniaxial compressive yield stress
σ_{yt}	uniaxial tensile yield stress
σ_o	applied stress
$\sigma_{11}, \sigma_{22}, \sigma_{33}$	principal stresses
τ_t	tear energy of rubber particles
Δ	displacement
tan ϕ	loss factor
ABS	acrylonitrile butadiene styrene
CDCB	contoured double cantilever beam
CT	compact tension specimen
CTB	carboxyl terminated butadiene rubber
CTBN	carboxyl terminated butadiene acrylonitrile rubber
CTBS	carboxyl terminated butadiene styrene copolymer
DGEBA	diglycidyl ether of bisphenol A
HIPS	high impact polystyrene
PPO	poly 2,6-dimethyl-1,4-phenylene oxide
PTFE	polytetrafluoroethylene
PVC	polyvinyl chloride
SEN	single edge notch specimen

PART ONE

INTRODUCTION AND LITERATURE SURVEY

CHAPTER ONE

INTRODUCTION AND AIMS

In recent years the use of thermosetting polymers such as epoxy resins, as adhesives and matrices for composites in structural engineering has increased significantly. This has been due essentially to the many desirable properties which they possess including high modulus, low creep and reasonably good temperature performance. Because of this increased structural use, knowledge of their mechanical properties is of major importance if they are to be employed safely and effectively. In particular, due to their brittle nature, it is of considerable importance to understand the mechanisms and conditions responsible for failure in such materials so that the properties of the adhesive joint or composite can be accurately predicted and understood. Attempts at studying fracture behaviour have been conducted in many investigations by the use of fracture mechanics, which enables the manner in which a crack propagates under stress to be analysed mathematically.

The majority of fracture investigations have been devoted to unmodified epoxy resins where parameters such as the type of curing agent, its concentration, cure conditions, resin molecular structure and testing variables (eg temperature and rate) have been studied in considerable detail. Generally these studies have been approached in a rather ad-hoc fashion where, for example, variations in curing agent type, concentration, cure conditions etc, have tended to impede comparisons between different investigations. However it has been possible to find general points of agreement and thus generate a reasonable understanding of the fracture behaviour of unmodified epoxies.

Studies of the fracture behaviour of rubber-modified epoxies, where a two-phase morphology results from the addition of a suitable liquid rubber, have been more limited. In this case the introduction of further variables such as rubber type and concentration, in addition to those mentioned above, has provided a further source of complication. As a result, a series of uncoordinated investigations by various research groups has produced data which, although providing some valuable information, has left unanswered important questions. For example, considerable doubt still exists as to the exact nature of the energy dissipating deformations that occur in the vicinity of a crack tip during loading. Such deformations are responsible for the substantial increases in fracture resistance which generally result from rubber addition. Perhaps of greater importance, detailed comparisons between the properties of rubber-modified epoxies and their unmodified counterparts have received little attention. This has hindered a greater understanding of the effects of rubber addition in thermosetting polymers.

The situation with adhesive joints and composites, where the adhesive or matrix is invariably present as a thin, highly constrained layer, is potentially more complex. Previous investigations have indicated that the fracture and crack growth characteristics of unmodified epoxies can be similar in bulk and adhesive joint form. However limited evidence has suggested that this may not be true of rubber-modified epoxies, where some substantial and possibly important differences are likely.

The present investigation is therefore concerned with overcoming the problem areas highlighted above. The main aims are two-fold. Firstly, to study and identify the differences and similarities in bulk fracture and mechanical properties between a rubber-modified

epoxy and its unmodified counterpart. The second is to compare in detail the fracture characteristics of the rubber-modified epoxy resin in bulk and adhesive joint form.

To achieve the first aim the two epoxy formulations will be identical, except of course for the presence of a rubbery additive in one, and will undergo the same curing conditions. Thus some of the problems mentioned above will be overcome. By investigating the effects of experimental variables such as temperature, rate and specimen thickness the detailed toughness and crack growth behaviour of the two materials will be identified. Crack tip deformation processes occurring in the two materials will be considered which should allow the development of a toughening mechanism to account for the effects of rubber modification. Finally an attempt will be made to develop a quantitative failure criterion which can be applied to both materials.

The second aim, as well as comparing adhesive joint and bulk fracture behaviour, will also attempt to provide a detailed understanding of the effects of certain design parameters such as adhesive bond thickness and joint width, and, as with the bulk studies, the effect of rate.

CHAPTER TWO

RUBBER-MODIFIED EPOXY RESINS

The usefulness of epoxy resins as structural adhesives and matrices for fibre reinforced composite materials is limited by their brittleness and susceptibility to catastrophic failure. Consequently materials of this type have been a target for the principles of rubber toughening (1). This modification produces tougher materials exhibiting greater resistance to crack initiation and propagation but with little sacrifice of other desirable properties (such as modulus and glass transition temperature). Attainment of the latter is usually dependent upon the polymer exhibiting a two-phase morphology.

The polymer which has probably received most benefit from this approach is polystyrene, the toughening of which dates back to Ostromislensky in 1927, who patented a process for producing a toughened polystyrene (2). The process, which involved polymerising a solution of rubber in styrene monomer, was not commercially exploited however, due to the product being crosslinked and thus not amenable to moulding operations.

Renewed interest in the toughening process occurred after the Second World War, due to the availability of cheap styrene monomer together with the realisation that a vast application potential was being restricted by the polymer's brittle characteristics. A research programme mounted by the Dow Chemical Company resulted in a rpocess, introduced in 1952, which overcame the problems inherent in the Ostromislensky process (3). In this case a processable polymer was produced by continuous stirring in the initial stages of the polymerisation reaction so that discrete rubber particles were dispersed in a polystyrene matrix. This basic idea is now commercially

employed in the production of high impact polystyrene (HIPS). Although numerous developments have occurred in HIPS technology since 1952, these have generally been more in the nature of modifications to the original process, rather than major alterations.

The development of rubber toughening in polystyrene has led to the extension of the basic principles to other thermoplastic polymers. Notable examples include acrylonitrile-butadiene-styrene (ABS), introduced initially in 1952 by the US Rubber Company and more recently modified poly 2,6-dimethyl-1,4-phenylene oxide (PPO) introduced by the General Electric Company in 1966 (4).

Thermosetting polymers differ from thermoplastics in being crosslinked, which, particularly if the degree of crosslinking is high, can result in extremely brittle characteristics. Consequently thermosets have been an obvious and logical target for rubber modification. Although it was at one time thought impossible to increase significantly their toughness, due to the energy absorption retarding influene of molecular crosslinks, work conducted by McGarry and co-workers in the late 1960s has shown otherwise. They demonstrated that the inclusion of a low molecular weight liquid rubber significantly increased the toughness of an epoxy resin (5,6). Furthermore they demonstrated that this improvement was achieved without a significant decrease in thermal and mechanical properties. This was assumed due to a two-phase morphology with rubbery particles dispersed in the crosslinked epoxy matrix. This discovery has been developed further by the B F Goodrich Company which now markets a range of rubbery materials which can act as toughening agents for epoxy resins as well as other thermosetting polymers.

Most of the rubbery materials which have been developed for thermoset polymer toughening have a backbone consisting of an acrylonitrile-butadiene copolymer with functional end groups as shown below.

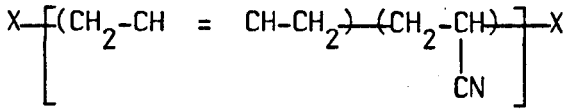

where X is a functional group designed to react with the matrix.

The choice of rubber for a particular thermoset is determined by two major factors (1).

Firstly there is a compatibility requirement. Essentially the rubber must initially dissolve and become dispersed, on a molecular level, in the resin, but precipitate when the resin begins to crosslink and thus form the required two-phase morphology. Thus an optimum degree of compatibility is required. The controlling factor with acrylonitrile-butadiene based copolymers is the acrylonitrile content (7). The solubility parameter of most DGEBA (diglycidyl ether of bisphenol A) epoxies, the structure of which is shown below, is approximately 9.0.

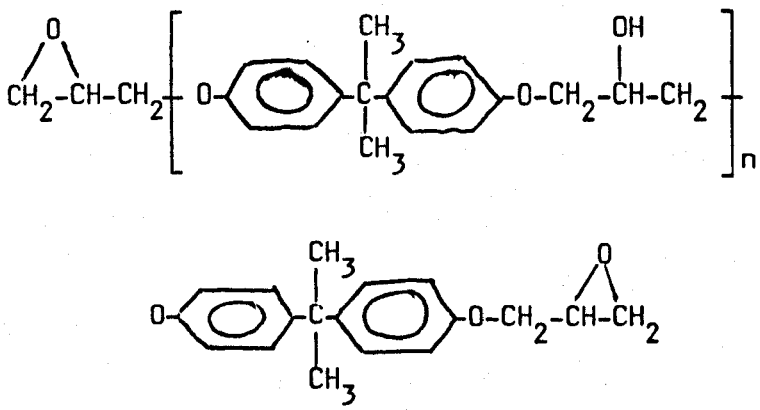

This value can be closely matched with acrylonitrile contents of approximately 20 to 30%. However in such circumstances the high degree of compatibility can result in resistance to precipitation when the resin crosslinks producing a danger of flexibilisation.

Conversely, too low an acrylonitrile level can lead to incompatibility with the epoxy resin and thus produce phase separation prior to reaction. The preferred composition for toughening epoxy resins is approximately 17%.

The second important factor concerns the reaction between the rubber and epoxy resin molecules. This is considered necessary for the development of strong particle-matrix bonding which is generally believed to be of importance for significant toughness enhancement. Consequently the choice of terminal functional group on the rubber molecule is important and will be dependent upon the molecular structure of the base polymer.

The most commonly employed liquid rubber which has been used with epoxy resins is carboxyl terminated butadiene-acrylonitrile rubber (1,5-9) which can be represented structurally in the following way,

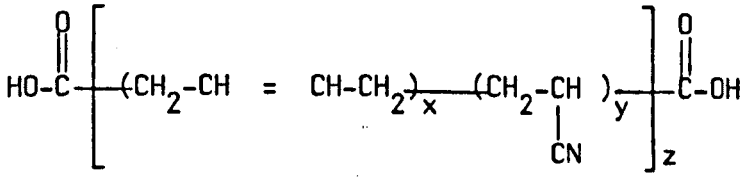

where for example x = 5, y = 1 and z = 10. However variations in these values can occur for the reasons stated earlier. Although, other types of terminal functional groups have been studied, such as phenol, epoxy, hydroxyl and mercaptan, the carboxyl group has shown most promise (10).

As will be discussed more fully in chapter 6, preparation of a cured rubber modified epoxy resin generally involves adequate mixing of the epoxy resin, rubber and curing agent. This is followed by curing under the appropriate conditions whereby in-situ rubber particle formation occurs prior to gelation.

CHAPTER THREE

FRACTURE MECHANICS

Fracture events depend on a number of factors, one of which is the presence of flaws, and fracture mechanics is essentially the study of the strength of materials containing such flaws. For convenience the subject can be divided into two inter-relatable parts. First there is the energy criterion arising from the work of Griffith (11) and later Orowan (12) which proposes that fracture occurs when sufficient energy is released from the stress field by growth of the crack to supply the requirements of the fracture surfaces. The second, due to Irwin (13), proposes that the stress field around a crack can be defined by a parameter called the stress-intensity factor. This is denoted by the term K, and states that fracture occurs when the value of K exceeds some critical value, K_c. Both approaches will be considered separately in some detail.

3.1 The Energy Balance Approach

The energy balance approach to fracture mechanics, describes the propagation of a crack in terms of the conversion of elastic energy, U, stored in the bulk of the sample, together with the work done, F, by the external force, into surface free energy, γ. Probably the most convenient way of demonstrating this approach is to consider a cracked body of uniform thickness, H, subjected to a load, P, as shown in Figure 3.1. The linear load - displacement diagram to be expected from the loading of such a system is shown in Figure 3.2. As indicated, the load - displacement trend is linear so that at load P_1 the elastic energy stored within the system is given by the area under the curve so that,

$$U_1 = \tfrac{1}{2} P\Delta \qquad (3.1)$$

where Δ is the displacement.

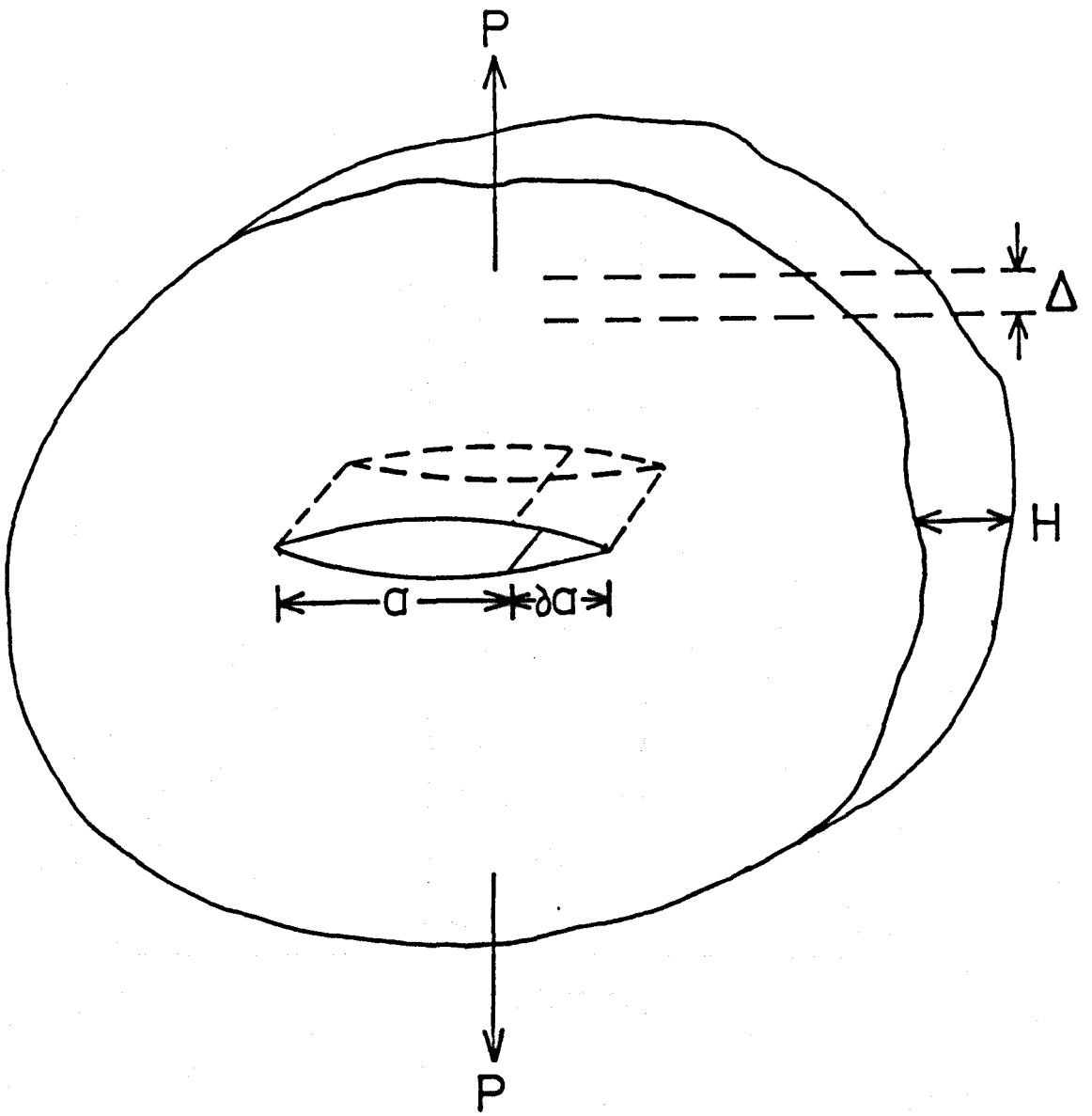

Figure 3.1 Loading of a cracked elastic body.

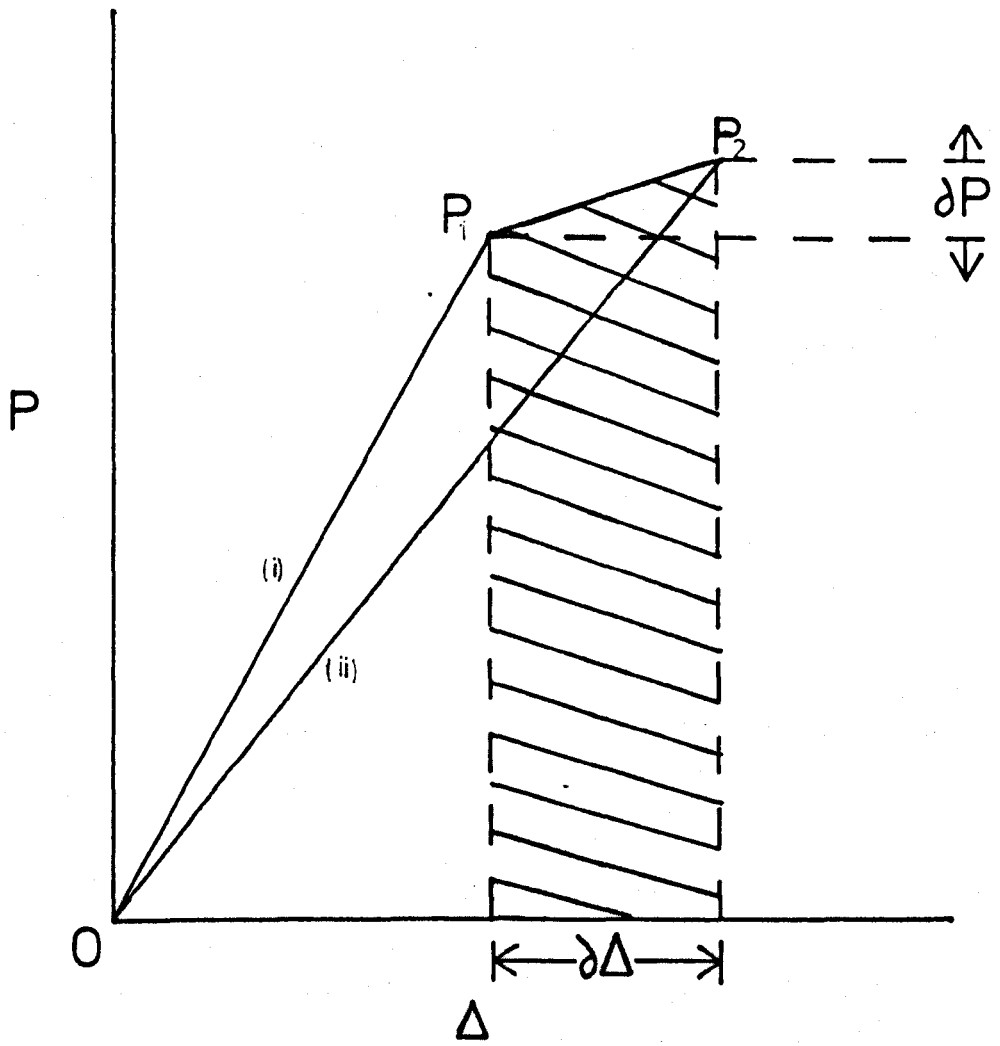

Figure 3.2 Load – displacement diagram from a cracked elastic body.

Let us now suppose that a crack of length a grows by a small amount ∂a. This will result in changes in both load, ∂P and displacement $\partial \Delta$. The crack growth will reduce the stiffness of the system and since the material exhibits bulk linear elastic behaviour, unloading would give the line (ii) shown. Thus, at load P_2, the energy stored within the system will be given by,

$$U_2 = \tfrac{1}{2} (P + \partial P)(\Delta + \partial \Delta) \tag{3.2}$$

Unfortunately the change in stored energy on crack growth from U_1 to U_2 does not provide a value for the energy of fracture since, in addition, external work will have been performed which is shown as the shaded area in Figure 3.2. This work performed by crack extension is given by,

$$\begin{aligned} F &= P\partial\Delta + \frac{\partial P}{2}\,\partial\Delta \\ &= \left(P + \frac{\partial P}{2}\right)\partial\Delta \end{aligned} \tag{3.3}$$

The change in energy of the whole system when the crack grows from a to $a + \partial a$ is thus given by,

$$\partial U = U_2 - U_1 - F \tag{3.4}$$

which is the wedge shaped area between lines (i) and (ii). By substituting from equations 3.1, 3.2 and 3.3, we obtain,

$$\partial U = \frac{1}{2} (\Delta \partial P - P \partial \Delta) \tag{3.5}$$

If the energy change within the system, ∂U is now defined in terms of the energy released per unit area of crack growth, then the fracture criterion becomes

$$\frac{\partial U}{H \partial a} = \frac{1}{2H} \left(\Delta \frac{\partial P}{\partial a} - \frac{P \partial \Delta}{\partial a} \right) = 2\gamma \tag{3.6}$$

where γ is the surface energy of the crack.

The Griffith theory as originally devised considered that the energy to fracture a material was simply equivalent to twice surface-free energy, γ, which for most materials would be in the region of 0.1 Jm^{-2}. However it has been observed in many cases that the values of γ obtained experimentally can be greater, by many orders of magnitude, than theoretical estimates (200-400 Jm^{-2} for polymethyl-methacrylate (14) and 1,000 to 2,000 Jm^{-2} for polystyrene (15)). It is known that even if a material exhibits brittle behaviour there invariably exists a small degree of plastic deformation, primarily at the crack tip. Thus, in the majority of cases this highly localised plastic deformation clearly swamps the surface-free energy contribution. This concept was considered by both Orowan (12) and Irwin (13) who suggested that γ be replaced by the symbol G_c which encompasses all the energy losses incurred around the crack tip. Thus equation 3.6 can be rearranged to give

$$G_c = \frac{1}{2H}\left(\frac{\Delta \partial P}{\partial a} - \frac{P \partial \Delta}{\partial a}\right) \qquad (3.7)$$

The usefulness of equation 3.7 in practice can be demonstrated by considering the compliance of the cracked body, C. This is given by,

$$C = \frac{\text{displacement}}{\text{load}} = \frac{\Delta}{P} \qquad (3.8)$$

Thus

$$\partial \Delta = P \partial C + C \partial P \qquad (3.9)$$

and by substituting this expression into equation 3.7 taking the load at crack extension to be P_c, we obtain

$$G_c = \frac{P_c^2}{2H} \frac{\partial C}{\partial a} \qquad (3.10)$$

The problem is resolved into determining the compliance of the specimen as a function of crack length, which provides a measure of $\partial C/\partial a$. If P at fracture is determined for a given crack length, then G_c can be found from equation 3.10.

3.2 The Stress - Intensity Factor Approach

The stress-intensity factor approach owes its existence to Westergaard (16) who developed stress-function solutions to relate the local concentration of stresses at a crack tip to the applied stress. The basis of these solutions is shown in Figure 3.3. This shows the coordinate stress system for the specification of stresses at a crack tip. The way in which the three principal stresses, σ_{11}, σ_{22} and σ_{33} vary with applied stress, σ_o, crack length, a, and the polar coordinates r and θ are given as,

$$\sigma_{11} = \sigma_o\sqrt{\frac{a}{2r}}\cos\frac{\theta}{2}\left[1 + \sin\frac{\theta}{2}\sin\frac{3\theta}{2}\right] - - -$$

$$\sigma_{22} = \sigma_o\sqrt{\frac{a}{2r}}\cos\frac{\theta}{2}\left[1 - \sin\frac{\theta}{2}\sin\frac{3\theta}{2}\right] - - -$$

$$\sigma_{33} = \nu(\sigma_{11} + \sigma_{22}) \quad \text{(plane strain)}$$

$$\sigma_{33} = 0 \quad \text{(plane stress)} \qquad (3.11)$$

where ν is poissons ratio.

As expected, in the elastic case the stresses are proportional to the applied stress, σ_o. Furthermore they vary with the square root of the crack size and tend to infinity at the crack tip where r is small.

Irwin (13) modified the above equations by introducing and utilising the term 'stress-intensity factor', K, which is given by,

$$K = \sigma_o\sqrt{\pi a} \qquad (3.12)$$

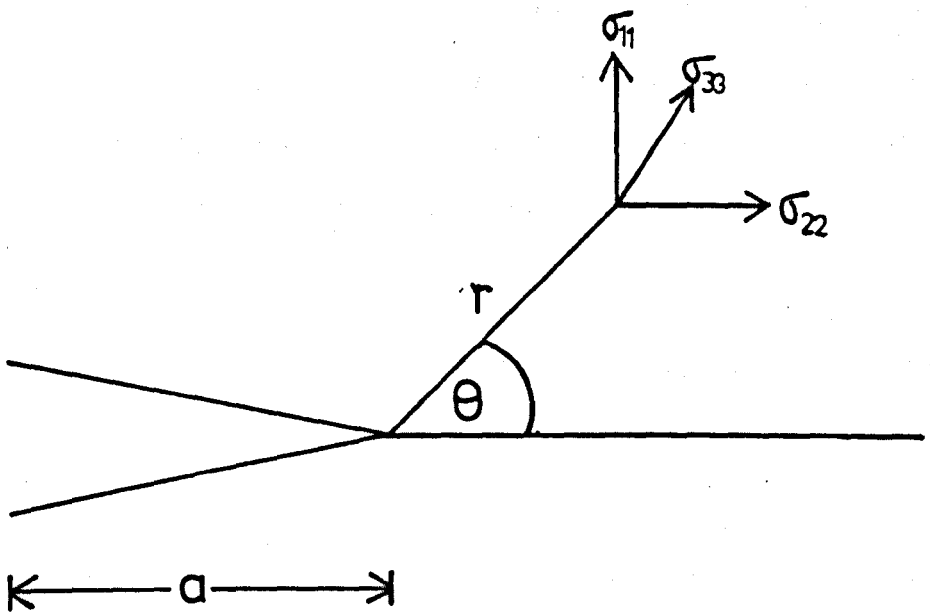

Figure 3.3 Coordinate stresses around a crack tip.

Thus the equations 3.11 can be rearranged to,

$$\sigma_{11} = \frac{K}{(2\Pi r)^{\frac{1}{2}}} \cos\frac{\Theta}{2}\left(1 + \sin\frac{\Theta}{2}\sin\frac{3\Theta}{2}\right) - - -$$

$$\sigma_{22} = \frac{K}{(2\Pi r)^{\frac{1}{2}}} \cos\frac{\Theta}{2}\left(1 - \sin\frac{\Theta}{2}\sin\frac{3\Theta}{2}\right) - - -$$

$$\sigma_{33} = \frac{2\nu K \cos \Theta/2}{(2\Pi r)^{\frac{1}{2}}} \quad \text{(plane strain)}$$

$$\sigma_{33} = 0 \quad \text{(plane stress)} \tag{3.13}$$

From equation 3.13 it can be seen that as $r \to 0$ then the principal stresses σ_{11}, σ_{22} and σ_{33} (plane strain) $\to \infty$. Thus stress cannot make a reasonable local fracture criterion. However since K uniquely defines the stress field around a crack Irwin (13) postulated that the condition,

$$K \geq K_c \tag{3.14}$$

represented a fracture criterion, where K_c is a critical value for crack growth and therefore a material property frequently termed the fracture toughness.

The main advantage of the stress intensity factor is that it combines in a single parameter the three test variables, namely applied stress, crack length and specimen geometry. This is represented in the following general equation,

$$K = Q\,\sigma_o\,a^{\frac{1}{2}} \tag{3.15}$$

where Q is a factor dependent upon the geometry of the structure and which can be obtained either experimentally or theoretically. Thus for crack growth,

$$K_c = Q\,\sigma_c\,a^{\frac{1}{2}} \tag{3.16}$$

where σ_c is the applied stress at the onset of crack propagation.

Thus the stress intensity factor approach to fracture can be employed by first determining the value of K for a cracked structure using equation 3.15 for known levels of applied stress and flaw size and second determining the value of fracture toughness, K_c, of the material in question by employing standard laboratory test-specimens.

For a crack in a homogeneous material the two approaches to fracture mechanics are related by (13),

$$K_c^2 = EG_c \text{ for plane stress} \qquad (3.17)$$

and

$$K_c^2 = \frac{EG_c}{(1-\nu^2)} \text{ for plane strain} \qquad (3.18)$$

where E is Youngs modulus.

For a crack in an adhesive layer these relations have been shown to be generally valid (17,18) particularly for thick adhesive layers. In such cases the appropriate value of E for the adhesive, E_a, may be employed to correlate K_c(joint) and G_c(joint). One particular problem however concerns the interpretation of the stress intensity factor for a crack at or near an interface, which can often be considerably more complex than for a homogeneous material. A further complexity is that significant differences may be observed in the stress-field from that predicted for the homogeneous material outside of a very limited distance ahead of the crack tip (18). Due to these difficulties with the stress intensity approach, many workers have preferred to employ the fracture energy approach for crack growth in adhesive joints.

In this present investigation, where studies were conducted into the fracture of both bulk and adhesive joint geometries, the stress intensity factor approach was used in the former. Because of the difficulties described above however, the fracture energy approach was

used in the adhesive joint studies. Comparisons between bulk and adhesive joints was permitted by simply converting K_c (bulk) to G_c (bulk) by equation 3.17.

3.3 Crack Tip Plasticity

As mentioned previously the major problem with the Griffith approach to fracture was that the value of γ, the surface-free energy term, was far greater when expermimentally determined than the theory would allow. To overcome this, Orowan (12) and Irwin (13) suggested that since, even with macroscopically brittle materials, γ measured > γ theory then inelastic processes would have to occur at the tip of a loaded crack. The elastic stress field solutions discussed earlier indicate that a stress singularity exists at the tip of an elastic crack whereby $\sigma_{11} \rightarrow \infty$ as $r \rightarrow o$. However in practice this would not occur since close to the crack tip σ_{11} would be greater than the tensile yield stress σ_{yt} of the material, which would therefore keep the stresses finite at the crack tip. Clearly a situation where $\sigma_{11} > \sigma_{yt}$ would result in a small region ahead of the crack tip becoming plastic in nature. This region is frequently referred to as the plastic zone and an estimate of its size (13) can be made by considering Figure 3.4. This figure shows the magnitude of the stress σ_{11} in the plane $\theta = 0$ as a function of the distance from the crack tip, r. Up to a distance, r_y, from the crack tip the stress is higher than the yield stress of the material, σ_y. Thus r_y can be assumed to be the size of the plastic zone. By taking the standard elastic stress field equation ie,

$$\sigma_{11} = \frac{K}{(2\pi r)^{\frac{1}{2}}} \tag{3.19}$$

and substituting σ_y for σ_{11}, r_y can be ascertained ie.,

$$\sigma_{11} = \frac{K}{(2\pi r_y)^{\frac{1}{2}}} \tag{3.20}$$

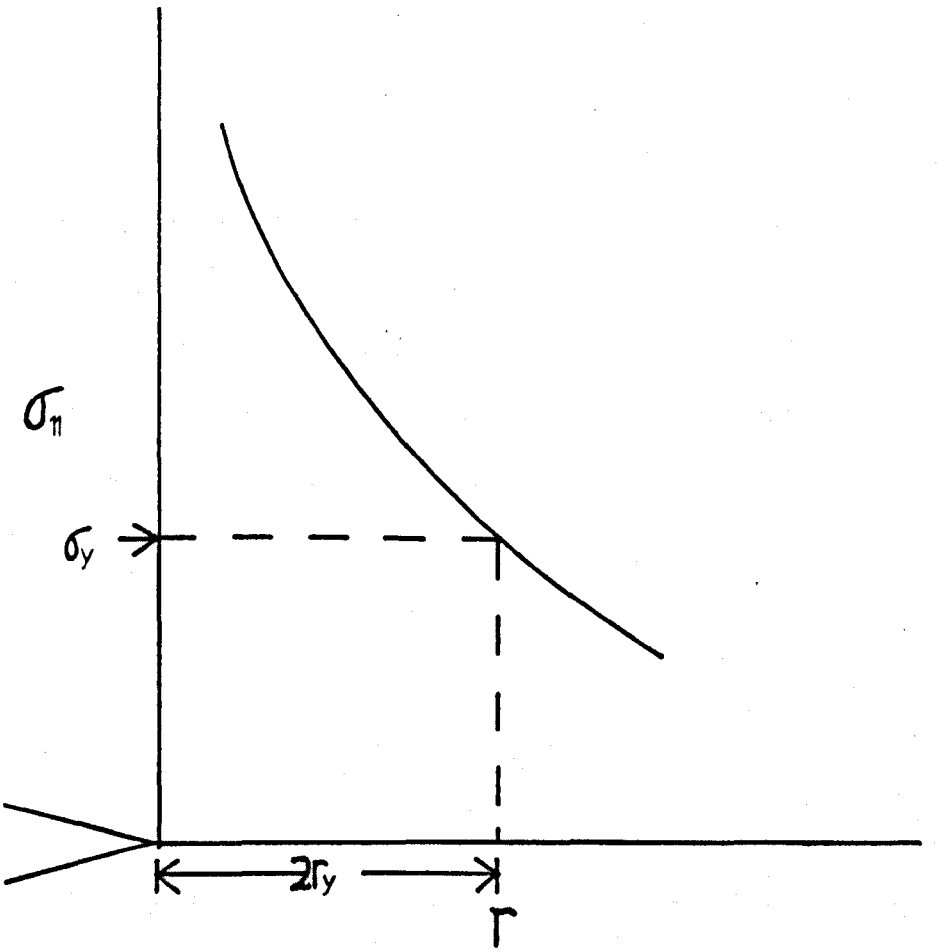

Figure 3.4 Principal stress, σ_{11}, as a function of distance, r, under plane stress conditions.

and thus

$$r_y = \frac{1}{2\pi}\left(\frac{K}{\sigma_y}\right)^2 \qquad (3.21)$$

Thus the plastic zone size, r_y can be directly related to the stress-intensity factor and the yield stress.

The above treatment is limited to plane stress conditions. For plane strain the increased constraint which exists would significantly elevate the tensile stress, σ_y, necessary for yielding. This effect is given the term plastic constraint. It can be theoretically demonstrated by considering the elastic stress field equations in combination with a yield criterion eg von mises, that under plane strain conditions, the plastic constraint factor has a value of approximately 3 (19). Thus the size of the plastic zone would be significantly smaller than that which would occur under plane stress conditions, as indicated in Figure 3.5. In this case,

$$r_y = \frac{1}{2\pi}\left(\frac{K}{3\sigma_y}\right)^2 \qquad (3.22)$$

$$= \frac{1}{18\pi}\left(\frac{K}{\sigma_y}\right)^2 \qquad (3.23)$$

In practical situations there is not usually a distinct boundary betwwen pure plane stress on the one hand and pure plane strain on the other. As a consequence Irwin (20) has proposed that the average plastic constraint factor for plane strain be $\sqrt{3}$, ie approximately 1.7, thus

$$r_y = \frac{1}{2\pi}\left(\frac{K}{1.7\sigma_y}\right)^2 \qquad (3.24)$$

$$= \frac{1}{6\pi}\left(\frac{K}{\sigma_y}\right)^2 \qquad (3.25)$$

Experimentally determined plastic constraint factors have been shown to be in the region of 1.5 to 2 (21), thus confirming the validity of

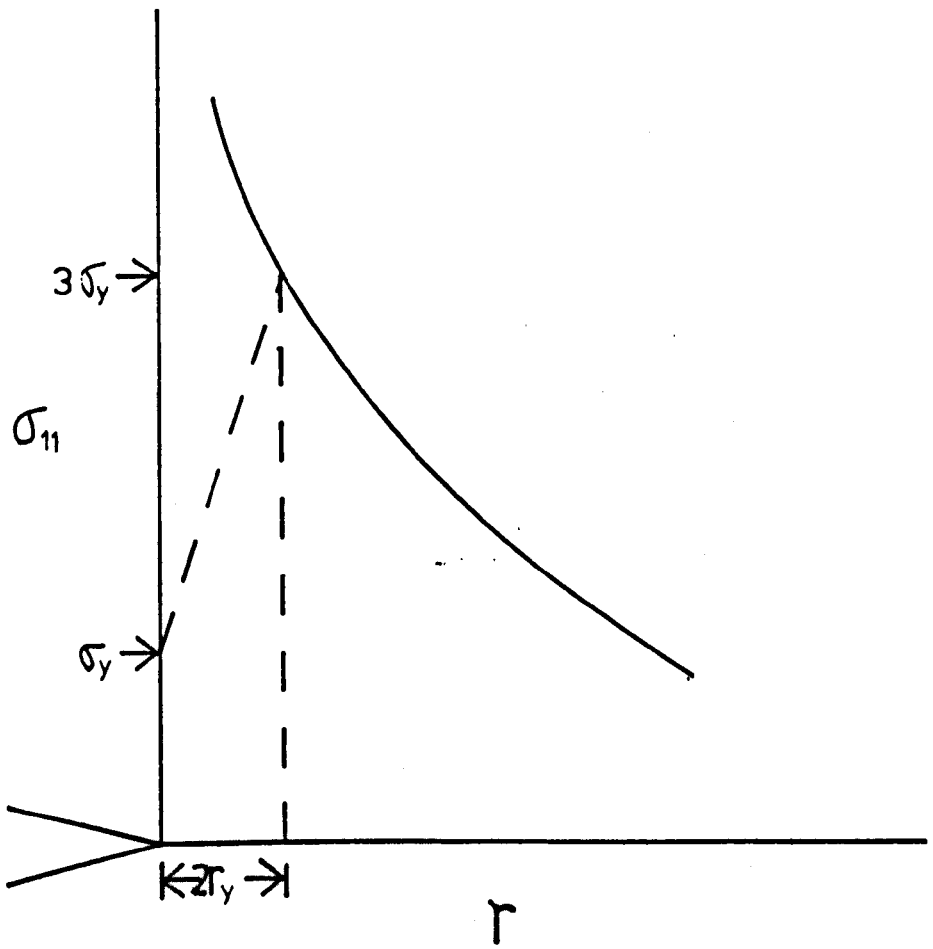

Figure 3.5 Principal stress, σ_{11}, as a function of distance, r, under plane strain conditions.

of equation 3.25.

3.4 Thickness Effects

It is frequently found that the thickness of a specimen can significantly influence the value of fracture toughness, K_c or fracture energy G_c. This is due to the manner in which the state of stress varies across the thickness of a specimen. Plane stress conditions predominate at a free surface whereas within the central regions of a specimen increased constraint results from plane strain conditions which consequently increases yield stress producing a corresponding reduction in plastic zone size. The variation of plastic zone size with thickness is typically demonstrated in Figure 3.6. If a specimen is comparatively thin then the plane stress zones at the free edges will occupy a large proportion of the total thickness and thus a comparatively high toughness will result. As specimen thickness is increased the plane stress zones will increasingly occupy lower proportions of specimen thickness until they have an insignificant contribution, upon which plane strain conditions occur.

The general form of the relationship between fracture toughness, K_c and specimen thickness is shown in Figure 3.7.

3.5 Modes of Loading

A crack in a solid may be stressed in three different modes as indicated in Figure 3.8. As shown these are denoted Modes I, II and III. The cleavage or tensile opening mode, Mode I, is technically the most important since it is the most commonly encountered and usually the one which most readily results in failure. This is also true of adhesive joints where attempts are generally made to design joints to exist under in-plane shear loading. Because of this, the work described in this thesis considers Mode I loading conditions only.

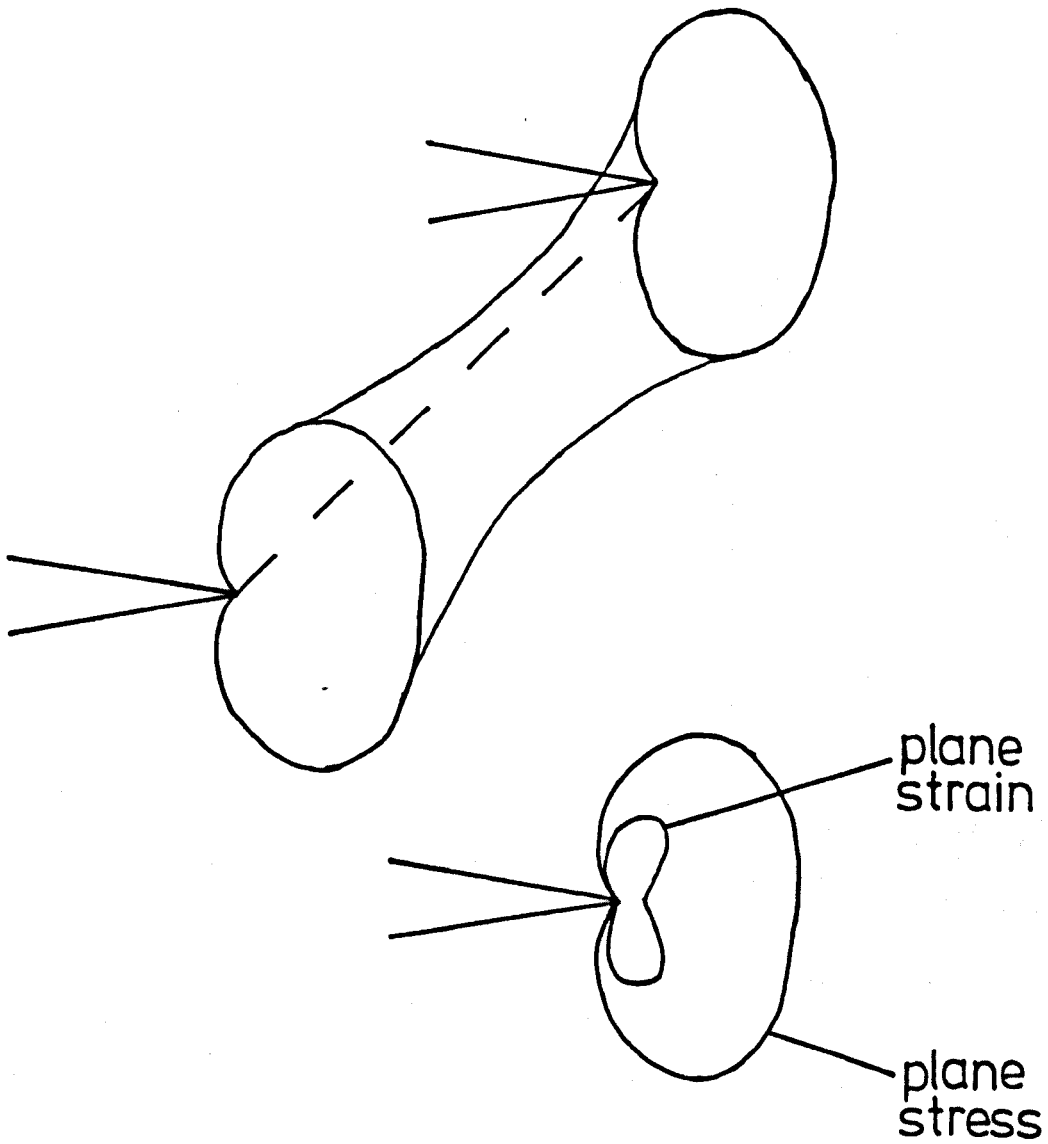

Figure 3.6 Plastic zone shapeas a function of specimen thickness

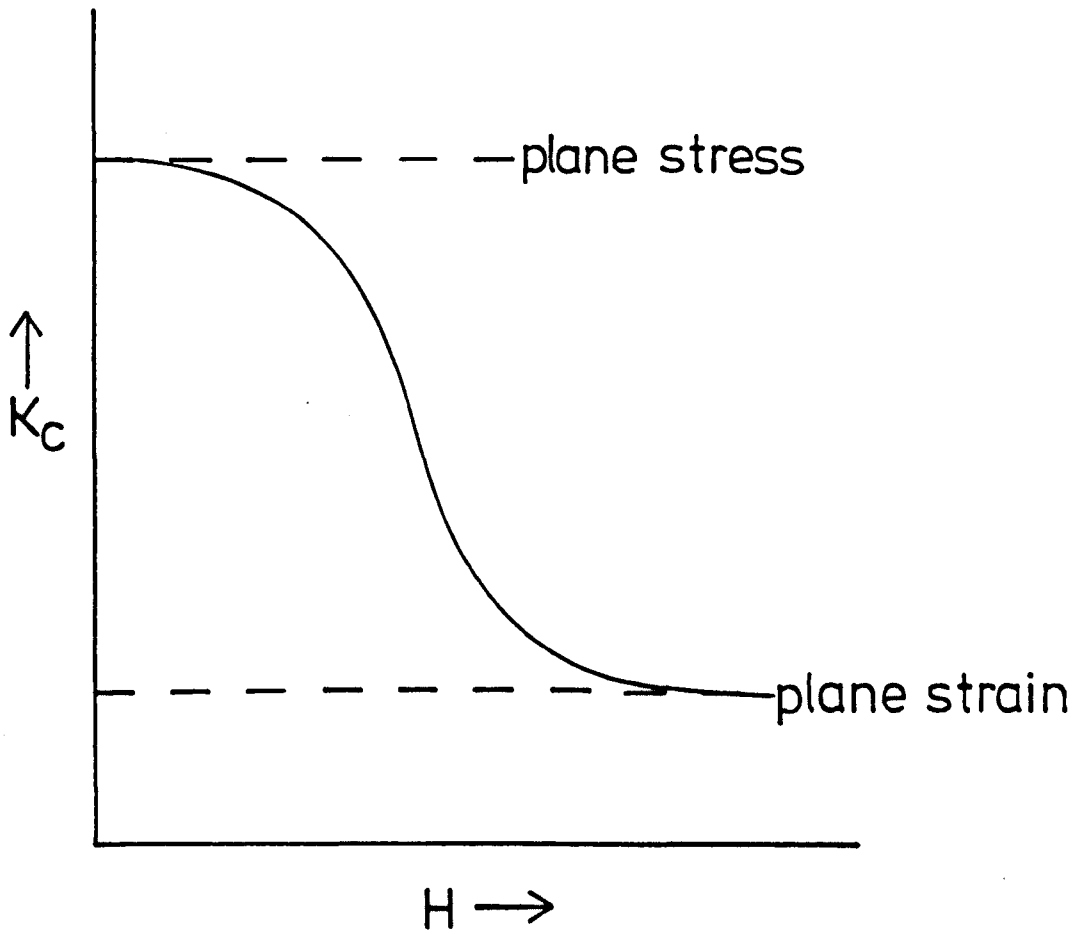

Figure 3.7 General effect of specimen thickness, H, on fracture toughness, K_C.

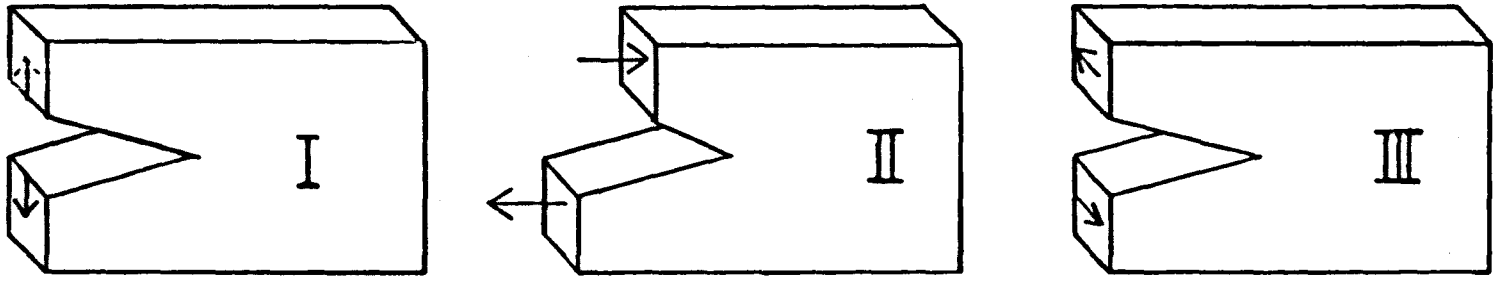

Figure 3.8 Modes of loading. I, tensile-opening; II, in-plane-shear; III, antiplane-shear.

CHAPTER FOUR

THE FRACTURE OF BULK EPOXY RESINS

4.1 Effect of Material Variables

The material variables discussed in this section are known to influence the manner in which cracks propagate in epoxy resins. Thus it is desirable at this point to describe the two main types of crack propagation which have been observed. They are,

(i) Brittle, stable crack propagation which may occur at a constant load with the rate of propagation being dependent upon the rate of crosshead displacement used. This has been termed stable crack growth and a typical load displacement trace for a specimen exhibiting this behaviour is shown in Figure 4.1 (a).

(ii) Alternatively, brittle crack propagation may occur intermittently in a "stick-slip" manner exhibiting load values appropraite to both crack initiation and arrest. This is termed unstable crack growth and a typical load-displacement trace is shown in Figure 4.1 (b).

The earliest investigations into the fracture of bulk epoxy resins were conducted by Broutman and McGarry (22) and Mostovoy and Ripling (23). From these studies it was observed that crack propagation took place in an unstable, stick-slip manner in epoxy resins, whilst with brittle thermoplastics, stable propagation generally occurred.

Since this early work, a number of workers have investigated the effects of different curing agents and curing conditions on the fracture of unmodified epoxy resins (24-32). As a result, a comprehensive list

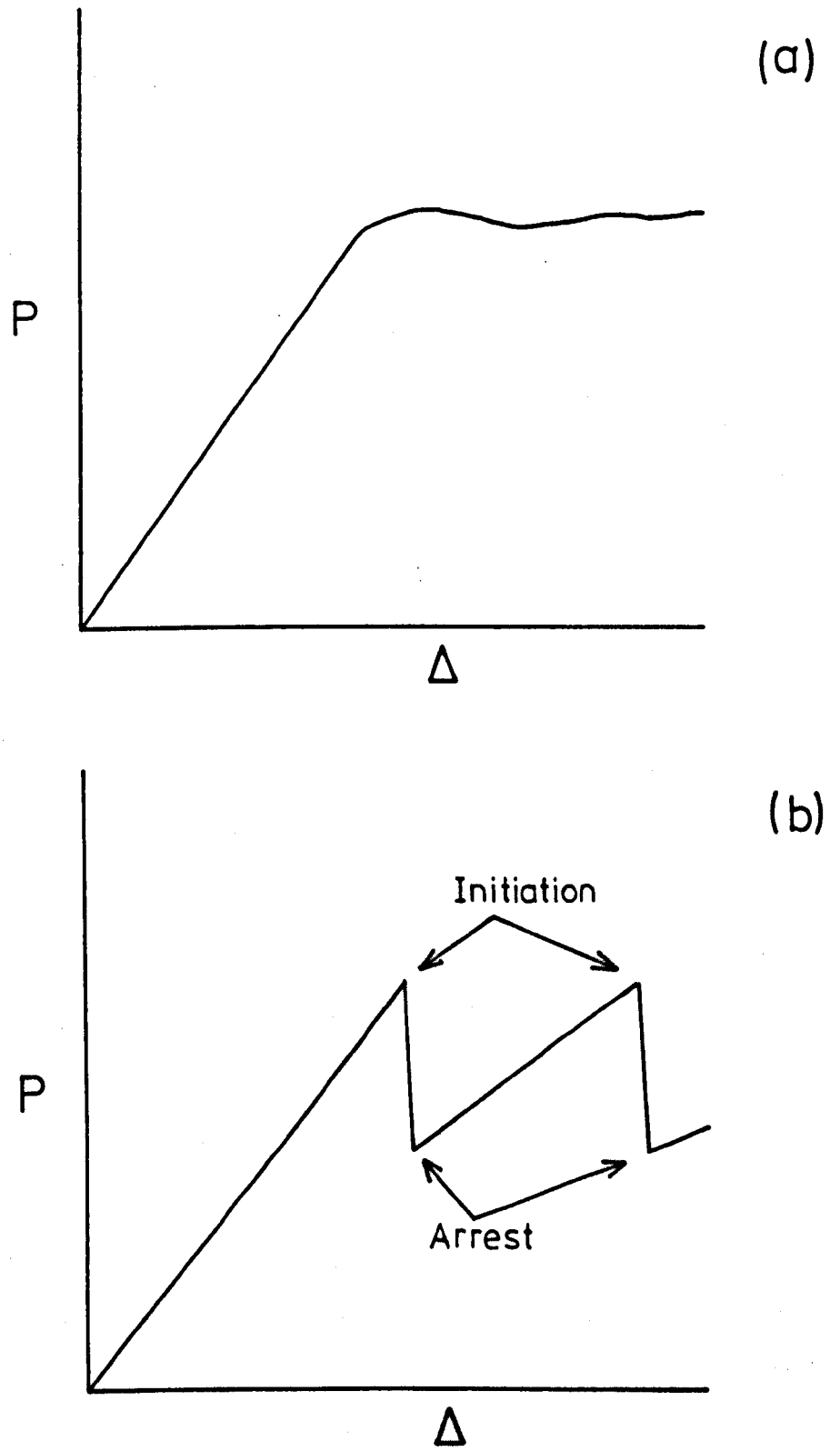

Figure 4.1 Typical load, P, – displacement, Δ, curves depicting (a) stable crack propagation and (b) unstable crack propagation

of curing agent/epoxy resin systems has been compiled providing fracture energy values ranging from approximately 50 to 1000 Jm^{-2}.

Although there have been exceptions, most studies have shown that an optimum curing agent concentration occurs producing a maximum in fracture energy. For example, Selby and Miller (26) using a tapered double cantilever beam geometry, obtained a maximum fracture energy of approximately 1000 Jm^{-2} with 35 pph of diaminodiphenyl methane in a diglycidyl ether of bisphenol A (DGEBA) resin. Similar results were found by Griffith and Holloway (27) with an anhydride cured system and by Mostovoy et al (23) with a tetraethylene pentamine cured epoxy. A more recent investigation by Yamini and Young (31), who studied a triethylenetetramine cured DGEBA epoxy using the double torsion geometry, indicated that fracture toughness, K_{Ic}, increased as the amount of curing agent was increased with no maximum observed over the concentration range employed. A similar effect was found by increasing the post-cure temperature, thereby indicating that toughness in such systems increases as the amount of crosslinking is increased. Similar experiments conducted by Mijovic and Koutsky (32), who studied crack propagation in diethylenetriamine cured systems found, in contrast to the work of Yamini and Young, that fracture energy reached a maximum at certain curing agent concentrations and post-cure periods.

The amount and type of curing agent employed and degree of cure has also been shown to influence crack propagation behaviour (23-32). Results suggest that unstable growth generally occurs when an increased degree of cure, brought about by, for example, increases in curing agent concentration, post-cure temperature and/or cure time is increased beyond a certain limit.

With rubber-modified epoxy resins, it has been clearly demonstrated that variables such as the type and concentration of rubber together with the nature of the curing agent can significantly affect toughness (5, 7-10, 25, 28, 33).

With the rubber component it is possible to vary its nature in a number of ways. Terminal functionality on the rubber molecule has been investigated for toughening ability on epoxy resins by Riew and co-workers (10). They employed a parallel double cantilever beam technique to study the effects of carboxyl, phenol, epoxy, hydroxyl and mercaptan terminal groups on butadiene-acrylonitrile rubbers. Their results indicated that carboxyl or phenol terminal groups were preferable for toughening with fracture energies of approximately 2.8 kJm^{-2} for rubber concentrations of 5 phr. All types of terminal group were shown to produce a cured system exhibiting a distinct two-phase morphology. The exception was the mercaptan terminated rubber where a low fracture energy of approximately 0.3 kJm^{-2} was obtained together with little evidence of a two-phase structure. Pendant functional groups on the rubber molecule, in addition to terminal functionality were shown to be less effective. A complete absence of terminal groups produced poor results, this being attributed to a lack of covalent bonding between resultant rubber particles and matrix. However fracture resistance was an improvement on the equivalent unmodified epoxy.

In a futher study, Riew investigated the toughening abilities of carboxyl terminated butadiene rubber (CTB) and carboxyl terminated butadiene styrene copolymer (CTBS) (10). Their toughening action in comparison to a carboxyl terminated butadiene acrylonitrile rubber (CTBN) was found to be poor and was attributed to poor initial compatibility with the epoxy resin.

It has been shown with CTBN rubbers that an increase in molecular weight produces an increase in fracture toughness up to an optimum level, which is dependent upon such factors as acrylonitrile level and the type of curing agent employed (6-8). Sultan and McGarry (6) have explained this dependence upon compatibility and copolymerisation effects. They argued that as CTBN molecular weight increases so the degree of incompatibility between rubber and epoxy resin likewise increases, thereby encouraging precipitation of the elastomeric component. They also pointed out that increasing molecular weight would decrease the density of reactive sites which would therefore increase the acrylonitrile-butadiene concentration of the rubbery phase.

The effects of rubber concentration on fracture toughness have been studied in some detail (6, 10). With the majority of epoxy/ curing agent combinations there exists an optimum concentration. Concentrations above the optimum have been shown to produce phase inversion where the rubbery phase forms the matrix with the epoxy resin separating out as spherical particles. Generally it has been shown that increased curing agent reactivity increases optimum rubber concentration since it produces a decreased gelation time and thus retards the phase separation process. Consequently a greater amount of rubber is required to produce a given effect in comparison to a low reactive curing agent where the rubber would be more efficiently utilised.

Two further aspects of the nature of a curing agent are also of importance. Firstly it is well known that the molecular structure of a curing agent contributes significantly to the final structure of the crosslinked polymer (34, 35). For example, epoxy systems requiring a degree of thermal resistance generally have comparatively high crosslink densities which can be obtained in part by the use of

polyfunctional curing agents. However the introduction of substantial crosslinking in polymers is known to suppress molecular flow and thus such materials frequently suffer from brittleness. The toughening of highly crosslinked epoxy resins has been reviewed by Laible and McGarry (33). They demonstrated that, although improvements in toughness can be imparted by the use of liquid rubber polymers such as CTBN, the magnitudes were consdierably less than those encountered with resins of significantly lower crosslink density. Secondly, as pointed out by Meeks (25) curing agent type and concentration can significantly alter the compatibility balance between the rubber and epoxy resin and thus interfere with the phase separation process. This effect would clearly be of greater potential significance for epoxy formulations having curing agents which, by necessity, have to be employed in fairly large concentrations, eg anhydrides.

4.2 Effect of Testing Variables

A large proportion of the fracture studies with epoxy resins has consisted of investigating the effects of material variables. However the most significant advances in understanding the mechanisms of fracture and crack propagation have resulted from investigations into the effects of testing variables such as rate (30, 36, 37, 38) and temperature (30, 31, 37, 38). The majority of these studies have concerned unmodified epoxy resins with only minor attention being paid to rubber-modified epoxies.

The influence of both displacement rate and temperature on the toughness and crack growth characteristics of unmodified epoxy resins has been studied by a number of workers. One of the earliest references to rate dependence was by Selby and Miller (26) who employed tapered double cantilever beam specimens to study a DGEBA resin cured with diaminodiphenyl methane. Although the main object of this work was

to study the influence of resin/curing agent ratio on fracture and mechanical properties, an experiment was conducted at three testing rates with one formulation. Increasing rate was shown to reduce fracture toughness, K_{Ic}, from 0.9 to 0.73 MN $m^{-3/2}$. Crack growth was found to be unstable at all three rates, in each case being preceded by a small degree of stable propagation which produced a degree of roughness on the fracture surface.

Later work by Young and Beaumont (36) on an anhydride cured epoxy resin (DGEBA/phthalic anhydride) also showed that K_{Ic} was rate dependent in a similar way. In this case however a transition in crack growth behaviour from unstable at slow rates to stable, continuous at high rates occurred at 20°C.

Yamini and Young (37) employed double torsion specimens to study the effects of rate and temperature on the fracture toughness and crack growth characteristics of a number of epoxy resin formulations. As with Young and Beaumont they found significant rate, and temperature dependence with a wide range of formulations, with K_{Ic} generally decreasing with increasing rate and decreasing temperature. Transitions from unstable to stable growth were also common, with high temperatures and slow rates favouring unstable behaviour.

Phillips, Scott and Jones (30) have recently studied an ethylene diamine cured epoxy resin using double torsion specimens. Fracture energy, G_{Ic}, was found to be both temperature and rate dependent with increases in the former and decreases in the latter increasing G_{Ic}. Furthermore, rate dependence was found to increase with increasing temperature. Throughout the range of temperatures and rates investigated, unstable crack growth predominated with stick-slip growth being preceeded by a small degree of stable growth which produced a region of roughness on the fracture

surface. The size of this rough zone and extent of stable growth prior to unstable fracture was found to decrease with decreasing temperature and increasing rate.

In a recent investigation Cherry and Thomson (39) studied a range of unmodified epoxy formulations using a parallel double cantilever beam geometry, where testing rate was the main variable of interest. As observed in previous studies, increasing rate was generally shown to decrease fracture energy, G_{Ic}. However of major interest in this work was the manner in which crack growth behaviour and fracture surface topography varied with both rate and formulation. The effect of rate varied significantly with the formulation employed. However the range of crack growth types observed varied from ductile stable at slow rates to brittle stable at fast rates. Two types of unstable propagation were observed at intermediate rates with the distinguishing features being the presence or absence of a small degree of stable growth prior to unstable fracture.

The effect of temperature on the fracture behaviour of a rubber-modified epoxy was studied by Bascom and Cottington in 1976 (40). They employed a tapered double cantilever beam geometry to show that fracture energy, G_{Ic}, increased with increasing temperature over the range -40°C to 50°C. Unstable crack propagation occurred throughout. More recent work by Rushford et al (41) extended this earlier work by also investigating the influence of rate at one particular temperature and were able to show that G_{Ic} increased with decreasing rate.

4.3 Stability of Cracking

It is only fairly recently that the factors controlling crack growth stability in epoxy resins have been identified. Some of these have already been mentioned, namely the effects of temperature and rate together with material variables which were discussed in section 4.1.

Further factors which are known to influence crack propagation stability are water and specimen geometry. Investigations by Young and co-workers (36, 37) have shown that with both anhydride and amine cured epoxy resins, water in the vicinity of a crack tip promotes unstable, stick-slip crack growth.

Studies by Mai and Atkins have shown that specimen geometry can influence crack stability (42, 43). They pointed out that stability of crack growth depends upon two factors, a geometric stability factor which varies with specimen geometry and a factor dependent upon material characteristics.

Although a number of theories have been proposed to explain crack growth characteristics in epoxy resins, the one proposed by Gledhill et al (38) appears to carry most weight. They have suggested that the main parameter controlling crack growth is simply the amount of localised plastic deformation that occurs at a crack tip prior to crack propagation. If this degree of plastic deformation is high, the crack tip will be severely blunted. Consequently when the crack eventually propagates the release of strain energy will be greater than that required for a stable moving crack. Thus unstable propagation would occur and vice-versa. In support of this model, Gledhill et al showed a correlation between type of crack growth in a tapered double cantilever beam geometry and the ability to undergo plastic deformation in uniaxial compression tests. Epoxy resin formulations showing high plastic deformation produced fracture specimens which underwent unstable crack growth and vice-versa.

This proposed crack tip blunting model, although basically simple, qualitatively explains some of the experimental observations stated earlier. For example, the increased tendency towards stable

propagation with increased testing rate and decreased temperature is logical when it is considered that molecular mobility would be hindered under such conditions and thus crack blunting processes restricted. The previously mentioned tendency of water to increase the extent of unstable growth also adds weight to this theory, since the plasticising action of water would almost certainly promote crack blunting.

4.4 Failure Criteria

The determination of a failure criterion, whereby fracture can be said to occur when a certain parameter reaches a critical value, irrespective of conditions, has been considered in recent years. With polymethylmethacrylate it has been shown that slow stable crack growth occurs at a constant crack opening displacement, δ_{tc} (44-46) (Figure 4.2) with propagation taking place through a region of crazed material ahead of the crack tip. With thermosetting polymers, failure criteria have generally been more difficult to elucidate due to the more complex crack propagation characteristics which they generally exhibit. However Gledhill et al (38) have recently calculated crack opening displacement values for a triethylene tetraamine cured epoxy resin tested at different temperatures. They have shown that a constant δ criterion appears to apply under certain conditions, as shown in Figure 4.3. As indicated, below about 10°C, where stable crack propagation occurs, δ is approximately constant. However above 10°C, unstable crack growth predominates and δ increases. Thus a constant δ criterion is certainly not applicable under these conditions. Clearly a more universal criterion is required which will encompass the two major types of crack growth which have been observed with epoxy resins.

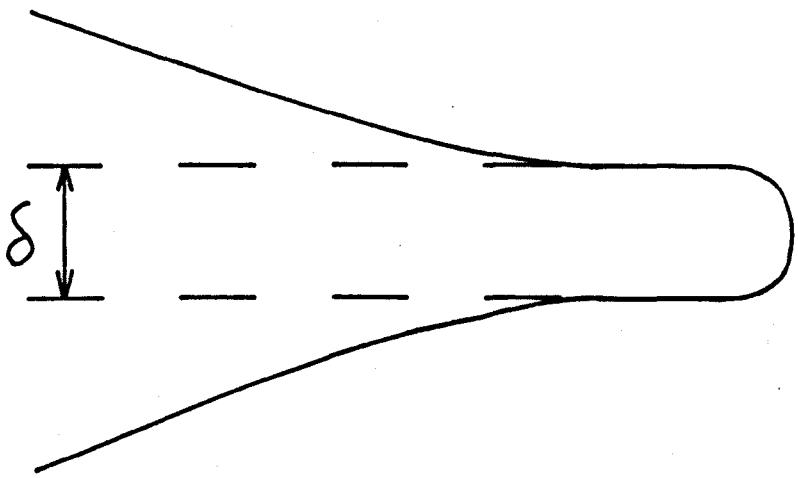

Figure 4.2 Schematic drawing of crack opening displacement, δ.

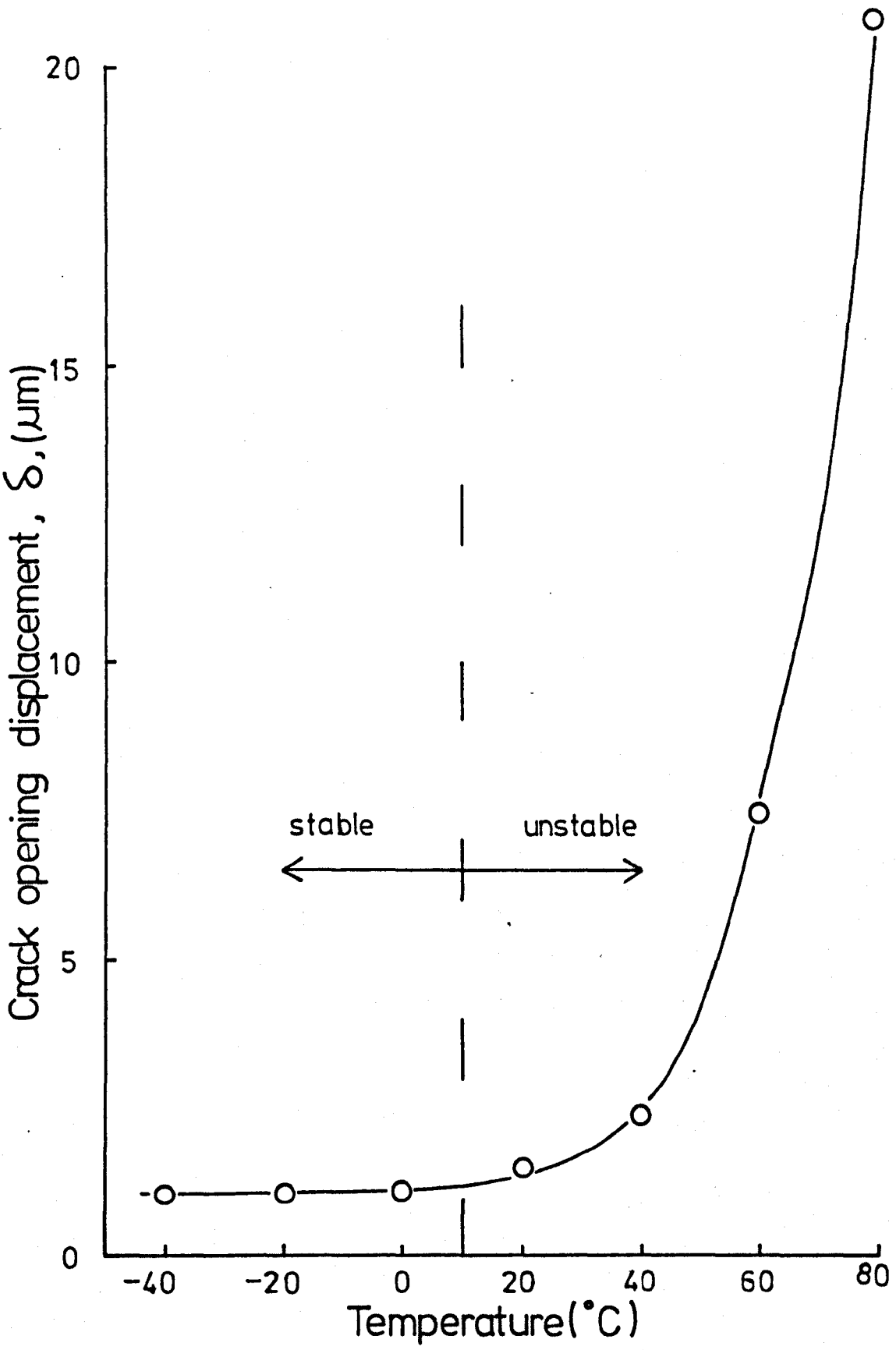

Figure 4.3 Variation of crack opening displacement, δ, with temperature for an epoxy resin cured with triethylenetetramine (after Gledhill et. al[38])

CHAPTER FIVE

THE FRACTURE OF ADHESIVE JOINTS

5.1 Effect of Joint Geometry

The term 'joint geometry' in this thesis refers essentially to the geometrical variables of adhesive bond thickness, joint width and mode of loading. Since only the contoured double cantilever beam specimen was used, the majority of this discussion will be centred around this type of specimen.

The effect of bond thickness on the toughness and crack growth behaviour of unmodified epoxy resin adhesive joints has been considered by various workers (28, 47,48). Mostovoy and Ripling (47,48) employed aluminium tapered double cantilever beam specimens bonded with amine and anhydride cured epoxy resins to study bond thickness effects. They found that, in most cases, adhesive fracture energy, G_{Ic}, was independent of bond thickness from approximately 0.05 to 0.5mm, ie the common range of thicknesses traditionally employed. However at greater bond thicknesses an optimum thickness existed with G_{Ic} passing through a maximum which was greater than that observed at the lowest feasible thickness by a factor of approximately 2.5. The decline in G_{Ic} at thicknesses greater than that pertaining to the maximum was associated with a change in mode of failure from cohesive within adhesive to apparent interfacial. This suggested that residual stresses developing during cooling from the cure temperature were causing separation at or near the interface. Indeed at very large thicknesses, interfacial separation was frequently observed during cooling after the bonding process.

A similar but less detailed investigation was conducted by Bascom et al (28) on a piperidine cured unmodified epoxy resin, once again using the tapered double cantilever beam geometry. They concluded that no significant bond thickness effect existed over a range of approximately 0.25 to 2 mm. Of far greater interest in this work was an investigation conducted on a rubber-modified epoxy cured with piperidine and using CTBN as the liquid rubber. The effect of bond thickness on fracture energy was studied over the thickness range 0.1 to 3.2 mm at 25°C. The result obtained is shown in Figure 5.1. As indicated, on increasing bond thickness from 0.1 mm, adhesive fracture energy, G_{Ic}, rises steeply and reaches a maximum at a bond thickness of approximately 0.6 mm. A further increase in bond thickness results in a sharp decline in G_{Ic} until a constant value is obtained. The authors were able to explain part of this effect by showing that the maximum G_{Ic} occurred when the bond thickness and plastic zone diameter, $2r_y$, calculated from equation 5.1,

$$r_y = \frac{1}{6\pi} \frac{EG_{Ic}}{\sigma_y^2} \qquad (5.1)$$

were approximately equal. Thus reducing bond thickness below the optimum would impose a physical barrier to the full development of a plastic zone, which would thus reduce G_{Ic}. The decline in G_{Ic} for bond thicknesses greater than the optimum was not understood. However it was suggested that it resulted from a change from plane strain conditions at the maximum to conditions approaching plane stress at higher bond thicknesses.

Variations in both crack propagation behaviour and fracture surface appearance were also shown to occur with bond thickness. Stable growth was observed at low bond thicknesses and unstable, stick/slip at high thicknesses with an apparent transition accompanying the maximum in G_{Ic}.

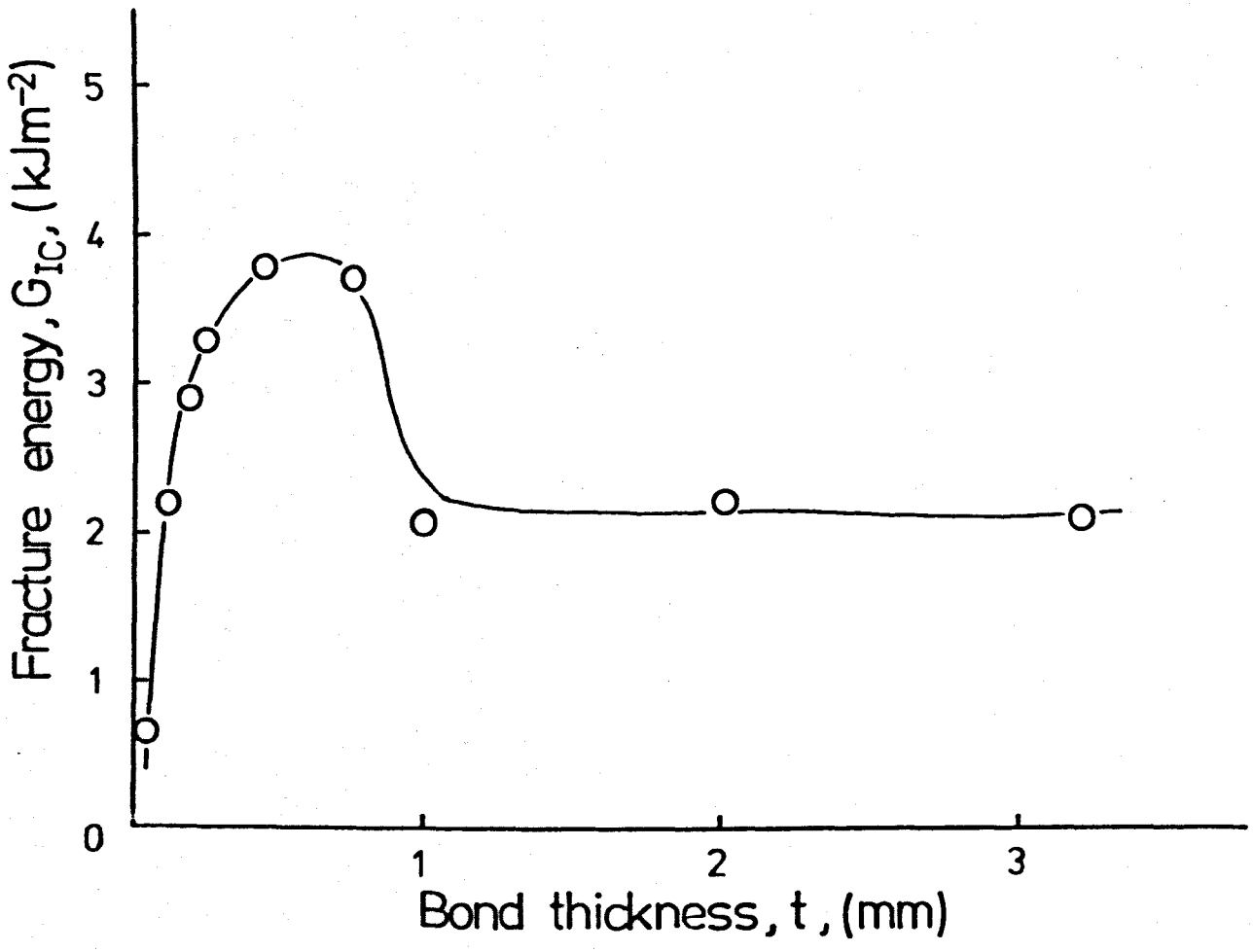

Figure 5.1 Effect of adhesive bond thickness, t, on fracture energy, G_{Ic}, (after Bascom et.al[28])

This transition was further accompanied by a change in the locus of failure from near the adhesive/substrate interface to the centre of the bond. Fracture surfaces resulting from stable propagation also exhibited pronounced stress whitening which was not observed to any major extent with specimens which experienced unstable fracture.

Mostovoy et al (48) briefly investigated the effect of varying the width of a tapered double cantilever beam joint using a tetraethylene pentamine cured unmodified epoxy resin. No significant change in G_{Ic} and crack growth behaviour was observed over the joint width range studied (12 to 75 mm).

No further major studies of joint width effects have been published.

5.2 Effect of Testing Variables

Mostovoy and Ripling (49) are the only workers to have studied in detail the effect of temperature on the fracture behaviour of unmodified epoxy adhesive joints. They employed a tapered double cantilever beam geometry, using aluminium alloy substrates, to study the effect of temperature on four adhesive systems. A typical result is shown in Figure 5.2. It can be seen that G_{Ic} remains fairly constant over a wide temperature range (approximately -100 to 100 °C). However a pronounced increase occurs at temperatures in excess of 100 °C as the glass transition temperature, T_g, of the adhesive is approached. The rather unexpected increase in G_{Ic} at very low temperatures has been attributed to an environmental effect due to the cryogen employed (50). Crack propagation behaviour for the four unmodified formulations was generally unstable at all temperatures, with the extent of instability possibly being greater at the temperature extremes where, as indicated, G_{Ic} is noted to rise steeply. Fracture surface appearance was found to vary greatly with temperature. Rough, partially interfacial fracture appearances were observed at temperatures which promoted comparatively

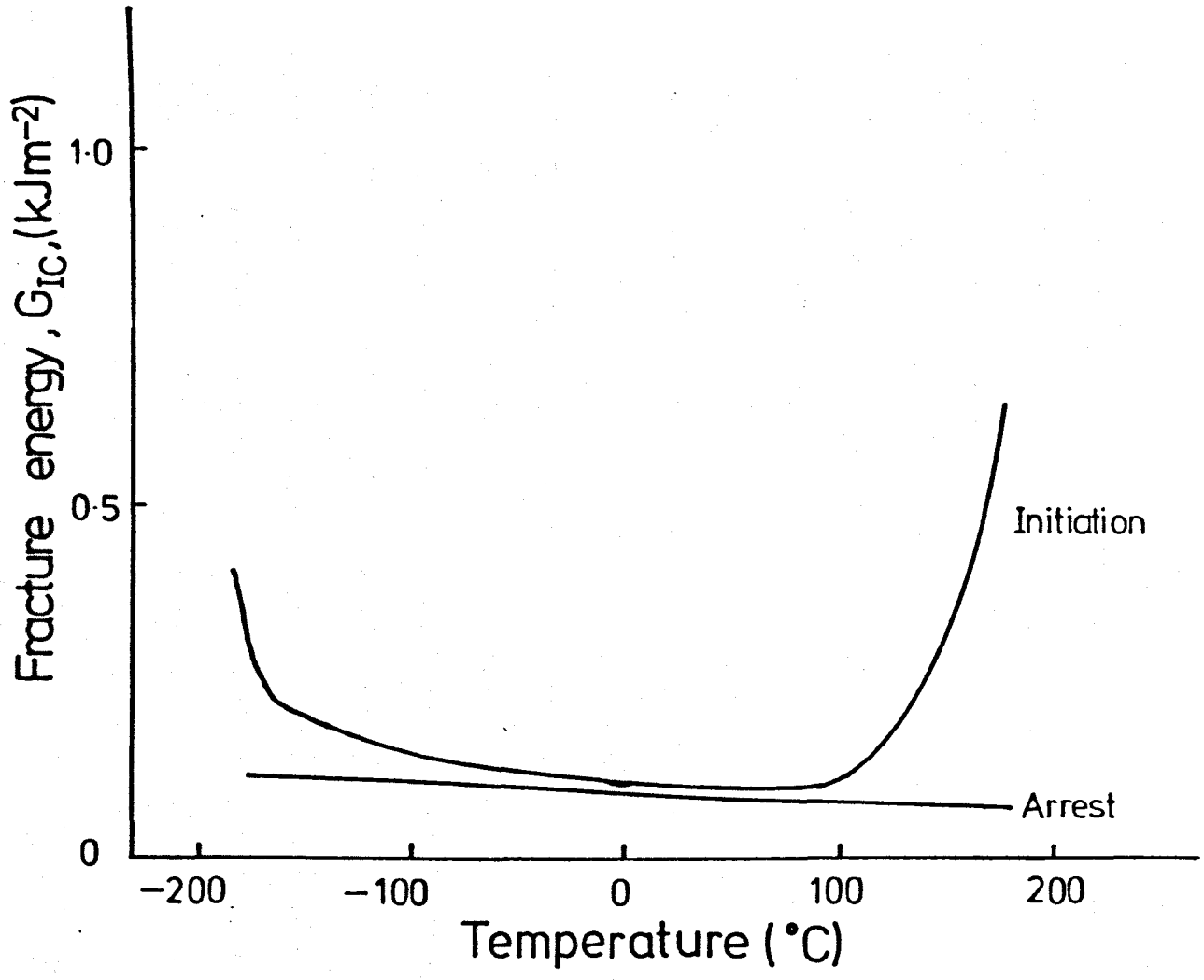

Figure 5.2 Effect of temperature on adhesive fracture energy, G_{Ic}, for an epoxy resin cured with hexahydrophthalic anhydride (after Mostovoy and Ripling[49])

high degrees of toughness. At room and fairly low temperatures, fracture surfaces were generally smooth and at the centre of the bond with fine 'finger-nail' markings indicating arrest/initiation events resulting from the unstable fracture characteristics. At extremely low temperatures (≈ -180 °C) fracture surface roughness was once again apparent.

In addition Mostovoy and Ripling studied a rubber-modified epoxy (49), which was said to be a commercial film adhesive. It was shown to exhibit considerably different behaviour at varying temperatures. This adhesive showed a pronounced fracture energy maximum at approximately room temperature which was roughly an order of magnitude greater than that found with the unmodified system. In the temperature range -30 to -70 °C, fracture energy dropped sharply, with a minimum value reached at about -130 °C. Further reductions in temperature resulted in a slight increase in G_{Ic}, presumably due to the cryogenic effects quoted above. Crack propagation was apparently stable, except at temperatures below about -70 °C where unstable fracture occurred. Fracture surface appearance varied significantly with temperature. At elevated temperatures a partial interfacial fracture was reported. Below 20 °C a rough centre of bond fracture resulted with a transition to a smooth centre of bond fracture occurring at temperatures below -50 °C.

The effect of testing rate on unmodified epoxy adhesive joints has been briefly investigated by Gledhill et al (38), for amine cured systems using aluminium alloy tapered double cantilever beam specimens. They found that a higher toughness and greater tendency for unstable crack growth occurred at the lower testing rates. However when stable growth occurred, increasing rate resulted in slight increases in toughness. At the temperature at which these investigations were conducted, namely 22 °C, centre of bond failure occurred.

The influence of temperature on the previously discussed fracture energy - bond thickness relationship for a rubber-modified epoxy adhesive (DGEBA-CTBN-Piperidine) has been studied by Bascom and Cottington (40). They used aluminium alloy tapered double cantilever beam specimens over the temperature range -40 to 50 °C. This study showed that the basic trend previously discussed and shown in Figure 5.1 was essentially maintained throughout the temperature range. However increasing temperature was clearly shown to shift the maximum in G_{Ic} to higher bond thickness levels. The authors once again attempted to correlate the bond thickness at maximum G_{Ic} with plastic zone diameter using equation 5.1. Although some success was achieved in the 25 to 50 °C region, poor correlation existed at lower temperatures. This discrepancy was partly attributed to the fact that tensile strength values, as opposed to yield stress, were used to determine values of $2r_y$ from equation 5.1. It was suggested that the former would increasingly underestimate yield stress as temperature was decreased. It was further proposed that this error would be aggravated by the use of σ_y^2 to calculate $2r_y$. The transition in both crack growth behaviour and fracture surface appearance at the bond thickness corresponding to the G_{Ic} maximum was reported to occur throughout the temperature range.

In an extension of this work, Bascom and Cottington (40) further demonstrated that, at a constant bond thickness of 0.25 mm, G_{Ic} was a maximum at approximately 25 °C. This trend was shown to resemble very closely the result obtained by Mostoroy and Ripling (49) on the commercial structural film adhesive discussed above. Bascom and Cottington explained this effect in terms of the plastic zone - bond thickness model previously discussed. At temperatures below 25 °C the rapid decline in G_{Ic} was attributed to a reduction in plastic zone size, $2r_y$, which would inevitably occur under these conditions. At the

G_{Ic} maximum it was suggested that $2r_y$ was equivalent to the bond thickness, whereas the decline at temperatures beyond 25 °C was due to a combination of two effects. Firstly, a further increase in plastic zone diameter, due to increased temperature would not occur due to the restrictive influence of the adherends. Secondly, other properties that influence G_{Ic} would also change with increasing temperature. This is clearly indicated by a simple rearrangement of equation 5.1, so that

$$G_{Ic} = \frac{6\pi r_y \sigma_y^2}{E} \qquad (5.2)$$

Increasing temperature generally results in reductions in both yield stress, σ_y and modulus, E with epoxy resins. Equation 5.2 clearly indicates that reductions in both these parameters would have opposite effects. However σ_y^2 suggests that increasing temperature in this case would produce a reduction in G_{Ic}.

5.3 Comparisons Between Bulk and Adhesive Joint Fracture

The earliest attempt at relating bulk and adhesive joint fracture behaviour was conducted by Mostovoy, Ripling and Bersch (48). They investigated an unmodified epoxy resin, cured by either tetraethylene-pentamine or hexahydrophthalic anhydride, using the tapered double cantilever beam geometry for both bulk and adhesive joint systems. It was concluded that for both types of formulation, bulk and adhesive joint toughness was not simply related and that adhesive joint toughness could not be predicted from bulk toughness. For the tetraethylenepentamine cured system it was stated that bulk toughness could give either an under or over estimate of bond performance over a range of post cure temperatures. However, bulk toughness was shown to be significantly greater than joint toughness for the anhydride cured formulation.

Conversely Bascom and co-workers (28) found similar G_{Ic} values for both bulk and adhesive joint specimens using a piperidine cured unmodified epoxy.

A more recent attempt at correlating bulk and adhesive joint fracture behaviour was conducted by Gledhill et al (38). They once again investigated an unmodified epoxy resin, this time cured with triethylene tetraamine, using double torsion and tapered double cantilever beam geometries for bulk and adhesive joint studies respectively. They were able to show that the type of crack propagation in the adhesive joint specimens was completely analogous to that in the bulk material. In both cases a transition between unstable and stable propagation occurred under identical testing conditions. Also, the values of K_{Ic} for both geometries were within about 20%. Although this degree of scatter is intuitively high, the authors argued that this discrepancy was possibly due to certain assumptions implicit in the conversion of adhesive joint G_{Ic} to K_{Ic}, which was necessary due to the double torsion geometry providing values of bulk K_{Ic}.

No detailed comparison of bulk and adhesive joint behaviour has been conducted with rubber-modified epoxy resins. Such a study is therefore long overdue.

PART TWO

EXPERIMENTAL AND RESULTS

CHAPTER SIX

EXPERIMENTAL PROCEDURES

6.1 Materials

6.1.1 Epoxy resin formulations

The epoxy resin formulations employed were,

(a) Unmodified epoxy

Epikote 828	100pph
Piperidine	5pph

(b) Rubber-modified epoxy

Epikote 828	100pph
CTBNX8	15pph
Piperidine	5pph

Epikote 828 is a liquid diglycidyl ether of bisphenol A, produced by the Shell Chemical Co., having a molecular weight of approximately 380 .

CTBNX8 is a high viscosity liquid carboxyl-terminated butadiene-acrylonitrile polymer, produced by B F Goodrich, having a molecular weight of 3,500 and an acrylonitrile content of 18%.

Piperidine was used as the curing agent.

To prepare the rubber-modified epoxy resin, the required quantity of CTBN was added to the resin, followed by mixing with a spatula for ten minutes. The resultant mixture was then raised to a temperature of 70 °C in a water bath and stirred for five minutes with an electric stirrer, followed by degassing in a vacuum oven at 60 °C. After cooling to 30 °C, the piperidine was added and the mixture gently stirred with a spatula. This was done so as to minimise air entrapment, since degassing of resins containing piperidine is generally inadvisable due to its volatility. The unmodified system was prepared by adding the

required quantity of piperidine to the epoxy resin at ambient temperature. Mixing was conducted by stirring gently with a spatula. The formulations at this stage were then ready either for casting to produce sheets for bulk studies or for adhesive joint preparation.

6.1.2 Substrates

For the adhesive joint studies the substrate material was mild steel to specification British Standard 970, EN3B. The mild steel was in the form of cantilever beams (to be described later). Prior to bonding, the mild steel surfaces were firstly degreased in 1,1,1 trichloroethane (five minutes complete immersion, five minutes vapour degrease) followed by grit-blasting with 180-220 mesh alumina. This was followed by a further identical degreasing process to remove contamination imparted by the grit-blasting procedure, after which they were allowed to air dry. A time limit of three hours was allowed between completion of surface pre-treatment and bonding so as to minimise atmospheric contamination.

6.2 Bulk Fracture Studies

6.2.1 Specimen preparation

A casting technique was employed to prepare bulk fracture mechanics specimens. A mould was made of stainless steel to produce sheets approximately 320 mm x 300 mm and of a thickness which was variable within set limits between 1.3 and 49 mm.

Prior to casting, the inner surfaces of the mould were treated with mould release agent (Araldite QZ 13), followed by heating to a temperature of 120 °C. Immediately following this, the epoxy formulation, at a temperature of 60 °C, was cast into the mould and cured at 120 °C for 16 hours in an air-circulating oven, followed by gradual cooling so as to minimise shrinkage stresses. On removal from the mould, the cured sheet was cut into compact tension (CT) specimens (51), with the dimensions shown in Figure 6.1. A number of single-edge-notch (SEN) specimens (51)

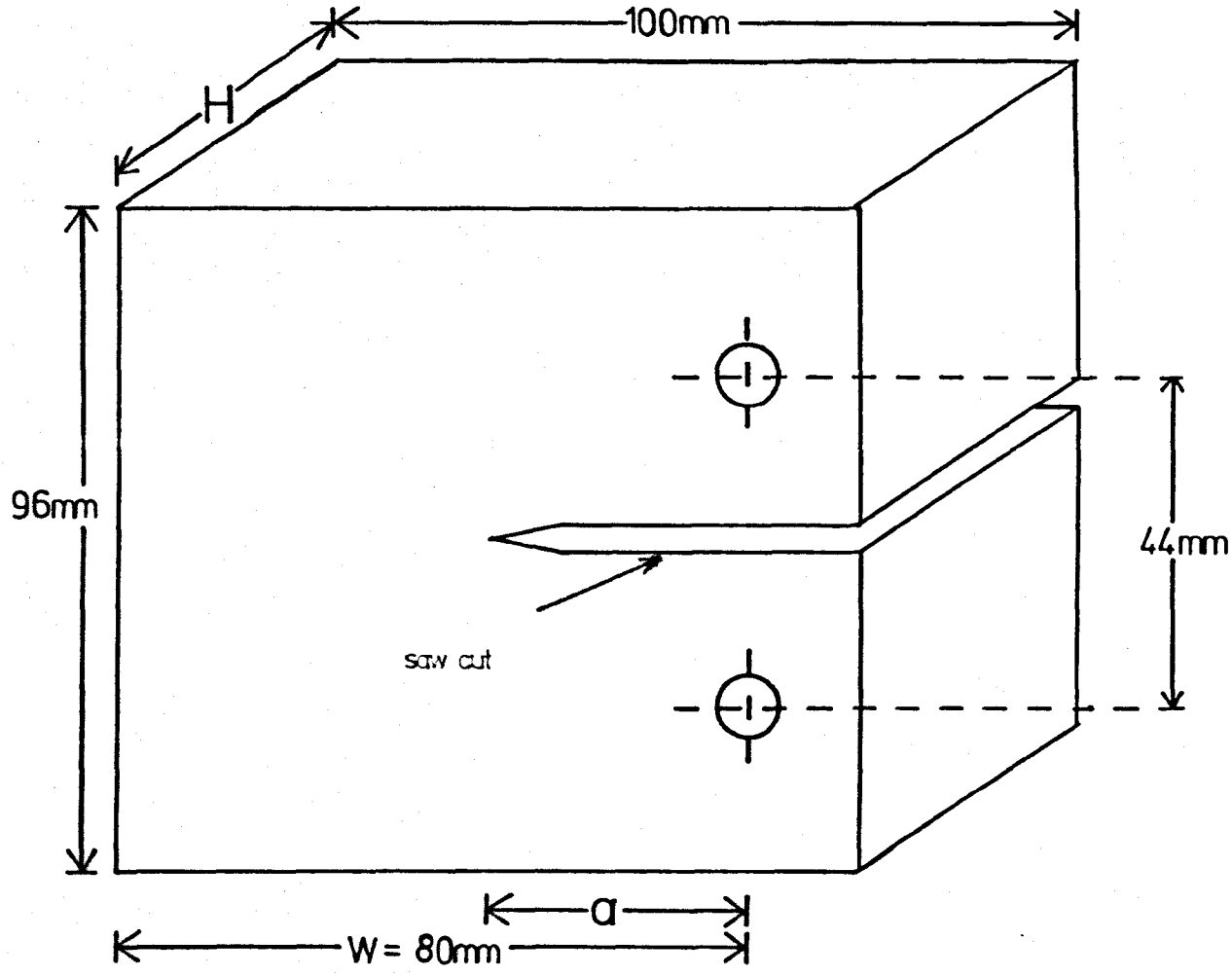

Figure 6.1 Compact – tension specimen.

were also produced having the dimensions shown in Figure 6.2.

6.2.2 Testing procedure

The experimental variables studied in the bulk fracture investigations were:

(i) cross-head displacement rate, $\dot{y}$, ranging from 0.05 to 10 mm min^{-1}

(ii) temperature, T, ranging from -90 to 60 °C and

(iii) thickness, H, ranging from 1.3 to 49 mm.

The detailed testing procedure employed with both types of specimen (CT and SEN) was essentially similar. If the specimens were to have crack lengths greater than 3 mm then a saw-cut was made in the positions indicated in Figures 6.1 and 6.2 just a little shorter in length than the final crack length required. This was followed by carefully tapping a fresh razor blade into the base of the saw-cut at 20 °C, which caused a natural crack to grow for a short distance ahead of the blade. With SEN specimens having intended crack lengths less than 3 mm the initial saw-cut was not needed.

The specimen dimensions outlined in Figures 6.1 and 6.2 were measured accurately with calipers and a micrometer. Specimens were then mounted in an Instron mechanical testing machine. With CT specimens, high tensile steel pins were used as indicated in Figure 6.1. Instron clamps were used to grip and locate the SEN specimens, and the length of the specimen was at least twice the specimen width. This was considered to be sufficient to prevent the stress-field at the crack tip being influenced by the clamps. Results from these investigations were obtained in the form of a load-displacement curve.

For experiments conducted at non-ambient temperatures, the specimens were tested in an Instron environmental chamber capable of maintaining the set temperature to within ± 0.5 °C. The required conditions were

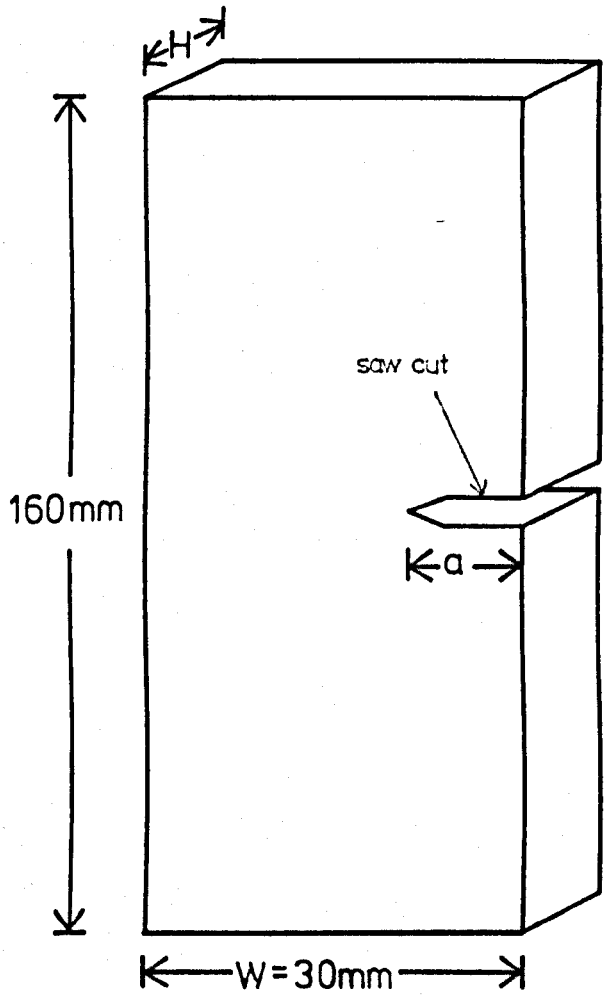

Figure 6.2 Single-edge-notch specimen.

provided by either electrical heating or liquid nitrogen cooling. Prior to testing, each specimen was allowed to achieve equilibrium under the prescribed temperature conditions.

For all room temperature tests (20 °C), a travelling microscope was used to observe the crack tip during the course of the experiment in an attempt to determine the onset of crack propagation. However at non-ambient temperatures, a travelling microscope was not used. Instead unaided visual observations were made. Prior to test, ink marks were made on the sides of the specimens to provide an approximate means for relating crack length to applied load.

6.2.3 Determination of fracture toughness

The critical stress intensity factor, K_{Ic}, is related to critical stress and specimen parameters by (51),

$$K_{Ic} = Q\sigma_c a^{\frac{1}{2}} \qquad (6.1)$$

where σ_c is the critical stress, a the crack length and Q a geometry factor. For CT specimens this factor is given by (51, 52)

$$Q = \left[29.6-185.5\left(\frac{a}{w}\right)+655.7\left(\frac{a}{w}\right)^2-1017\left(\frac{a}{w}\right)^3+638.9\left(\frac{a}{w}\right)^4\right]$$

where w is the width of the specimen (as described in Figure 6.1), with in this investigation $\frac{a}{w}$ being restricted to values between 0.45 and 0.55 (53). Results obtained from specimens outside this range were ignored.

For SEN specimens the geometry factor, Q, is given by (51),

$$Q = \left[1.99-0.41\left(\frac{a}{w}\right)+18.7\left(\frac{a}{w}\right)^2-38.48\left(\frac{a}{w}\right)^3+53.85\left(\frac{a}{w}\right)^4\right]$$

with $\frac{a}{w} < 0.2$.

The results obtained from the SEN specimens were expressed as a plot of $\sigma_c^2 Q^2$ versus a^{-1}, which, as can be seen from equation 6.1 should yield a linear relationship, K_{Ic} being given by the square root

of the gradient.

The critical stress intensity factor, K_{Ic}, values were, where convenient, converted to fracture energy, G_{Ic}, by the equation,

$$G_{Ic} = \frac{K_{Ic}^2}{E} \qquad (6.2)$$

where E is Young's modulus.*

6.3 Adhesive Joint Fracture Studies

6.3.1 Joint preparation

It is possible to employ a variety of specimens to study crack growth in adhesive joints (54). Probably the most popular, and the one used in this investigation, is the contoured-double-cantilever-beam (CDCB) (23,28,29,40,48,54-60), shown in Figure 6.3.

Detailed investigations were conducted on the rubber-modified epoxy, which, due to its comparatively low viscosity, necessitated the use of a casting technique. Initially a number of minor problems were encountered as will be mentioned, however these were eventually overcome and the final procedure employed is embodied in Figure 6.4.

A glass sheet completely covered with double-sided adhesive tape, was used as a rigid base. Three pieces of PTFE tape, 70 μm thick, 12 mm wide and 300 mm long were positioned so as to enable the finished joint to be easily removed from the tape-covered sheet. The pre-treated mild steel cantilever beams were then pressed onto the tape-covered sheet so that the bond line was directly over one of the pieces of PTFE tape. Poly(ethylene terephthalate) or in certain cases, brass spacers were positioned at each end of the specimen to control bond thickness and to provide a casting reservoir for the adhesive. A piece of PTFE tape approximately 60 mm long and 12 mm wide was placed at the loading end of the specimen so as to assist starter crack formation. Steel plates,

* (It should be noted that the terms K_{Ic} and G_{Ic} do not necessarily imply the attainment of plane strain behaviour).

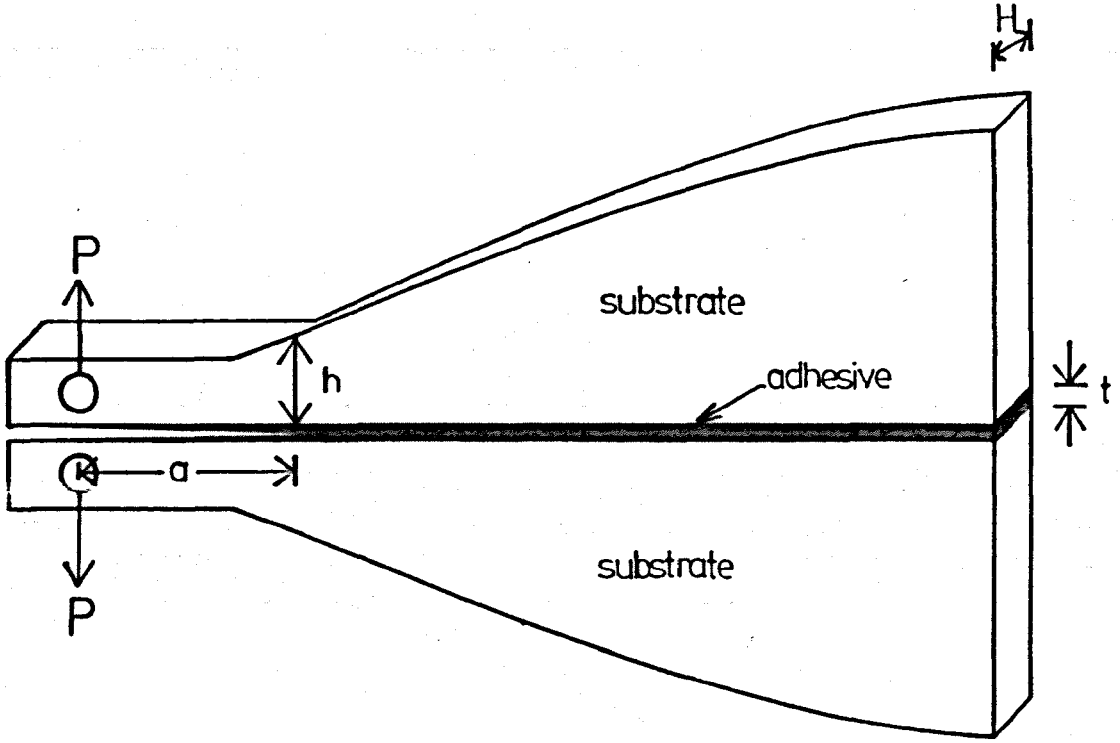

Figure 6.3 Contoured-double-cantilever-beam adhesive joint specimen.

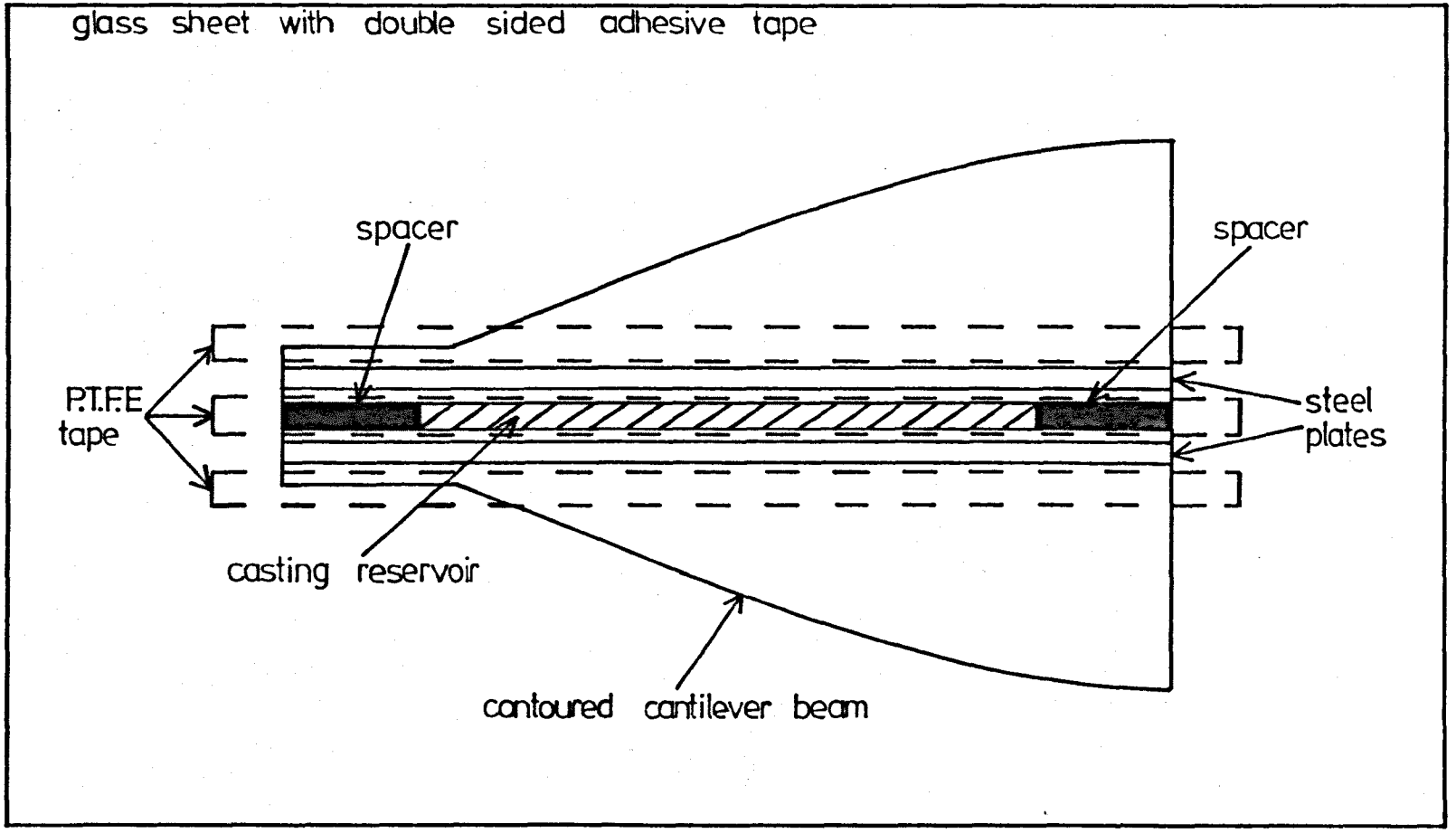

Figure 6.4 Plan view of adhesive joint casting arrangement.

300 mm x 25 mm x 5 mm were then positioned, using double-sided adhesive tape, on the specimen so as to provide an increased casting volume. This was found necessary for two resons: loss of adhesive invariably occurred during cure which produced adhesive starvation and; on a number of occasions discolouration of the adhesive which was in contact with the air occurred. However, with the above arrangement discolouration was restricted to excess adhesive. The whole specimen assembly was then suitably bound using PVC adhesive tape to maintain specimen integrity and ensure minimum loss of adhesive during cure. This was followed by heating the complete assembly to 120 °C in an air-circulating oven. Adhesive at 60 °C was then poured into the casting reservoir and the assembly returned to the oven for a cure cycle of 16 hours at 120 °C followed by slow cooling. After cure, excess adhesive remaining on the joint was removed using a hand file.

In a limited number of cases, were plastic zone observations were required, hand filing was followed by abrading with various grades of silicon carbide paper and polishing with 6 μm diamond paste. This was done so as to present a smooth surface for detailed observation.

6.3.2 Testing procedure

The experimental variables studied in the adhesive joint fracture investigations were:

(i) adhesive bond thickness, t, ranging from 0.1 to 3.0 mm

(ii) joint width, H, (see Figure 6.3) ranging from 3 to 49 mm, and

(iii) cross-head displacement rate, $\dot{y}$, ranging from 0.05 mm min^{-1} to 50 mm min^{-1}.

The adhesive bond thickness, t, of each joint was measured by a travelling microscope equipped with an eyepiece graticule unit. A number of readings for each joint were taken so as to determine an average and a measure of scatter. Joints having coefficients of variation greater than 25% were discarded.

A starter crack was inserted by separating the arms of the joint at a constant rate of 1mm min^{-1}, at 20 °C, using an Instron mechanical testing machine, until a crack existed in the adhesive layer about 70 to 100 mm long. The joints were then re-loaded to failure under the required conditions, with the results being recorded as a load - displacement curve.

In a limited number of cases the crack tip and deformation zone was observed in detail. These experiments were conducted on 12 mm wide specimens at bond thicknesses of 0.6, 0.9 and 1.5 mm. The testing procedure employed was similar to that described above but the tip of the crack and its associated deformation zone was observed with a travelling microscope whilst being subjected to a displacement rate of 0.05 mm min^{-1}.

6.3.3 Determination of fracture energy

With a contoured-double-cantilever-beam specimen the fracture energy, G_{Ic}, of the adhesive layer is given by,

$$G_{Ic} = \frac{P_c^2}{2H} \frac{\partial C}{\partial a} \qquad (6.3)$$

where P_c is the critical load, H the joint width and $\partial C/\partial a$ the change in compliance of the specimen with crack length. According to beam theory this compliance dependence is given by (61,62),

$$\frac{\partial C}{\partial a} = \frac{8}{E_s H} \left(\frac{3a^2}{h^3} + \frac{1}{h} \right) \qquad (6.4)$$

where E_s is the modulus of the substrate, a the crack length and h the corresponding beam height. Combining 6.3 and 6.4 yields,

$$G_{Ic} = \frac{4P_c^2}{E_s H^2}\left(\frac{3a^2}{h^3} + \frac{1}{h}\right) \qquad (6.5)$$

where the term in brackets is known as the geometry factor and given the symbol, mg. The specimen shown in Figure 6.3 was designed to have a constant geometry factor (in this case $2mm^{-1}$) along the whole length of the specimen, hence making the fracture energy independent of crack length and removing the necessity of monitoring crack length during the experiment.

Values of adhesive fracture energy, G_{Ic}, were calculated using equation 6.5.

6.4 Deformation Studies

The main objective of these studies was to obtain values of yield stress and modulus which could be of use in the further characterisation of the fracture data. Two techniques were employed, namely three-point-bend and compression.

6.4.1 Three-point-bend

(a) Specimen preparation

Sheets of rubber-modified and unmodified epoxy were prepared as described in section 6.2.1 with a thickness of 5.8 mm. The cured sheets were cut into rectangular plates 20 mm by 130 mm.

(b) Testing procedure

The dimensions of the specimen were accurately determined with calipers. The specimen was then located in a three-point-bend assembly attached to an Instron mechanical testing machine. The loading arrangement is shown schematically in Figure 6.5. The specimen was then tested under pre-selected conditions, with the results of the test being recorded as a load-displacement curve. The results were

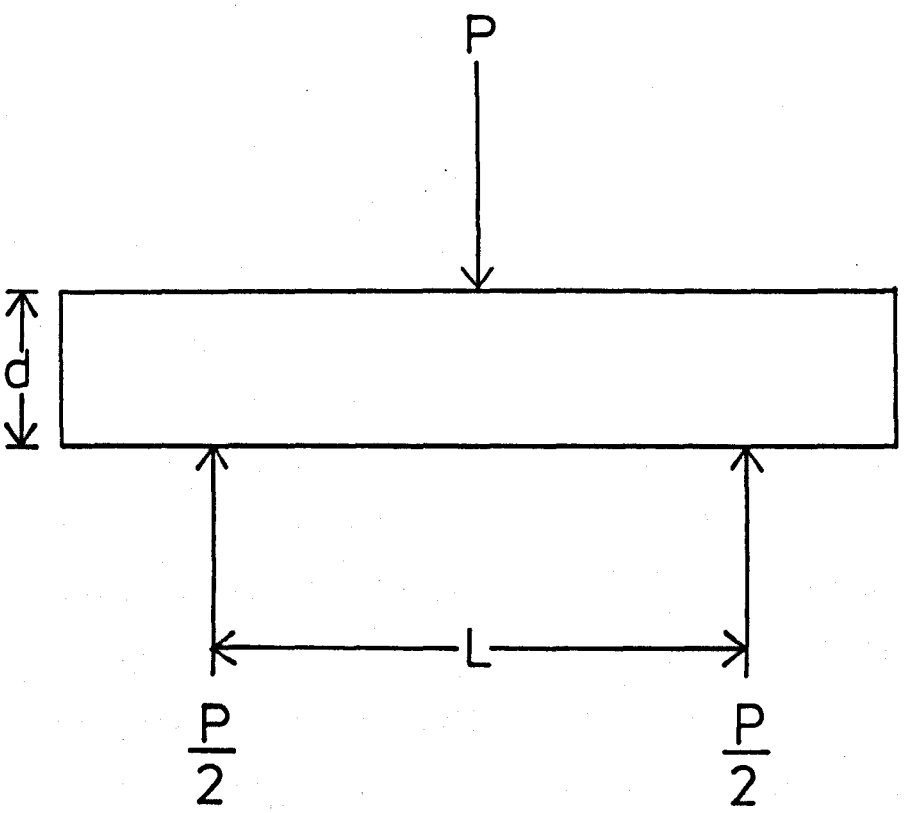

Figure6.5 Three– point bend test.

used to determine values of Young's modulus, E, by use of the equation (63),

$$E_a = \frac{L^3 m}{4bd^3} \qquad (6.6)$$

where L is the support span (85 mm), b the specimen width, d the specimen depth and m the gradient of the tangent to the initial straight line portion of the load-displacement curve. The displacement of the specimen was determined from the movement of the machine cross-head, taking into account correction for machine softness by prior testing with a steel blank.

Tests were conducted at 20 °C at displacement rates of 0.05, 1 and 10 mm min^{-1}.

6.4.2 Compression

(a) Specimen preparation

Compression specimens were prepared by casting the epoxy resin into cylindrical holes drilled out of a brass block, followed by curing for 16 hours at 120 °C. The resultant rods, wich had a diameter of approximately 8 mm, were cut into lengths of approximately 16 mm. The specimen ends were then carefully machined using a lathe to minimise end distortion and frictional effects. The resultant 2:1 length - diameter ratio was found to produce a good compromise between end frictional effects and specimen buckling (64).

(b) Testing procedure

The dimensions of each rod were accurately determined with calipers. The rods were then deformed in a compression cage between polished steel plates, lubricated with molybdenum disulphide grease, in an Instron mechanical testing machine. A constant cross-head displacement rate was used for each test and this was converted to a strain rate using the specimen dimensions. The nominal strain, e, was determined from

the cross-head displacement corrected for the machine deflection using a steel blank. The result of the test was recorded in the form of a load-displacement curve. The main parameters of interest were the true compressive yield stress, σ_{yc}, and modulus, E_a. The former was obtained from the load, P_y, at yield and the initial specimen cross-sectional area, Ao, by the equation,

$$\sigma_y = \frac{P_y}{Ao} (1 - e) \qquad (6.7)$$

The value for modulus was obtained from the slope of a tangent to the initial linear part of the load-displacement curve.
(See Figure 6.6 for a typical load - displacement curve).

Rates of cross-head displacement employed ranged from 0.05 to 10 mm min^{-1} over a temperature range of -60 to 60 °C. All tests were conducted in an Instron environmental chamber.

6.4.3 Dynamic mechanical studies

To obtain values of both storage and loss shear moduli, G' and G'', and loss tangent, tan Ø, dynamic mechanical studies on both rubber - modified and unmodified epoxy formulations were conducted using a mechanical spectrometer (Rheometrics Ltd).

Rectangular specimens 85 mm long and 10 mm wide were machined from 5.8 mm thick sheets, produced by the casting procedure specified in section 6.2.1. The specimens were mounted vertically in the spectrometer and clamped securely at both ends. The upper fixture was subjected to torsional sinusoidal oscillations at a frequency of 1 Hz actuated by a voltage signal from a generator. The resultant torque in the specimens was transmitted to the lower fixture which was locked in position and connected to a transducer system, which through a transfer function analyser provided values of storage shear modulus, G' and loss shear modulus, G''. Values of the loss tangent, tan Ø, were calculated from

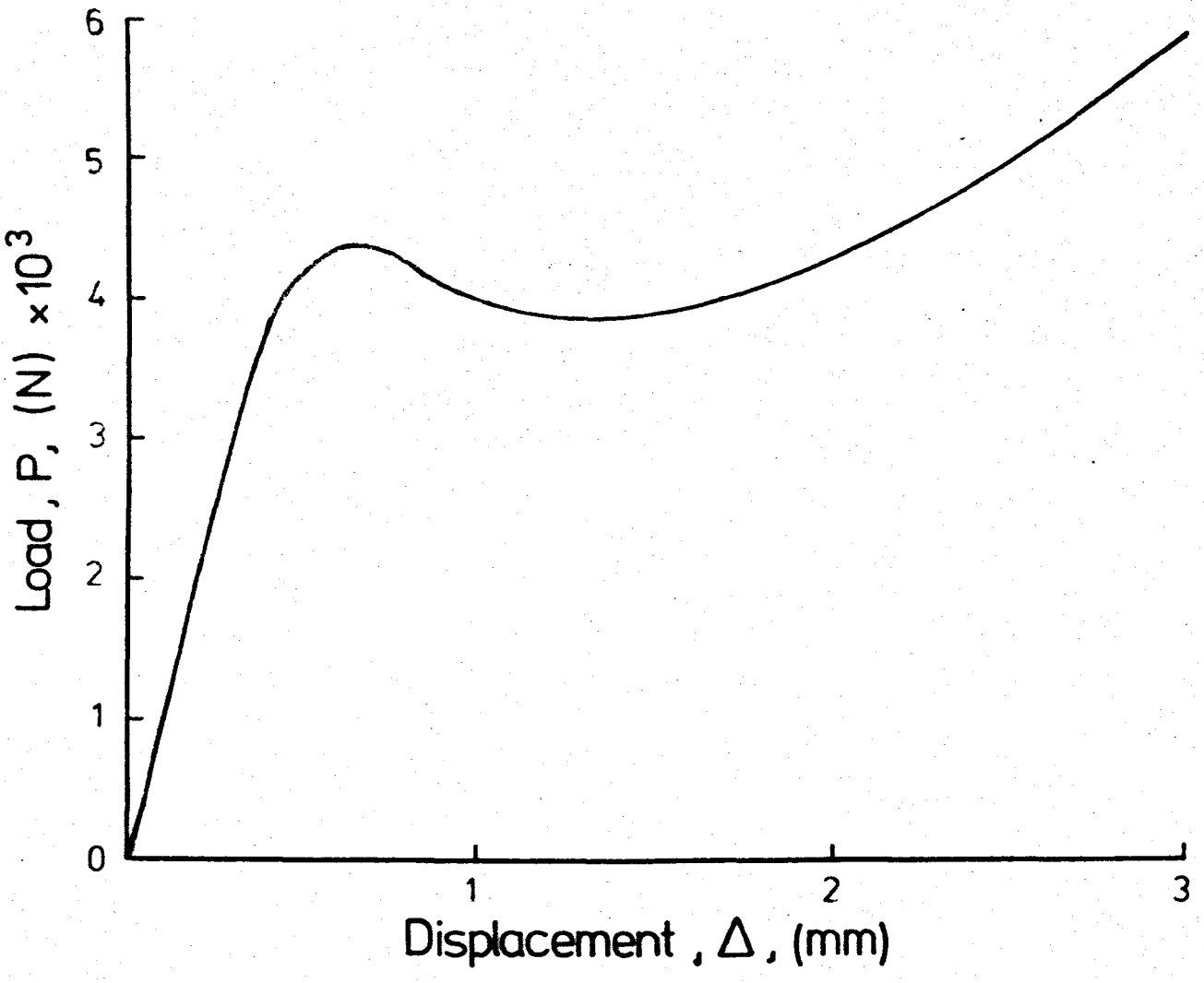

Figure 6.6 Typical load–displacement curve obtained from a uniaxial compression test. Unmodified epoxy, 20°C, 1 mm min^{-1} displacement rate.

equation 6.8,

$$\tan \emptyset = \frac{G''}{G'} \qquad (6.8)$$

Measurements were taken at approximately 5 °C intervals between -160 °C and 150 °C. The specimen was allowed to reach equilibrium for five minutes at each test temperature with a heating rate between test temperatures of approximately 5 °C per minute. Electrical heaters and liquid nitrogen were used to obtain high and low temperatures respectively.

6.5 Fractography

Both bulk and adhesive joint fracture surfaces were examined visually and in reflected light with a Nikon optical microscope for evidence of general surface features. Bulk fracture surfaces were further studied by both scanning and transmission electron microscopy.

6.5.1 Scanning electron microscopy

Relevant areas of the fracture surfaces were mounted on metal stubs and coated with a thin layer of gold to improve conductivity and prevent charging. The surfaces were examined in a scanning electron microscope (Cambridge Instruments Ltd) at a relatively low beam current and accelerating voltage of 175 mA and 20 kV respectively.

6.5.2 Transmission electron microscopy

Transmission electron microscopy was performed on both rubber-modified and unmodified epoxy bulk fracture surfaces. A two-stage replication procedure was used involving the preparation of a carbon replica by means of an intermediate polymeric stage. The technique needed some exploration but the method generally involved applying a polymeric material (see below) in either a liquid or softened form, to the fracture surface. The polymer was allowed to harden and was then stripped from the surface and placed in a carbon coating unit, where it

was first shadowed at an angle of 45 ° with platinum/carbon. This was followed by carbon evaporation normal to the surface to strengthen the replica. The polymer was then dissolved in a suitable solvent, thus leaving the final carbon replica for investigation in the transmission electron microscope.

A number of different polymeric replicating materials were tried in the investigation. Initial experiments used gelatin sheet as the intermediate replica; the gelatin being softened in water before being applied to the fracture surface. Unfortunately, on drying, the gelatin sheet had a tendency to lift off the surface, giving rise to considerable doubt as to its replicating accuracy. So an alternative material was considered necessary.

A second series of replicas were produced using a 2% solution of nitrocellulose in amyl acetate. This was applied to the fracture surface and allowed to dry, and the film stripped with sellotape. However, although this technique appeared adequate for the majority of the unmodified fracture surfaces, a number of problems were encountered with the rubber-modified surfaces, with stripping resulting in evidence of replica damage. A third replicating material, consisting of cellulose acetate dissolved in acetone, was therefore examined and showed some minor improved stripping characteristics.

Therefore in this investigation, two replicating polymeric solutions, nitrocellulose and cellulose acetate were employed; both being used for rubber-modified fracture surfaces, but only nitrocellulose in amyl acetate for unmodified surfaces.

Investigations were conducted on different regions of the fracture surfaces obtained at temperatures ranging from -60 to 60 °C, at magnifications of 500 to 70,000 in a transmission electron microscope.

CHAPTER SEVEN

BULK STUDIES. RESULTS

7.1 Introduction

This chapter describes results obtained from studies of bulk materials and is divided into four principal sections. The first two deal with results obtained from uniaxial compression and flexural bending, and dynamic mechanical experiments. The third section deals with the fracture investigations. Finally, the fourth section summarises the results obtained from all these bulk investigations.

7.2 Uniaxial Compression and Flexural Bending Experiments

Table 7.1 shows the modulus, E, data obtained from the three-point-bend and unaxial compression techniques for both unmodified and rubber-modified formulations. For both formulations it is of interest to note that modulus values obtained from the two techniques were within 10% thus suggesting that the well known practical difficulties with uniaxial compression tests of buckling and frictional constraint (64), did not significantly affect the results.

TABLE 7.1

Modulus, E, obtained from compression and three-point-bend experiments. 20°C

Displacement rate ($mm\ min^{-1}$)	Unmodified Epoxy Modulus, GPa		Rubber-Modified Epoxy Modulus, GPa	
	Compression	Three-point-bend	Compression	Three-point-bend
0.05	3.20[a](0.16)[b]	3.41 (0.03)	2.78 (0.15)	2.57 (0.10)
1	3.19 (0.06)	3.47 (0.02)	2.77 (0.19)	2.57 (0.07)
10	3.19 (0.13)	3.52 (0.04)	2.68 (0.09)	2.64 (0.05)

(a) Mean calculated from three results

(b) Standard deviation

The more detailed results obtained from the uniaxial compression tests are shown in Figures 7.1 to 7.4. These show that for both systems, modulus and yield stress increase with increasing displacement rate and decreasing temperature. This is frequently found with a wide range of polymers (65-70) and indeed is to be expected of such viscoelastic materials.

The modulus and yield stress values for the rubber-modified epoxy are approximately 17 to 50% lower than the corresponding unmodified data; the greater differences existing at the higher temperatures.

7.3 Dynamic Mechanical Studies

The results obtained from the dynamic mechanical experiments conducted on both formulations are shown in Figure 7.5, where loss tangent, tan ϕ, is plotted as a function of temperature at a frequency of 1 Hz. In both cases the high temperature region is dominated by a peak at approximately 100°C, which can be attributed to the glass transition, Tg, of the crosslinked epoxy. This value compares favourably with that obtained by other workers for a similar formulation (71-73) as indicated in Table 7.2. The presence of the

TABLE 7.2

Glass transition temperatures, Tg, for epoxy resin - piperidine cured systems

Glass transition temperature (°C)	Ref
110[a]	71
99[a]	72
85[b]	73
100[a]	This work

(a) from mechanical loss measurements

(b) heat distortion temperature

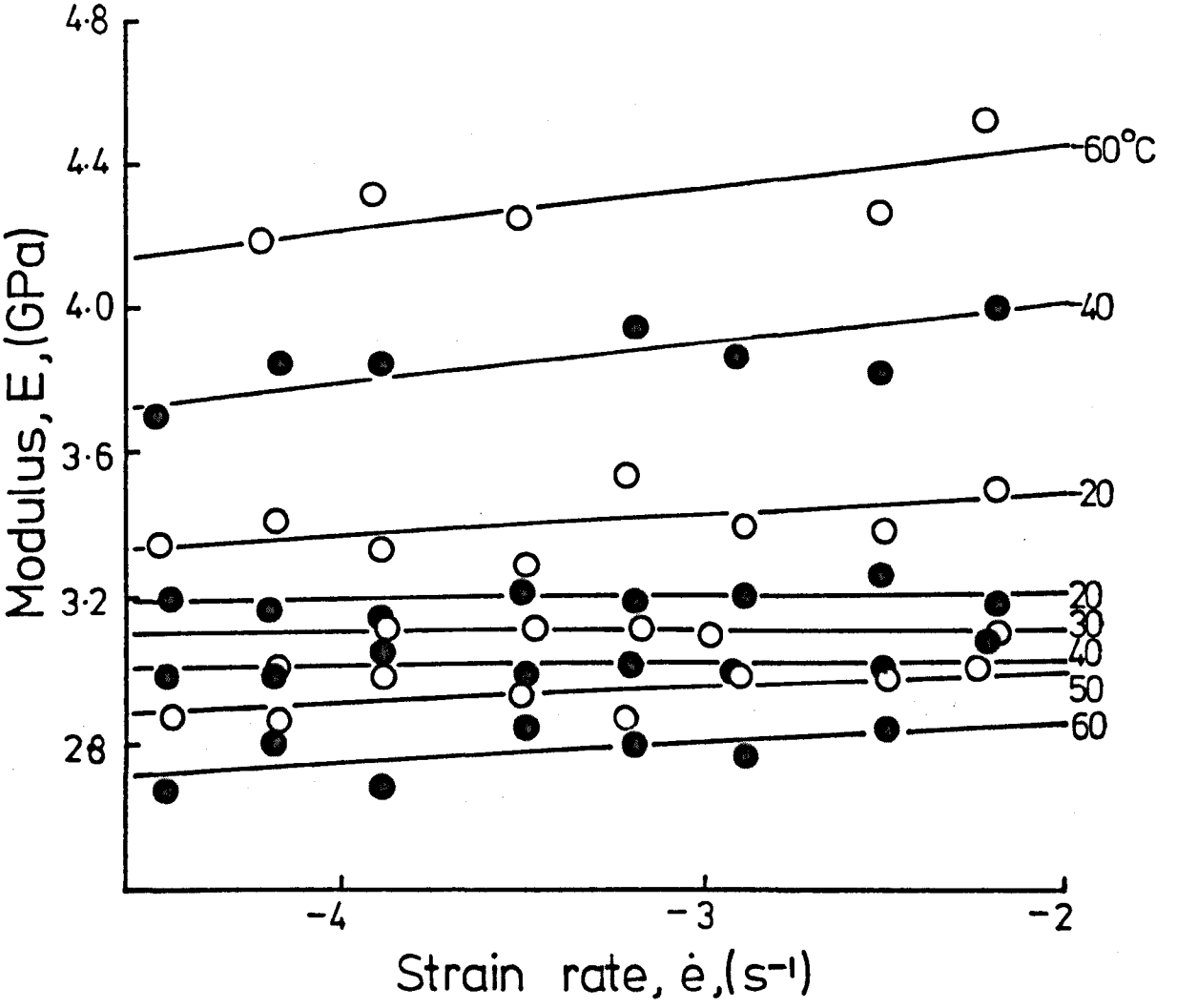

Figure 7.1 Modulus as a function of strain rate at various temperatures. Unmodified epoxy.

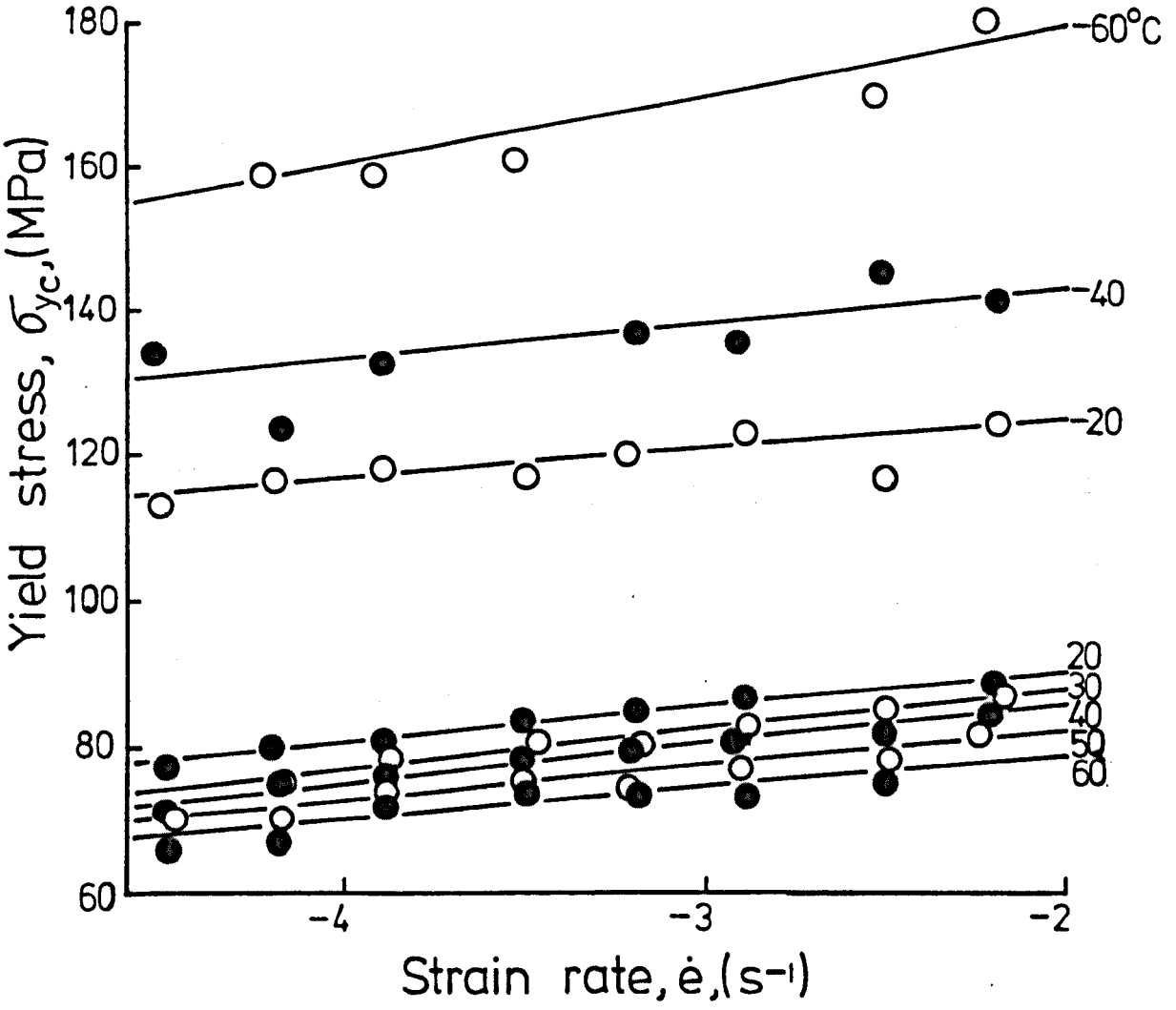

Figure 7.2 True compressive yield stress as a function of strain rate at various temperatures. Unmodified epoxy.

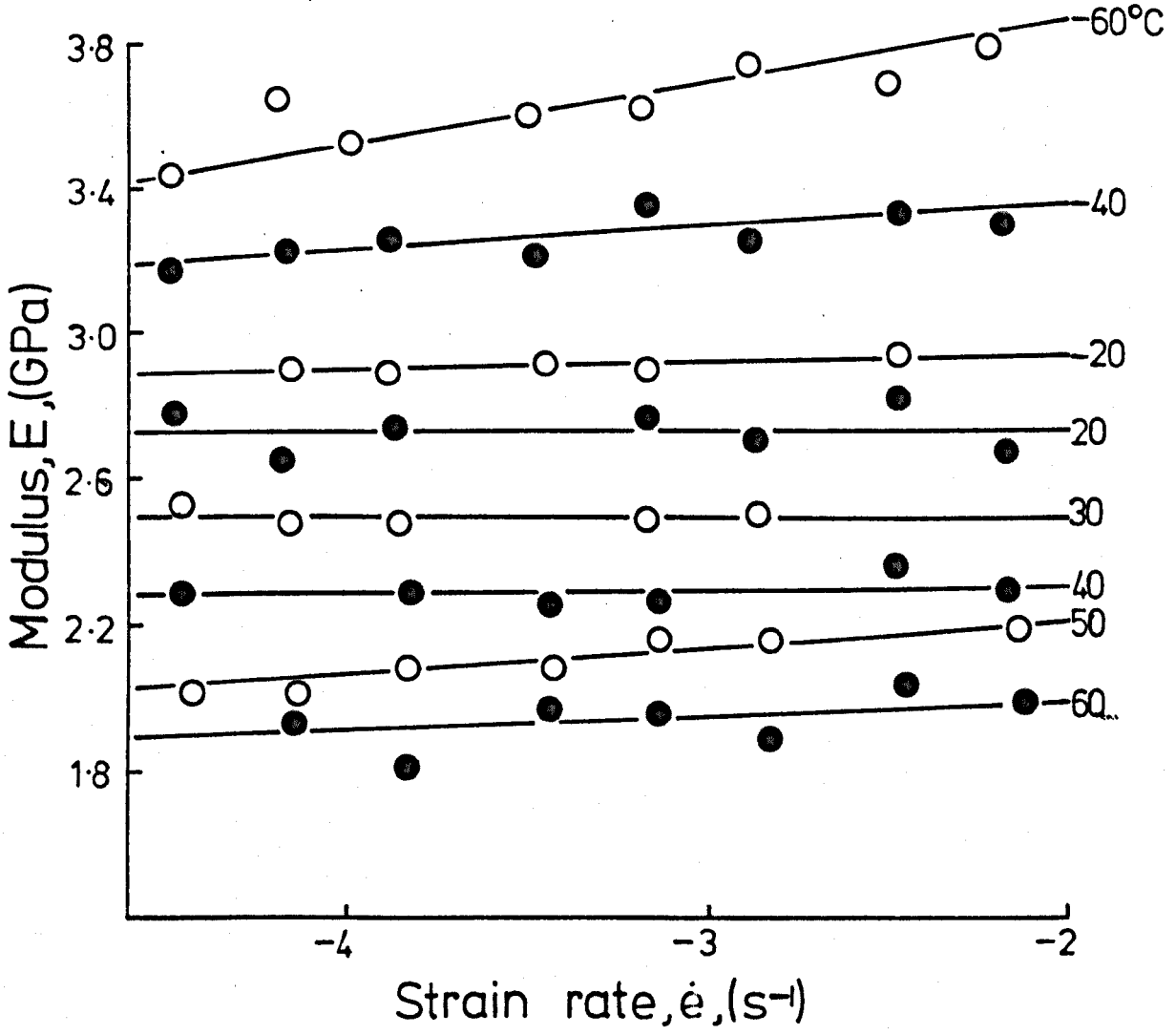

Figure 7.3 Modulus as a function of strain rate at various temperatures. Rubber modified epoxy.

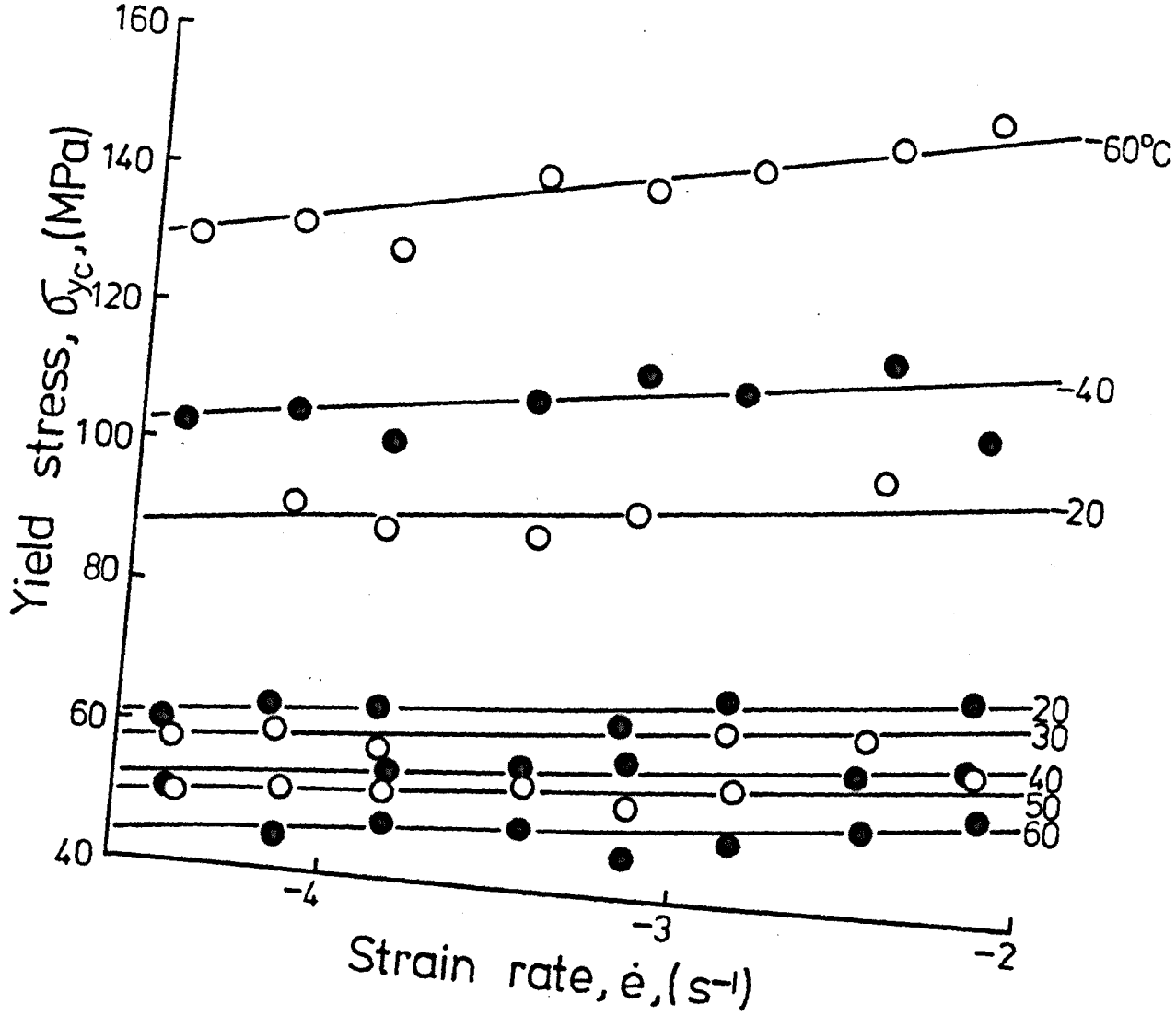

Figure 7.4 True compressive yield stress as a function of strain rate at various temperatures. Rubber-modified epoxy.

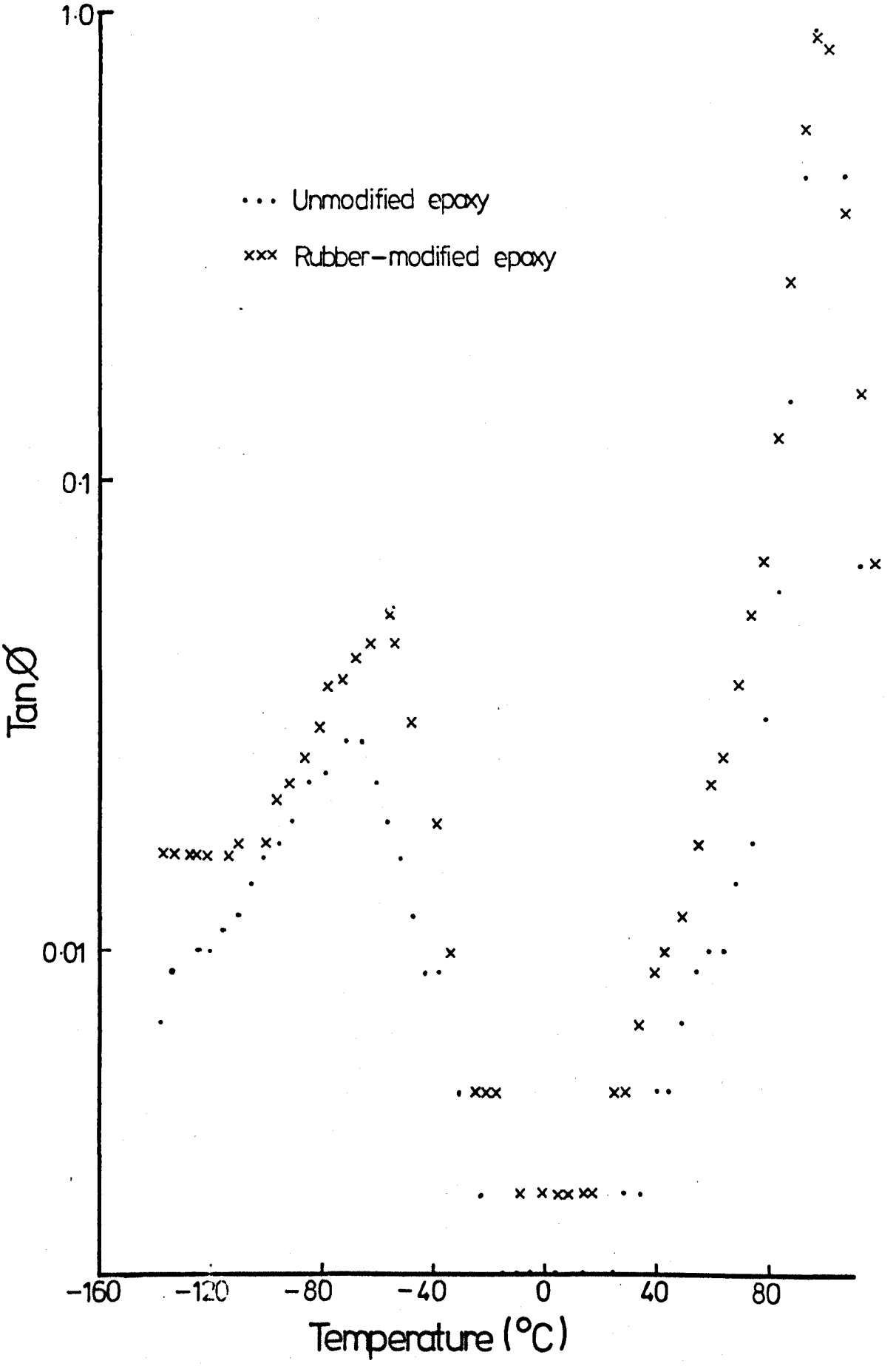

Figure 7.5 Loss factor, tanØ, as a function of temperature. Frequency 1 Hz.

elastomeric carboxyl terminated acrylonitrile butadiene rubber in the epoxy formulation does not significantly affect Tg. This suggests that most of the rubber phase separates prior to gelation with only a minimal amount remaining in the epoxy matrix.

Both systems show a second, much smaller peak with a maximum tan ø at approximately -70°C. Relaxations in this temperature region are common with amine cured epoxy resins and are frequently referred to as β relaxations (74-82). They are believed to result from crankshaft rotations of glyceryl units, $-CH_2-CH(OH)-CH_2-O-$, in the epoxy matrix (76, 78, 82).

With the rubber-modified epoxy this peak exhibits a greater value of tan ø over an approximately similar temperature range. It would therefore appear that this increased tan ø value is associated with the presence of CTBN rubber, which would be expected to exhibit a Tg in this temperature region (83, 84). This peak is therefore composed of both the β relaxation of the epoxy phase, $T_\beta E$ and the Tg of the rubber phase, Tg R. An estimate of the loss peak for the rubbery phase can be obtained by simply subtracting tan ø for the unmodified epoxy from tan ø for the modified epoxy, allowing for the reduced concentration of epoxy in the modified material. The result is shown in Figure 7.6, where it can be seen that the rubber phase has a tan ø maximum at approximately -55°C. All of the major transitions determined for the two systems are shown in Table 7.3.

TABLE 7.3

Transition temperatures for both epoxy systems

Transition	Temperature (°C)	
	Unmodified	Rubber-modified
Tg E	100	100
T_β E	-70	-70
Tg R	-	-55

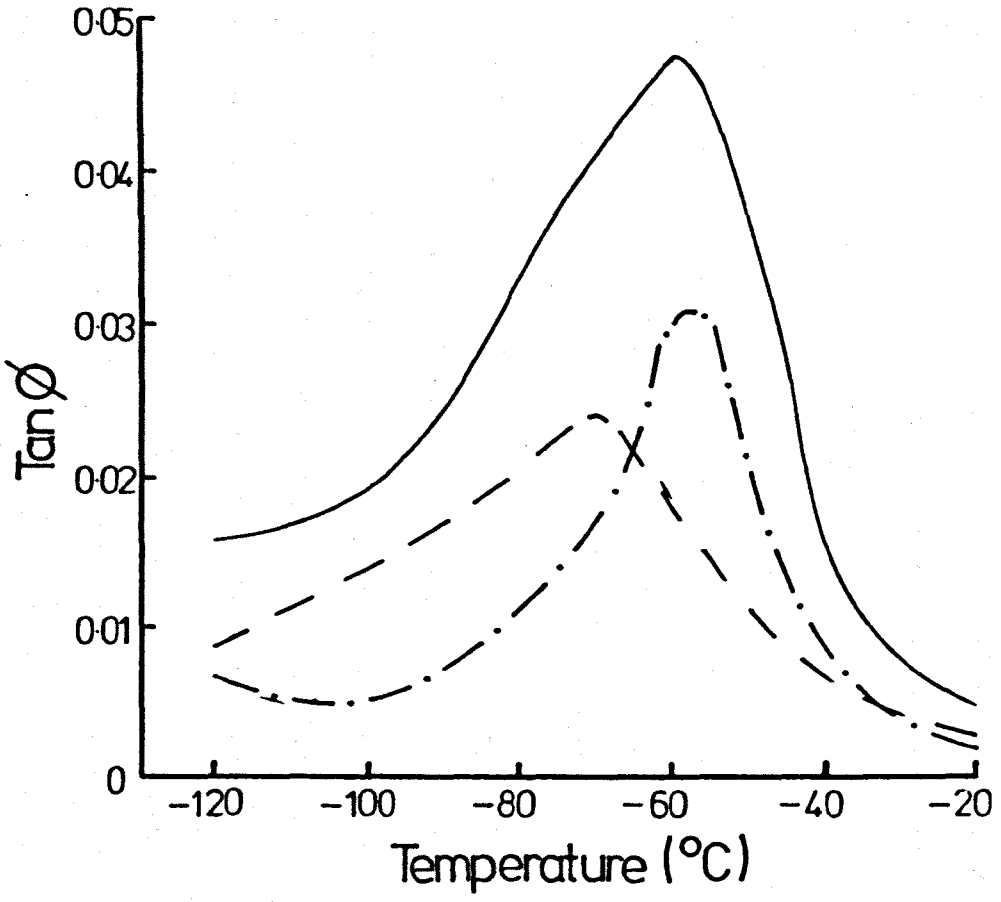

Figure 7.6 Loss factor, tan Ø, as a function of temperature, -120°C to -20°C. —— Rubber-modified epoxy, – – – –Unmodified epoxy, –·–·– Δtan Ø.

7.4 Fracture Studies

7.4.1 Types of load-displacement curves

Over the range of displacement rates and temperatures that fracture behaviour was studied, three main forms of load-displacement curve were obtained for both systems. These reflected three major types of crack growth behaviour, which are all illustrated in Figure 7.7.

Figure 7.7(a) shows one type, designated A, which was associated with slow, stable crack extension. With this behaviour the onset of crack extension did not occur at the maximum load but at a load of approximately 0.8 of this value. However all fracture toughness calculations were based on maximum load data due to experimental uncertainty regarding the 0.8 value.

Figure 7.7(b) shows a load-displacement curve which was associated with unstable, stick-slip crack extension. This has been designated type B. In this case the point at which maximum load occurred coincided with the onset of crack extension.

Figure 7.7(c) shows the third main form of load-displacement curve, Type C, which again was associated with stable crack extension. As with type B growth, the onset of crack extension appeared to occur at the maximum load. Fracture toughness values for types B and C crack growth were calculated from maximum load data.

Two intermediate forms of crack growth were also observed with both formulations which resulted in slight changes in corresponding load-displacement curves. These crack growth regimes, which will be discussed more fully later in this chapter, were given the designations A→B and C→B, and gave load-displacement curves similar to type B.

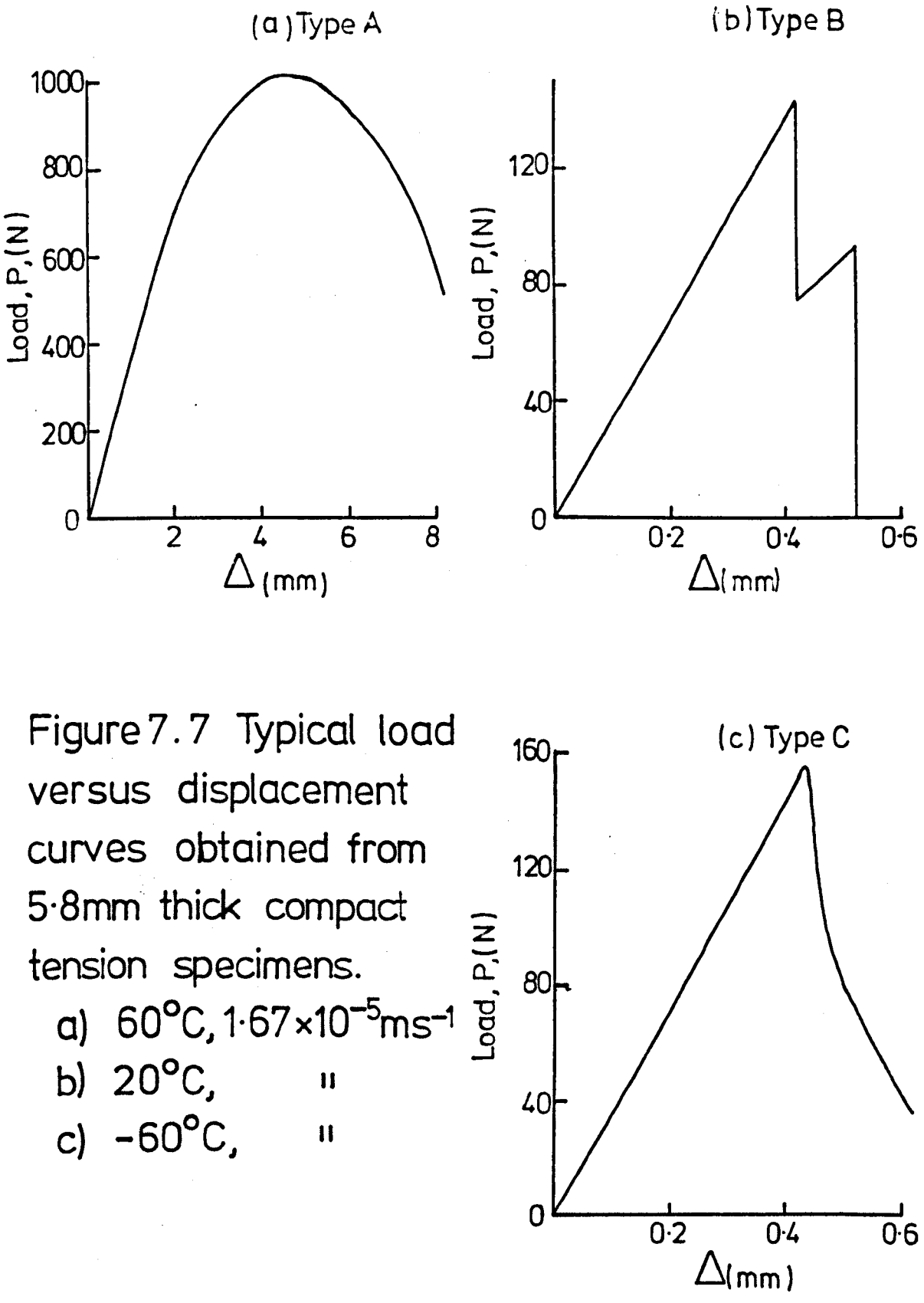

Figure 7.7 Typical load versus displacement curves obtained from 5·8mm thick compact tension specimens.

a) 60°C, $1{\cdot}67\times10^{-5}ms^{-1}$

b) 20°C, "

c) -60°C, "

7.4.2 Fracture toughness, K_{Ic}, data

This section is divided into two parts. The first deals with the effects of rate and temperature on the fracture behaviour of 5.8 mm thick compact tension specimens. The second deals with the effect of specimen thickness, which was studied at 20°C only.

(a) Rate and temperature

The effects of rate and temperature on fracture toughness, K_{Ic}, for the unmodified system are shown in Figures 7.8 and 7.9. Figure 7.8 shows the influence of displacement rate on fracture toughness at various temperatures from -90°C to 60°C. Figure 7.9 shows the influence of temperature on fracture toughness at three different values of displacement rate. The crack growth types are also indicated.

Both figures show clear evidence of tough-brittle transitional behaviour under certain conditions, where relatively high temperatures and low rates lead to a sharp increase in the values of K_{Ic}. Furthermore this transition is also associated with a transition from type A to type B crack growth. Also indicated, but far less pronounced, are indications that K_{Ic} in the brittle regime is both rate and temperature dependent.

Although values of K_{Ic} associated with type A crack growth are shown in Figures 7.8 and 7.9 it should be noted that, under such ductile crack growth conditions, the assumptions of linear elastic fracture mechanics previously invoked in deriving equation 3.16 (Chapter 3) would be grossly violated.

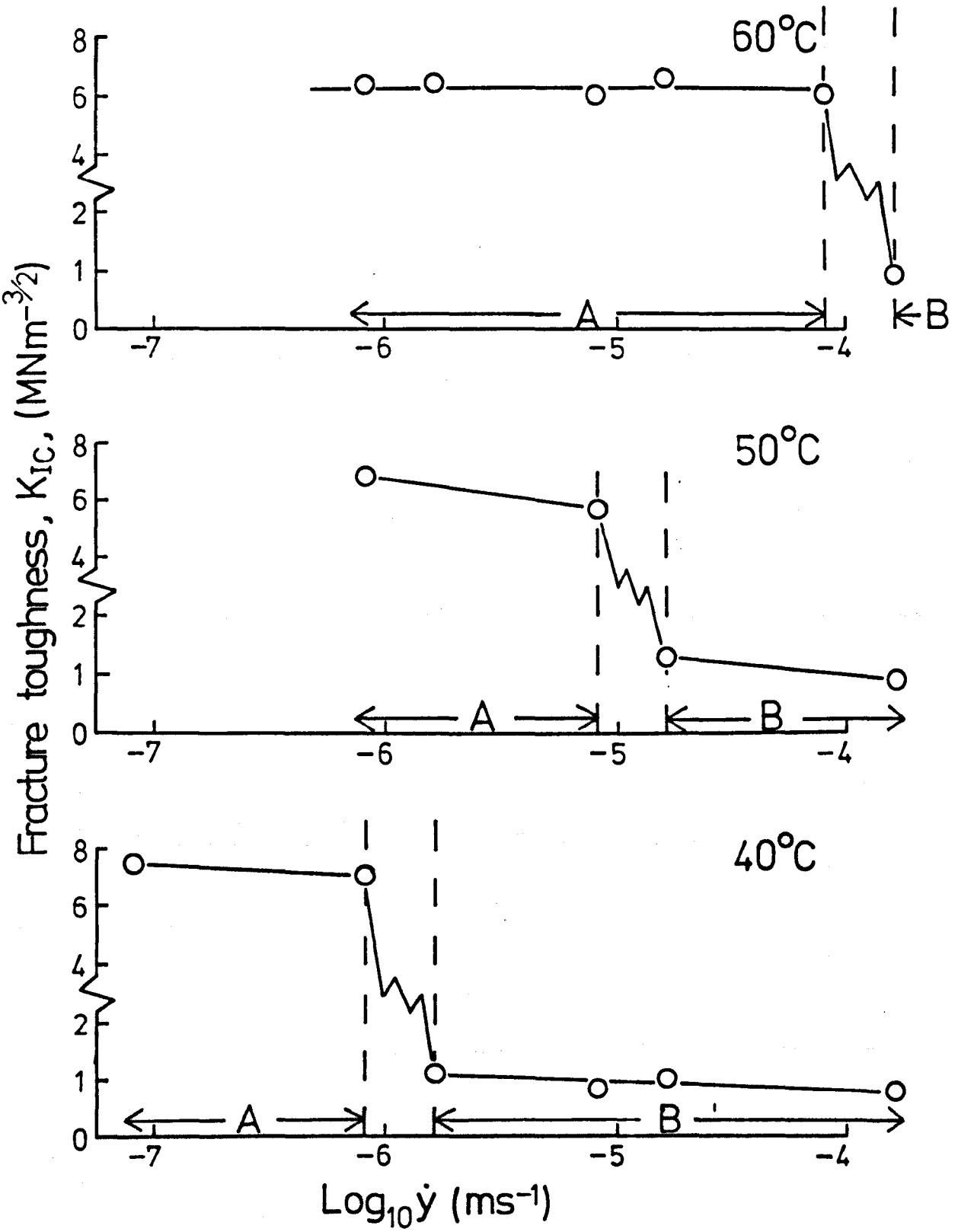

Figure 7.8 Fracture toughness, K_{IC}, versus displacement rate, $\dot{y}$. Unmodified epoxy, 5·8 mm thickness.

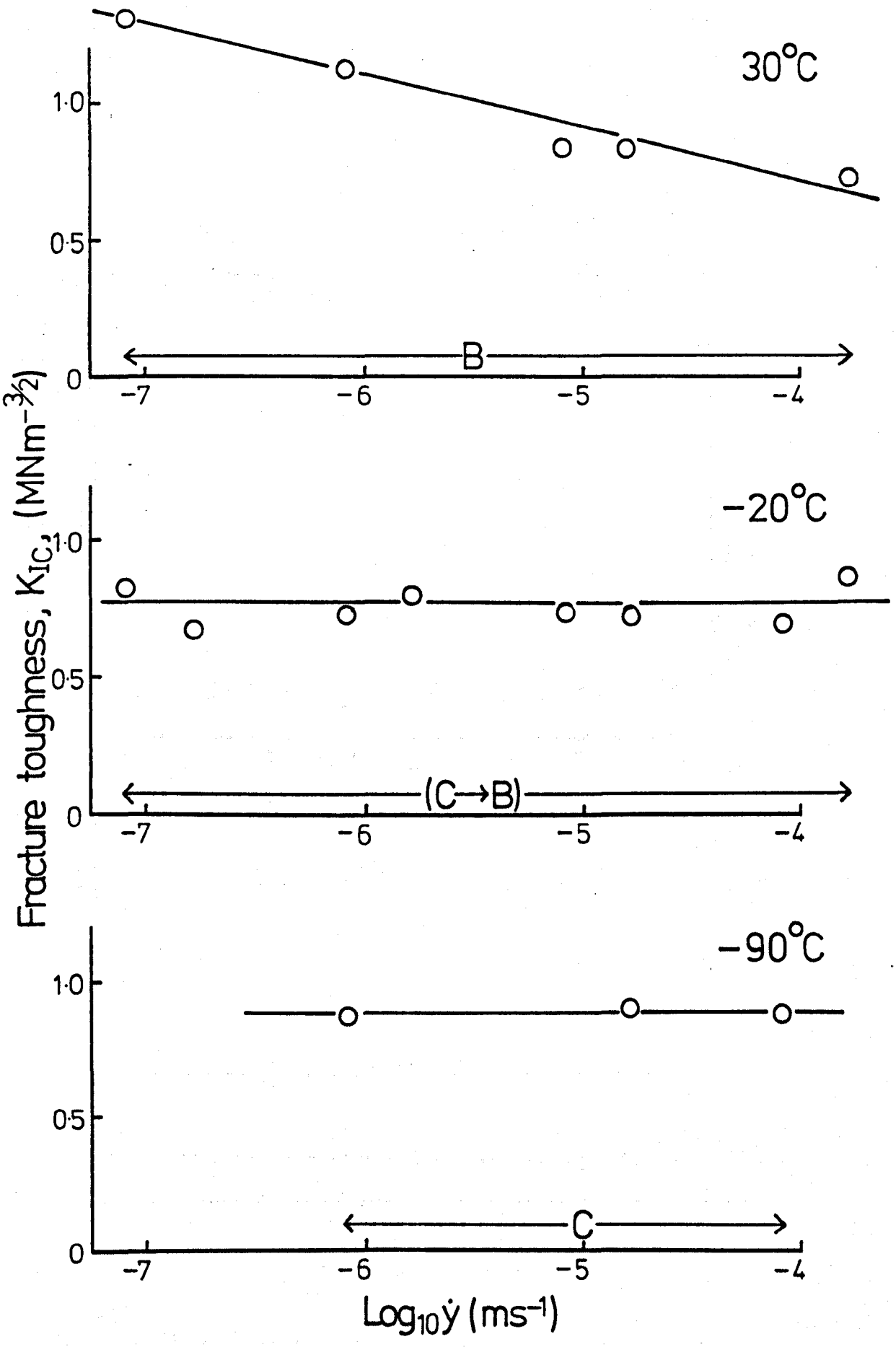

Figure 7.8 continued.

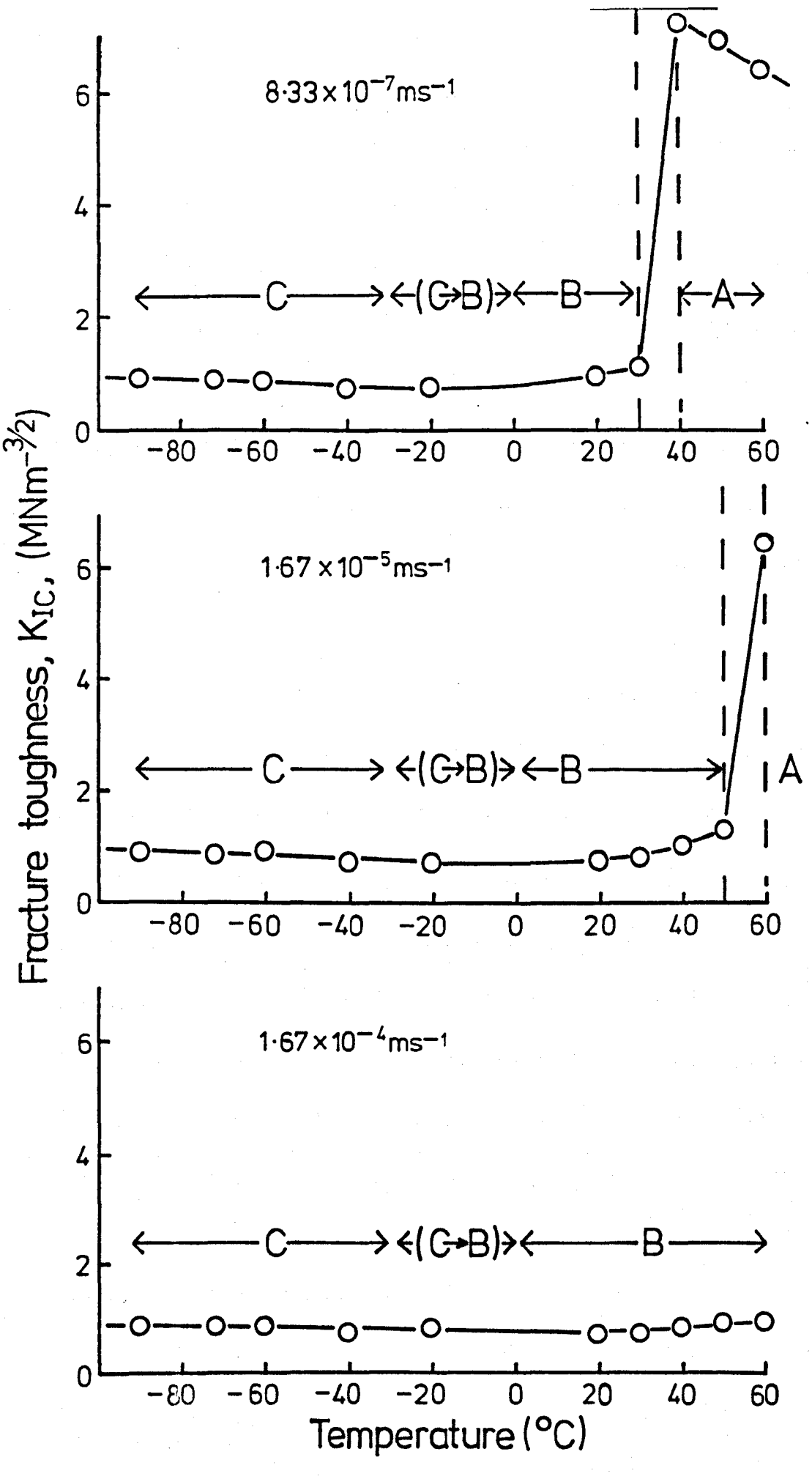

Figure 7.9 Fracture toughness, K_{IC}, versus temperature. Unmodified epoxy. 5·8mm thickness.

In contrast to the sharp type A/type B crack growth transition, the change from type B to type C was more gradual. For example, within the type B crack growth regime, reduced temperature and increased rate were generally found to increase the number of crack jumps required to cause total failure of the specimen. At -20°C evidence obtained from both the load-displacement trace and visual observations of the crack suggested that arrest/initiation points were showing a limited degree of stable crack extension prior to the re-initiation of unstable growth.

The effects of rate and temperature on K_{Ic} for the rubber-modified system are shown in figures 7.10 and 7.11. Also indicated are the crack growth regimes observed, namely A, A↛B, B, C↛B and C.

In figure 7.10 a difference in rate dependence is apparent between the 60°C and 40°C data with the former showing an apparent transition between rate dependent and independent trends. At 60°C it is of interest to note that, unlike the unmodified epoxy, the K_{Ic} transition does not coincide with a crack growth transition. At temperatures below 60°C rate dependency gradually decreases with decreasing temperature. This is accompanied by a gradual change in crack growth behaviour from type A at high temperatures/low rates to type C at low temperatures/high rates with A↛B, B and C↛B at intervening temperatures.

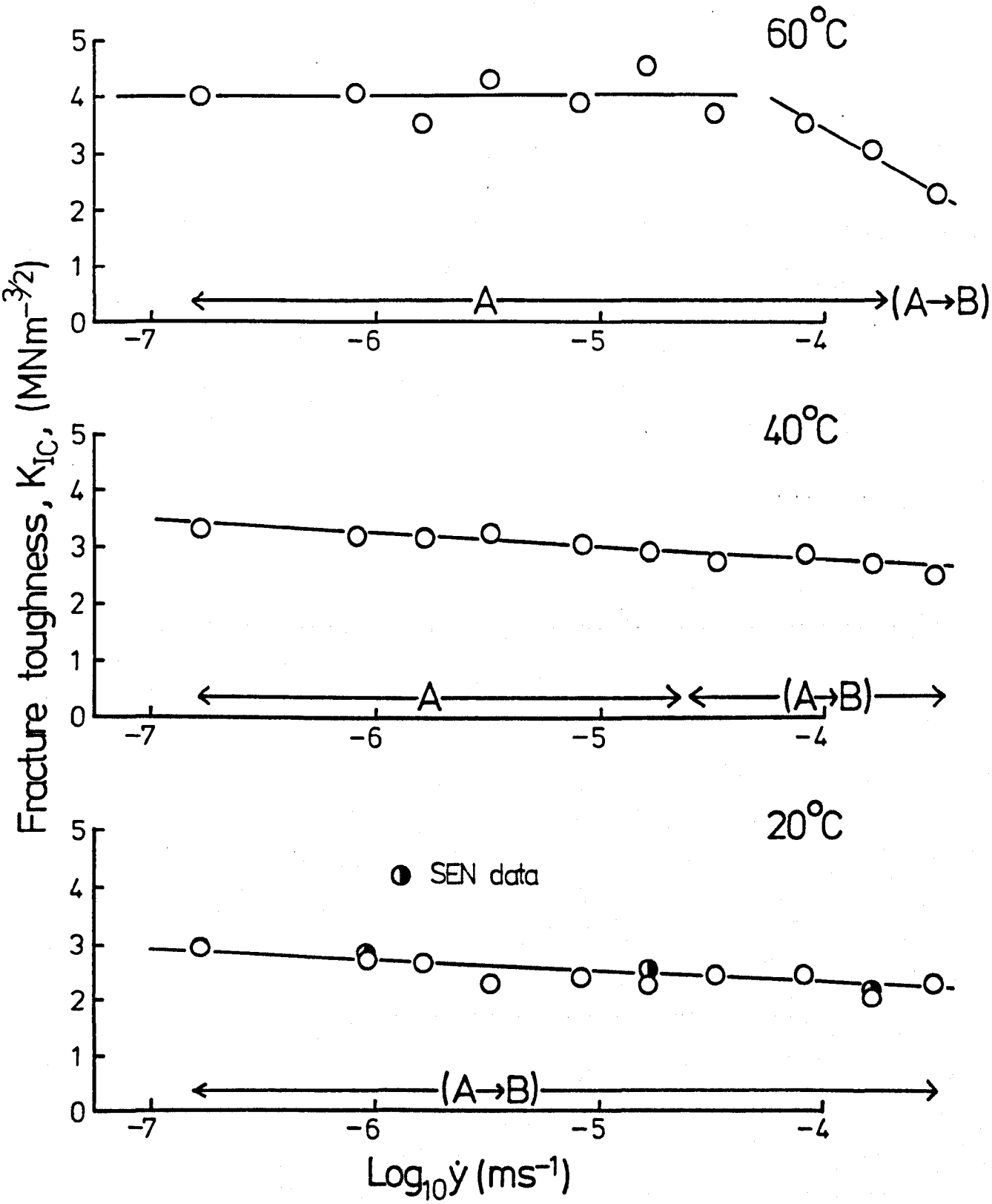

Figure 7.10 Fracture toughness, K_{IC}, versus displacement rate, $\dot{y}$. Rubber-modified epoxy. 5·8mm thickness.

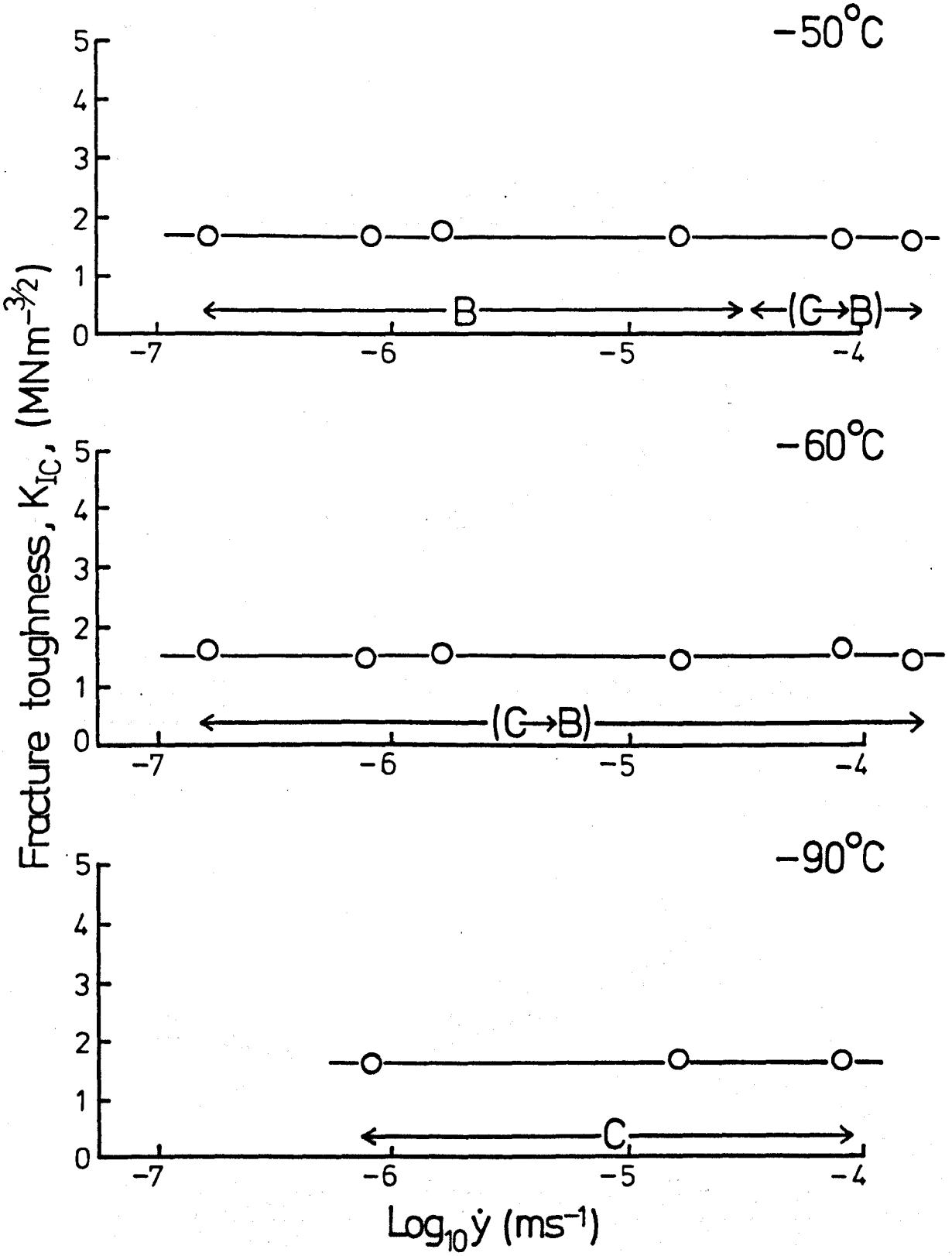

Figure 7.10 continued.

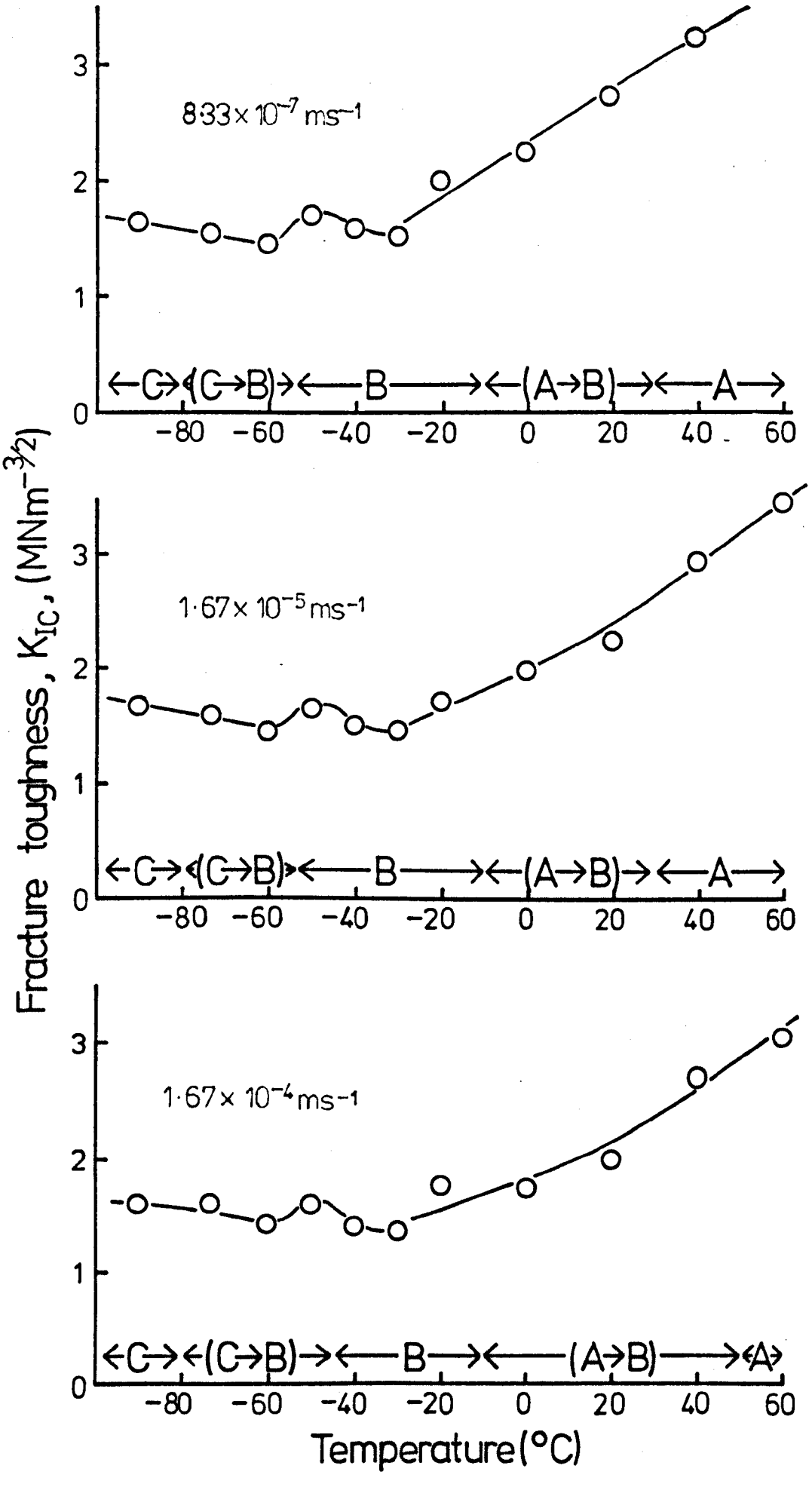

Figure 7.11 Fracture toughness, K_{IC}, versus temperature. Rubber-modified epoxy. 5·8 mm thickness.

Figure 7.11 shows that an increase in temperature from approximately -30°C produces an increase in K_{Ic}. At temperatures below -30°C two main effects are observed. Firstly an apparent peak in K_{Ic} at approximately -50°C exists. Secondly decreasing temperature from -60°C to -90°C causes a further minor increase in K_{Ic}. In order to determine whether these effects are real and not merely a result of experimental scatter or batch to batch variation, further experiments were conducted in the -30°C to -90°C temperature region. They were found to confirm statistically the low temperature trend indicated in Figure 7.11.

As discussed previously in section 7.3, a loss peak at approximately -55°C with the rubber-modified epoxy was attributed to the rubber phase. It is therefore difficult to resist the conclusion that a correlation exists between the K_{Ic} peak at -50°C, and the loss peak. Similar correlations have been observed with other polymeric materials such as polytetrafluoroethylene (85, 86), polysulphones (85) and poly2,6-dimethylene 1,4-phenylene ether (85).

Similarly the increase in K_{Ic} which occurs from -60°C to -90°C can be attributed to the presence of the β relaxation of the epoxy matrix which occurs in this temperature region.

The 20°C data for the rubber-modified epoxy shown in Figure 7.10 is worthy of brief discussion. At this temperature single-edge-notch specimens were also employed at three displacement rates in order to confirm geometry independence at 20°C. The results obtained from

these experiments were expressed as a plot of $\sigma_c^2 Q^2$ as a function of a^{-1} and fracture toughness calculated from the gradient of the plot, as discussed in Chapter 6. Figure 7.12 shows one of these plots, where it can be seen that a linear correlation exists indicating crack length independence. This, together with the similarity in K_{Ic} values found for the two types of specimen indicated in the 20°C data, clearly indicates geometry independence for 5.8 mm thick specimens at 20°C.

(b) Specimen thickness

The effect of specimen thickness on the fracture behaviour for the unmodified epoxy is shown in Figure 7.13 for three displacement rates at 20°C. As indicated, four specimen thicknesses were used, namely 1.3, 2.3, 5.8 and 49 mm. Attempts at using the compact tension geometry for the two lower thicknesses produced evidence of appreciable mode III, anti-plane shear loading. This problem was not found with single-edge-notch specimens and therefore this geometry was employed. The compact tension geometry was used for the 5.8 and 49 mm thick specimens.

As figure 7.13 shows, a change in specimen thickness produces a pronounced tough/brittle transition in the region of 1.3 to 2.3 mm. This is accompanied by a crack growth transition from type A (at the onset of crack growth) to type B. Thus it would seem that the tough/brittle transition brought about by all the variables studied, namely temperature, rate and now specimen thickness can be considered as resulting from the same mechanism.

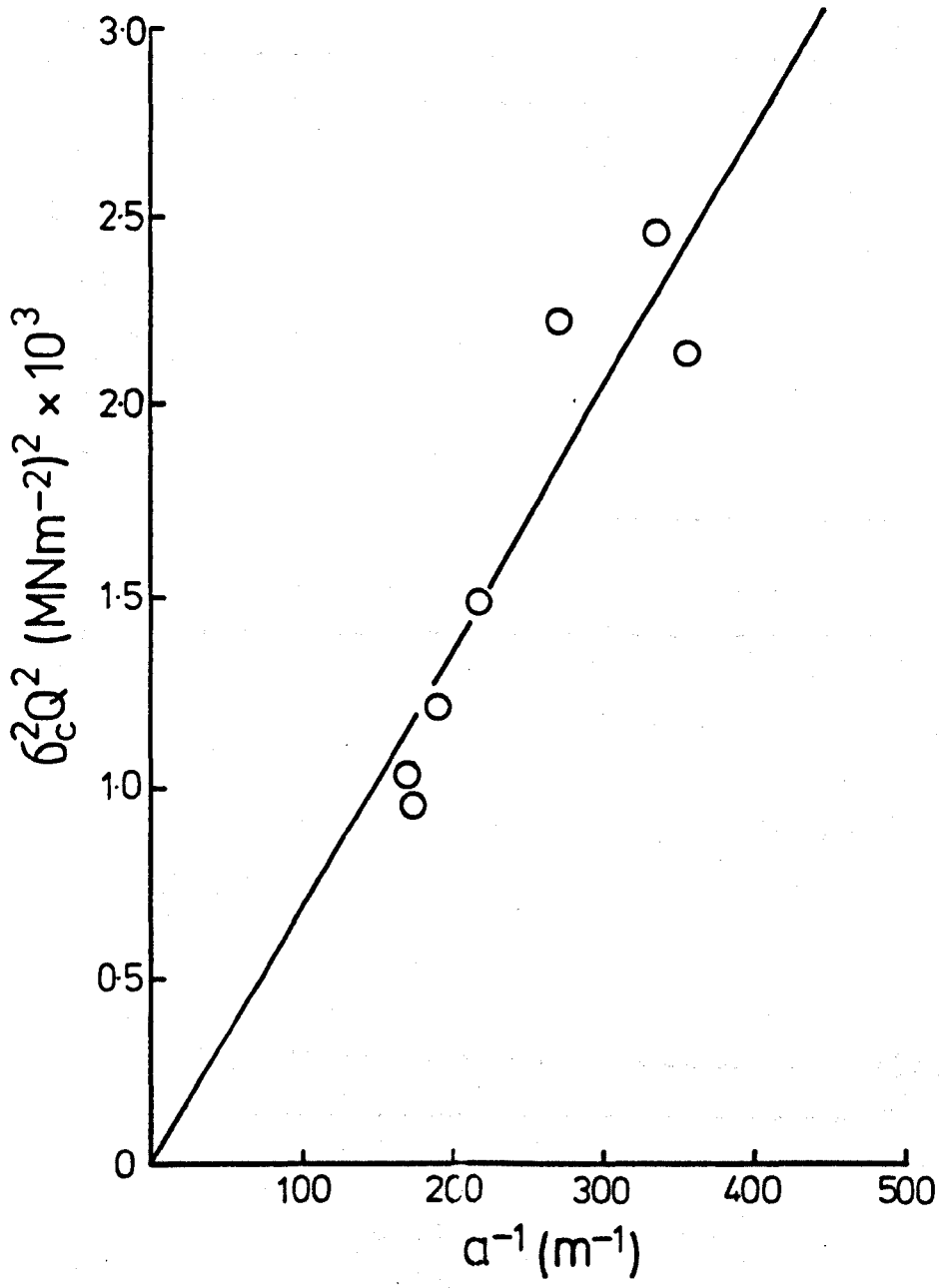

Figure 7.12 $\sigma_c^2 Q^2$ versus a^{-1} for 5·8mm thick SEN specimens. Rubber-modified epoxy. 20°C.

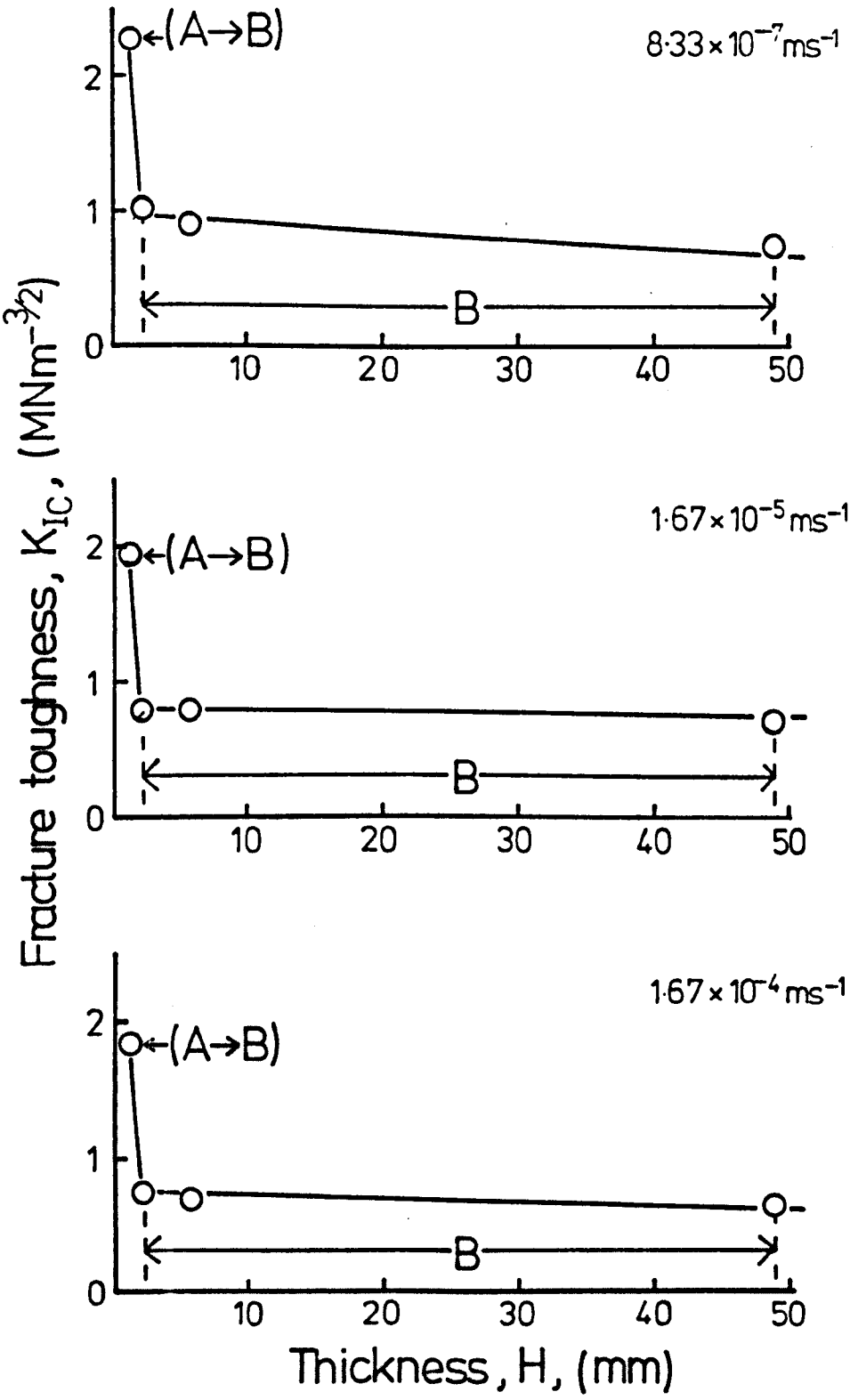

Figure 7.13 Fracture toughness, K_{IC}, versus specimen thickness, H. Unmodified epoxy. 20°C

Figure 7.14 illustrates the effect of specimen thickness on the fracture behaviour for the rubber-modified epoxy, obtained under the same conditions shown earlier for the unmodified system. As before, single-edge-notch specimens were used for thicknesses of 1.3 and 2.3 mm and compact tension specimens for thicknesses of 5.8, 29 and 49 mm. The results show that an increase in thickness from 2.3 to 49 mm produces a minor reduction in K_{Ic}, ranging from 9% to 37% at the slowest and highest rates respectively. It is initially tempting to view these trends as being due to a fundamental effect of specimen thickness, such as a plane stress-plane strain transition. However it is necessary to consider two major problems which arise in interpreting this data.

Firstly, the degree of experimental scatter was a problem with the 2.3 and, particularly, the 1.3 mm thick single-edge-notch specimens. Least squares analysis of the $\sigma_c^2 Q^2$ .v. a^{-1} data, in most cases, indicated an intercept considerably greater than zero thus suggesting a fundamental divergence from linear elastic conditions. Thus the trend depicted in the 1.3 to 2.3 mm region in Figure 7.14 is clearly open to some doubt.

Secondly, visual observations of the fracture surfaces obtained from both 29 and 49 mm thick specimens showed, in many cases, indications of liquid rubber domains in the central regions of the specimens. This suggests an epoxy/CTBN rubber incompatibility problem in the initial stages of cure (1). In order to determine

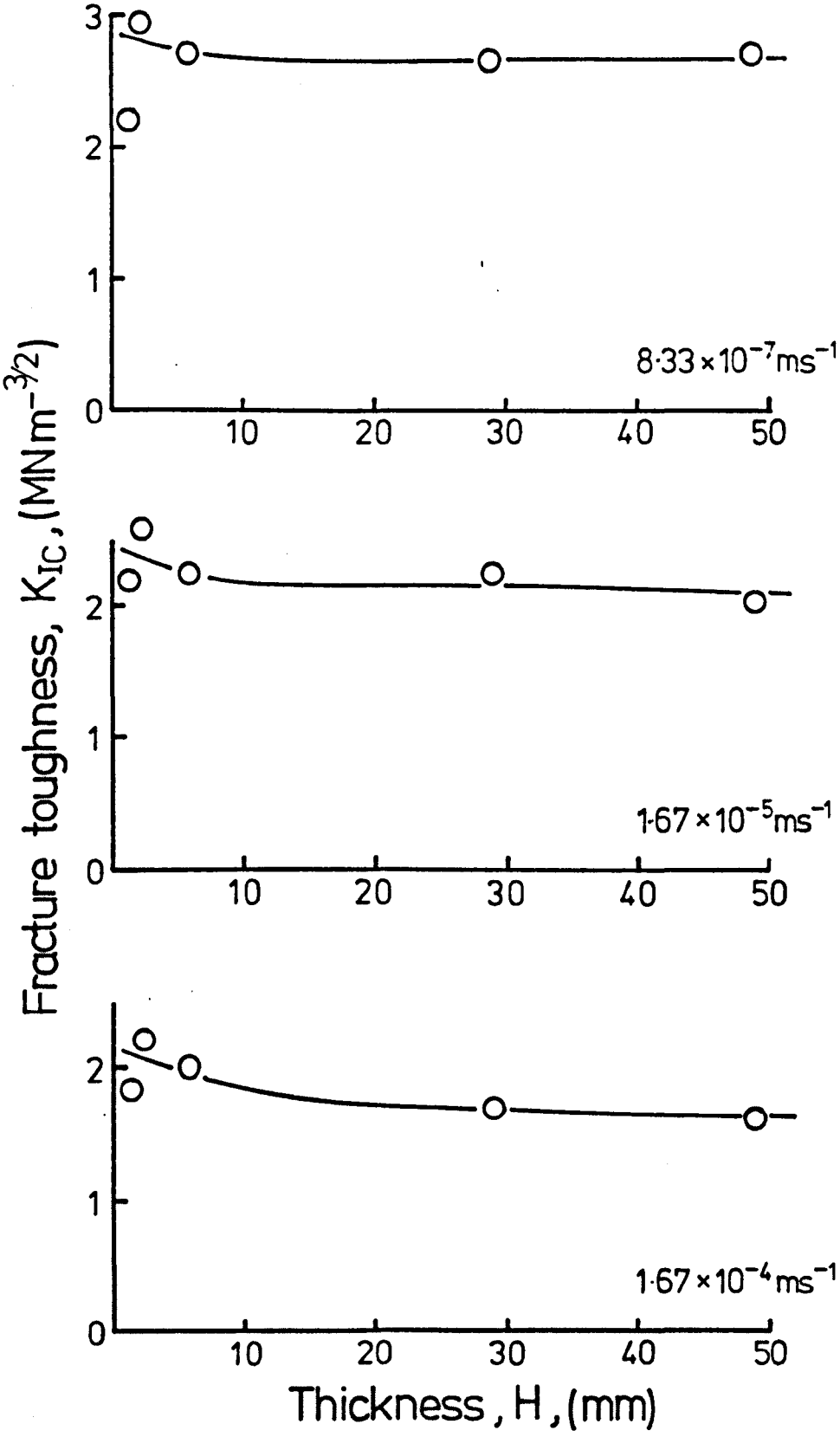

Figure 7.14 Fracture toughness, K_{IC}, versus specimen thickness, H. Rubber-modified epoxy. 20°C

its effect on K_{Ic}, a number of 49 mm thick compact tension specimens were sectioned into five 6 mm thick specimens and tested at 20°C. In all cases the data showed a tendency towards reduced K_{Ic} in the central regions of the original 49 mm specimen. Specimens which had been sectioned from the outer 12 mm of the original specimens were not generally affected. Thus it seems likely that the K_{Ic}-thickness trends beyond the 12 mm thickness region would have been, at least partly due to this problem.

Consequently, the data suggests that a substantial thickness dependence probably does not exist with the rubber-modified epoxy.

7.4.3 Crack growth characteristics and fractography

Type A: This crack growth behaviour was observed with both systems and occurred under conditions of relatively high temperatures (40 to 60°C in both cases) and low rates. Type A crack growth was stable with the rate of propagation being governed by the machine displacement rate. Figure 7.15 shows typical type A fracture surfaces for the unmodified and rubber-modified systems. Both indicate a system of ridges diverging away from the central region of the specimen making contact with the specimen edges at an angle of approximately 45°. Pull-in of the specimen edges is also apparent with both systems. However the magnitude of this effect is substantially reduced in the case of the rubber-modified epoxy. Furthermore the modified epoxy fracture surfaces exhibited pronounced stress whitening which was completely absent with unmodified surfaces.

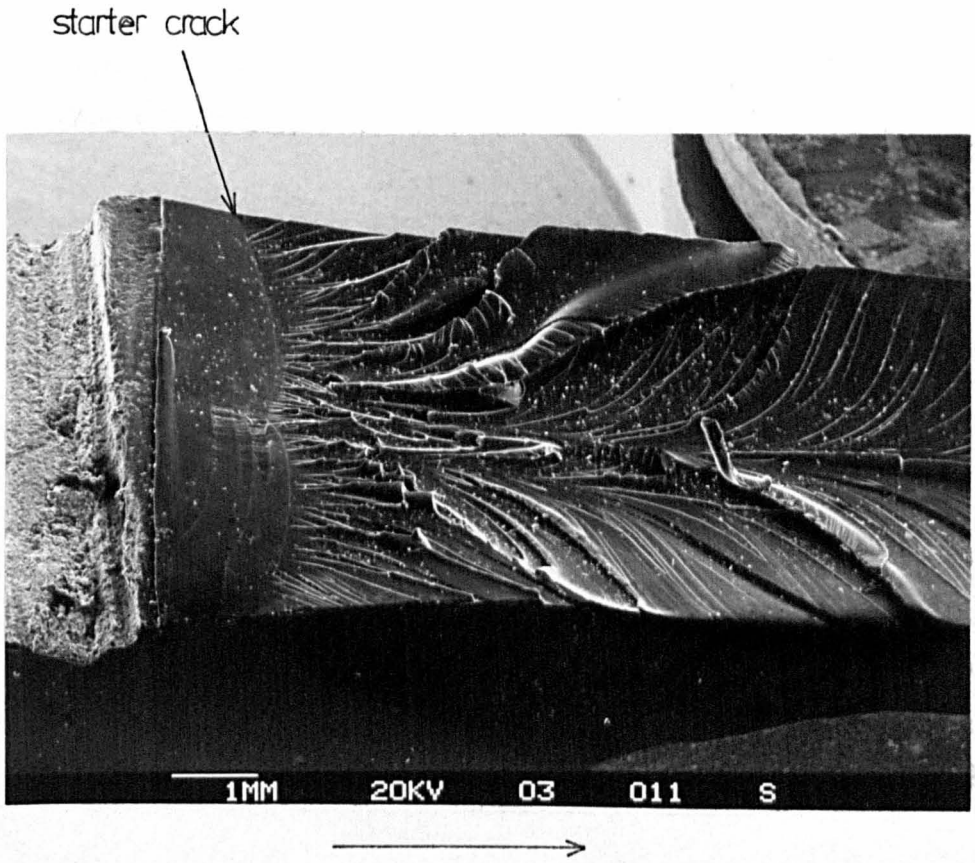

Figure 7.15(a) Typical type A fracture surface for the unmodified epoxy (scanning electron micrograph).

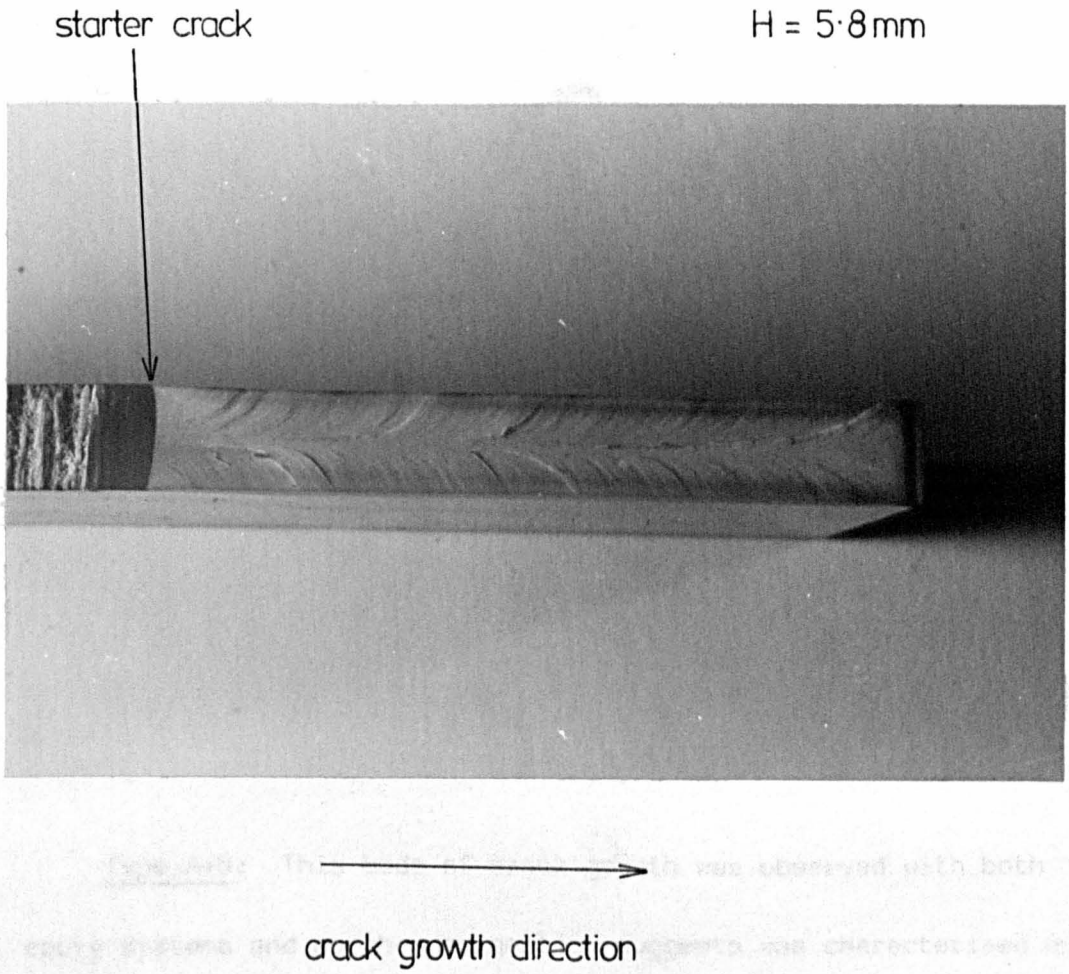

Figure 7.15(b) Typical type A fracture surface for the rubber–modified epoxy (optical photograph).

Figure 7.16 shows a high magnification scanning electron micrograph of a rubber-modified type A surface. It exhibits a fairly uniform distribution of holes, having diameters of approximately 2 to 5 μm. A high degree of roughness is also apparent with clear evidence of plastic shear flow of the matrix. Although some of the holes show signs of rubber, which had undergone a tearing process, in the majority of cases they appear relatively deep with no signs of remaining rubber. The presence of this rubber was however demonstrated by immersing a type A fracture surface in tetrahydrofuran followed by observation in the scanning electron microscope. The result is shown in Figure 7.17. Protrusions are clearly visible and are the result of rubber debris, lining the insides of the holes, swelling in the solvent.

Variations in temperature and displacement rate did not produce any significant changes in the details just described for both systems.

Type A→B: This mode of crack growth was observed with both epoxy systems and as the designation suggests was characterised by stable, type A growth followed by rapid unstable fracture. A typical A→B fracture surface obtained from a rubber-modified epoxy is shown in Figure 7.18. This indicates a crescent shaped stress-whitened zone which had developed from the initial starter crack. Adjacent to this zone, in the direction of crack growth, is a relatively smooth 'mirror' region. This is followed by a 'mist' appearance, followed eventually by a return to relatively smooth features. Crack tip observations at 20°C with a travelling microscope, suggested that the extent of

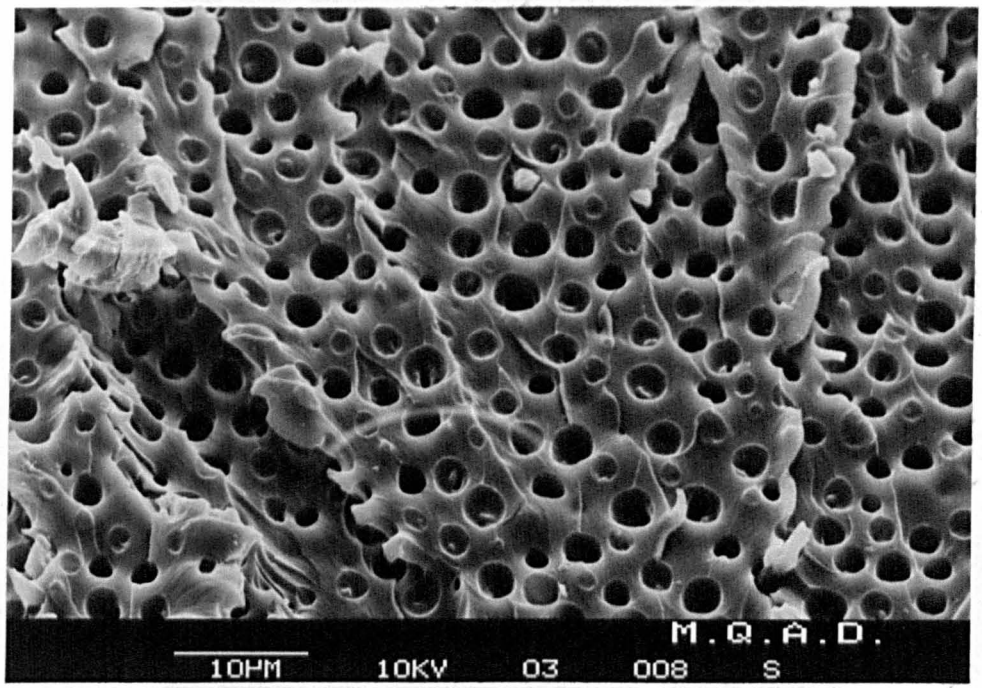

crack growth direction

Figure 7.16 Scanning electron micrograph of a rubber-modified epoxy type A fracture surface.

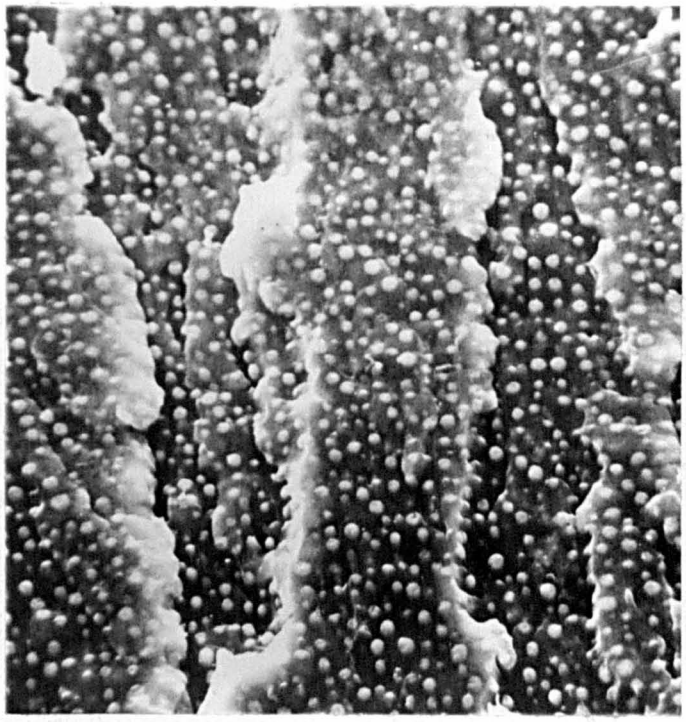

20 μm

Figure 7.17 Rubber particles on a type A fracture surface swollen by tetrahydrofuran.

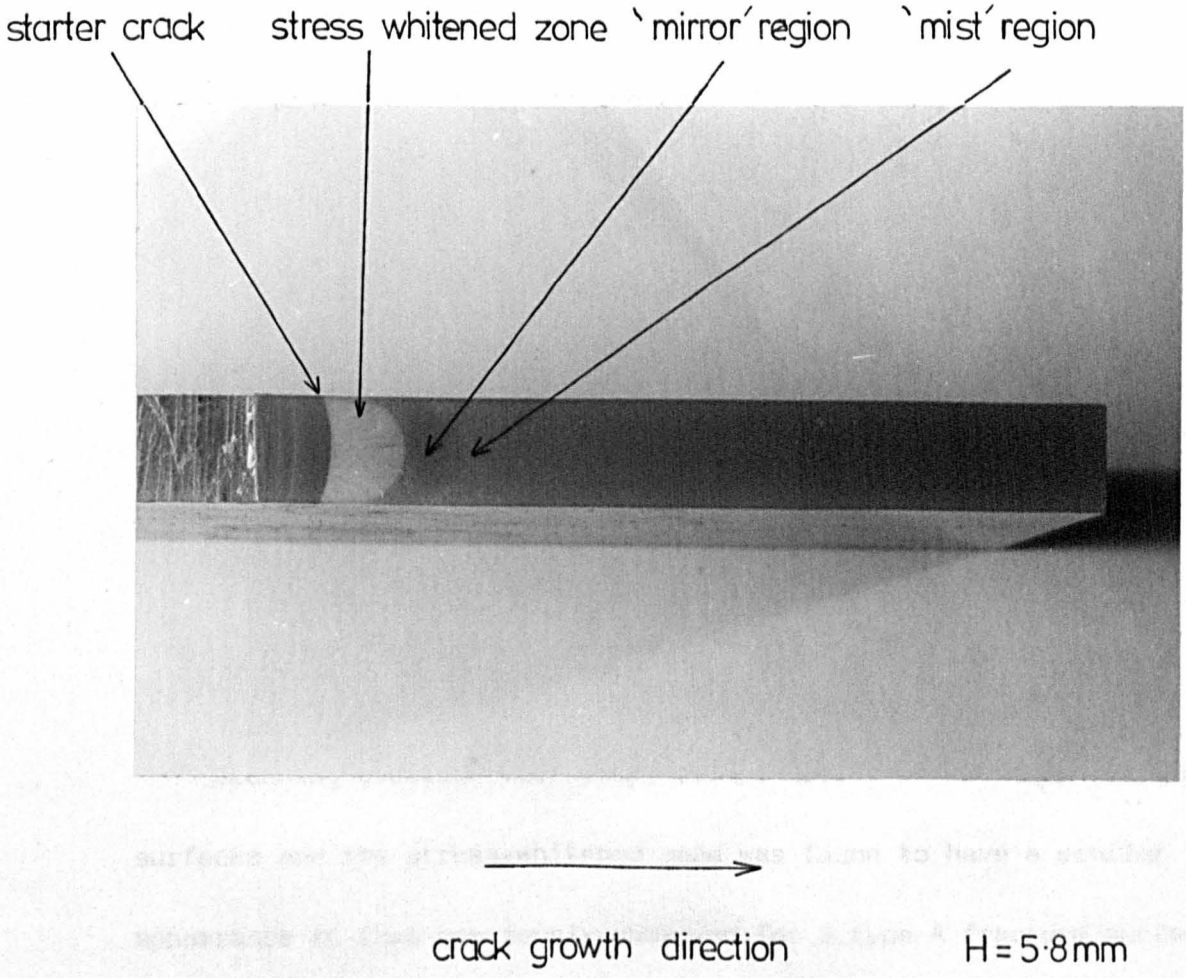

Figure 7.18 Type A→B rubber–modified epoxy fracture surface.

stable growth with specimens exhibiting A↛B fracture was equivalent to the length of the stress-whitened zone measured at the specimen edge. It would therefore appear that the stress-whitened region occurs as a direct result of slow stable crack growth. The 'mirror' and 'mist' regions probably result from the rapid initiation of unstable growth whereas the reduced roughness observed further along the fracture surface results from an eventual reduction in crack velocity. This behaviour would be expected from a compact tension specimen.

Variations in temperature and displacement rate were found to strongly influence the length of the stress-whitened zone and hence the degree of stable, type A growth preceeding unstable fracture. Increased rate and decreased temperature produced a similar effect, namely a reduction in the length of this zone.

Scanning electron microscopy was conducted on the A↛B fracture surfaces and the stress-whitened zone was found to have a similar appearance to that previously observed for a type A fracture surface. Figure 7.19 shows a scanning electron micrograph of the 'mirror' region mentioned above. Although the surface has a high degree of roughness, the size, population and depth of the holes previously observed in the stress-whitened regions of A and A↛B fracture surfaces appear to be significantly reduced. A similar effect was observed for the region further along the specimen which underwent rapid unstable growth and did not therefore exhibit stress-whitening.

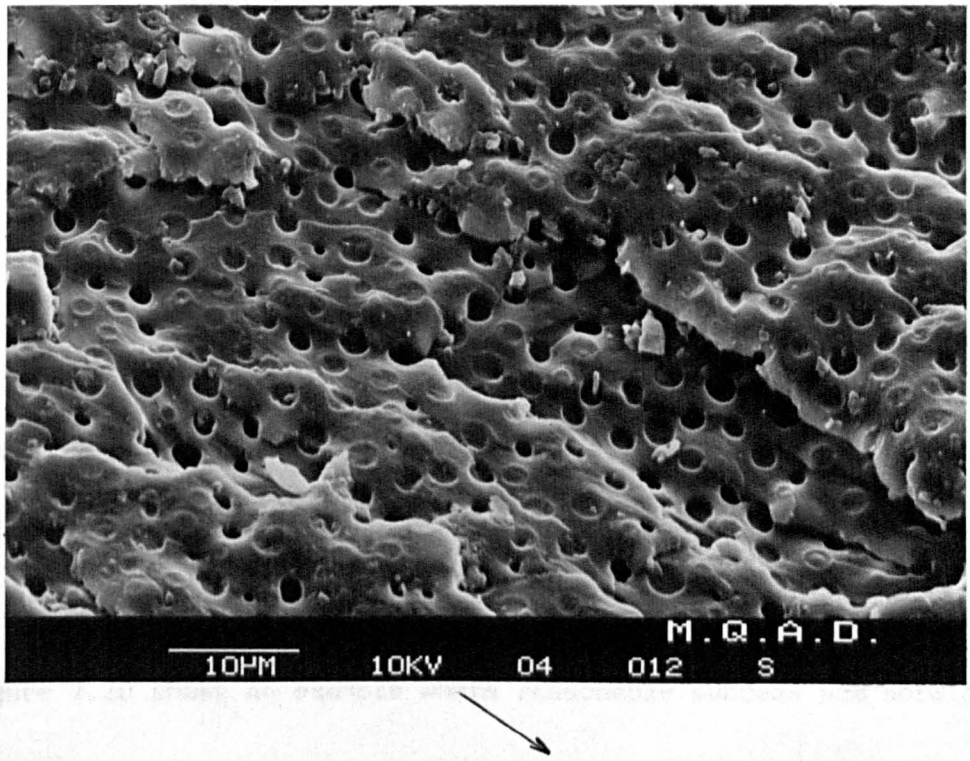

crack growth direction

Figure 7.19 Scanning electron micrograph of the mirror region of a type A→B rubber-modified epoxy fracture surface.

A→B crack growth was also observed with the unmodified system with 1.3 mm thick single-edge-notch specimens tested at 20°C. It did not occur with any other thickness under any conditions. It exhibited many of the characteristics described for the rubber-modified epoxy with two main exceptions. Firstly stress-whitening and the presence of holes were not observed on the type A part of the fracture surfaces. Secondly, gross roughness was apparent on the fracture surfaces remote from the type A region. This was due to the occurrence of crack bifurcation which undoubtedly resulted from the attainment of a critical velocity.

As previously discussed in Chapter 6, attempts at studying rubber-modified epoxy fracture surfaces using transmission electron microscopy proved difficult due to the problem of replica damage. Consequently only limited information was provided by this technique. Figure 7.20 shows an example where reasonable success was obtained. This shows a transmission electron micrograph obtained from the stable, type A region of an A→B fracture surface, where the characteristic two-phase morphology generally exhibited by rubber-modified epoxies is apparent. Also it is particularly interesting to note the absence of craze-like structures spanning the rubber particles. In fact evidence indicating the presence of crazes on fracture surfaces was never obtained in this study.

Type B: This type of crack growth behaviour was observed with both systems and was unstable, stick/slip with no visible evidence of any preceeding stable growth. The number of crack jumps required

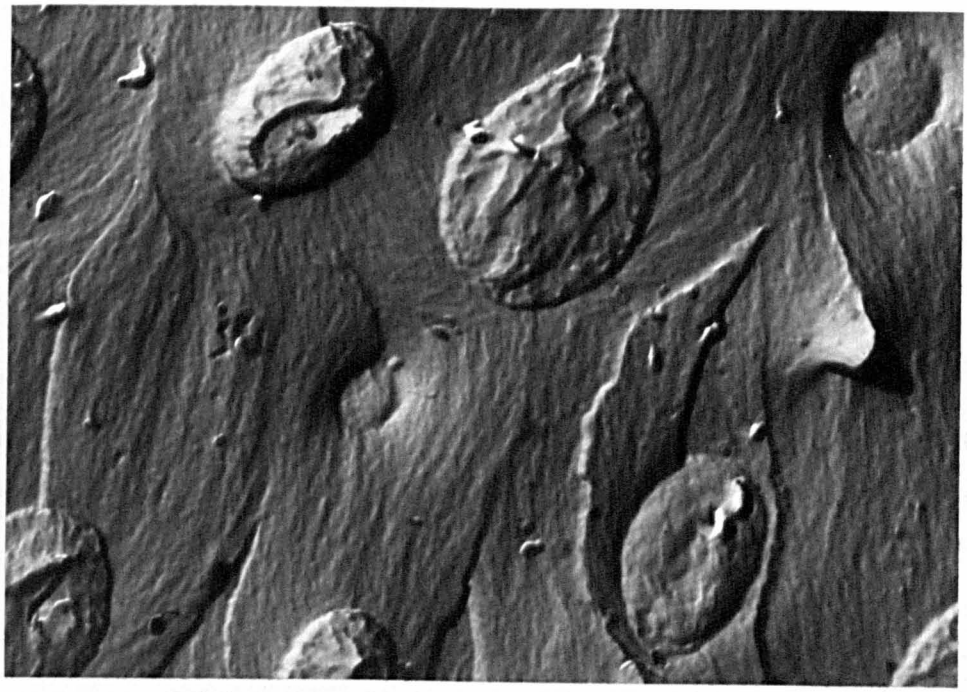

Figure 7.20 Transmission electron micrograph of the stable, type A region of an A→B rubber-modified epoxy fracture surface.

to cause total failure of the specimen was dependent upon the conditions of test: increasing temperature and decreasing rate generally decreasing the number of crack jumps.

For the unmodified epoxy, type B fracture occurred over a temperature range of approximately -20 to 60°C. Figure 7.21 shows a low magnification micrograph of a type B surface. In this case the general lack of any appreciable surface features is indicated.

With the rubber modified system, type B crack growth was observed at temperatures below 0°C and produced the type of fracture surface shown in Figure 7.22. Stress whitening in the starter crack region is not observed suggesting the absence of any significant stable, type A growth prior to rapid unstable fracture. Also absent are indications of a 'mirror' zone and 'mist' regions, suggesting that unstable crack growth velocities with type B fracture are significantly slower than those obtained with A→B growth.

Figure 7.23 shows a scanning electron micrograph of an arrest/ initiation locus from a type B rubber-modified fracture surface. Clearly indicated are the holes left by the rubber particles after the fracture event. However of significance is a band of holes showing a greater depth than observed for holes found either side of this band. This observation suggests that some very limited degree of stable growth is indeed occurring prior to unstable fracture with type B specimens. Thus the distinction between types A→B and B crack growth is merely one of convenience and does not indicate any fundamental difference in crack growth behaviour.

Scanning electron microscopy conducted on the fast, unstable regions of type B fracture surfaces indicated hole populations and dimensions similar to that observed from the unstable regions of A→B fracture surfaces.

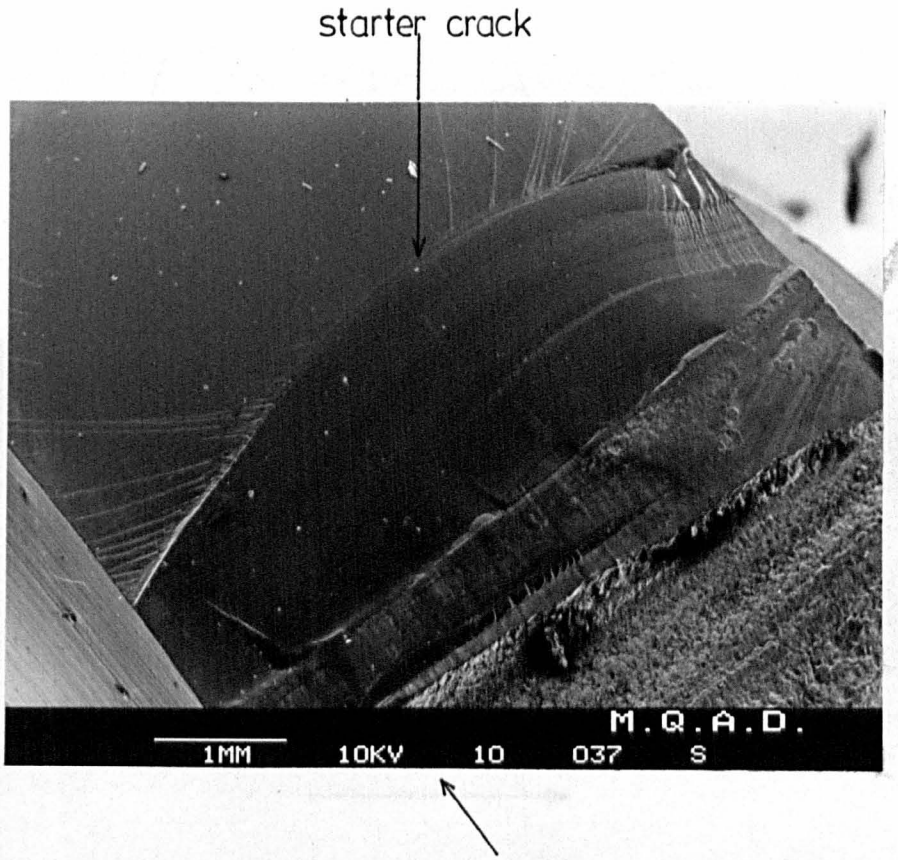

Figure 7.21 Type B unmodified epoxy fracture surface (scanning electron micrograph).

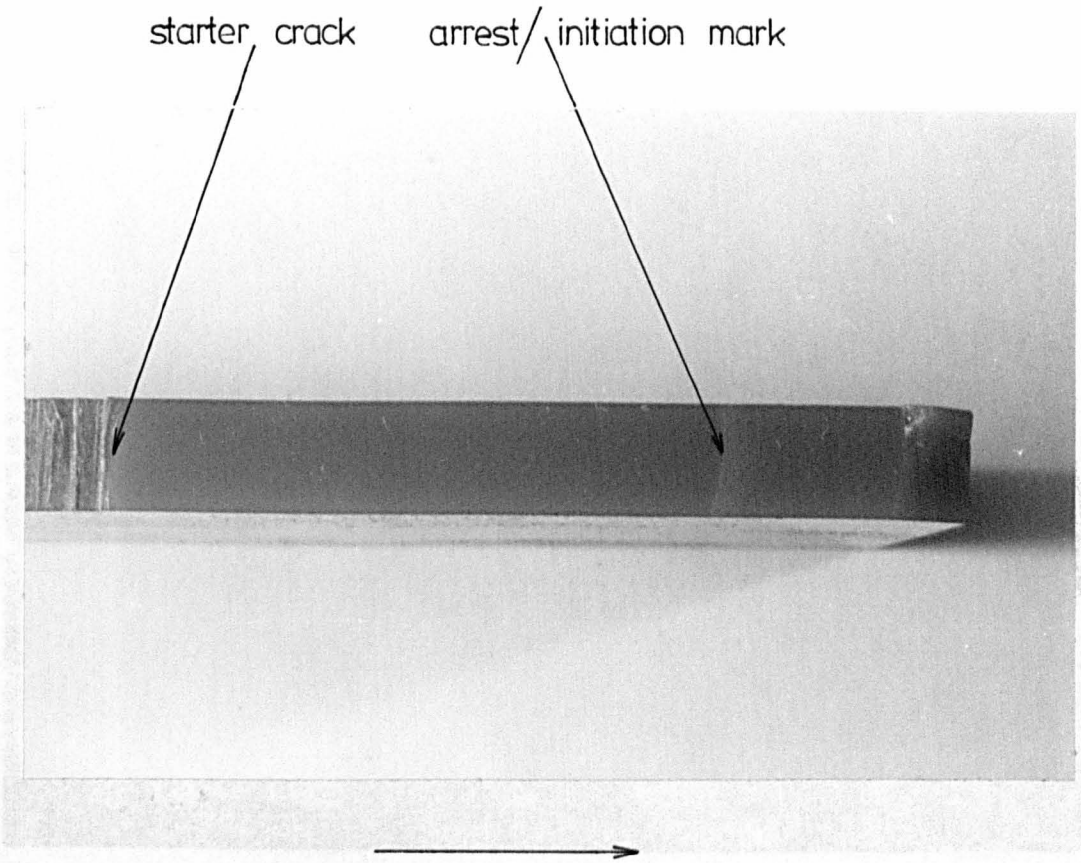

Figure 7.22 Type B rubber–modified epoxy fracture surface.

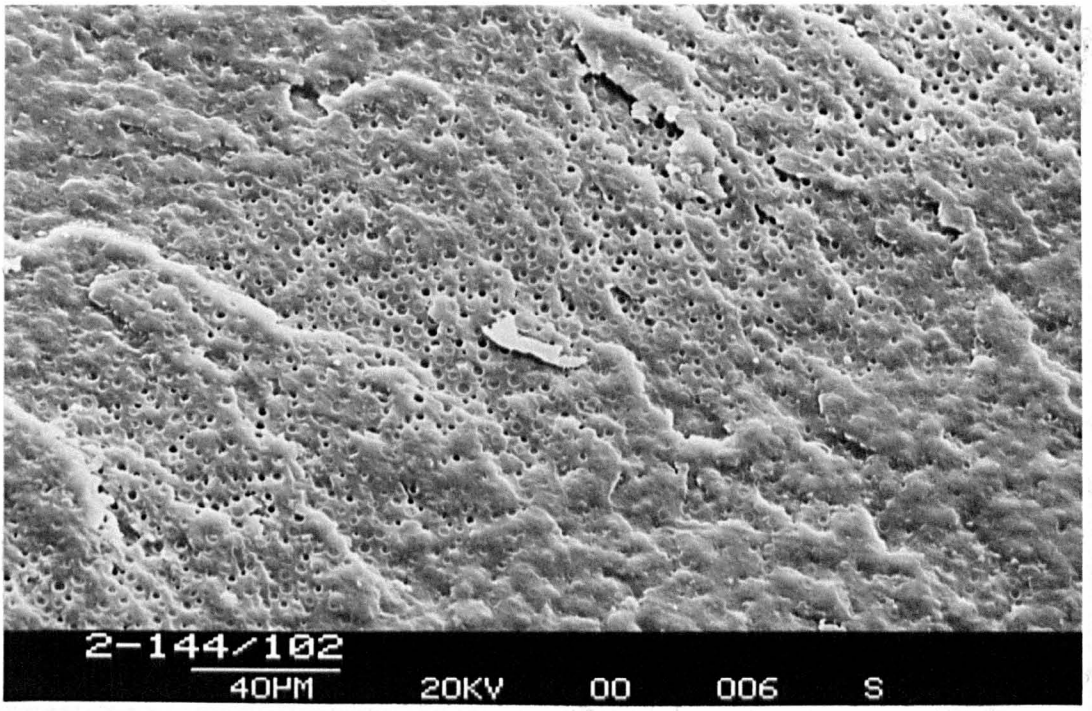

Figure 7.23 Scanning electron micrograph of an arrest/initiation locus from a type B rubber–modified epoxy fracture surface.

Type C: This crack growth behaviour was observed with both epoxy systems at low temperatures and took the form of stable, continuous crack extension. In this case crack extension occurred at a significantly faster rate than with type A growth; displacement rate once again having a controlling influence.

Typical fracture surfaces obtained from type C crack growth are shown in Figure 7.24 for both systems. It can be seen that in contrast to that observed with type A crack growth, type C produces a relatively smooth and featureless surface.

Of further interest with the rubber-modified system was a distinct difference in type C fracture surface colour from that observed with any other type of crack growth or indeed for the as-moulded material. In this case fracture surfaces were intermediate in colour between those obtained from type A and type B growth, thus suggesting that some, albeit small degree of stress-whitening accompanied type C growth. Scanning electron microscopy revealed a topography similar in appearance to that observed in the fast growth regions of types A↦B and B fracture.

A further observation of interest was the occasional presence of Wallner type markings (87) on unmodified type C fracture surfaces. Wallner phenomena is a term generally applied to surfaces exhibiting an evenly rippled undulating appearance. In this case the markings exhibited a high degree of periodicity and were of a similar curved shape to the arrest/initiation points observed with type B fracture. It is generally believed that such markings occur as a result of interaction between the crack front and reflected stress waves which momentarily alter the stress distribution at the crack front (87).

Although type C fracture surfaces were examined by transmission electron microscopy, little detail was observed with no evidence for

Figure 7.24(a) Typical type C fracture surface for the unmodified epoxy (scanning electron micrograph).

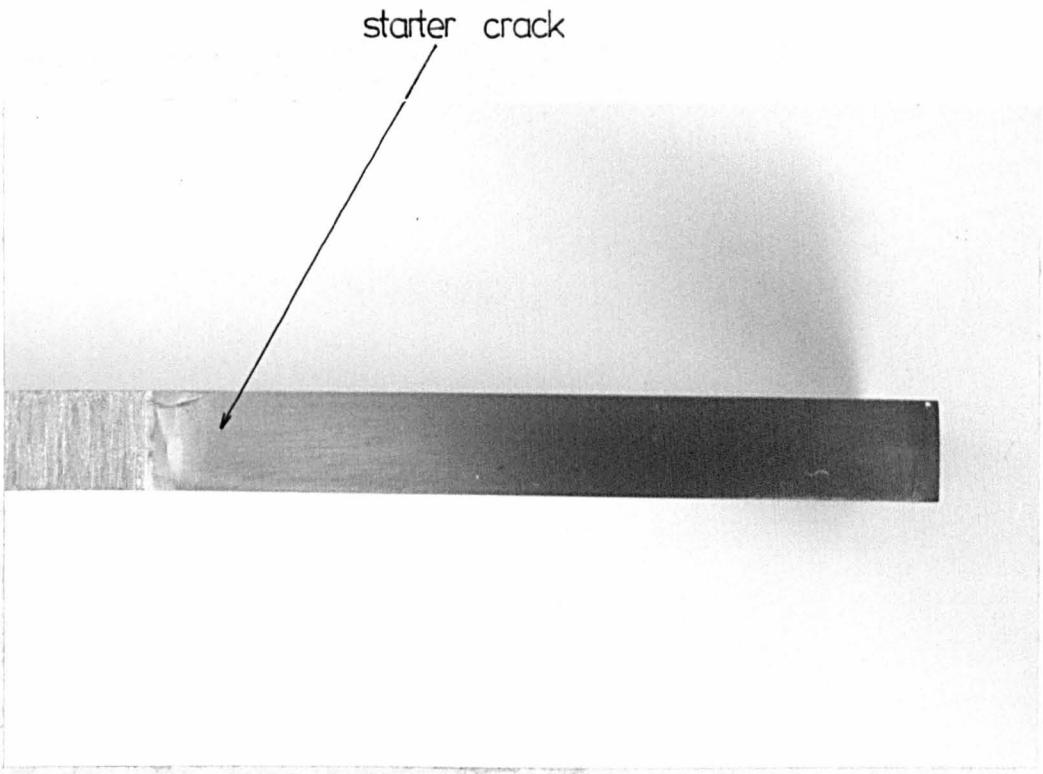

Figure 7.24(b) Typical type C fracture surface for the rubber–modified epoxy (optical photograph).

the existence of such entities as crazing or shear banding. However in some cases evidence for the presence of an underlying nodular structure was apparent (51). This is demonstrated in Figure 7.25 where it would appear that the nodular structure is of the order of 10-30 nm. Clearly the apparent nodules demonstrate a greater resistance to fracture than the remainder of the epoxy-material. In this work nodular structure was observed on fracture surfaces obtained from all types of crack growth with both epoxy systems. However it occurred with most regularity with type C crack growth. Of further interest was the observation that this morphology was more pronounced with replicas prepared using a nitrocellulose solution as the replicating agent rather than a cellulose acetate solution.

Considerable controversy currently exists concerning nodular structures in crosslinked polymers. It might seem theoretically reasonable that such polymers, which are generally prepared by the addition of a crosslinking agent to a low molecular weight oligomer, should have a non-uniform structure. Indeed, Koutsky and co-workers (32, 88) have recently suggested a close correlation between the mechanical properties and nodular structure of epoxy resins. However others believe they are simply artefacts resulting from the replication procedure. Probably the major evidence against their existence is the lack of small angle X-ray scattering which should arise from such a morphology (89-91).

The results obtained from this work clearly does not provide conclusive evidence either way. However the previously mentioned dependence of the structure upon the replicating agent used does raise questions about the interpretation of such electron micrographs as evidence for nodular structure.

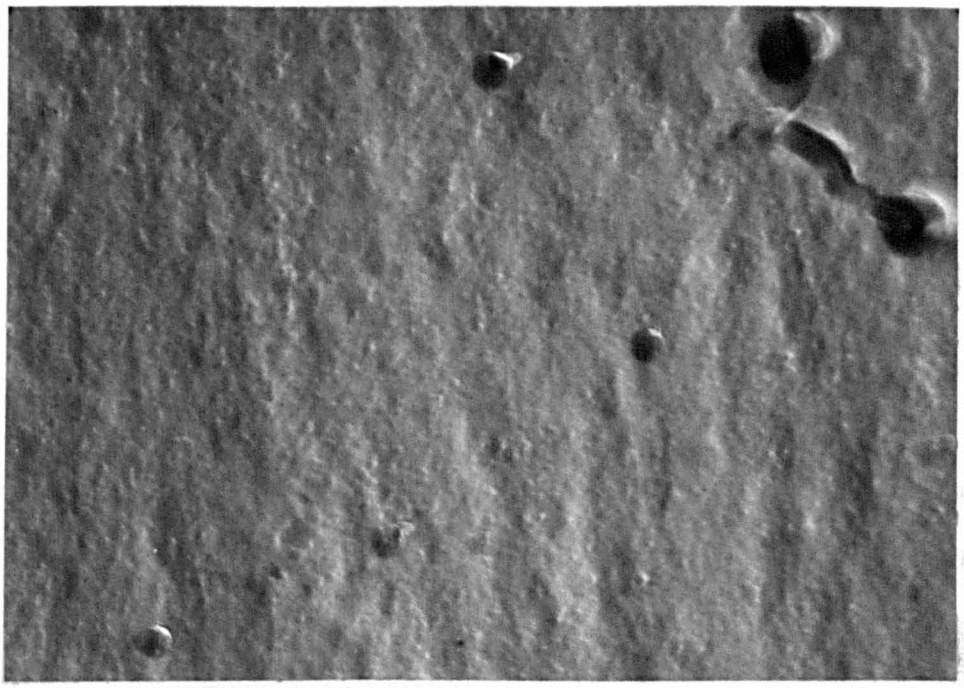

Figure 7.25 Transmission electron micrograph of an unmodified epoxy, type C fracture surface.

Type C↛B: As the designation suggests this form of crack growth was a combination of both types B and C. In most cases where it was observed, initial crack extension was predominantly stable type C, which eventually reverted to type B followed frequently by a return, once again, to type C and so on. With the unmodified epoxy this behaviour was only observed at -20°C; type B and type C modes occurring above and below -20°C respectively. With the rubber-modified system C↛B behaviour was observed at temperatures of -50, -60 and -73°C.

7.5 Summary

7.5.1 Unmodified epoxy

(i) A sharp tough/brittle transitional effect was observed. All of the experimental variables studied, namely temperature, displacement rate and specimen thickness were shown to exhibit a pronounced influence on this behaviour.

(ii) In the brittle regime K_{Ic} was both rate and temperature dependent.

(iii) Three main types of crack growth were observed and were designated A, B and C. A and C refer to stable, continuous growth; A exhibiting pronounced ductility and C occurring in a brittle manner. B refers to unstable stick-slip growth. Both rate and temperature influenced crack growth with, in particular, the tough/brittle transition coinciding with an A/B transition. Two intermediate types of crack growth, designated A↛B and C↛B, were also observed. The former occurred only with 1.3 mm single-edge-notch specimens. C↛B

growth was observed at -20°C and exhibited both types B and C characteristics. The fracture surfaces obtained from these crack growth regimes were studied and several interesting features observed.

(iv) Modulus data obtained from three-point-bend and compression tests showed that the two techniques produced results within 10%. More extensive experiments using the compression technique indicated that decreasing temperature and increasing rate increased both modulus and yield stress.

(v) Dynamic mechanical studies showed the glass transition temperature, Tg, to be approximately 100°C with a β relaxation occurring in the vicinity of -70°C.

7.5.2 Rubber-modified epoxy

(i) Increasing temperature and decreasing rate have been shown to increase K_{Ic} with no major evidence of the tough/brittle transitional behaviour found with the unmodified system.

(ii) Specimen thickness has been shown to have no appreciable effect on K_{Ic}.

(iii) Five types of crack growth behaviour were observed, namely A, A↔B, B, C↔B and C. All exhibited similar characteristics to those described for the unmodified epoxy and both temperature and rate were found to influence crack growth behaviour. Fracture surface features were similar in a number of respects to the unmodified epoxy. Possibly the most notable difference was the observation of stress whitening on rubber-modified surfaces which had undergone type A fracture.

(iv) Once again modulus data obtained from three-point-bend and compression tests showed reasonable agreement (within 10%). More extensive compression tests showed that decreasing temperature and increasing rate increases both modulus and yield stress.

(v) Dynamic mechanical studies indicated a Tg of approximately 100°C together with evidence of a low temperature relaxation in the vicinity of -60°C.

CHAPTER EIGHT

ADHESIVE JOINT STUDIES. RESULTS

8.1 Introduction

This chapter describes the influence of adhesive bond thickness, cross-head displacement rate and joint width on the fracture behaviour of rubber-modified epoxy adhesive joints.

The most striking observation found in these studies is the effect of bond thickness on adhesive fracture energy and this is the subject of the first section. The following two sections deal primarily with the effects of test rate and joint width on the bond thickness-fracture energy relationship. Finally, data obtained from crack tip deformation zone studies are described.

8.2 Effect of Adhesive Bond Thickness

The effect of bond thickness on the adhesive fracture energy is shown in Figure 8.1 for a joint width of 12 mm tested at 0.05 mm min^{-1} displacement rate and 20 °C. As shown the fracture energy passes through a maximum, G_{Icm}, at a specific bond thickness, t_m, which in this case occurred at approximately 1 mm. At thicknesses beyond t_m the fracture energy declines until a value is reached which remains essentially constant with increased thickness. The linear relationship shown at the bottom of Figure 8.1 refers to the arrest energy values obtained when unstable growth occurs and produces at least one crack jump, and hence an arrest point (discussed below). As may be seen the arrest energy values appear independent of bond thickness.

The bond thickness was also found to have a significant influence on crack growth behaviour. At low values of bond thickness ie below t_m, crack growth was generally of a stable, continuous nature and Figure 8.2(a) shows a schematic load displacement record obtained under

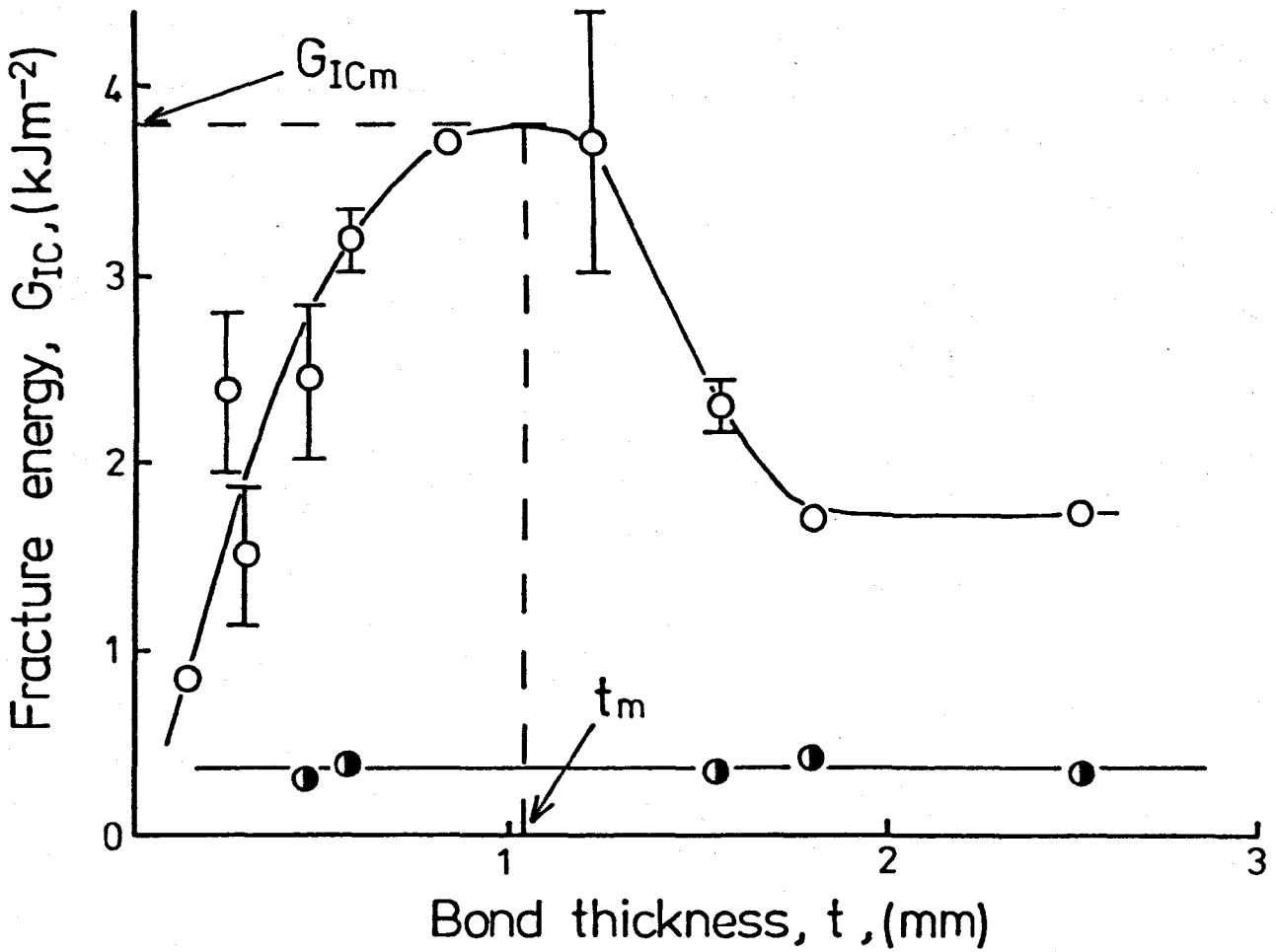

Figure 8.1 Adhesive fracture energy, G_{IC}, versus bond thickness, t.
0·05mm min^{-1} displacement rate, 20°C.
–o– stable or initiation, –◑– arrest.

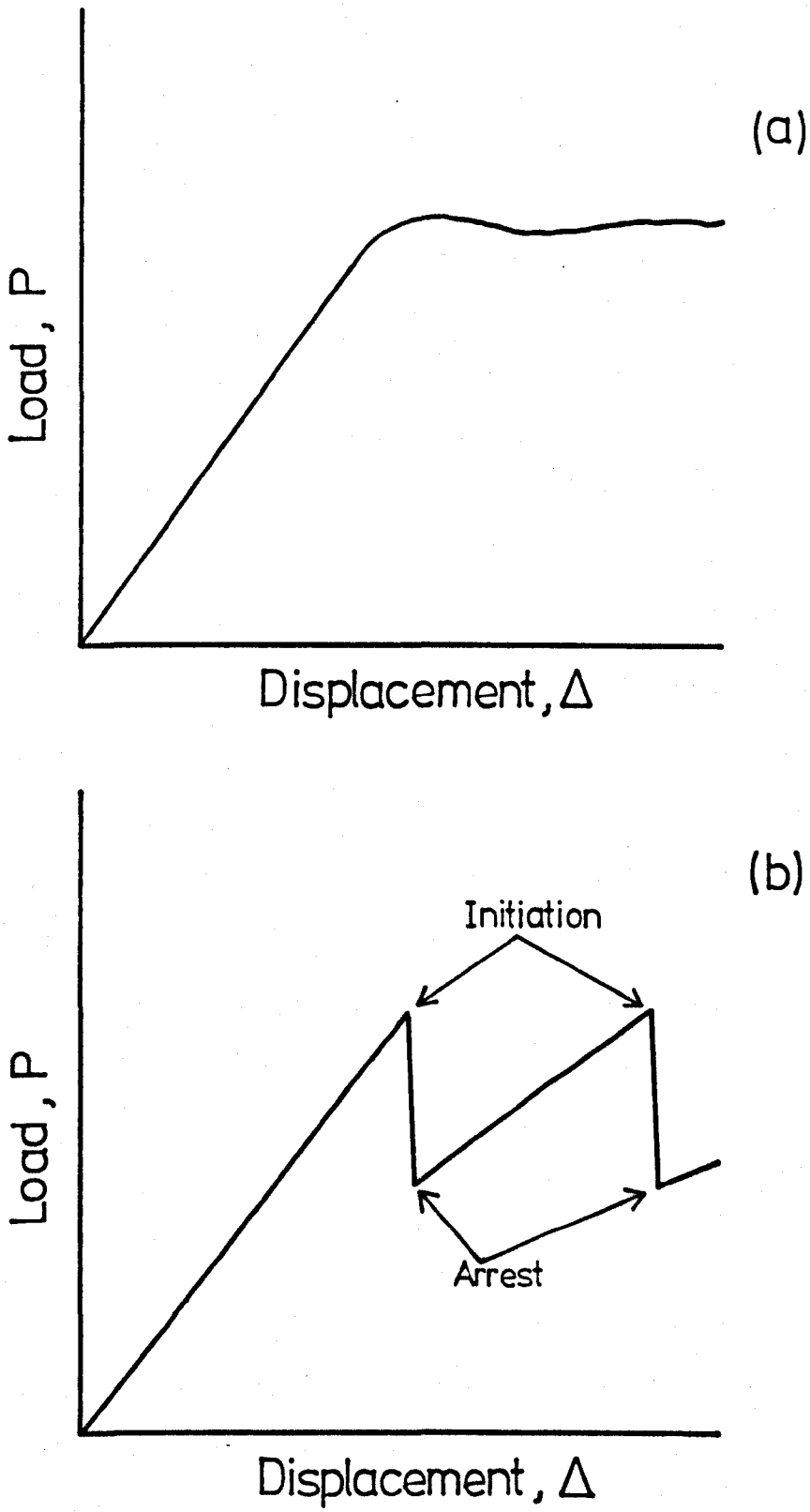

Figure 8.2 Schematic extreme load versus displacement curves obtained from rubber-modified epoxy joints (a) stable growth (b) unstable growth.

such conditions. At high values of bond thickness, unstable stick-slip fracture predominated producing the type of load-displacement curve shown in Figure 8.2(b).

The fracture surfaces obtained from these two types of crack growth were somewhat different. In the former case it was found that the entire adhesive layer was severely stress-whitened, as indicated in Figure 8.3, with the locus of failure close to the interface. At high bond thicknesses, evidence of unstable crack growth was clearly apparent, with each arrest/initiation point being represented by a curved, stress-whitened 'finger-nail' mark on the fracture surface. Such a mark is shown in Figure 8.4. Evidence of stress-whitening or apparent interfacial failure was not observed in the fast unstable growth regions.

The transition from stable to unstable growth was found to be gradual, with instances of crack jumping occurring even at very low bond thicknesses (see Figure 8.1). This trend is further demonstrated in Figure 8.5 where total stress-whitened length per specimen is shown as a function of bond thickness.

One further interesting observation with respect to the arrest/initiation 'finger-nail' markings was that increasing the bond thickness was found to increase the degree of curvature of the marking, as shown in Figure 8.6.

8.3 Effect of Displacement Rate

The effect of displacement rate on the fracture energy bond thickness relationship discussed in the last section is shown in Figure 8.7 for a series of 12 mm wide joints tested at 20 °C. This shows that the general trend previously discussed for one particular rate, is maintained over a fairly wide range of rates. Furthermore it can be seen that an increase in displacement rate produces the following two effects,

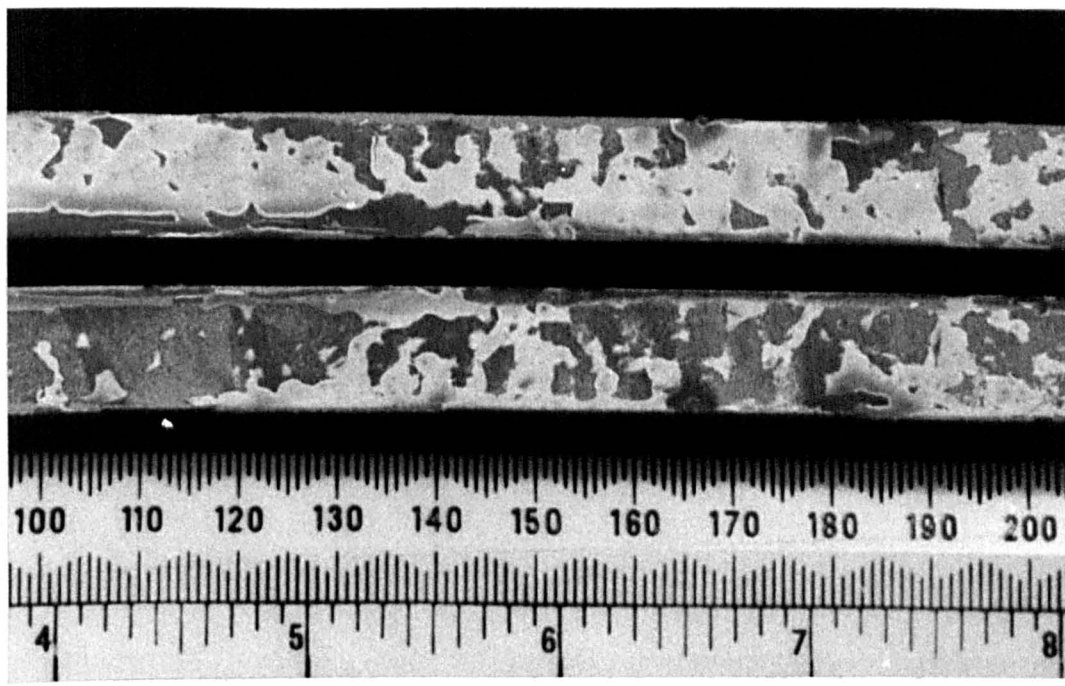

Figure 8.3 Rubber–modified epoxy adhesive fracture surface (0·13mm bond thickness, 12mm joint width, 10mm min^{-1} displacement rate, 20°C).

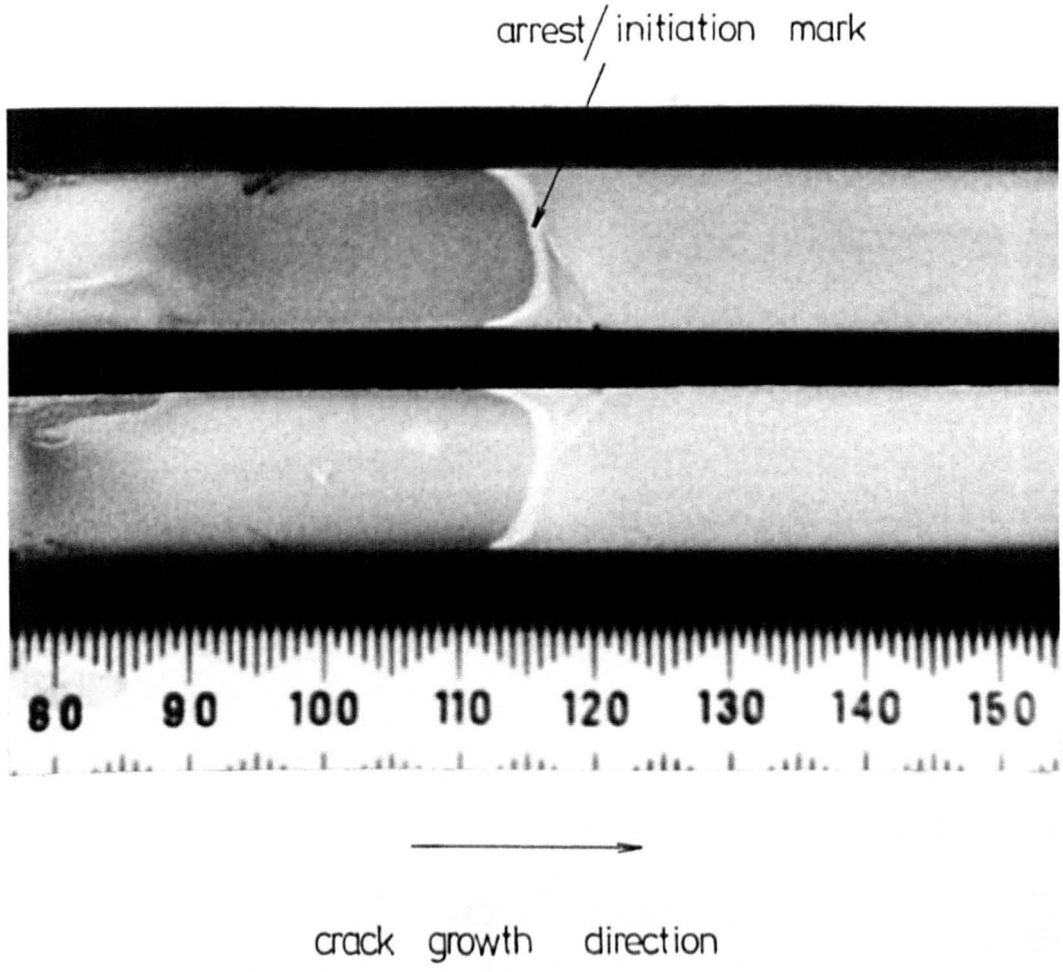

Figure 8.4 Rubber–modified epoxy adhesive fracture surface (1·98mm bond thickness, 12mm joint width, 10 mm min^{-1} displacement rate, 20°C).

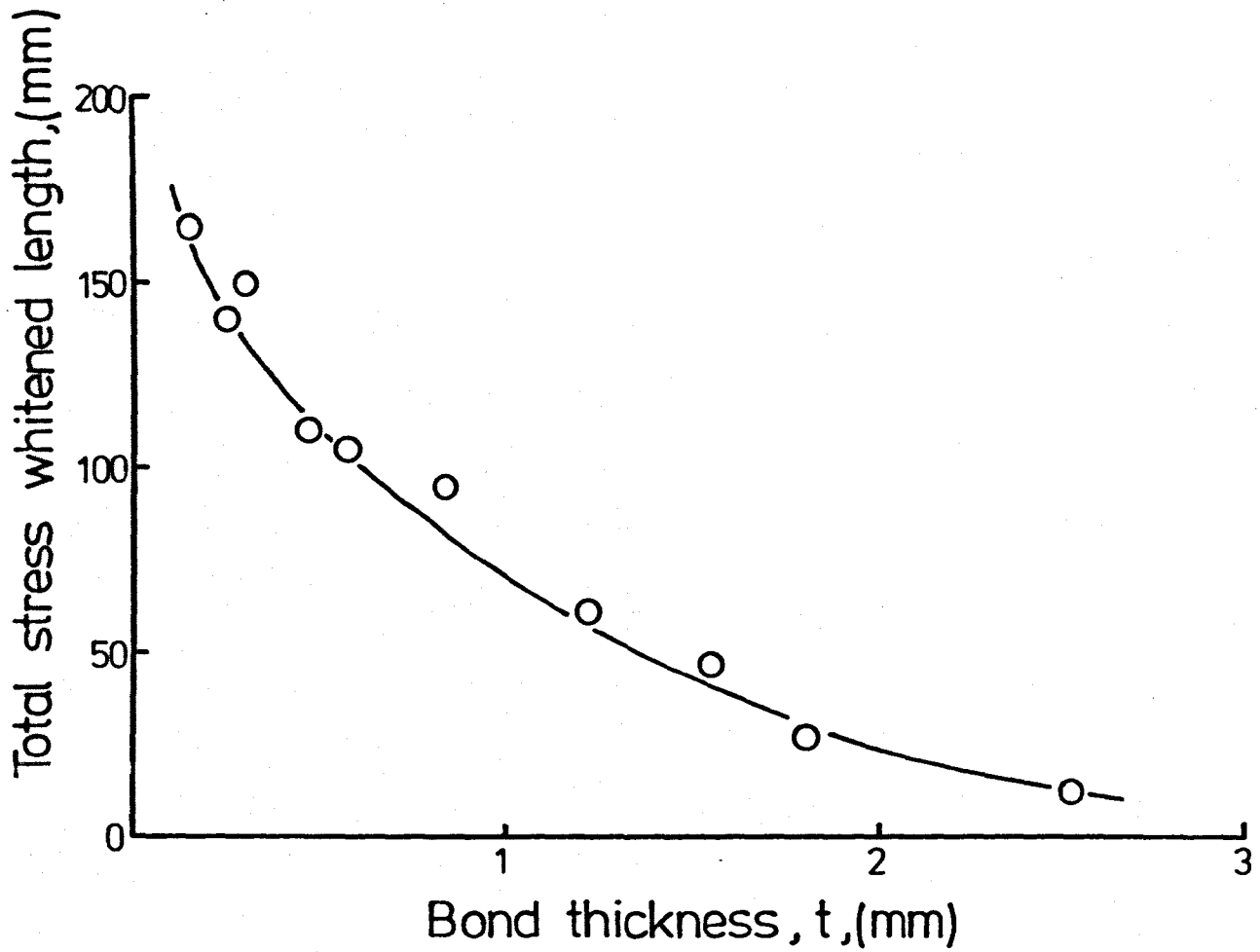

Figure 8.5 Total stress whitened length per specimen versus bond thickness, t. 0·05mm min^{-1} displacement rate, 20°C, 12mm joint width.

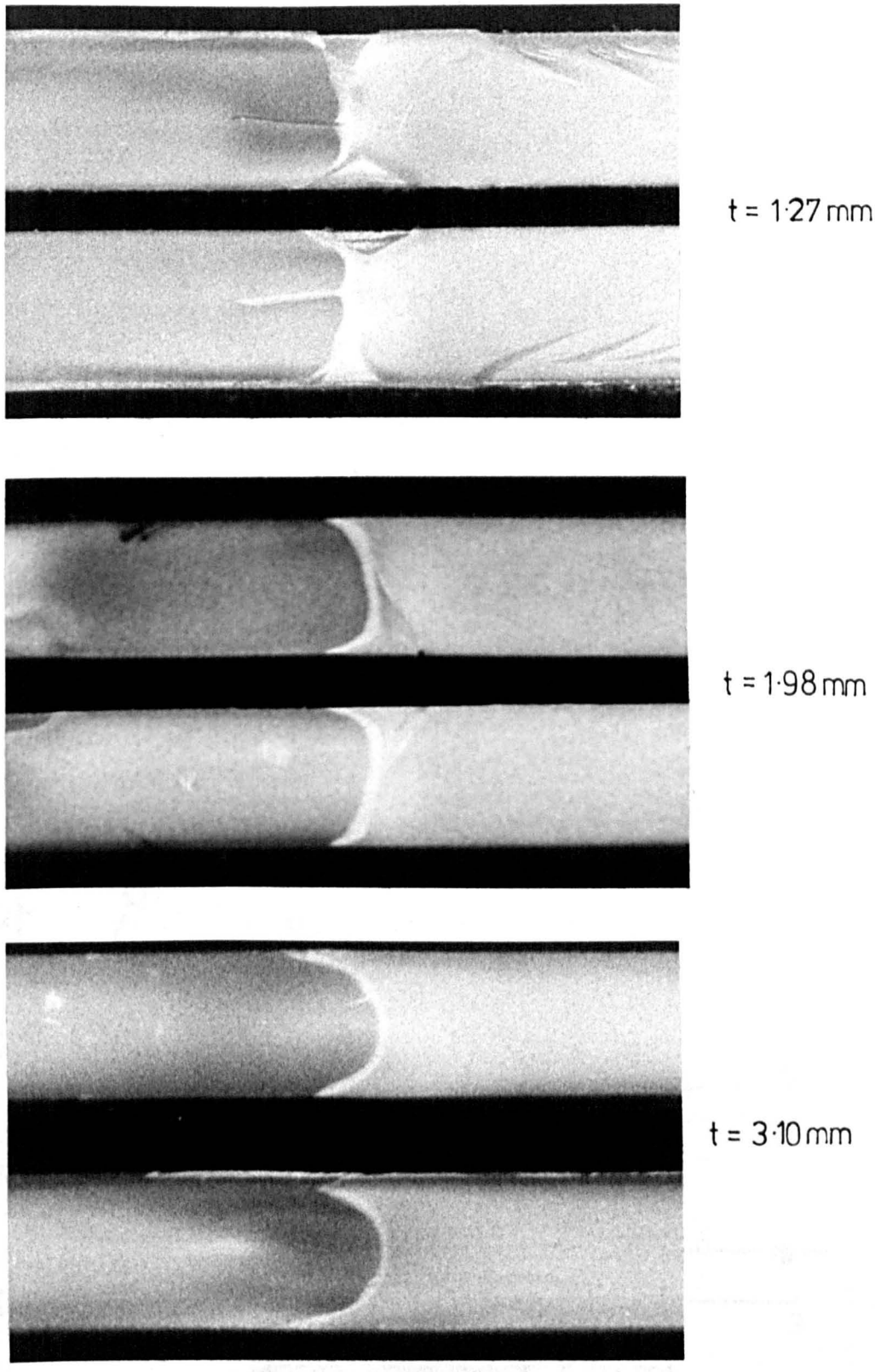

Figure 8.6 Arrest/initiation zone curvature as a function of bond thickness.

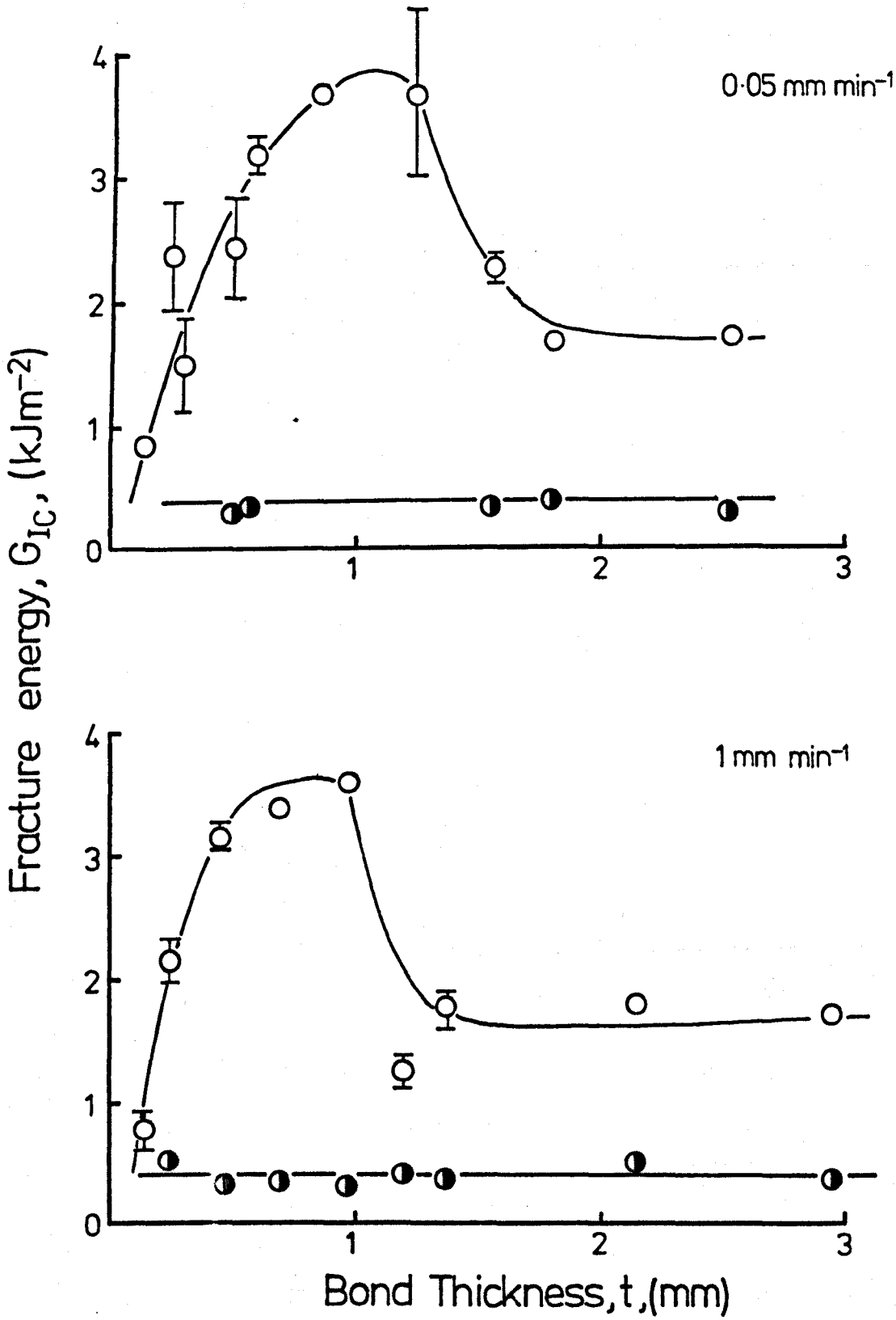

Figure 8.7 Adhesive fracture energy, G_{IC}, versus bond thickness, t, for various displacement rates. 20°C, 12mm joint width.-o-stable or initiation,-◐- arrest.

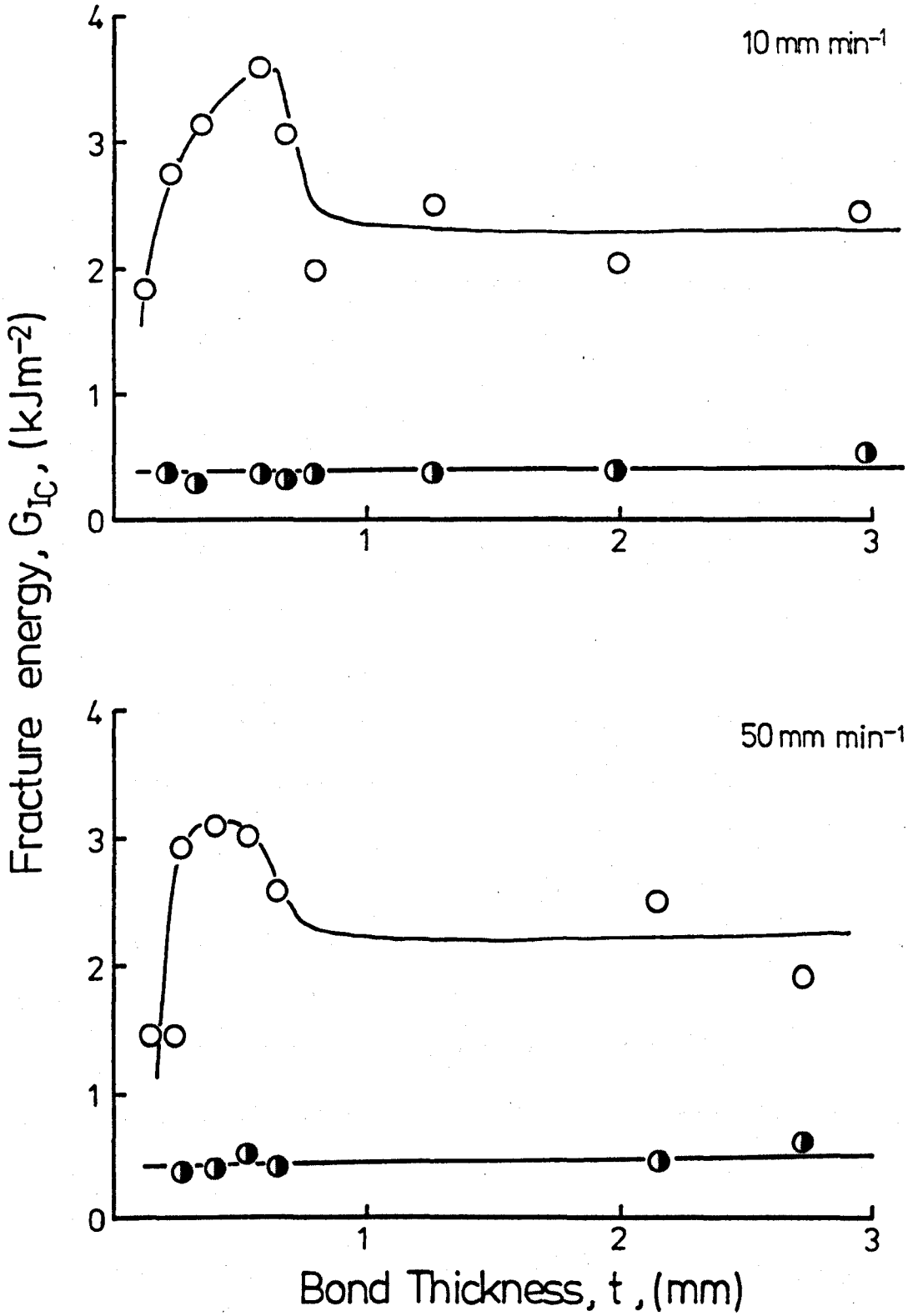

Figure 8.7 continued.

(i) a reduction in the value of the maximum fracture energy, G_{Icm} and

(ii) a reduction in the bond thickness, t_m, corresponding to G_{Icm}.

It may be seen that the arrest energy values, which are independent of bond thickness, are also independent of rate.

Increasing the displacement rate generally produced a reduction in the degree of stable crack growth. The fracture surface appearance which, as discussed previously was related to crack growth behaviour, was similarly affected; decreased stable growth behaviour at fast rates resulting in less stress whitening. This trend is demonstrated in Figure 8.8 as a plot of total white zone length per specimen against displacement rate.

8.4 Effect of Joint Width

The effect of joint width on the previously discussed fracture energy-bond thickness relationship is demonstrated in Figure 8.9. It can be seen that the general trend observed previously (width = 12 mm) is essentially maintained throughout the range studied. However the peak becomes more pronounced and 'sharper' with increased width and the value of G_{Icm} increases significantly. As indicated, arrest energies were generally independent of joint width.

Increasing joint width was also found to reduce the extent of stable crack growth and consequently the extent of stress whitening. These trends are depicted in Figures 8.10 and 8.11. The former shows clearly the change from stable to unstable crack growth behaviour on increasing the width from 3 to 49 mm. Of further interest is the shape of the arrest/initiation 'finger-nail' markings at 12 and 49 mm. As indicated, the increase in width reduces the degree of curvature of the marking.

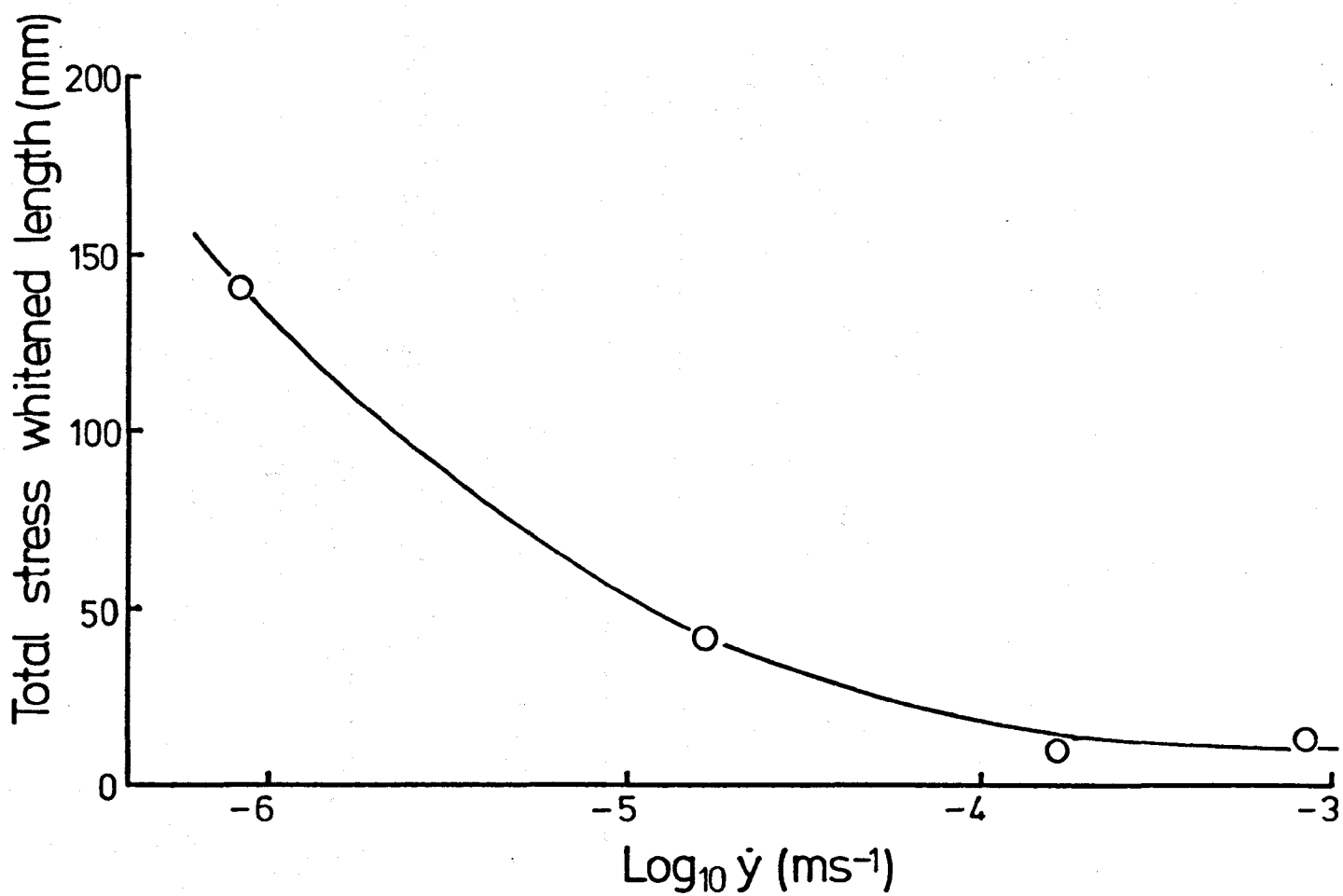

Figure 8.8 Total stress whitened length per specimen versus displacement rate, $\dot{y}$. 20°C, 12mm joint width, 0·25mm bond thickness.

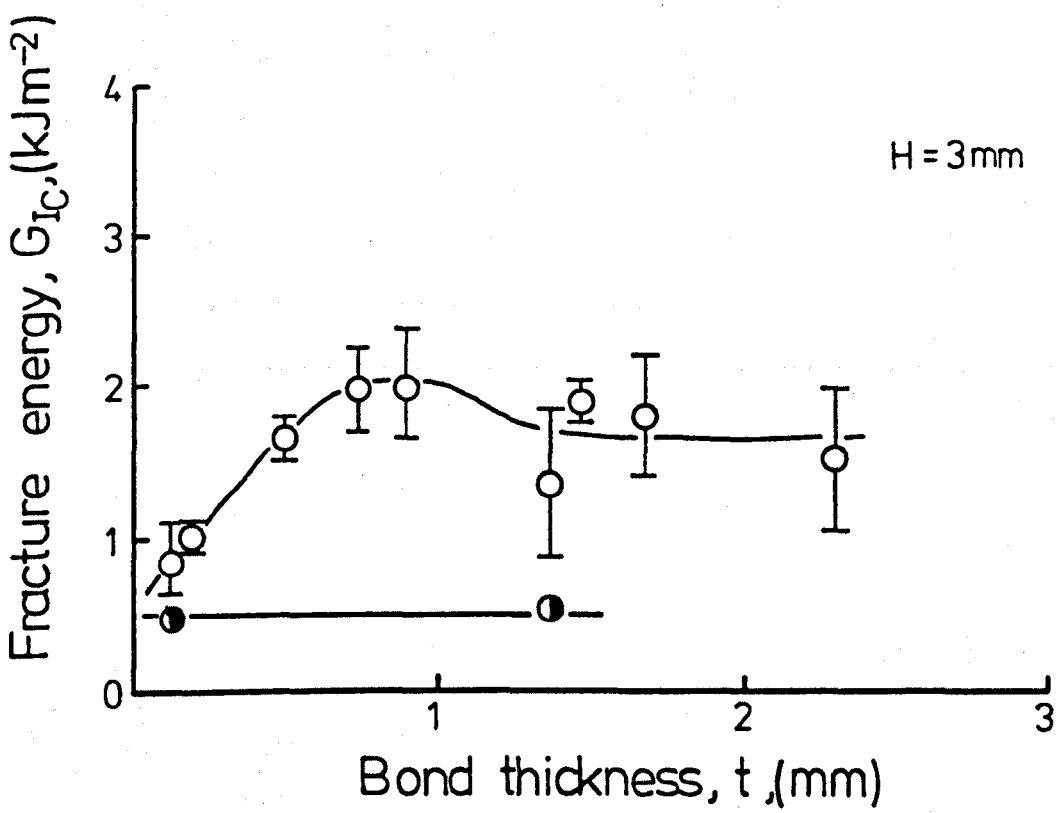

Figure 8.9 Adhesive fracture energy, G_{IC}, versus bond thickness, t, for various joint widths. 20°C, 1mm min^{-1} displacement rate. -o- stable or initiation, -◑- arrest.

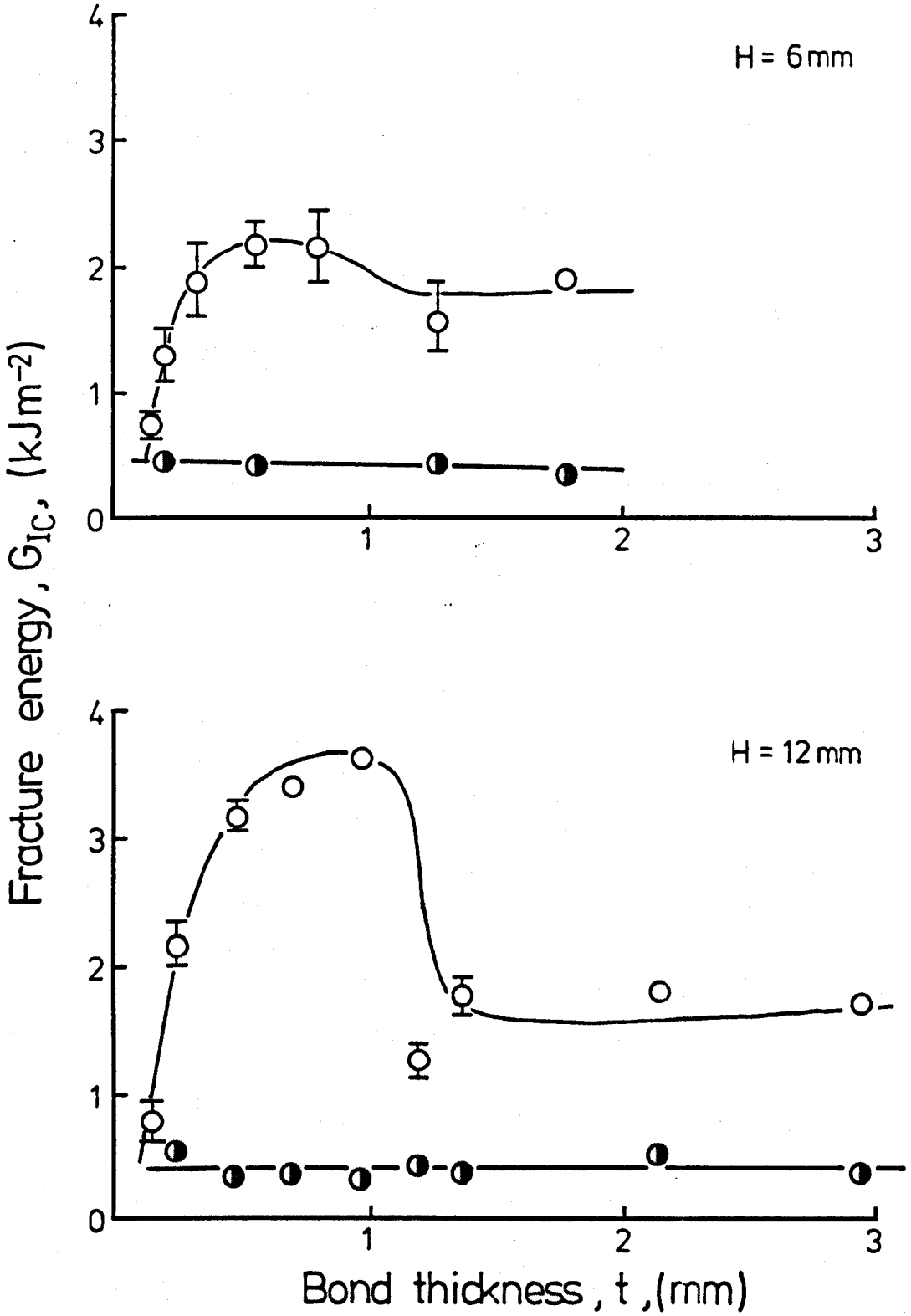

Figure 8.9 continued.

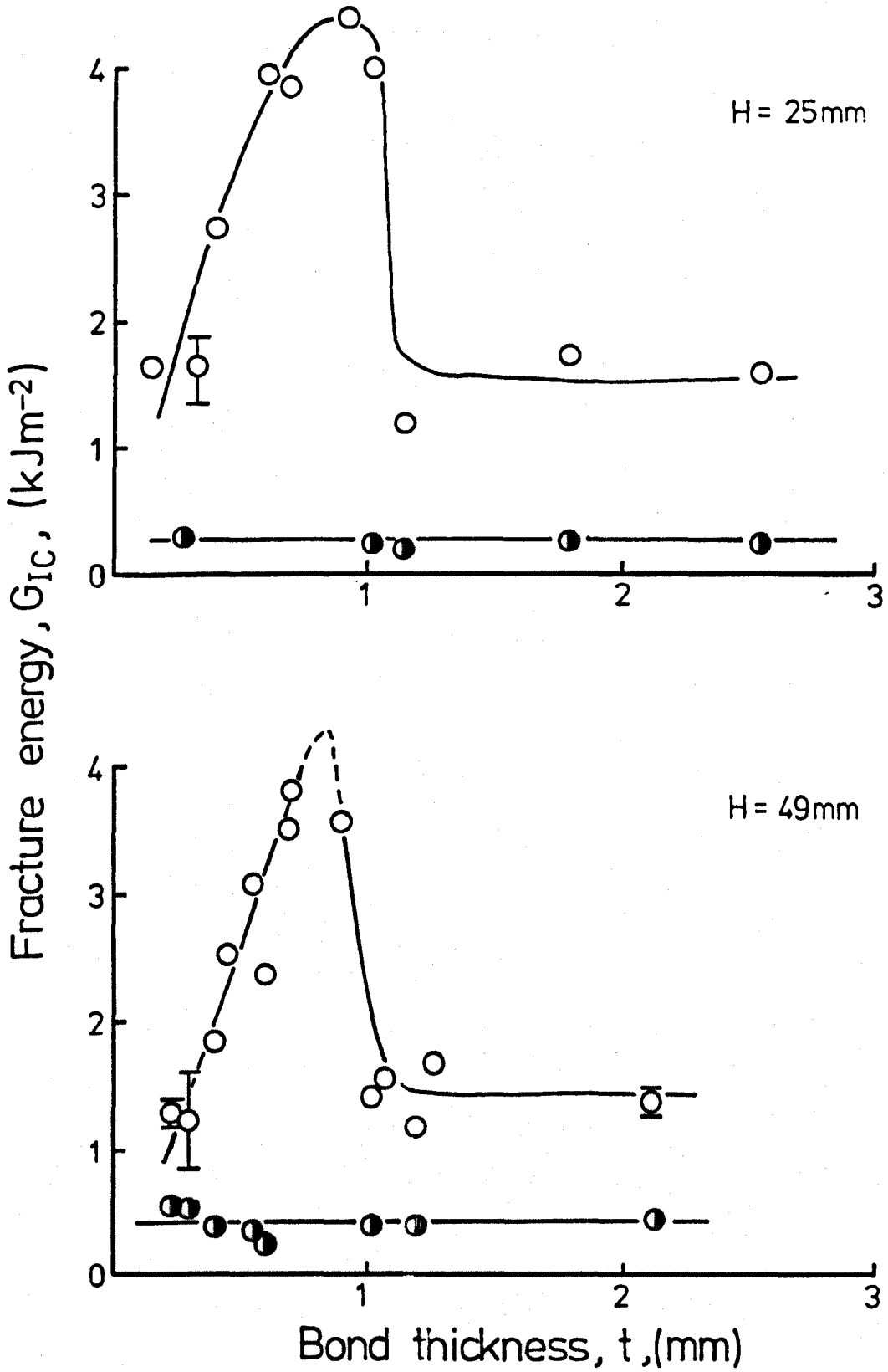

Figure 8.9 continued.

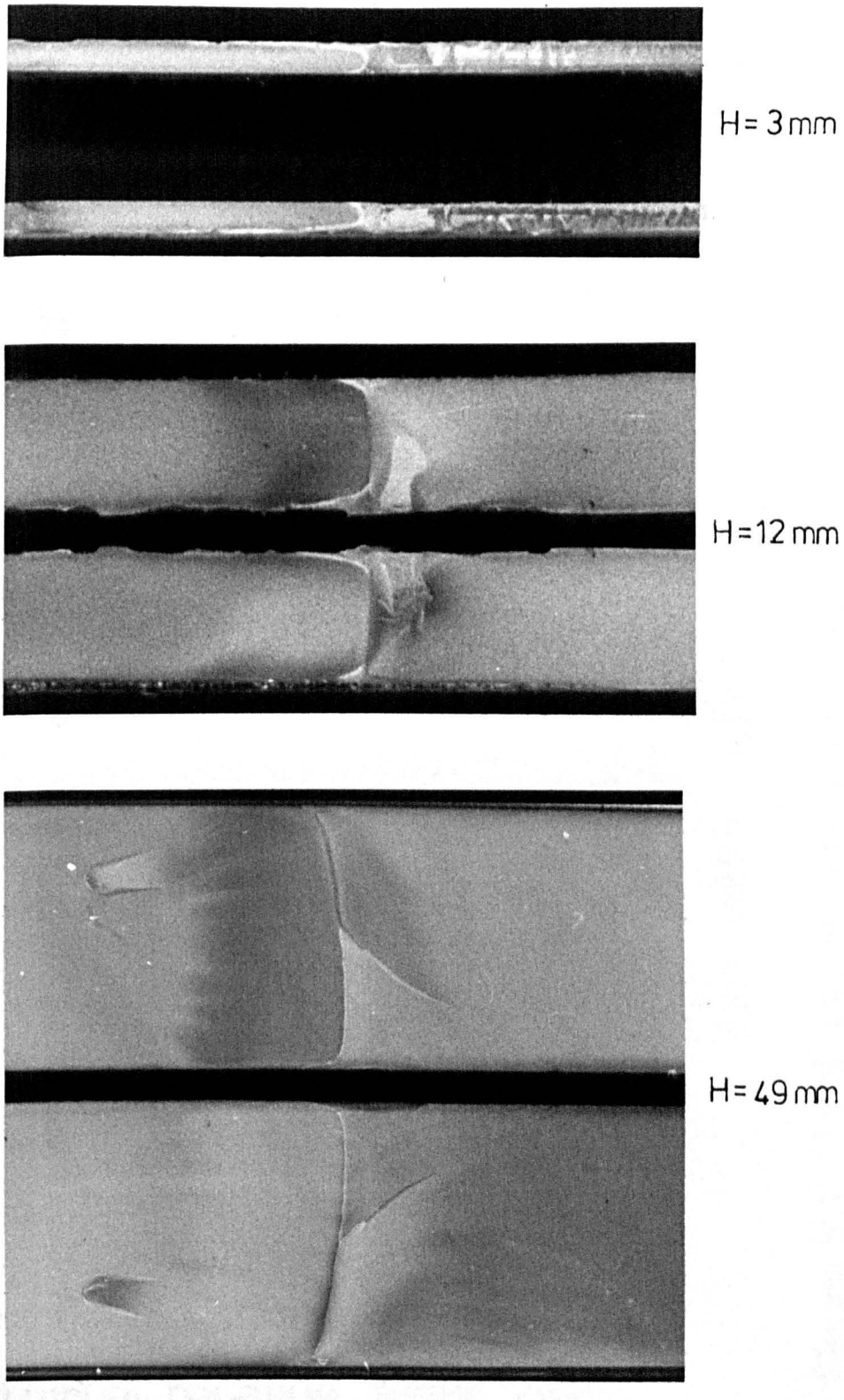

Figure 8.10 Adhesive joint failure mode as a function of joint width (1·76mm bond thickness, 0·05mm min^{-1} displacement rate, 20°C).

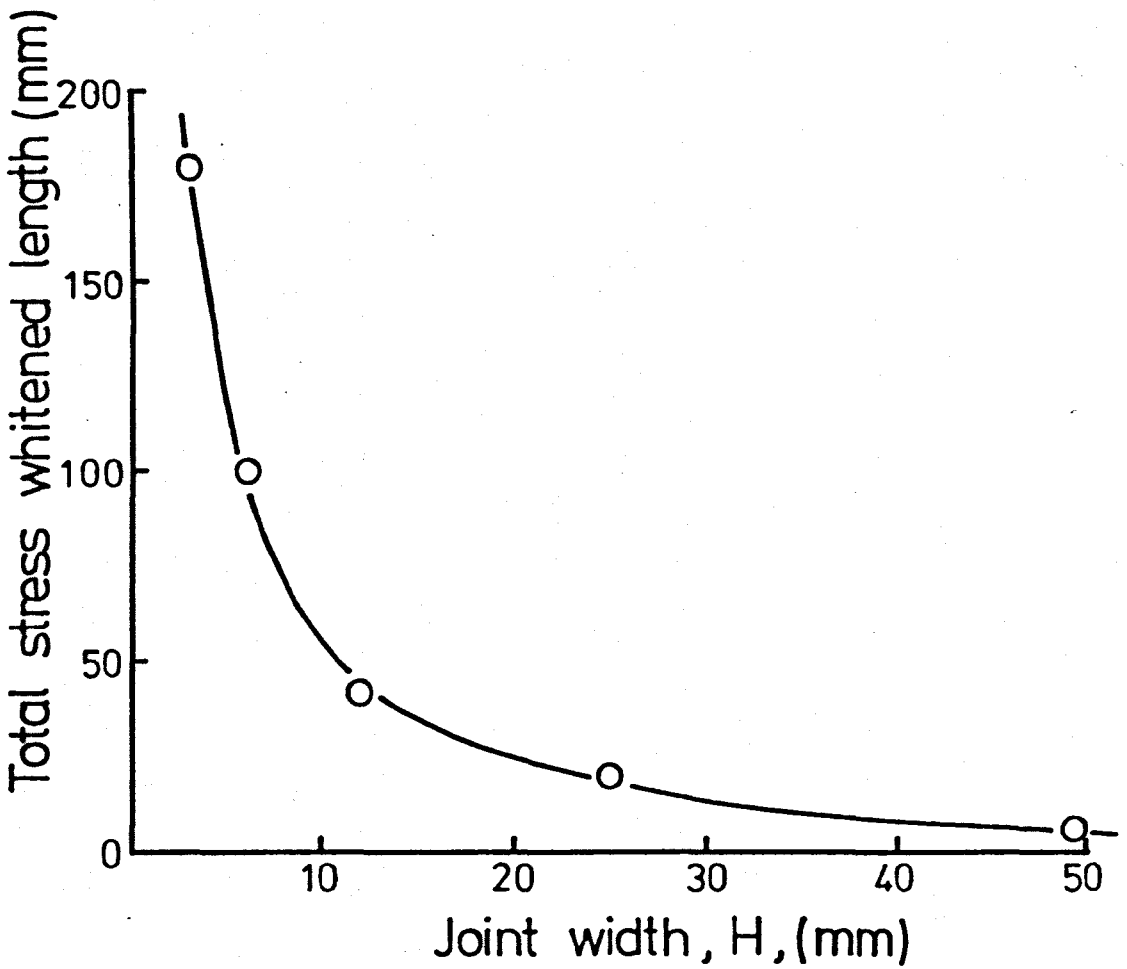

Figure 8.11 Total stress whitened length per specimen versus joint width. 20°C, 1 mm min^{-1} displacement rate, 0·25 mm bond thickness.

8.5 Deformation Zone Studies

The rubber-modified epoxy employed in this investigation exhibited stress-whitening under certain conditions, as seen from the fractographic studies. It was also possible to observe this process at the tip of the crack in the adhesive layer during loading. Hence, in a limited number of cases, detailed observations of the stress-whitened zone were attempted during testing.

Experiments were conducted on 12 mm wide joints at bond thicknesses of 0.6, 0.9 and 1.5 mm. The procedure employed was to pre-crack the specimen as outlined in section 6.3.2, and follow this by loading at a displacement rate of 0.05 mm min^{-1}. The development of the stress-whitened deformation zone during loading was followed with the naked eye. The results obtained are demonstrated in Figure 8.12, which indicates an elongated crack tip stress-whitened zone which had developed during the loading of the joint (1.5 mm bond thickness). The tests conducted on the 0.6 and 0.9 mm joints indicated an increase in elongation of the zone with decreasing bond thickness. However, as Figure 8.12 indicates, the degree of stress-whitening tended to decrease significantly in intensity with increased distance from the crack tip, thus making it extremely difficult to locate the zone boundaries. Consequently it was not considered worthwhile to embark on a detailed study to correlate stress-whitened zone length with parameters such as displacement rate and joint width.

These studies also indicated a pronounced difference in the mechanism of crack growth between thin and thick bonds. The 0.6 mm thick joint underwent crack growth by a micro-crack coalescence process, which occurred close to the adhesive/adherend interface. The 1.5 mm joint did not show this behaviour. Instead crack growth occurred in a similar manner to that found with bulk specimens, ie by a gradually increasing crack opening displacement followed eventually by unstable

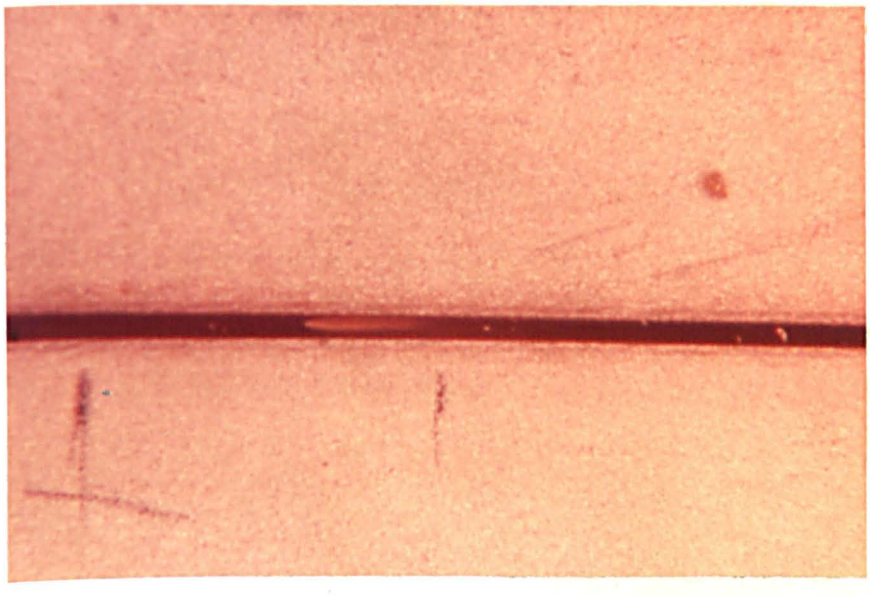

crack growth direction

Figure 8.12 Crack tip plastic zone in a rubber-modified epoxy adhesive layer (1·5mm bond thickness, 12mm joint width).

growth.

8.6 Summary

(i) The results have shown that adhesive fracture energy, G_{Ic}, is strongly dependent upon bond thickness and a maximum, G_{Icm}, occurs ata specific bond thickness, t_m.

(ii) The variation of such factors as displacement rate and joint width have shown that the basic adhesive fracture energy - bond thickness trend is maintained, but with some important effects. For example, the rate affects the value of G_{Icm} and t_m and the joint width affects the value of G_{Icm}.

(iii) Two major types of crack growth have been observed, namely stable and unstable, stick-slip. The former produces fracture surfaces exhibiting pronounced evidence of stress-whitening and apparent interfacial failure whilst the latter shows only minor evidence of this behaviour. Increases in bond thickness, testing rate and joint width increase the extent of unstable cracking.

(iv) Crack tip deformation zone studies have indicated that the stress-whitened zone which develops at the crack tip during loading, is extended along the adhesive bond line. It thus differs significantly in both shape and volume from that observed with the bulk rubber-modified system.

PART THREE

DISCUSSION AND CONCLUSIONS

CHAPTER NINE

BULK FRACTURE

9.1 Introduction

This chapter discusses the results obtained from the bulk fracture studies given in Chapter 7. It is divided into three principal sections. The first section deals with toughening mechanisms. The second discusses failure criteria and the third section considers the sudden brittle/ductile transitions exhibited by the unmodified epoxy.

9.2 Toughening Mechanisms

Before proceeding with a discussion of a toughening mechanism based upon both the increased toughness exhibited by the rubber-modified epoxy and the many detailed fractographic observations, it is useful to review some of the major mechanisms which have been proposed previously.

9.2.1 Current theories

(a) Rubber Tear

This theory was initially proposed by Merz, Claver and Baer in 1956 (92). It proposes that rubber particles simply hold the opposite faces of a propagating crack together. The energy absorbed in fracture is the sum of the energy to fracture the glassy matrix and rupture the rubber particles.

Kunz-Douglas and co-workers (93) have recently proposed a quantitative model for a rubber-modified epoxy based upon similar principles. It is depicted mathematically in equation 9.1,

$$G_{Ic} = G_{Ice}(1 - vp) + \left[1 - \frac{6}{\lambda t^2 + \lambda t + 4}\right] 4\tau_t vp \qquad (9.1)$$

where Vp is the volume fraction of the rubbery particles, τ_t is the tear energy of the particles, λ_t is the extension ratio at failure for a rubber particle and G_{Ice} is the fracture energy of the epoxy matrix.

This mechanism has the obvious advantage of being simple together with the ability of allowing a quantitative estimate of fracture energy, G_{Ic}, from a knowledge of measurable parameters such as Vp, τ_t and λ_t.

A number of studies (93, 94) have shown evidence of particles spanning loaded cracks, thus suggesting a rubber tearing contribution to overall toughness. However there are a number of major inconsistencies between the mechanism and experimental observations. They include,

(i) It does not explain the existence of stress whitening observed on numerous occasions.

(ii) It does not account for a yielding and plastic flow contribution to toughness which would clearly be necessary from the fracture surface studies described in Chapter 7.

(iii) The rubber particle tear energy, τ_t would have to be quite large (≈ 5 kJm^{-2}) to account for the high fracture toughness values obtained at high temperatures in this work. Experiments conducted by Kunz-Douglas and co-workers (93), designed to estimate τ_t for the rubber particles, resulted in much smaller values.

(iv) Since τ_t would be expected to rise as temperature is reduced towards rubber particle Tg (95), the value of τ_t at, for example -60°C, would be much greater than 5 kJm^{-2} and therefore extremely high indeed.

(v) The rate and temperature dependence of fracture toughness, K_{Ic}, observed in this work, is opposite to the manner in which the tearing energy of rubbers varies with the same experimental variables. In this case the extension ratio term, λ_t in equation 9.1 would have to completely dominate τ_t in order to produce a strong effect in the opposite direction. This appears unlikely.

(vi) Since equation 9.1 has a dominant contribution to toughness from the unmodified epoxy matrix, tough/brittle transitional behaviour would also be expected with the rubber-modified epoxy under exactly the same conditions. This did not occur.

(b) Multiple Crazing

This theory, due to Bucknall and Smith (96), proposes that toughness enhancement is attributed to the generation and efficient termination of crazes by rubber particles. This process has been adequately demonstrated with thermoplastics such as high-impact polystyrene. Craze initiation occurs at regions of high stress concentration which, with rubber particles embedded in a brittle matrix, is at the equatorial region normal to the applied stress direction. Craze termination occurs when the craze encounters another rubber particle. This stabilises the craze and prevents it growing into a larger crack-like structure.

No evidence was found during the present investigation to indicate a crazing process in the unmodified epoxy, or the matrix of the rubber-modified material. Although some evidence has been put forward to suggest that crazing can occur in epoxy resins (97, 98) it is generally believed that crazing is the exception rather than the

rule under most conditions. In support of this, recent studies with thermoplastics (99) have indicated a transition from a crazing to a shear yielding mechanism as the length of polymer chain between physical entanglements decreases. This suggests that with thermosetting polymers, where crosslink density is high and thus chain length between crosslinks is short, crazing would be suppressed.

(c) Shear Yielding

This theory was proposed by Newman and Strella (100) in 1965 following work on ABS thermoplastics. It is proposed that shear deformation can occur either as shear bands or as a result of more diffuse shear yielding. It has been shown that shear bands, like crazes, also initiate at stress concentrations resulting from the presence of rubber particles (101).

Probably the greatest difficulty with the shear yielding theory is that it cannot explain stress whitening, due to shear yielding being a constant volume deformation process. As a result it has been suggested that crazing and shear yielding occur simultaneously in many polymers (101), with the former accounting for the frequently observed stress-whitening effect. This crazing with shear yielding mechanism has been able to explain many of the fundamental differences in mechanical behaviour between two of the most common toughened thermoplastics, high-impact polystyrene and ABS. Furthermore this theory has been proposed by Sultan and McGarry (102) to explain the deformation behaviour of various rubber-modified epoxy systems. They proposed that rubber particle size controls deformation behaviour with small particles (< 0.1 μm) favouring shear yielding and large particles (> 5 μm) favouring crazing, with intermediate particle sizes producing both mechanisms. Again however, evidence for the presence of crazing

was lacking in this work. Furthermore it is now believed (103) that particle size does not greatly influence toughness, with rubber-phase volume being the important parameter.

9.2.2 Proposed toughening mechanism

(a) Introduction

The results of the experiments conducted in the present investigation clearly indicate a correlation between fracture toughness and the extent of plastic deformation found either throughout the fracture surface for stable growth or in the initiation region in the case of unstable growth (type B). For example, type A and A→B fracture surfaces, where toughness was comparatively high, showed a high number of comparatively large, deep holes together with extensive plastic shear flow in the matrix. Furthermore, hole diameters were generally greater on these surfaces than obtained with type B and C surfaces. Evidence for the presence of a typical crazing mechanism was not observed. Such observations suggest a mechanism based upon yielding and plastic shear flow of the matrix as the primary source of energy dissipation during fracture in both the unmodified and rubber-modified epoxies. Clearly however the main cause of the improved toughness of the modified epoxy is the rubber particles dispersed in the epoxy matrix. Thus it is necessary to firstly consider the rubber particles and in particular the stress fields which would exist around them at a loaded crack tip.

(b) Stress fields around rubber particles at crack tips

Goodier (104) in 1933 considered the case of an isolated spherical particle embedded in an istropic elastic matrix which is subjected to a uniform uniaxial tensile stress at points remote from the particle. He derived equations which indicated that for a rubbery particle, which possesses a considerably lower shear modulus than the

matrix, the maximum stress concentrations occurred in the equatorial regions of the particle with a value of approximately 1.9. With the present material, where a fairly large volume fraction of rubber particles exists, there is the added complication of particle stress-field interaction. In such cases the maximum stress concentrations would almost certainly be greater than 1.9. However, in the region ahead of a crack tip a state of triaxial stress would exist, as opposed to the uniaxial tensile stress employed in the Goodier model. This would be in addition to triaxial stresses which would develop during cooling from the curing temperature, due to differences in thermal contraction between the rubber particles and epoxy matrix. This triaxial stress-field would reduce the stress concentrating effect at the equatorial regions of the particles by approximately 20% (105). Thus, allowing for the various factors which would influence the extent of the stress concentration, it would probably have a value of approximately 1.6.

(c) Voiding and shear yielding

The interactions between the triaxial stress field in the vicinity of a loaded crack tip and that existing around rubber particles in close proximity would lead to the initiation of two important processes.

First, the development of a triaxial stress would lead to dilatation of the matrix. This, in combination with triaxial stresses inherent in the rubber particles, due to differential thermal contraction effects, would cause cavitation of the particles. This would occur either within the particles (particularly if the particle/matrix bond is strong) or at the particle/matrix boundary. Indeed, it is commonly found that rubbers undergo cavitation quite readily under the action of a triaxial stress field (95). This rubber particle cavitation is responsible for the stress-whitening effects observed in this work.

The second process that occurs is the initiation and growth of shear yield deformations in the matrix. During loading, stress concentrations will develop at the equators of the rubber particles, which will act as sites for the initiation of shear deformations. Due to the large number of particles present, the degree of yielding generated will be substantially greater than would otherwise occur in an unmodified material. However particles would also act as sites for shear yield termination which would therefore keep the yielding localised.

It is possible and indeed likely that both of the above processes occur during the early stages of loading. However the first, involving rubber particle cavitation, will be the most dominant, since evidence for particle failure has been clearly demonstrated in Chapter 7. Once extensive shear yielding has initiated this might be expected to inhibit cavitation and rubber particle failure.

Once cavitation of rubber particles has begun, leading to void formation, the generation of these voids will greatly enhance further shear yielding in the matrix. This will be partly attributable to an increased stress concentration which is likely to accompany cavitation and void formation. However of greater importance, the void formation will result in reduced constraint on the matrix adjacent to voided particles, thus relieving the degree of triaxiality. This important process would mean that the matrix never experiences simple plane stress or plane strain loading but rather a more complex stress state. The reduction in triaxiality would lower yield stress in the inter-particle regions and thus promote further extensive shear yielding. However, a fully ductile situation would be prevented since such shear deformations would only occur in regions ahead of the crack tip where stresses are sufficiently high to promote cavitation and

void formation either in the rubber particles or at the particle/ matrix boundary. This shear yielding process leads to a greatly increased plastic zone size at the crack tip, which in turn produces extensive blunting. This results in a reduction in crack tip stress concentration and thus an increase in toughness. Clearly, the degree to which this shear yielding process can occur will depend upon both temperature and time. Thus the fracture toughness of the rubber-modified epoxy will be rate and temperature dependent.

(d) Toughening at temperatures below the rubber glass transition

At temperatures below -60°C, the rubber particles would be below their glass transition temperature and would therefore no longer exhibit rubbery characteristics. As discussed in Chapter 7, the rubber-modified epoxy maintained an increased fracture toughness over its unmodified counterpart at temperatures below -60°C. Thus it is of interest to consider the mechanism responsible for this behaviour.

It might initially seem reasonable that a rubber particle could behave similarly to a rigid particulate filler when below its glass transition temperature. Various workers have investigated the toughening effects of particulate fillers such as alumina trihydrate and glass spheres on epoxy resins (106-110). These investigations have found that filler incorporation can significantly increase toughness. A crack-pining mechanism (111-113) has been proposed to explain the improvements in toughness brought about by particulate fillers. The mechanism proposes that a propagating crack front, when encountering an inhomogeneity, becomes temporarily pinned at that point. An increase in load increases the degree of bowing between pining points resulting in both new fracture surface and an increase in the length of the crack front. These processes will

absorb energy and therefore fracture toughness will increase. However three factors suggest that this mechanism does not operate with the current rubber-modified system.

Firstly, the crack-pinning model relies on 'inpenetrable' obstacles, ie obstacles which pin the crack but do not fracture under the applied stress. Consequently the presence of unfractured particles on a fracture surface would be expected. Scanning electron microscopy conducted on fracture surfaces obtained at -60°C and below, showed no signs of unfractured particles.

Second, for particles to be 'inpenetrable' it would seem desirable that they should have high levels of modulus and fracture resistance in comparison to the epoxy matrix. The modulus of the rubber particles at sub Tg temperatures encountered in this work would be approximately 1 GPa. This compares with values in excess of 20 GPa for particulate fillers such as glass and alumina trihydrate. Thus it is unlikely that the rubber particles could be considered as exhibiting a high degree of 'inpenetrability'. Indeed Evans has reported that the crack-pining mechanism is of minor significance for composites containing relatively ductile filler particles (112).

Third, as explained by Phillips and Harris (114), a crack-pining process would produce 'steps' behind particles on fracture surfaces. This would result from the two arms of the crack front meeting on different planes after the crack front has broken away from the pinning position. In this work 'steps' were observed under all conditions.

Thus a major contribution to toughness at temperatures below -60°C by the crack-pining mechanism is not substantiated from the observations in this work.

Of greater significance is the fact that Goodier's analysis (104) indicates that the stress concentration at the equator of a rubber particle would still exist at temperatures below its glass transition. Under these circumstances the shear modulus of the rubber would almost certainly remain lower than that of the comparatively highly cross-linked epoxy matrix. However the difference would be much reduced and thus the stress concentrating effect would be reduced in intensity. Consequently the ability of the rubber particles to act as sites for the initiation of shear deformations would be diminished. This effect would be aggravated by two further factors.

Firstly, the resistance to cavitation of the rubber particles would be comparatively high below their glass transition temperature. Thus the ability to reduce the extent of triaxiality within the epoxy matrix would be curtailed. (It is of interest to note that a very limited degree of stress-whitening was observed on rubber-modified fracture surfaces at temperatures below -60°C, thus indicating the existence of an albeit small amount of particle cavitation.)

Second, the yield stress of the epoxy matrix increases with decreasing temperature. Thus the value at temperatures below the glass transition of the particles would be comparatively high. This would result in a high resistance to shear deformations within the epoxy matrix.

Thus it can be argued that the mechanism proposed would still operate at temperatures below the rubber particle glass transition. However due to the factors mentioned above, the toughness enhancement would be substantially curtailed.

(e) Concluding remarks

The toughening mechanism proposed suggests that two basic deformation processes, namely rubber particle cavitation and plastic shear flow, serve to magnify the degree of shear yielding in the matrix. This results in a pronounced increase in plastic zone size and thus increased toughness. This mechanism would appear to operate at all the temperatures studied.

9.3 Failure Criteria

In recent years there have been two major criteria proposed to describe failure in polymeric materials. The first, known as the constant crack-opening displacement criterion, has been shown to apply to thermoplastics such as polymethyl methacrylate. The second, a more recent proposal, is based upon the concept of crack tip blunting. It is of interest to consider both approaches.

9.3.1 Constant crack-opening displacement

The models proposed by both Irwin (13) and Dugdale (115) to describe the extent and shape of the plastic zone which exists at a crack tip under load, also define the parameter, crack-opening displacement (previously demonstrated in Figure 4.2, Chapter 4). From these models the value of crack-opening displacement at the onset of crack growth, δ_{tc}, is given by the expression,

$$\delta_{tc} = e_y \left(\frac{K_{Ic}}{\sigma_{yt}}\right)^2 \qquad (9.2)$$

where σ_{yt} is the uniaxial tensile yield stress and e_y the yield strain.

A critical crack opening displacement criterion has been shown to apply to the fracture of polymethyl methacrylate (45, 46). Furthermore recent evidence suggests that such a criterion may also apply to epoxy resins when undergoing stable crack propagation (38).

In order to determine whether this criterion applies to the current epoxy materials, values of δ_{tc} were calculated from equation 9.2. The relevant values of K_{Ic} were taken from the data previously presented in Chapter 7. Values of σ_{yt} and e_y were determined from the uniaxial compression experiments. Now the yield stress obtained from a compression test, σ_{yc}, will not be equivalent to a tensile yield stress, σ_{yt}. This is because yield stress is usually dependent upon both the hydrostatic and deviatoric components of the stress tensor, with these components differing in the two types of test. Various yield criteria embodying hydrostatic stress components have indicated that the ratio of the tensile to the compressive yield stress is approximately 0.75 (116, 117). Thus this ratio was employed to calculate values of σ_{yt} from the uniaxial compression data. The K_{Ic} results were related to the yield data by approximately equating the time-to-failure in the former tests to the time-to-yield in the latter. This resulted in a displacement rate for a fracture test being equivalent to a strain rate for a compression test with a two decade difference; for example 8.3×10^{-7} ms^{-1} $\equiv$ 8.3×10^{-5} s^{-1}. The appropriate data is shown in Tables 9.1 and 9.2 for the unmodified and rubber-modified epoxies respectively. Figures 9.1 and 9.2, showing the variation of δ_{tc} with temperature for both systems show a number of interesting points.

Firstly, a reduction in δ_{tc} occurs with decreasing temperature and increasing rate, having values of approximately 2 μm and 10 μm for the unmodified and rubber-modified systems respectively at -90°C. However the degree of scatter does not allow accurate assessment of a constant δ_{tc} criterion within the low temperature, type C, crack growth region. This is in contrast to results obtained from polymethyl methacrylate (45, 46) and indeed some other unmodified epoxy formulations (38). In these cases a constant δ_{tc} value has been shown to govern

TABLE 9.1

Critical crack opening displacement values at various temperatures and rates. Unmodified epoxy

Temperature (°C)	Log_{10} $\dot{y}$ (ms^{-1})	K_{Ic} ($MNm^{-3/2}$)	Type Crack Growth	Log_{10} $\dot{e}$ (s^{-1})	e_y	σ_{yt} (MPa)	δ_{tc} (μm)
-90	- 6.08	0.98	C	-4.08	0.070	148.0	3.1
-73	"	0.93	C	"	0.065	130.0	3.3
-60	"	0.75	C	"	0.061	117.8	2.5
-40	"	0.70	C	"	0.055	98.4	2.8
-20	"	0.75	C→B	"	0.055	87.0	4.1
20	"	0.91	B	"	0.038	60.0	8.8
30	"	1.12	B	"	0.038	57.6	14.3
40	"	7.19	A	"	0.036	56.3	587
50	"	6.88	A	"	0.034	53.8	556
60	"	6.36	A	"	0.033	52.1	492

TABLE 9.1 (Cont'd)

Temperature (°C)	$\text{Log}_{10}\ \dot{y}$ (ms^{-1})	K_{Ic} ($MNm^{-3/2}$)	Type Crack Growth	$\text{Log}_{10}\ \dot{e}$ (s^{-1})	e_y	σ_{yt} (MPa)	δ_{tc} (μm)
-90	-4.78	0.89	C	-2.78	0.075	156.0	2.4
-73	"	0.87	C	"	0.070	140.0	2.7
-60	"	0.93	C	"	0.068	127.5	3.6
-40	"	0.72	C	"	0.060	104.4	2.8
-20	"	0.73	C→B	"	0.058	90.4	3.7
20	"	0.80	B	"	0.038	64.5	6.0
30	"	0.83	B	"	0.038	63.0	6.4
40	"	1.03	B	"	0.035	60.3	10.0
50	"	1.31	B	"	0.034	58.3	17.1
60	"	6.61	A	"	0.033	56.7	449

TABLE 9.1 (Cont'd)

Temperature (°C)	$\text{Log}_{10}\ \dot{y}$ (ms^{-1})	K_{Ic} ($MNm^{-3/2}$)	Type Crack Growth	$\text{Log}_{10}\ \dot{e}$ (s^{-1})	e_y	σ_{yt} (MPa)	δ_{tc} (μm)
-90	-3.78	0.89	C	-1.78	0.075	164.0	2.2
-73	"	0.95	C	"	0.070	150.0	2.8
-60	"	0.85	C	"	0.072	135.0	2.7
-40	"	0.72	C	"	0.060	109.1	2.5
-20	"	0.87	C→B	"	0.058	93.0	5.1
20	"	0.71	B	"	0.048	67.9	5.2
30	"	0.71	B	"	0.044	67.1	4.9
40	"	0.87	B	"	0.036	64.7	6.5
50	"	0.93	B	"	0.035	61.9	7.8
60	"	0.97	B	"	0.033	60.0	8.7

TABLE 9.2

Critical crack opening displacement values at various temperatures and rates. Rubber-modified epoxy

Temperature (°C)	$\text{Log}_{10}\ \dot{y}$ (ms^{-1})	K_{Ic} ($MNm^{-3/2}$)	Type Crack Growth	$\text{Log}_{10}\ \dot{e}$ (s^{-1})	e_y	σ_{yt} (MPa)	δ_{tc} (μm)
-90	-6.08	1.66	C	-4.08	0.080	131.0	12.8
-73	"	1.58	C→B	"	0.075	112.0	14.9
-60	"	1.47	C→B	"	0.070	98.6	15.6
-50	"	1.70	B	"	0.065	88.5	24.0
-40	"	1.62	B	"	0.063	78.9	27.4
-30	"	1.53	B	"	0.058	72.8	26.5
-20	"	2.00	B	"	0.054	66.8	49.3
0	"	2.26	A→B	"	0.043	56.3	72.5
20	"	2.72	A→B	"	0.036	47.1	133.4
40	"	3.19	A	"	0.040	40.5	248.0
60	"	4.07	A	"	0.040	34.3	563.0

TABLE 9.2 (Cont'd)

Temperature (°C)	$\log_{10} \dot{y}$ (ms^{-1})	K_{Ic} ($MNm^{-3/2}$)	Type Crack Growth	$\log_{10} \dot{e}$ (s^{-1})	e_y	σ_{yt} (MPa)	δ_{tc} (μm)
-90	-4.78	1.67	C	-2.78	0.080	134.0	11.7
-73	"	1.61	C→B	"	0.075	116.0	14.4
-60	"	1.45	C→B	"	0.070	110.4	12.1
-50	"	1.67	B	"	0.065	96.8	19.4
-40	"	1.52	B	"	0.056	84.3	19.3
-30	"	1.46	B	"	0.057	78.8	20.1
-20	"	1.72	B	"	0.056	73.4	20.2
0	"	1.97	A→B	"	0.045	62.3	45.0
20	"	2.27	A→B	"	0.039	50.8	79.9
40	"	2.94	A	"	0.040	45.0	170.7
60	"	3.52	A	"	0.040	38.6	332.0

TABLE 9.2 (Cont'd)

Temperature (°C)	$\text{Log}_{10}\ \dot{y}$ (ms^{-1})	K_{Ic} ($MNm^{-3/2}$)	Type Crack Growth	$\text{Log}_{10}\ \dot{e}$ (s^{-1})	e_y	σ_{yt} (MPa)	δ_{tc} (μm)
-90	-3.78	1.62	C	-1.78	0.080	138.0	7.3
-73	"	1.59	C→B	"	0.075	121.0	13.0
-60	"	1.43	C→B	"	0.070	119.5	10.0
-50	"	1.60	C→B	"	0.065	102.8	15.8
-40	"	1.43	B	"	0.060	88.5	15.7
-30	"	1.37	B	"	0.058	83.3	16.2
-20	"	1.77	B	"	0.059	78.2	30.7
0	"	1.75	A→B	"	0.049	66.0	35.2
20	"	2.02	A→B	"	0.039	53.6	56.8
40	"	2.70	A→B	"	0.036	48.8	122.0
60	"	3.05	A	"	0.040	42.0	210.9

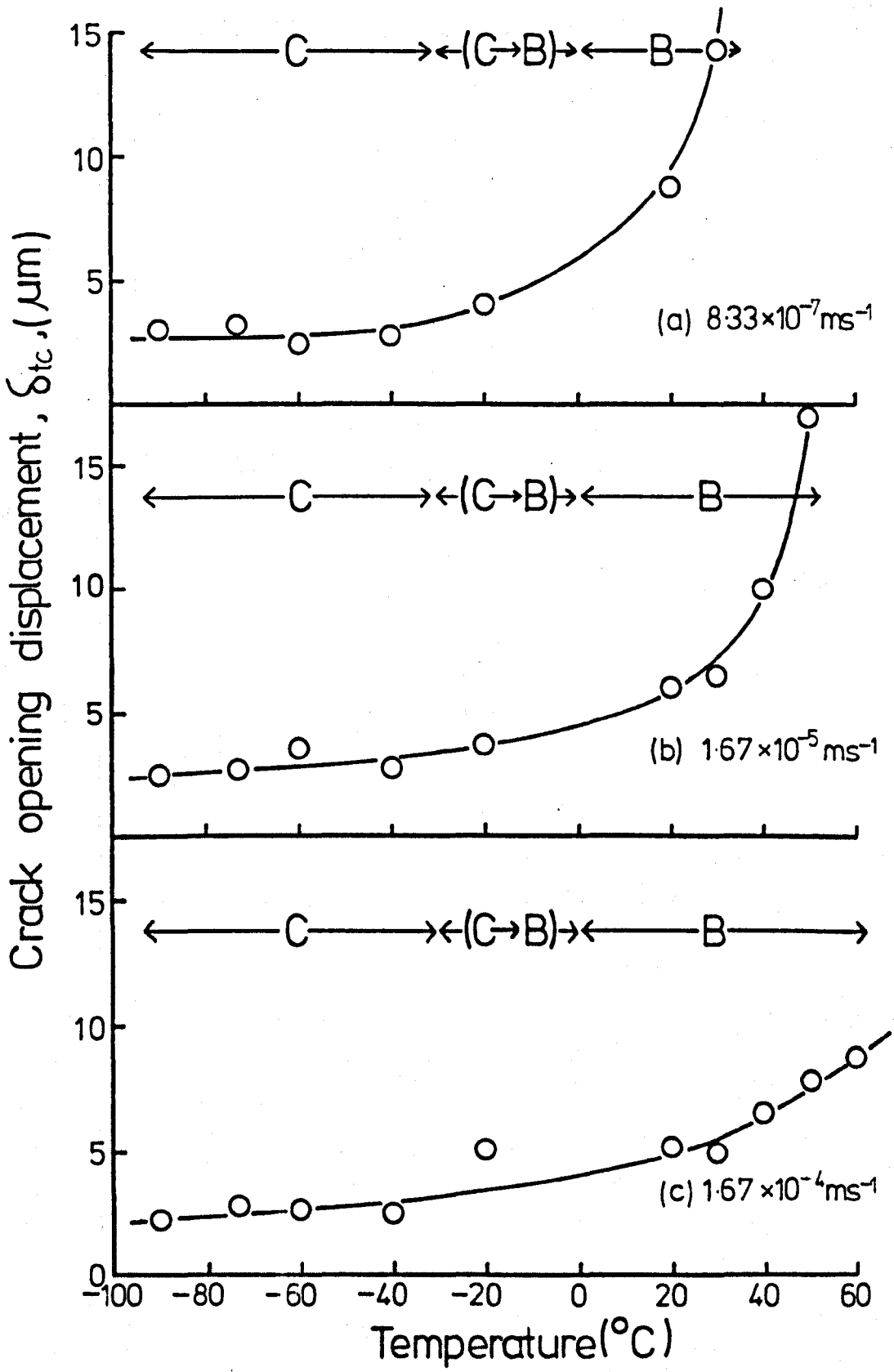

Figure 9.1 Critical crack opening displacement, δ_{tc}, versus temperature. Unmodified epoxy.

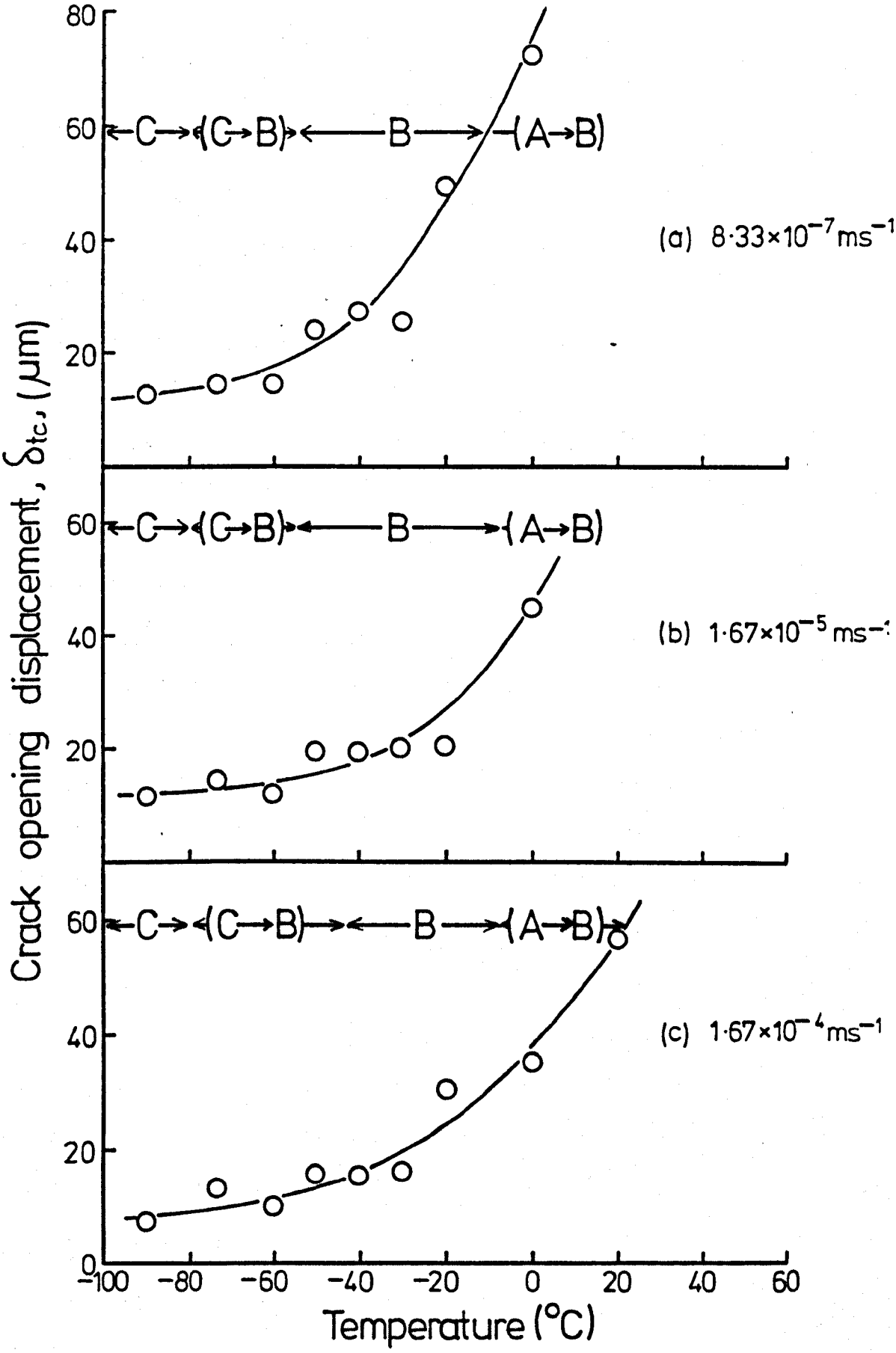

Figure 9.2 Critical crack opening displacement, δ_{tc}, versus temperature. Rubber-modified epoxy.

fracture behaviour during this type of crack growth. With polymethyl methacrylate this difference may be due to a different energy dissipating mechanism being operative. With this polymer, crazing at the crack tip occurs (44, 46) whereas localised shear yielding is the dominant mechanism with the present epoxy systems. The apparent differences in behaviour between the present and previously studied epoxies cannot be attributed to differences in mechanism. In this case it seems possible that the difference may be non-existent. In the previous studies (38) a far more limited temperature range was employed. Thus any small variation in the value of δ_{tc} could have been obscured by experimental scatter.

Secondly, δ_{tc} increases with increasing temperature and decreasing rate. This implies a steadily increasing degree of localised plastic deformation at the crack tip and associated crack tip blunting, as the temperature is increased or rate decreased. This would clearly be associated with a reduction in the material's yield stress. Accompanying this gradually increased degree of crack tip blunting are the transitions in crack growth from type C to type B to type A.

These observations clearly indicate a correlation between fracture behaviour and crack tip blunting resulting from the viscoelastic yield characteristics of the materials. Thus it is of interest to consider this correlation in greater detail.

9.3.2 Crack tip blunting

(a) Correlation between fracture and yield behaviour

The concept of crack tip blunting influencing both toughness and crack growth characteristics was initially proposed by Gledhill et al (38). They demonstrated that if a resin had a high yield stress then crack propagation was brittle, stable, whereas a low

yield stress generally produced stick/slip, unstable propagation with a corresponding increase in fracture toughness. In this work, the transition from stable, type C to unstable, type B through to type A growth was generally brought about by combinations of increasing temperature and decreasing rate ie the conditions which would produce reductions in yield stress. Thus there exists a relationship between the fracture behaviour and yield characteristics of the two epoxy materials studied.

This relationship is expressed more quantitatively in Figures 9.3 and 9.4, which show K_{Ic} as a function of σ_{yt} for both systems. As indicated, the data falls upon a mastercurve, suggesting in each case a unique relationship between fracture toughness, K_{Ic} and yield stress, σ_{yt}. Similar correlations have been observed by Yamini and Young (118) for various epoxy resin formulations tested at a variety of rates and temperatures and also by Kinloch and Williams (119) for a series of resins crosslinked with different curing agents (some of which were taken from this investigation).

The manner in which δ_{tc} varies with both temperature and rate indicates that the variations in yield behaviour are manifested in crack tip blunting. Such blunting would decrease the local stress concentrations at a crack tip and thus higher applied loads would be required to cause failure. At low temperatures, yield stress would be high and thus crack initiation would involve a comparatively small degree of crack tip yielding. Resultant crack tip blunting would be small, the crack relatively sharp and thus fracture toughness low. As temperature is increased (or testing rate decreased) the yield stress would decline and thus a greater degree of crack tip yielding would occur with greater crack tip blunting. This would result in a higher value of K_{Ic} and a tendency towards unstable crack growth.

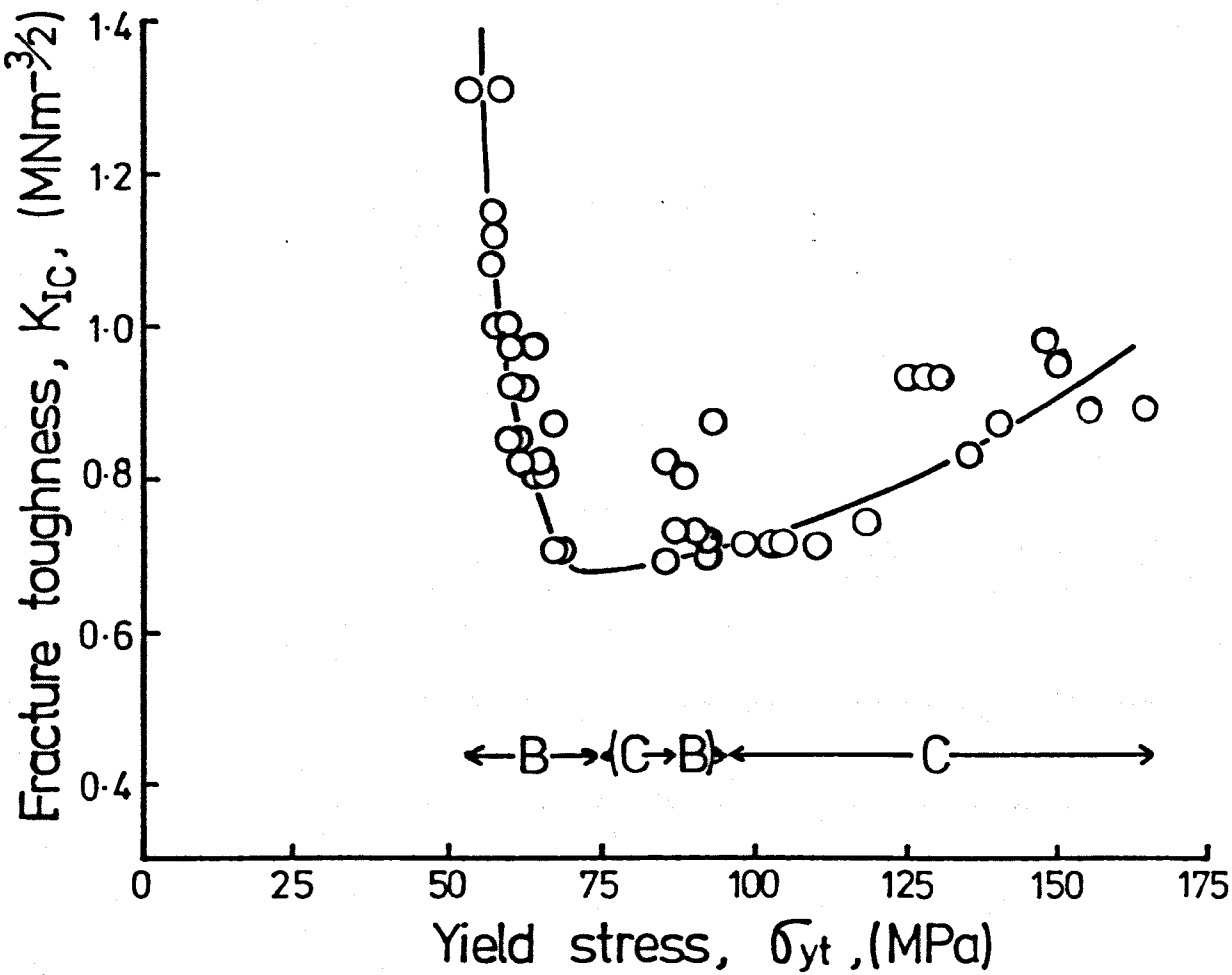

Figure 9.3 Fracture toughness, K_{IC}, versus true tensile yield stress, σ_{yt}. 5·8mm thick specimens tested at various temperatures and rates. Unmodified epoxy.

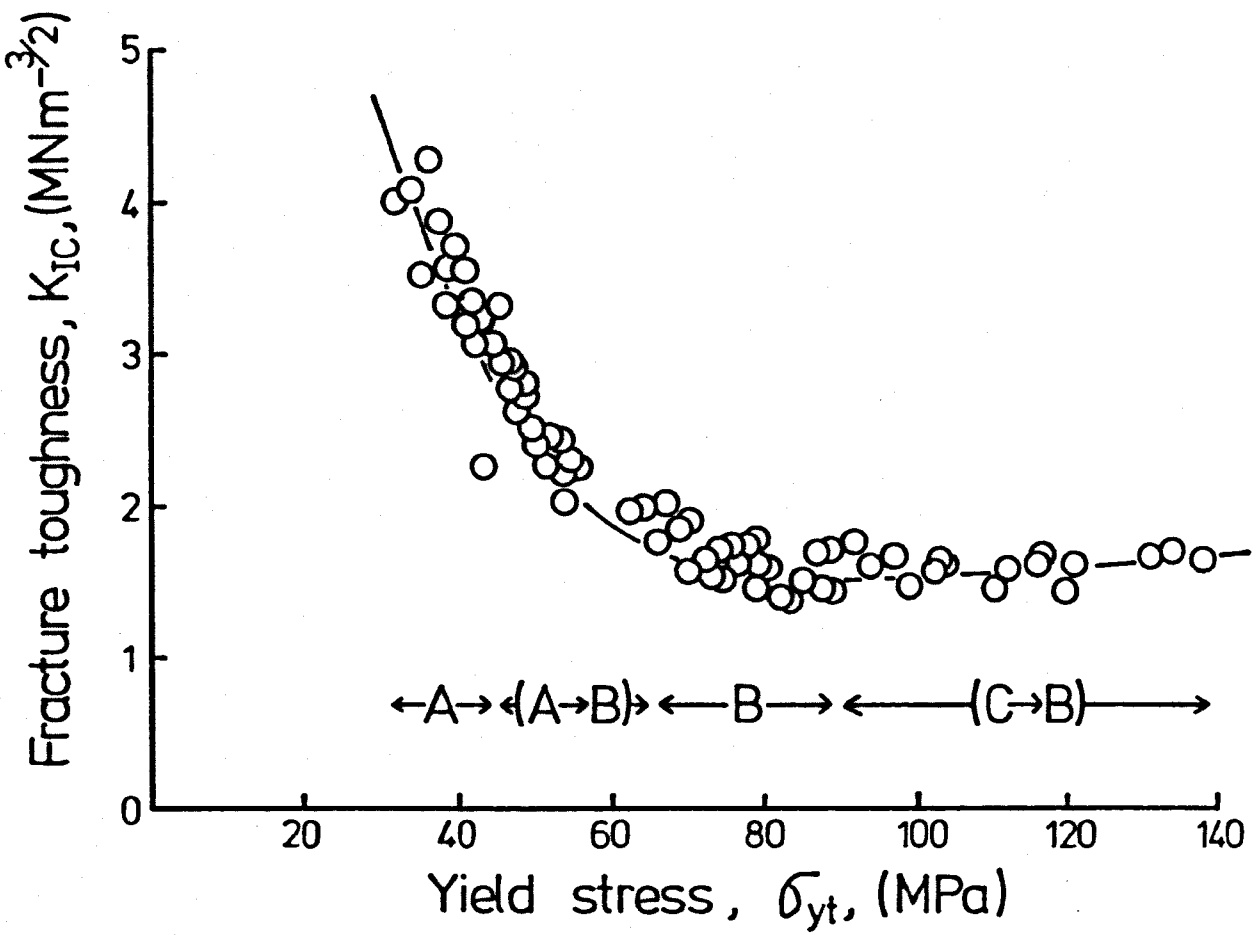

Figure 9.4 Fracture toughness, K_{IC}, versus true tensile yield stress, σ_{yt}. 5·8mm thick specimens tested at various temperatures and rates. Rubber–modified epoxy.

These arguments can explain some previously observed effects regarding static fatigue and high humidity/water exposure on epoxy resins. Gledhill et al (60) have shown that the application of a constant load just below the short term fracture load, can cause both an increase in toughness and a change from stable to unstable crack growth on subsequent testing of a specimen. Furthermore an increase in duration of the constant load was shown to produce a gradually increasing toughness. Also Yamini and Young (37) have shown that the presence of water in the vicinity of a crack tip with epoxy resin specimens has a similar effect to static fatigue loading. These effects can be explained simply in terms of the above arguments. Such conditions would be expected to increase the ability of the material to undergo relatively greater deformation in the vicinity of the crack tip. This would be due to a reduction in strain rate or plasticisation respectively, both of which would reduce yield stress.

(b) Theoretical considerations of crack tip blunting

So far, a relationship between toughness/crack growth characteristics and yield characteristics has been demonstrated and discussed. Furthermore it is clear that variations in yield behaviour, resulting from changes in temperature and rate, are manifested in crack tip blunting to a greater or lesser degree. In the light of these observations it is of interest to examine models which combine yield behaviour with various failure criteria to see if any such theory can adequately describe the fracture data obtained for the current epoxy systems.

Kinloch and Williams (119) have developed such a model based upon the stress distribution around a blunt crack. They showed that, for a crack tip radius, ρ, and length, a, the stress σ_{11} normal to the axis of the crack at a small distance, r, ahead of the tip is given by,

$$\sigma_{11} = \frac{\sigma_o\sqrt{a}}{\sqrt{(2r)}} \frac{(1 + \rho/r)}{(1 + \rho/2r)^{3/2}} \qquad (9.3)$$

where σ_o is the applied stress. They proposed a failure criterion based upon the premise that fracture occurs when a critical stress, σ_{tc}, is reached at a distance r = c. Thus equation 9.3 can be rearranged to,

$$\sigma_{tc} = \frac{\sigma_o\sqrt{a}}{\sqrt{(2c)}} \frac{(1 + \rho/c)}{(1 + \rho/2c)^{3/2}} \qquad (9.4)$$

The experimentally determined value of the stress intensity factor, K_{Ic}, can be related to the applied stress, σ_o, by,

$$K_{Ic} = \sigma_o \sqrt{(\pi a)} \qquad (9.5)$$

whereas the propagation of a 'sharp' crack at a value of K_{Ics} may be interpreted as requiring the critical stress, σ_{tc}, to be attained at the distance, c, such that,

$$K_{Ics} = \sigma_{tc} \sqrt{(2\pi c)} \qquad (9.6)$$

Thus, rearrangement of equation 9.4 produces,

$$\frac{\sigma_o \sqrt{(\pi a)}}{\sigma_{tc} \sqrt{(2\pi c)}} = \frac{(1 + \rho/2c)^{3/2}}{(1 + \rho/c)} \qquad (9.7)$$

Substituting for equation 9.5 and 9.6 yields,

$$\frac{K_{Ic}}{K_{Ics}} = \frac{(1 + \rho/2c)^{3/2}}{(1 + \rho/c)} \qquad (9.8)$$

As indicated, equation 9.8 relates the ratio K_{Ic}/K_{Ics} to the radius of a blunt crack, ρ, by assuming a failure criterion based upon the attainment of a critical stress acting over a critical distance ahead of the crack tip. Furthermore this equation indicates

the same general trends with regard to both rate and temperature dependence that were used successfully in the yield stress discussion to explain qualitatively the observed fracture behaviour.

(c) Quantitative description of fracture data

In order to test the validity of this expression and determine its ability to provide a quantitative description of the fracture data, it is necessary to obtain values of crack tip radius, ρ. Direct measurement of ρ is difficult for naturally blunted cracks, where radii in the vicinity of 10 μm and less are commonly encountered. It was therefore considered necessary to conduct experiments with specimens containing cracks of know tip radii. These were conducted on 5.8 mm thick compact tension specimens. Blunt crack tips were formed by drilling holes at the ends of saw-cuts, which were inserted in the specimens in the manner described in Chapter 6. Various drill sizes were employed so as to cover a radius range of approximately 190 to 750 μm. The results obtained are shown as filled circles in Figures 9.5 and 9.6 as plots of K_{Ic}/K_{Ics} .v. $\rho^{\frac{1}{2}}$. K_{Ics} was assigned values of 0.85 $MNm^{-3/2}$ and 1.60 $MNm^{-3/2}$ for the unmodified and rubber-modified epoxies respectively. These were considered representative of low temperature results and thus equivalent to a 'sharp' crack. Also shown are the results (open circles) taken from the data given in Chapter 7, where self-blunting of the crack tips had occurred. In this case ρ was not measured directly. An estimate was calculated using equation 9.2 together with equation 9.9

$$\rho = k\delta_{tc} \qquad (9.9)$$

where k is a proportionality constant relating ρ to δ_{tc}. The value of k was taken to be unity since a recent theoretical analysis by McMeeking (120) has indicated that the value of ρ may be taken to be equivalent to crack opening displacement, δ_{tc}.

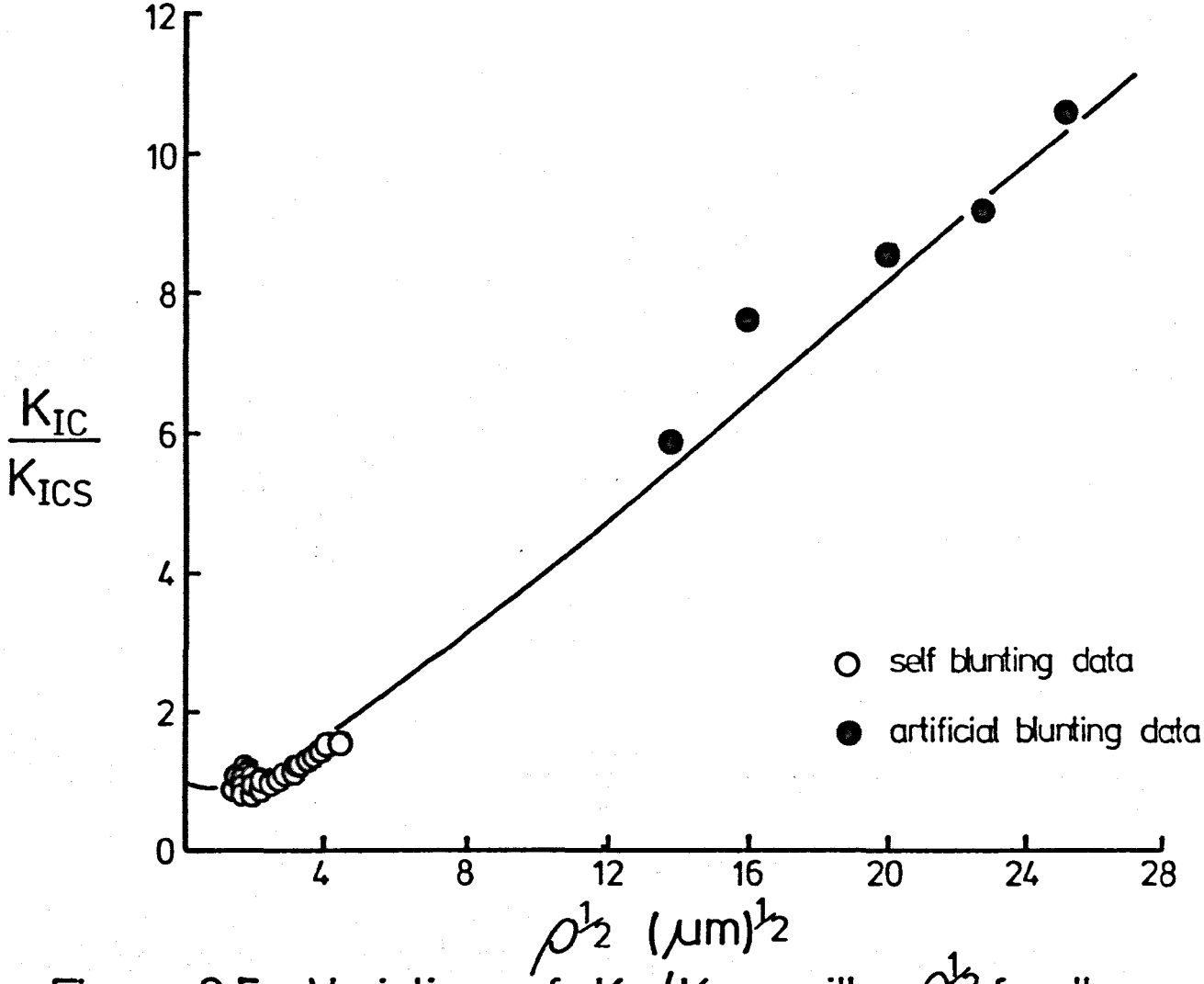

Figure 9.5 Variation of K_{IC}/K_{ICS} with $\rho^{1/2}$ for the unmodified epoxy. Line is theoretical curve from equation 9.8.

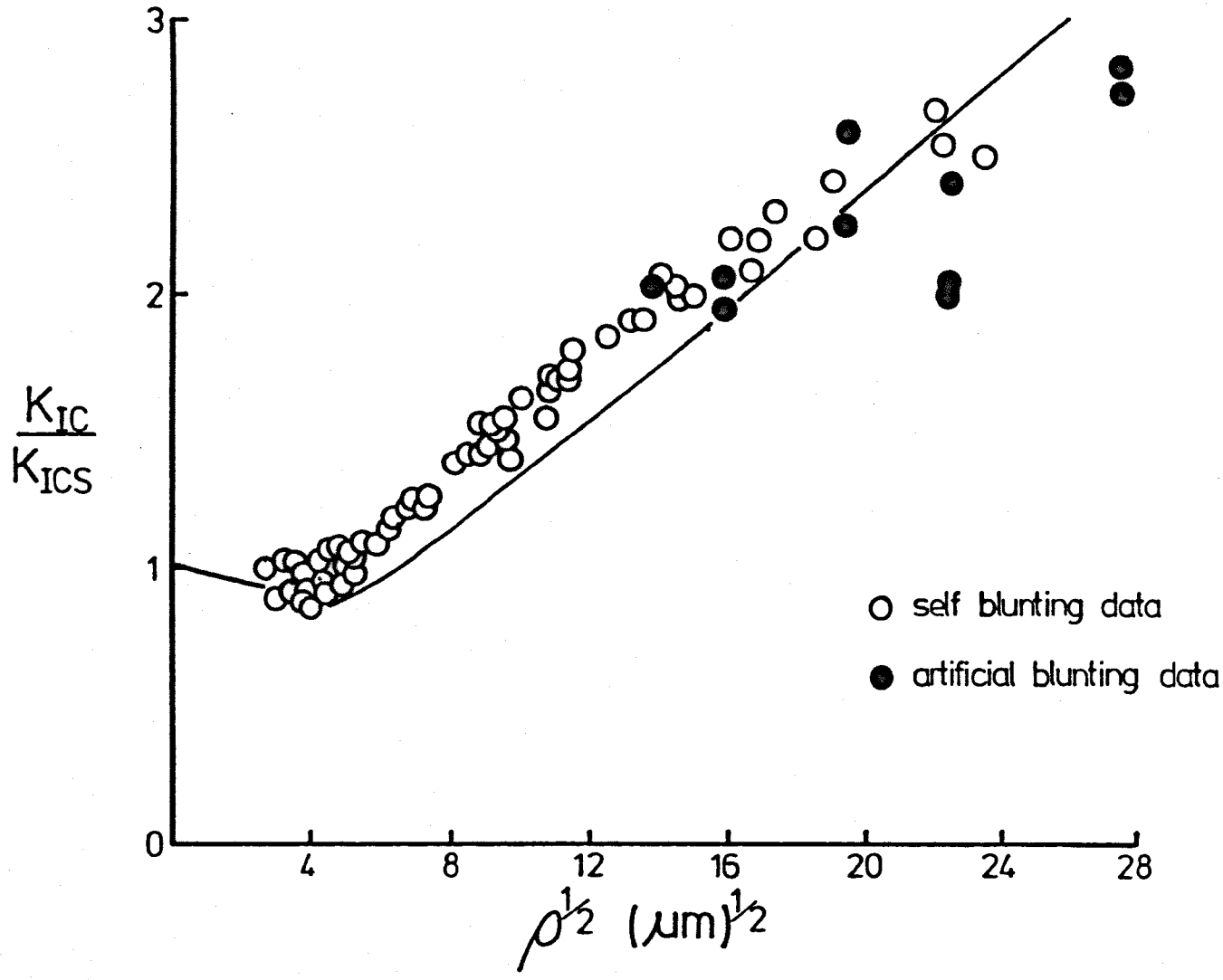

Figure 9.6 Variation of K_{IC}/K_{ICS} with $\rho^{1/2}$ for the rubber-modified epoxy. Line is theoretical curve from equation 9.8.

The solid lines in Figures 9.5 and 9.6 are the theoretical curves based on equation 9.8. They were fitted to both sets of experimental data by choosing values for c of 0.8 μm and 10 μm for the unmodified and rubber-modified epoxies respecitvely. As shown, for both systems, reasonable agreement is demonstrated firstly between the results obtained from both types of experimentally induced blunting and secondly between the experimental data and theoretical relations.

(d) Failure criterion

Figures 9.5 and 9.6 indicate that equations 9.2 and 9.8 provide a quantitative description of fracture toughness, K_{Ic}, based upon knowledge of σ_{yt}, e_y and two adjustable parameters, c and K_{Ics} (or σ_{tc}). Values of σ_{tc}, calculated from equation 9.6 using the known values of K_{Ics} and c, were 379 MPa and 200 MPa for the unmodified and rubber-modified epoxies respectively.

Since the σ_{tc} and c parameters are constants for each material, they can be considered as providing unique failure criteria over the whole range of conditions investigated.

The values of σ_{tc} and c obtained for both epoxy systems are compared with data obtained from other unmodified epoxy formulations in Table 9.3. These data are further demonstrated in Figure 9.7 which shows a linear inverse relationship between the two parameters when plotted on logarithmic axes. As indicated, the data for the present epoxy systems fit into the general trend reasonably well with the toughest materials having the lowest critical stresses but the longest critical distances.

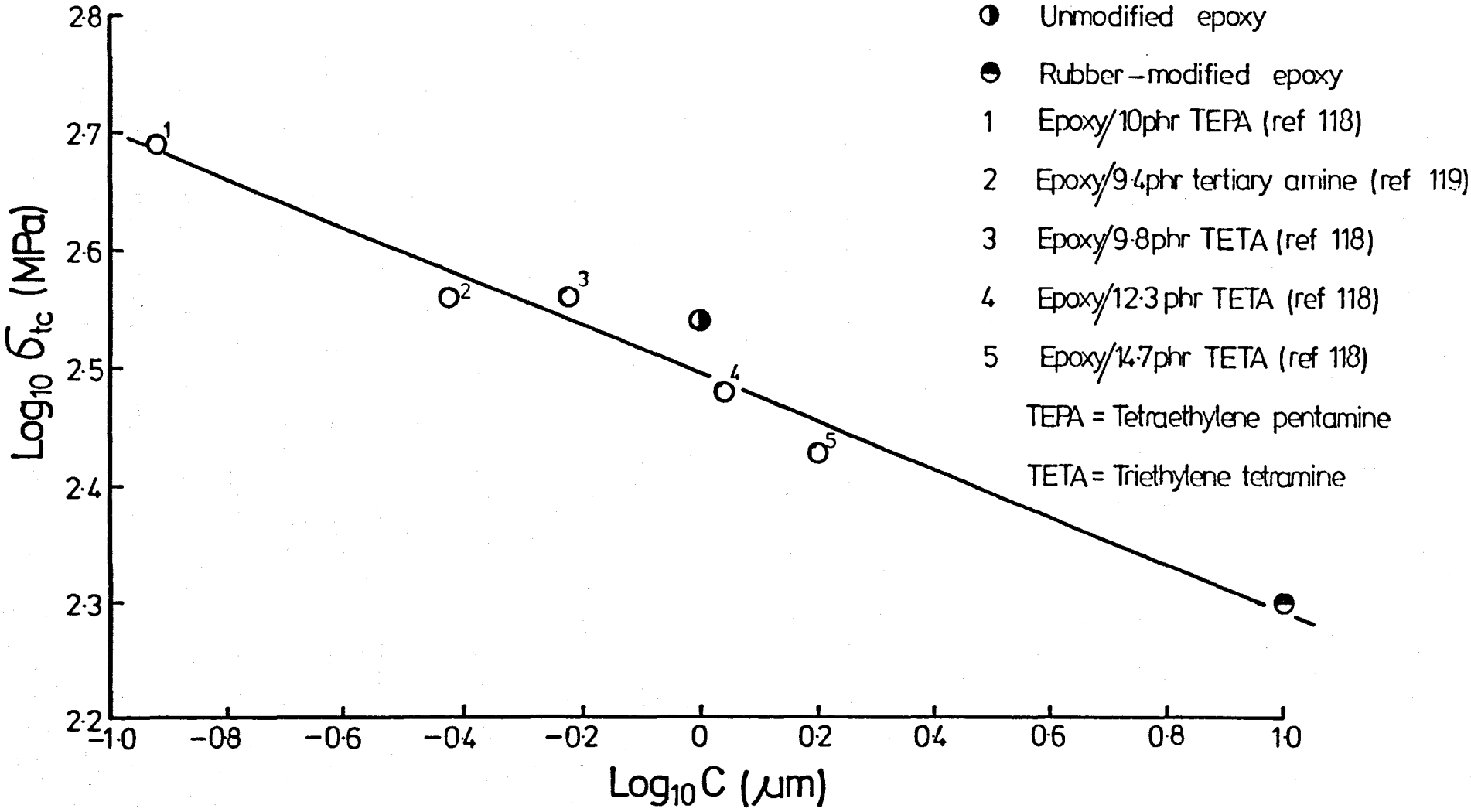

Figure 9.7 Critical stress, σ_{tc}, versus critical distance, c, for a range of epoxy resin formulations.

TABLE 9.3

Values of critical stress, σ_{tc}, and critical distance, c, for various epoxy formulations

Formulation	σ_{tc} (MPa)	c (μm)	Ref
9.8 phr TETA	360	0.60	118
12.3 phr TETA	300	1.10	118
14.7 phr TETA	270	1.60	118
9.4 phr 3° Amine	360	0.38	119
10 phr TEPA	495	0.12	119
5 phr Piperidine	379	0.80	This work
5 phr Piperidine 15 phr CTBN	200	10.00	This work

Although these two constants are fitting parameters which provide a reasonable first-order fit of the fracture data over a wide range of conditions, it is of interest to speculate on their physical significance. It has been proposed that, since the values obtained for σ_{tc} are significantly greater than the uniaxial tensile yield stress, σ_{yt}, then σ_{tc} can be considered as a constrained yield stress (51). Table 9.4 shows values of the ratio σ_{tc}/σ_{yt} for both epoxy systems as a function of temperature. As indicated an increase in temperature increases σ_{tc}/σ_{yt} quite considerably with maximum values of approximately 7.2 and 5.5 for the unmodified and rubber-modified epoxies respecitvely. These ratios are far in excess of the stress intensificiation which would be expected from a consideration of plastic constraint factors under plane strain conditions 19). In such cases a maximum stress within the plastic zone of approximately three times the uniaxial tensile stress would be expected. The values of σ_{tc} obtained in this investigation are in reasonable agreement with analyses of crack tip stress distributions obtained from several studies (120-123). In particular McMeeking (120) and Ritchie et al (123) has

demonstrated that with certain metals, enhanced stress intensification only occurs with materials exhibiting post-yield strain hardening. Materials which did not show this behaviour exhibited maximum crack tip stresses of approximately three times the tensile yield stress ie the theoretically expected value.

TABLE 9.4

σ_{tc}/σ_{yt} values for both epoxy systems as a function of temperature

Temperature (°C)	σ_{tc}/σ_{yt}	
	Rubber-modified	Unmodified
-60	1.9	3.0
-40	2.4	3.7
-20	2.8	4.4
20	4.0	6.1
30	4.2	6.3
40	4.7	6.6
50	4.9	6.7
60	5.5	7.2

The present epoxy systems were shown to exhibit post-yield strain hardening tendencies and thus it is reasonable to attribute the high σ_{tc}/σ_{yt} values to an effect of this type.

One problem which arises from these findings is an apparent paradox between the toughening mechanism previously proposed for the rubber-modified epoxy and the high degrees of stress intensification indicated by the σ_{tc}/σ_{yt} values. The toughening mechanism proposed two main deformation processes, one being rubber particle cavitation which leads to a relief of triaxiality within the epoxy matrix. This would lead to a reduction in stress in the vicinity of the crack tip which is clearly in complete contrast to the high σ_{tc} values obtained. It seems likely that this may simply be associated with differences

in size between the critical distance over which σ_{tc} acts and the crack tip plastic zone. Plastic zone sizes with the rubber-modified epoxy would generally be substantially greater than the critical distance zones. Thus the critical distance zone, over which substantial stress intensification exists, would occupy only a small proportion of the plastic zone, the remainder experiencing a much reduced degree of stress intensification. Thus, from this albeit qualitative argument, the toughening mechanism and failure criteria proposed would not be in conflict.

Although some degree of physical interpretation is possible with the critical stress, σ_{tc}, the significance of the critical distance term, c, is obscure. Detailed fractographic studies here have shown that it does not correlate with any observable microstructural features. Indeed Knott and co-workers (123, 124) have suggested that the most satisfactory interpretation of c may be simply statistical in nature, based on the probability of there existing a weak region ahead of the crack which can act as a site for microcrack initiation. Clearly more effort is needed to clarify further the physical significance of the critical distance parameter.

Finally it is of interest to note that this critical stress/critical distance criterion applies even at relatively low temperatures where indications of stable, type C propagation exist and where, as stated earlier, the constant crack opening displacement criterion appears not to apply.

9.4 The Unmodified Epoxy Tough/Brittle Transition

Probably one of the most obvious differences in the fracture behaviour of the unmodified and rubber-modified epoxies was the sharp tough/brittle transitions exhibited by the unmodified epoxy, but not in the rubber-modified epoxy. As discussed above, the value

of K_{Ic} for the rubber-modified epoxy was usually greater than for the unmodified epoxy. However when the unmodified material underwent the transition to ductile behaviour this was not necessarily the case. This transitional behaviour is considered in this section.

9.4.1 General observations

The tough/brittle transitions observed with the unmodified epoxy were found to be dependent upon the three experimental variables studied, namely rate, temperature and specimen thickness.

Tough/brittle transitions have received attention in the literature (13, 20, 125-128). Irwin (128) has argued that tough/brittle transitions are associated with a relationship between specimen thickness, H, and plane stress plastic zone radius, r_{y2}. Specifically he proposed from experimental observations that when $H < 4\ r_{y2}$, tough, ductile characteristics would occur since insufficient material would exist under constraint in the central regions of a specimen to give a plane strain contribution to toughness and vice versa.

The fracture toughness - specimen thickness relationship, previously discussed in Chapter 7 and demonstrated in Figure 7.13 is, in many respects, similar to that typically observed with a range of polymers (127, 129-133). This typical relationship was depicted schematically in Figure 3.7 of Chapter 3, where it was shown that the value of K_{Ic} under plane strain conditions was less than under plane stress. This can be attributed to the yield stress under triaxial stress conditions being greater than in plane stress where biaxial stress exists. Thus in the former case a more limited degree of plasticity would develop and thus a comparatively lower value of K_{Ic} would result. The one major difference between the K_{Ic}-thickness trend observed with the present unmodified epoxy and that

observed by others using a range of polymeric materials, is the very sharp transition observed. Such sharp transitions have not been reported previously with any other polymers.

9.4.2 Theoretical models

With many of the above mentioned specimen thickness studies the K_{Ic}-thickness dependence has been explained quantitatively in terms of a bimodal model based on plane stress, K_{c2}, and plane strain, K_{c1}, fracture toughness values (127, 129, 131, 133). The model is based upon the premise that the apparent fracture toughness of a material K_{Ic}, consists of contributions from both K_{c1} and K_{c2}. The plane stress behaviour will clearly be localised near the free surface of the specimen. In many of the studies this behaviour has been assumed to extend into the specimen for a distance comparable to the plane stress plastic zone radius, r_{y2}, given by,

$$r_{y2} = \frac{1}{2\pi} \left(\frac{K_{c2}}{\sigma_{yt}}\right)^2 \qquad (9.10)$$

where σ_{yt} is the uniaxial tensile yield stress under the appropriate experimental conditions. The apparent fracture toughness, K_{Ic}, is given by,

$$K_{Ic} = \left(\frac{H - 2r_{y2}}{H}\right) K_{c1} + \frac{2r_{y2}}{H} K_{c2} \qquad (9.11)$$

where H is specimen thickness.

Substituting for r_{y2} from equation 9.10 into 9.11 gives,

$$K_{Ic} = K_{c1} + \frac{K_{c2}^2 (K_{c2} - K_{c1})}{\pi \sigma_{yt}^2 H} \qquad (9.12)$$

Thus experimentally measuring two values of K_{Ic} (K_{Ic}' and K_{Ic}'') at two different thicknesses, H_1 and H_2, enables simultaneous

equations based upon equation 9.12 to be established and solved to yield values of K_{c1} and K_{c2}.

As stated above, the K_{Ic}-thickness relationship obtained with the present unmodified epoxy exhibited sharp transitional effects, which has not been reported for the other polymeric systems. However it is of interest to apply the bimodal analysis to the present data and see whether the transitions are controlled by an H/r_{y2} criterion.

Clearly what are needed are values of K_{c2} from which r_{y2} can be calculated using equation 9.10. With the unmodified epoxy, four specimen thicknesses were studied, of which three, 2.3, 5.8 and 49 mm, exhibited brittle, type B fracture. The 1.3 mm specimens exhibited tough, ductile behaviour, at least at the start of the crack extension process, thus suggesting the attainment of essentially plane stress behaviour. Values of K_{c1} and K_{c2} can be determined using equation 9.12 for each of the three thickness pairs exhibiting type B crack growth. The results obtained are shown in Table 9.5 which indicate that the mean values of K_{c2} agree fairly closely with K_{Ic} for the 1.3 mm specimens.

9.4.3 Criterion for the transition

Values of r_{y2} calculated from equation 9.10, using the mean values of K_{c2} shown in Table 9.5, are given in Table 9.6. A simple calculation provides values for the ratio H/r_{y2} for the tough/brittle transition region (1.3 to 2.3 mm thickness). The ratio range is shown in Figure 9.8 as a function of the three displacement rates employed. If it is assumed that a potential critical H/r_{y2} ratio is independent of rate, then a common ratio of approximately 10 would appear to exist. This suggests that the transition occurs when the plane stress zones occupy approximately 20% of the specimen thickness.

TABLE 9.5

Values of K_{c1} and K_{c2} obtained from three specimen thickness pairs. Unmodified epoxy

Rate (ms^{-1})	K_{c1} and K_{c2} ($MN\ m^{-3/2}$)							
	2.3/5.8 mm		2.3/49 mm		5.8/49 mm			
	K_{c1}	K_{c2}	K_{c1}	K_{c2}	K_{c1}	K_{c2}	K_{c1}	K_{c2}
8.33×10^{-7}	0.84	2.00	0.74	2.14	0.73	2.53	$\bar{x} = 0.77$ $\sigma = 0.06$	$\bar{x} = 2.22$ $\sigma = 0.27$
1.67×10^{-5}	-	-	0.71	1.90	0.71	2.15	$\bar{x} = 0.71$ $\sigma = 0$	$\bar{x} = 2.03$ $\sigma = 0.18$
1.67×10^{-4}	0.70	1.47	0.64	1.98	0.64	2.15	$\bar{x} = 0.66$ $\sigma = 0.03$	$\bar{x} = 1.87$ $\sigma = 0.35$

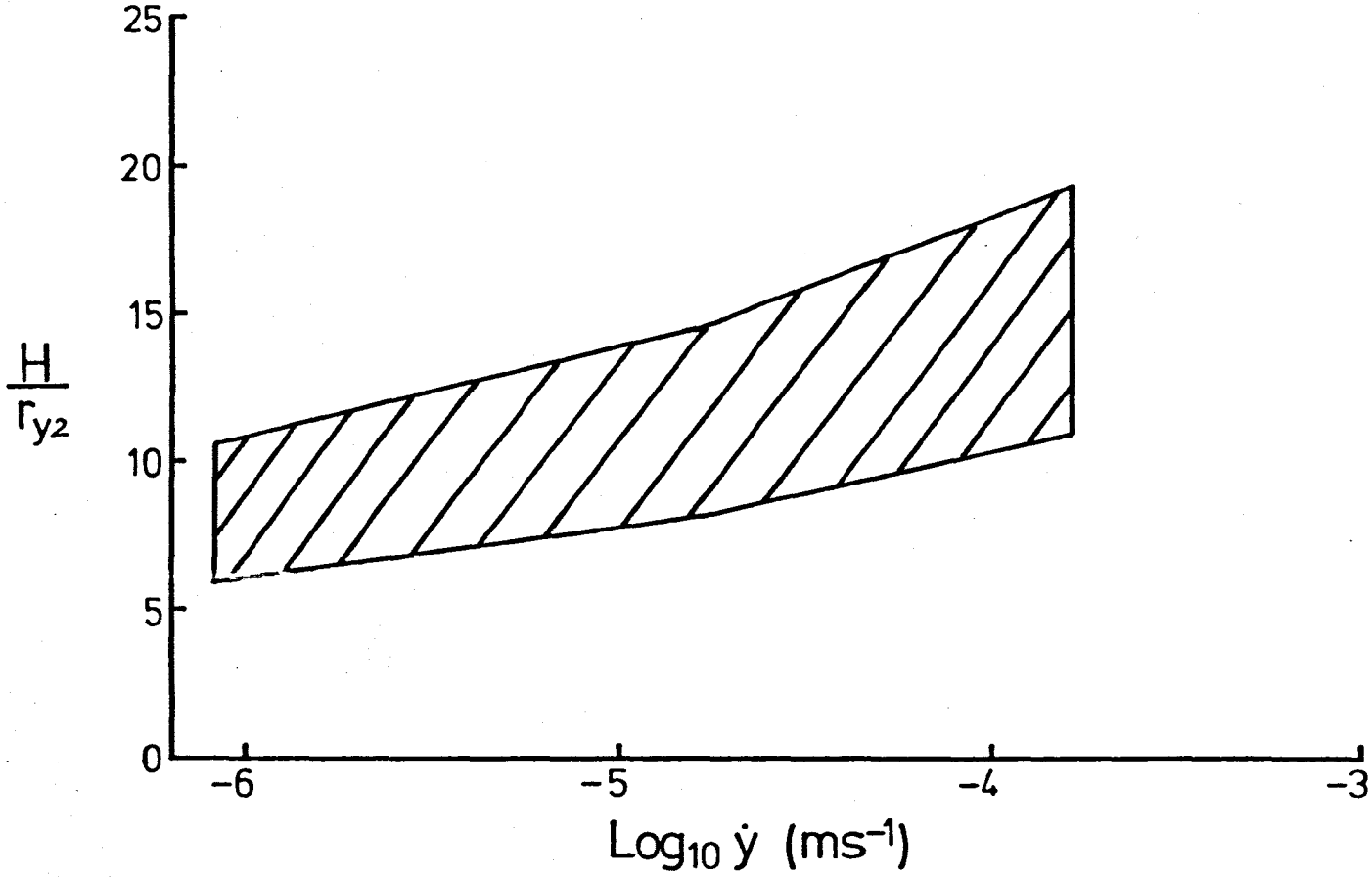

Figure 9.8 Specimen thickness/ plane stress plastic zone size ratio, H/r_{y2}, versus displacement rate, $\dot{y}$, for the unmodified epoxy. 20°C.

TABLE 9.6

Plane stress plastic zone radii, r_{y2}. Unmodified epoxy

Rate (ms^{-1})	σ_{yt} (MPa)	K_{c2} ($MN\ m^{-3/2}$)	r_{y2} (mm)
8.33×10^{-7}	60.2	2.22	0.22
1.67×10^{-5}	64.5	2.03	0.16
1.67×10^{-4}	68.0	1.87	0.12

It is not possible to apply this model to the rate and temperature dependent transitional data obtained from 5.8 mm thick specimens for two reasons. Firstly this would require values of K_{Ic} for at least two specimen thicknesses over the range of temperatures and rates employed. These values are not available. Secondly it is doubtful whether this extra data would be of use. The K_{Ic} results obtained from the tough side of the transition would almost certainly be invalid due to the high levels of ductility obtained. Thus values of K_{c1} and K_{c2} for the brittle regime only, could be calculated and therefore only one side of the transition characterised in terms of H/r_{y2}.

A value of approximately 10 for the critical H/r_{y2} value is substantially greater than would be expected theoretically. The reasons for this are at present unknown. However it is of interest to speculate on some potential causes. These are:

(i) Figure 7.13, Chapter 7, from which the critical H/r_{y2} values were originally determined, showed K_{Ic} values varying only by 10 to 35% over a thickness range of 2.3 to 49 mm. Such small variations in K_{Ic} over this thickness range indicate a potential complication from experimental scatter. This would be particularly true

of the 10% variations obtained at the slowest rate. However the 35% reduction obtained at the fastest rate, together with the observations that, throughout the experiments, K_{Ic} never increased with thickness, suggests that the trends obtained are real.

(ii) The potential effects of thickness on other factors which could have influenced toughness other than plane stress/plane strain effects needs consideration. With thermosetting polymers, the generation of an exotherm during the crosslinking reaction can give rise to significant variations in temperature through the thickness of a casting, such as was used in this work. The maximum temperature obtained would clearly depend upon thickness and the reactivity of the system; large thicknesses and highly reactive systems producing the highest temperatures. The curing agent employed in this work, piperidine, is generally regarded as being relatively immune from serious exothermic effects. No attempt was made to measure experimentally the actual temperature in the casting. However an attempt was made to determine the effects of any exotherm during cure on the fracture toughness by sectioning two 49 mm compact tension specimens into five, 6 mm thick specimens. The resultant specimens were tested at 20°C as described in Chapter 6. The results obtained indicated no significant variation of K_{Ic} with location in the original 49 mm specimens. Thus, from these admittedly very limited experiments, it would appear that exothermic effects had no major influence on K_{Ic}.

(iii) It is necessary to examine briefly the previous assumption that the extent of the plane stress contribution to toughness can be equated with the plane stress plastic zone size given by equation 9.10. A major problem frequently encountered with polymers is that, although fracture toughness is often found to vary with specimen thickness, indicating a plane stress contribution to the fracture process, features such as shear lips are rarely observed. On the rare occasions where they have been detected, for example certain grades of polycarbonate (130, 132), shear lip sizes have been significantly smaller than the plane stress plastic zone sizes calculated from equation 9.10. Recently Yap and co-workers (134) have suggested that equation 9.13 more adequately describes the extent of plane stress penetration into the thickness of a specimen,

$$r_{y2} = \frac{1}{2\pi}\left(\frac{K_{Ic}}{\sigma_{yt}}\right)^2 \qquad (9.13)$$

where K_{Ic} is the experimentally measured fracture toughness. This equation clearly indicates that, since K_{Ic} will be thickness dependent, then r_{y2} will also vary with specimen thickness. Although it is claimed that equation 9.13 provides values of r_{y2} which agree more closely with observed shear lip sizes (134), there is no theoretical justification for relating r_{y2} to K_{Ic}.

Thus, although relating a calculated value or r_{y2} from equation 9.10 with the plane stress contribution may seem intuitively reasonable, there is clearly some doubt to its validity. Thus the H/r_{y2} value of 10 previously quoted must be open to doubt.

9.4.4 Unmodified .v. Rubber-modified epoxy

Since the unmodified epoxy exhibits such sharp transitional effects it is particularly intriguing that the addition of just a small amount of rubber should almost completely erase these characteristics. It seems that a likely explanation is associated with the toughening mechanism proposed in section 9.2.2 of this Chapter. This mechanism was based upon two basic deformation processes ie rubber particle cavitation and plastic shear flow of the matrix. It was proposed that cavitation and void formation within the rubber particles reduces constraint on the matrix adjacent to the particles consequently allowing the local build-up of triaxiality to be relieved. This means that the matrix would never experience simple plane stress or plane strain deformation under virtually any conditions but rather a combination of the two. This complex stress state would (i) remain essentially constant across the specimen thickness and (ii) vary only gradually with rate and temperature conditions. Thus a tough/brittle transition dependent upon a plane stress/plane strain transition would not be expected.

9.5 Summary

(i) A toughening mechanism has been proposed which considers that the greater fracture toughness exhibited by the rubber-modified epoxy arises as a result of greater energy dissipating deformations occurring in the vicinity of the crack tip. Two basic deformation mechanisms are proposed, rubber particle cavitation and plastic shear yielding which, together with an interaction that occurs between them, magnifies the degree of shear yielding in the matrix. This results in a pronounced increase in plastic zone size and thus increased toughness.

(ii) The crack opening displacement at the onset of crack growth, δ_{tc}, increases with increasing temperature and decreasing rate for both systems. Little evidence for a constant δ_{tc} at low temperatures was apparent and thus does not appear to provide a unique failure criterion under any conditions.

(iii) A unique failure criterion based upon the attainment of a critical stress, σ_{tc}, that must be reached at a critical distance, c, ahead of the crack tip has been developed.

(iv) It is considered that the tough/brittle transition found with the unmodified epoxy systems results from a plane stress/plane strain transition. It is suggested that the absence of this effect with the rubber-modified epoxy is associated with the distinct difference in crack tip stress state which exists between the two systems.

CHAPTER TEN

ADHESIVE JOINT FRACTURE

10.1 Introduction

The major results obtained from investigations on the fracture of joints based upon the rubber-modified epoxy, which were previously given in Chapter 8, can be briefly summarised as follows,

(i) the adhesive fracture energy, G_{Ic}, is a function of bond thickness, t, with a maximum, G_{Icm}, occurring at a specific bond thickness, t_m,

(ii) variations in both displacement rate and adhesive joint width influence the specific values of both G_{Icm} and t_m,

(iii) crack tip plastic zone observations show that the stress-whitening at the crack tip is extended along the adhesive bond line.

This chapter will attempt to explain these observations and will be divided into six main sections. The first will deal with the adhesive bond thickness effect, where a model will be proposed to explain its occurrence. The next two sections will discuss the effects of displacement rate and joint width respectively. The next section will be concerned with failure criteria followed by a discussion of the comparisons between bulk and adhesive joint fracture. Finally, the last section summarises the main findings.

10.2 Adhesive Bond Thickness Effect

10.2.1 General model

As previously discussed in Chapter 8 and shown in Figure 8.1, adhesive bond thickness was found to have a significant effect on both fracture energy and crack propagation. The adhesive fracture energy was found to pass through a maximum value, G_{Icm}, at a certain bond

thickness, t_m. Furthermore, both G_{Icm} and t_m were dependent upon rate and joint width and both these factors will be discussed later in this chapter.

A similar bond thickness effect has been observed by Bascom and co-workers (28, 40) working on a similar rubber-modified epoxy adhesive. To interpret a maximum in fracture energy, they employed an elastic-plastic model for the deformation zone surrounding the crack tip. The basis of this model is shown schematically in Figure 10.1, where a crack is depicted in an adhesive layer between rigid substrates. At the tip of the crack is a plastic zone, the radius of which is given by,

$$r_{y1} = \frac{1}{6\pi}\left(\frac{K_{Ic}}{\sigma_{yt}}\right)^2 \frac{1}{(1-\nu^2)} = \frac{1}{6\pi}\frac{E_a G_{Ic}}{\sigma_{yt}^2}\frac{1}{(1-\nu^2)}$$

in plane strain (10.1)

$$r_{y2} = \frac{1}{2\pi}\left(\frac{K_{Ic}}{\sigma_{yt}}\right)^2 = \frac{1}{2\pi}\frac{E_a G_{Ic}}{\sigma_{yt}^2}$$

in plane stress (10.2)

where r_{y1} and r_{y2} are the plane strain and plane stress plastic zone radii respectively, E_a is the modulus of the adhesive, G_{Ic} is the fracture energy of bulk adhesive and σ_{yt} is the uniaxial tensile yield stress. Bascom and co-workers employed equation 10.1 and assumed the value of σ_{yt} to be the uniaxial tensile fracture stress, which they obtained from uniaxial tensile experiments. They showed that, at the fracture energy maximum, G_{Icm}, the plane strain plastic zone, $2r_{y1}$ was approximately equal to the bond thickness, t_m. Unfortunately uniaxial tensile tests suppress yielding and generally result in brittle failure, thus making it difficult to determine a yield stress. As described in Chapter 9, tensile yield stress, σ_{yt}, values were obtained from uniaxial compression tests by equation 10.3,

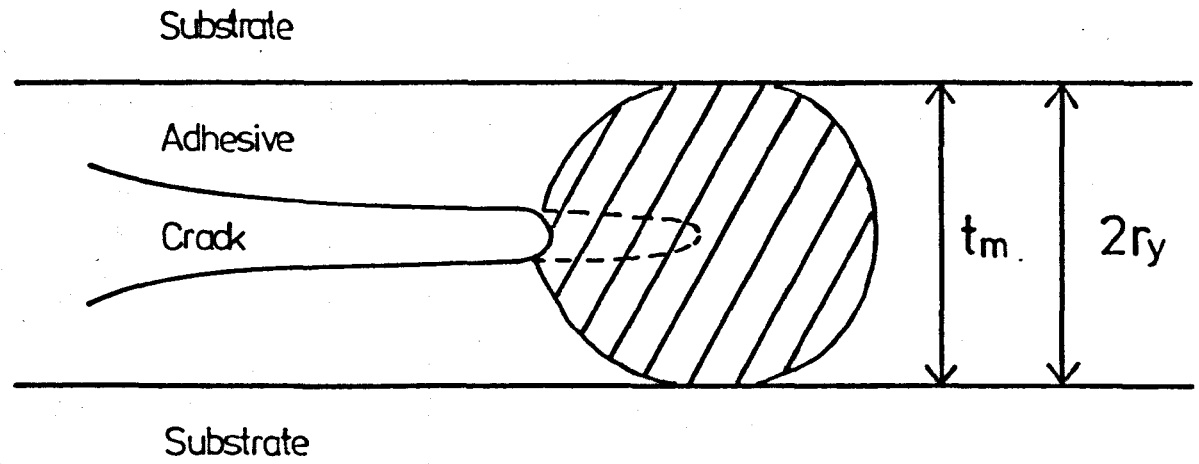

Figure 10.1 Simple elastic–plastic model for the deformation zone at a crack tip in an adhesive layer.

$$\sigma_{yt} = 0.75\ \sigma_{yc} \qquad (10.3)$$

where σ_{yc} is the uniaxial compressive yield stress.

The values of both $2r_{y1}$ and $2r_{y2}$ calculated from equations 10.1 and 10.2, using σ_{yt} values, are shown, together with the value of t_m obtained from Figure 8.1, in Table 10.1. The value of G_{Ic} used in these calculations was obtained by interpolating a value of K_{Ic} (and hence G_{Ic}) from the bulk data for a specimen thickness of 12 mm from Figure 7.14 Chapter 7. As indicated, the correlation between t_m and $2r_{y2}$ is excellent and thus supports the proposal of Bascom and co-workers, although via a slightly modified argument.

TABLE 10.1

Comparison of adhesive bond thickness, t_m, at maximum fracture energy, G_{Icm}, and the plane-stress and plane-strain plastic-zone diameters

Temp (°C)	$\text{Log}_{10}\dot{\gamma}$ (ms^{-1})	Joint Width (mm)	t_m (mm)	$2r_{y1}$ (mm)	$2r_{y2}$ (mm)
20	-6.08	12	1.04	0.40	1.02

Certain aspects of the fracture energy-bond thickness relationship can be explained in terms of this plastic zone-bond thickness equivalence model. The decline in G_{Ic} at $t < t_m$ can be described in terms of plastic zone restriction. The presence of the high modulus substrates will restrict full development of the plastic zone. Since toughness is mainly derived from the energy dissipated in forming this zone, then clearly adhesive G_{Ic} will be steadily reduced as the bond thickness is decreased.

10.2.2 Explanation of behaviour at $t>t_m$

The decline in adhesive fracture energy at $t>t_m$ has in the past been the cause of much conjecture, and two main reasons have been previously suggested:

(i) Bascom and co-workers (28) have suggested that the decline is due to a change from plane strain conditions at the maximum to conditions approaching plane stress as the bond thickness is increased. Some of the present observations appear to agree with this view. As discussed in Chapter 8, increasing bond thickness generally increased the degree of curvature of arrest/initiation 'finger-nail' markings. This would be consistent with increased plane stress character. Recognising that this should increase G_{Ic} with increasing bond thickness rather than decrease the G_{Ic} value, Bascom suggested that the increased plane stress character would reduce the degree of triaxial dilatation experienced by the rubber particles. This in turn would hinder the toughening mechanism which was believed responsible for the high degrees of toughness associated with rubber-modified epoxies. Thus, according to this approach, a reduction in G_{Ic} would be expected at $t>t_m$. However this study has shown that the toughness of the present rubber-modified epoxy is not specimen thickness dependent (see section 7.4.2, Chapter 7). This indicates that variations in plane stress and plane strain conditions would not influence toughness and thus the present findings are in conflict with Bascoms proposal.

(ii) It has been suggested that the cantilever beam compliance equation (6.4 in Chapter 6) should incorporate a correction

factor to take into account the thickness of the adhesive layer (135). However early work by the author on a commercial rubber-modified epoxy adhesive, indicated that adhesive bond thickness, t, did not invalidate equation 6.4 and therefore does not give rise to the trend observed at $t>t_m$.

An observation from the present studies, concerning the shape of the crack tip stress-whitened deformation zones, resolves this issue. Basically it was observed (section 8.5, Chapter 8) that:

(i) the deformation zones in bulk and adhesive joint specimens differ in shape; the former being circular, with the latter being elongated along the bond line, and

(ii) increasing the bond thickness decreases the length of the zone along the bond line.

The above observations may be placed upon a theoretical basis by drawing upon the work of Wang et al (18) to provide a semi-quantitative explanation for the trend at $t>t_m$. In this work, Wang and co-workers used a hybrid stress model finite-element analysis incorporating an advanced crack tip element to examine cracked adhesive double-cantilever-beam specimens. They computed the stresses, using an elastic analysis as a function of adhesive/substrate modulus ratio, E_a/E_s, and adhesive bond thickness and compared these results to a bulk system. They found that in an adhesive layer a given level of the σ_{11} local tensile stress ahead of a crack could act over a considerably longer distance than that expected from a comparison with a similar bulk specimen of the adhesive. This conclusion was valid when the distances involved were greater than about 2.5 μm. It was further shown that the distance over which the σ_{11} stress level acted was greater the higher the degree of constraint imposed upon the adhesive layer by, for example, the higher the E_s/E_a ratio and thinner the adhesive layer.

These effects are shown qualitatively in Figure 10.2. Since the stresses at a crack tip are singular then clearly the yield criterion, which can be taken as $\sigma_{11} = \sigma_{yt}$, will be exceeded in a zone in the crack tip region. To a first approximation the length of this zone will be equivalent to $2r_y$.

Now at the crack tip in the adhesive layer the thickness of the plastic zone will be as predicted from bulk considerations. However, the length of the zone, ahead of the crack may be longer for distances, r, greater than approximately 2.5 μm. Since plastic zones in rubber-modified epoxies are measured in hundreds of microns, then the volume of plastic deformation ahead of the crack will be greater for an adhesive joint than for a corresponding bulk specimen. This will be particularly so when the degree of constraint on the adhesive layer is increased. Consequently, from this argument, decreasing bond thickness from a comparatively large value would increase the degree of constraint on the adhesive layer. This would increase the length of the deformation zone and, providing development of plastic deformation in the bond thickness direction is not restricted, increase plastic zone volume. Thus adhesive G_{Ic} would be expected to increase.

This argument is developed further in Figure 10.3. As indicated, the maximum volume of plastic deformation ahead of the crack tip in the adhesive layer occurs when $t_m = 2r_y$. That is when the maximum degree of constraint exists, at a given bond thickness, commensurate with the condition that there is no restriction on the development of the plastic zone from the high modulus substrates. Under this situation G_{Ic} joint will be at its maximum value, G_{Icm}. At $t<t_m$, a high degree of constraint will exist and thus the deformation zone will extend a considerable distance along the adhesive layer. However restriction in the development of the zone in the bond thickness direction will also occur thereby reducing plastic zone volume and thus G_{Ic}. At $t>t_m$,

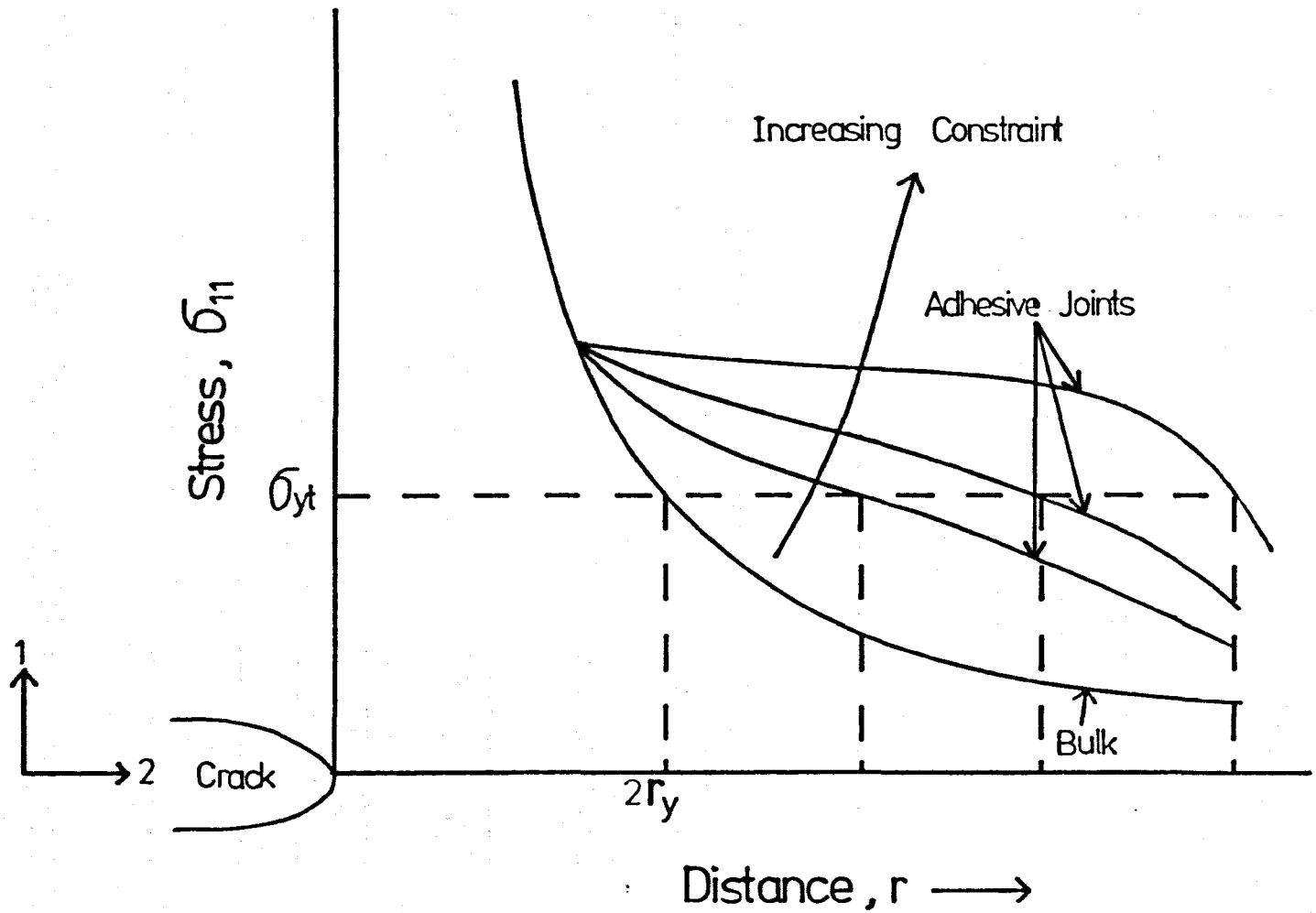

Figure 10.2 Effect of constraint on the σ_{11} stress level ahead of a crack tip.

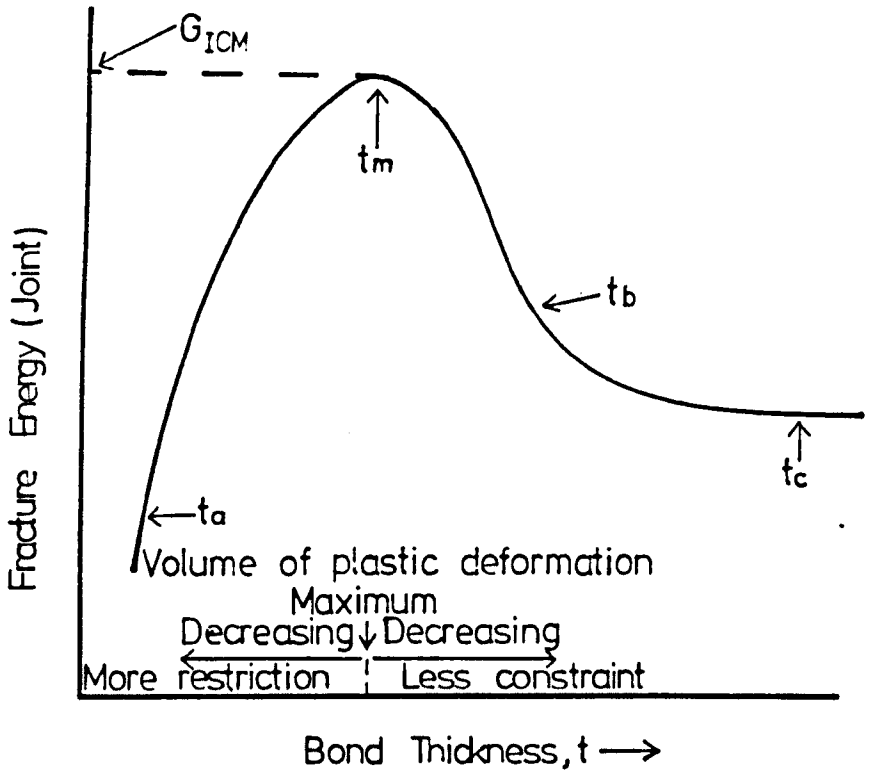

t —Value	Degree of constraint due to bond thickness	Plastic-zone shape	G_{Ic}(Joint)
$t_a(<2r_y)$	High		Comparatively Low
$t_m(=2r_y)$	Moderate		At Maximum
$t_b(>2r_y)$	Low		Below G_{ICM}
$t_c(\gg 2r_y)$	Almost Nil		Approx Equal To G_{Ic} Bulk

Figure 10.3 Schematic model for explaining the fracture energy versus bond thickness relationship.

restriction in the bond thickness direction will no longer apply but constraint on the adhesive layer will decrease, thereby reducing zone length and consequently zone volume, thus reducing G_{Ic}. Further support for this model is shown in Table 10.2, where adhesive G_{Ic} values at $t>t_m$ are shown to be similar, in the majority of cases, to bulk G_{Ic} values.

Thus to summarise, the evidence available shows that the entire G_{Ic} - bond thickness relationship occurs as a result of two effects, namely plastic zone restriction and constraint on the adhesive layer.

10.2.3 Crack growth behaviour

The crack growth variations which were observed as a function of bond thickness, namely increased unstable growth with increasing bond thickness, were also observed by Bascom and co-workers (28,40). However the crack growth transition at t_m, to which they referred, was not observed in this work. Instead the change from stable to unstable propagation occurred gradually. This was previously indicated in Figure 8.5 Chapter 8 where the length of stress-whitening observed on fracture surfaces (resulting from stable crack growth) was shown to decrease gradually with increasing bond thickness.

The mechanisms responsible for these two forms of crack growth can be considered separately. At $t>t_m$, G_{Ic} joint was approximately equivalent to G_{Ic} bulk and thus the factors influencing crack propagation in the latter could be expected to apply to adhesive joints.

At $t<t_m$, the mild steel substrates would restrict the development of the plastic zone. Thus crack propagation would be expected to involve an interaction between the deformation zone and the substrate surface. As outlined in Chapter 8, examination of fracture surfaces from stable growth regions indicated a locus of failure at, or close to, the adhesive-substrate interface. Furthermore, observations of stable

TABLE 10.2

Comparisons between G_{Ic} bulk and G_{Ic} joint at $t > t_m$.

Rate (ms^{-1})	Width (mm)	Bond thickness at $t>t_m$ (mm)	G_{Ic}(joint) (kJm^{-2})	G_{Ic}(bulk) (kJm^{-2})
8.33×10^{-7}	12	1.55	2.30	
"	"	1.80	1.70 $\bar{x}$ =2.03	2.63
"	"	2.52	1.73 σ =0.36	
"	"	2.96	2.38	
1.67×10^{-5}	12	1.20	1.27	
"	"	1.37	1.77 $\bar{x}$ =1.64	1.81
"	"	2.15	1.80 σ =0.25	
"	"	2.95	1.71	
1.67×10^{-4}	12	0.79	1.98	
"	"	1.27	2.51 $\bar{x}$ =2.25	1.26
"	"	1.98	2.06 σ =0.27	
"	"	2.98	2.46	
1.67×10^{-5}	3	1.37	1.35	
"	"	1.47	1.89 $\bar{x}$ =1.64	2.30
"	"	1.68	1.79 σ =0.25	
"	"	2.29	1.52	
1.67×10^{-5}	6	1.27	1.57 $\bar{x}$ =1.74	1.85
"	"	1.78	1.91 σ =0.24	
1.67×10^{-5}	25	1.15	1.21 $\bar{x}$ =1.52	
"	"	1.79	1.74 σ =0.27	1.73
"	"	2.54	1.60	
1.67×10^{-5}	49	1.02	1.41	
"	"	1.07	1.56 $\bar{x}$ =1.44	1.50
"	"	1.19	1.18 σ =0.19	
"	"	1.27	1.67	
"	"	2.13	1.38	

growth behaviour during loading indicated that the mechanism involved, was one of micro-crack coalescence (see section 8.5, Chapter 8), which occurred close to the interfacial regions.

10.3 Effect of Displacement Rate

As previously discussed in Chapter 8, increasing displacement rate was shown to have the following effects,

(i) the G_{Ic}-bond thickness relationship is maintained over the range of displacement rates investigated,

(ii) a reduction in the magnitude of the G_{Ic}-bond thickness peak, and

(iii) a reduction in the values of G_{Icm} and t_m.

Similar observations have been found for the effects of decreasing test temperature (40) on a similar adhesive system. This expected inter-relation between rate and temperature emphasises the importance of the visco-elastic response of the adhesive in influencing joint fracture behaviour.

The practical consequences of the effects of rate and temperature on G_{Icm} and t_m are demonstrated in Figures 10.4 and 10.5. As indicated, the selection of the optimum value of bond thickness, t_m, to achieve maximum toughness will depend upon the service conditions the joint is likely to experience. Thus the designer will be presented with considerable potential difficulties if these adhesive materials are to be employed with maximum efficiency.

The existence of the bond thickness effect exerts a complicating influence on dependence of G_{Ic} (joint) upon rate. As discussed previously in Chapters 7 and 9, bulk specimens indicated a reduction in fracture toughness with increasing rate. For the adhesive joints however, much more complicated results are obtained. As shown in

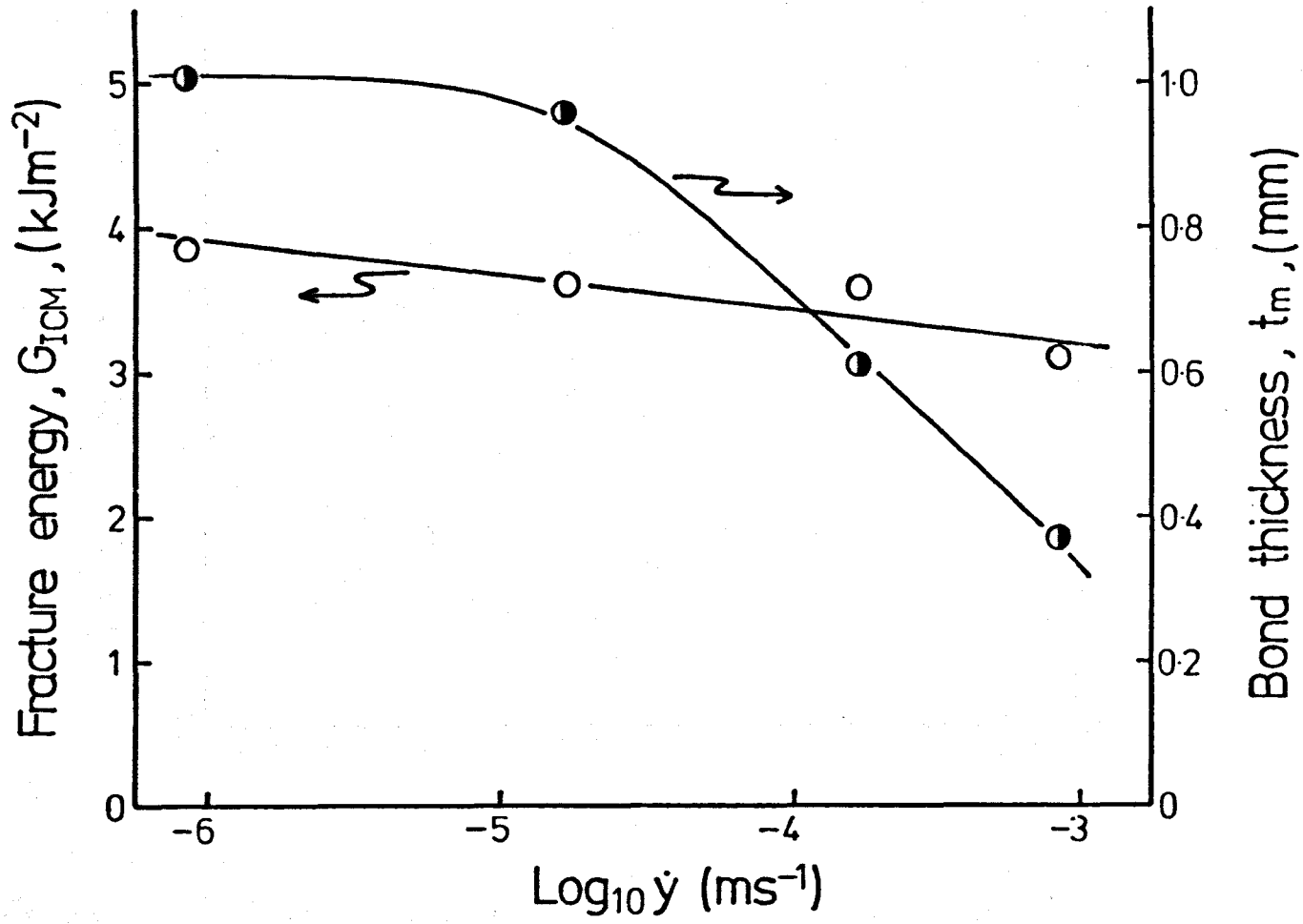

Figure 10.4 Adhesive fracture energy maximum, G_{ICM}, and corresponding bond thickness, t_m, versus displacement rate, $\dot{y}$. 20°C.

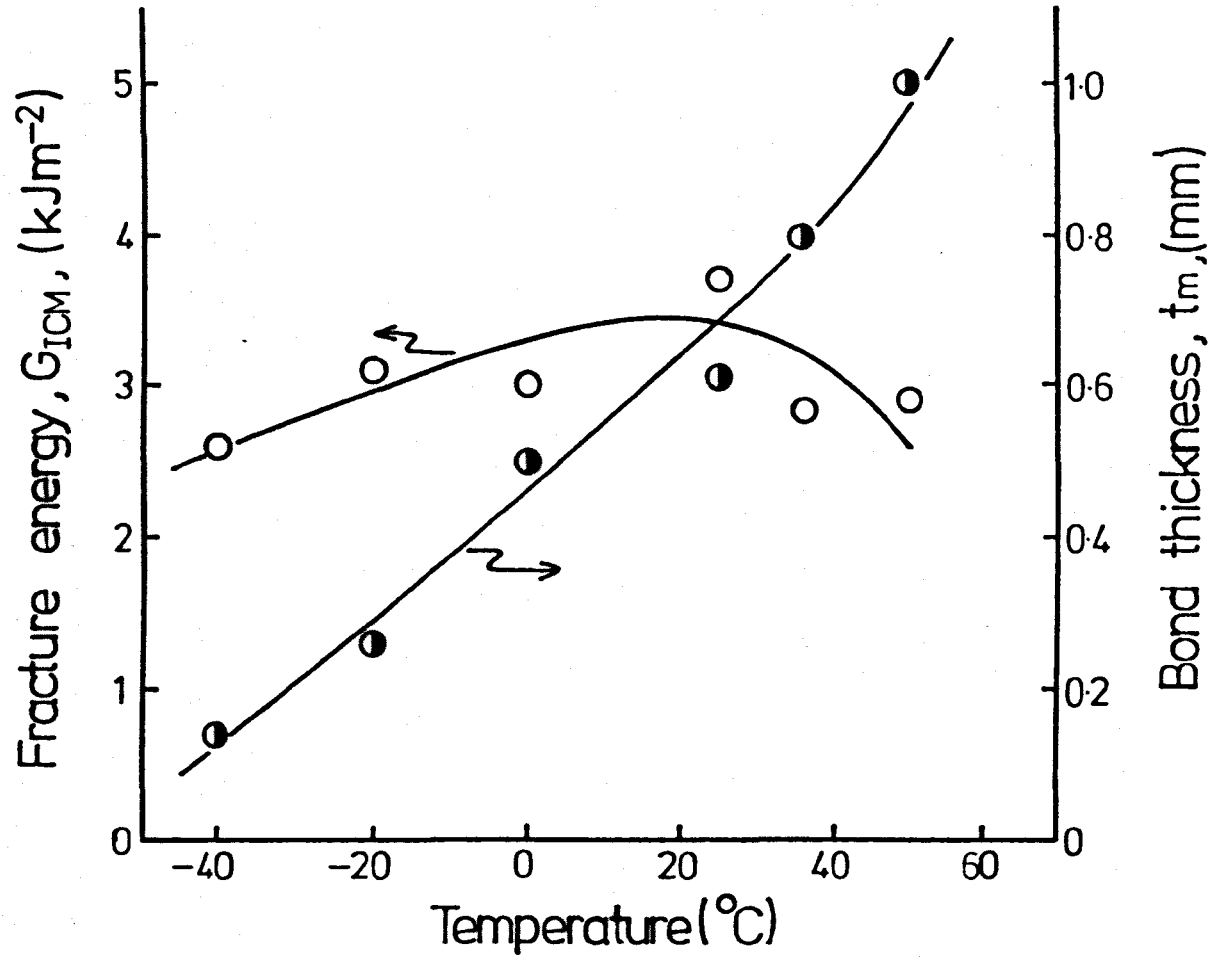

Figure 10.5 Adhesive fracture energy maximum, G_{ICM}, and corresponding bond thickness, t_m, versus temperature. Rate: $2{\cdot}2\times10^{-5}ms^{-1}$.

Figure 10.6 increasing rate can produce either an increase or a decrease in G_{Ic}. Consequently the trend can be the same as, or opposite to, those seen in bulk samples.

The reasons for this complex behaviour can be explained in terms of plastic zone restriction. As noted above, the G_{Ic}-bond thickness relationship was maintained over the entire range of rates investigated. Thus it is reasonable to assume that the proposed plastic zone restriction-adhesive layer constraint model applies over the rate range studied. Evidence to support this assumption is shown in Table 10.3, where correlations between t_m and both $2r_{y1}$ and $2r_{y2}$ are presented. Also shown is data published by Bascom and co-workers (40) for a similar adhesive system studied at one rate over the temperature range -40 to 50 °C. As indicated good agreement is evident between t_m and $2r_{y2}$ under all the temperature and rate conditions shown. Now as indicated in Figure 10.4, t_m increases significantly as the rate is decreased. Consequently, at $t<t_m$, G_{Ic} will decrease with decreasing rate. Conversely, at $t>t_m$, the behaviour will be reversed and will be similar to that shown by bulk specimens. A similar effect has been described by Hunston and co-workers (136) with temperature as the variable.

10.4 Effect of Joint Width

As discussed in Chapter 8, increasing joint width was shown to have the following effects,

(i) the G_{Ic}-bond thickness relationship is maintained over the joint width range investigated, namely 3 to 49 mm,

(ii) the G_{Ic}-bond thickness peak becomes 'sharper',

(iii) an increase in the value of G_{Icm}, and

(iv) t_m is independent of joint width.

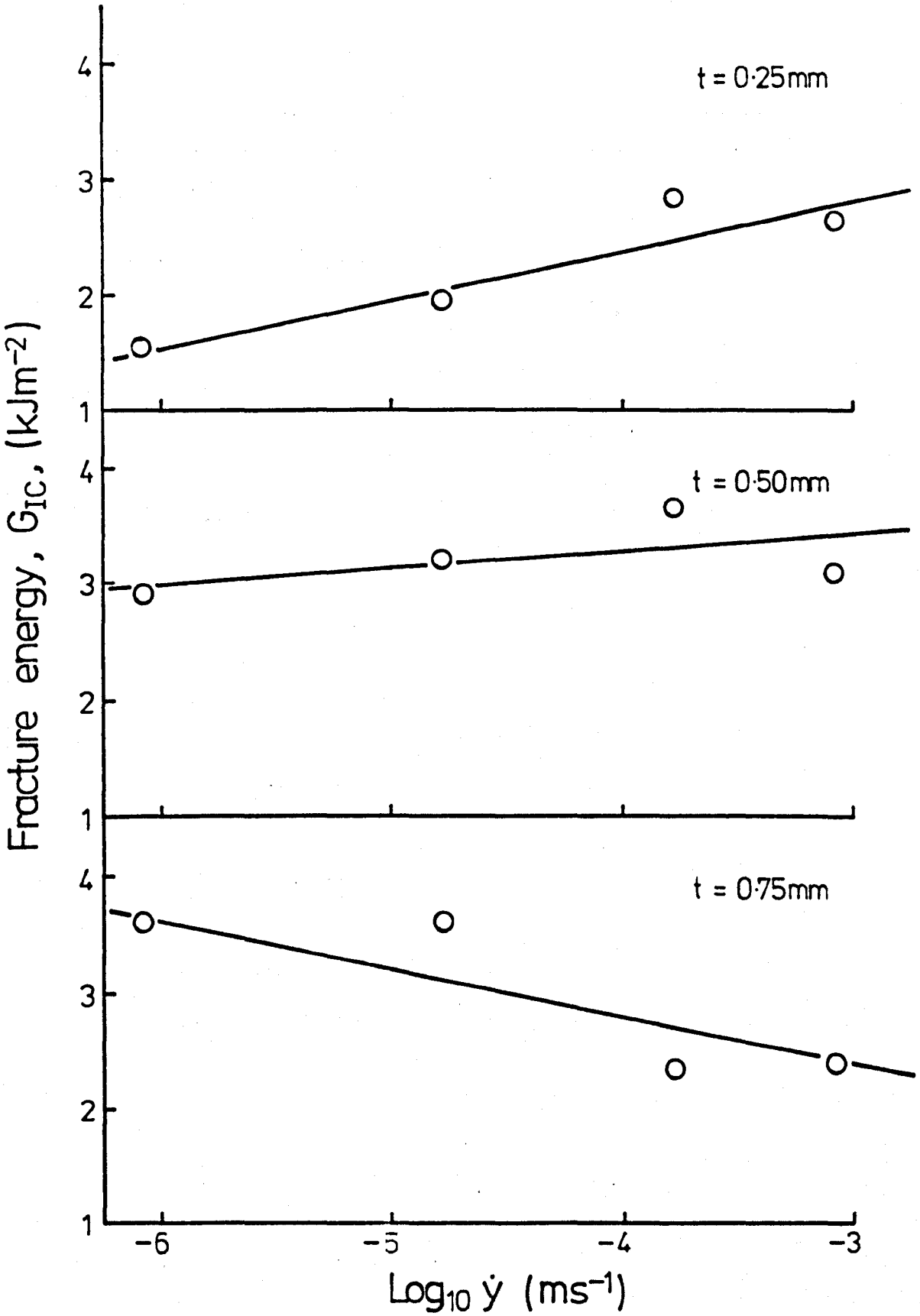

Figure 10.6 Adhesive fracture energy, G_{IC}, versus displacement rate for three bond thicknesses. Joint width, 12mm. 20°C.

TABLE 10.3

Comparison of adhesive bond thickness, t_m, and plane stress and plane strain plastic zone diameters, $2r_{y1}$ and $2r_{y2}$ at various rates and temperatures.

Temperature (°C)	$\log_{10}\dot{y}$ (ms^{-1})	Joint Width (mm)	t_m (mm)	$2r_{y1}$(a) (mm)	$2r_{y2}$(b) (mm)
20	-6.08	12	1.00	0.40	1.02
20	-4.78	12	0.80	0.18	0.62
20	-3.78	12	0.55	0.11	0.38
20	-3.08	12	0.40	0.09	0.30
50	-4.66	12	1.10(c)	0.48(d)	1.60(d)
37	-4.66	12	0.90	0.35	1.16
25	-4.66	12	0.60	0.17	0.57
0	-4.66	12	0.50	0.12	0.39
-20	-4.66	12	0.25	0.05	0.15
-40	-4.66	12	<0.10	0.02	0.05

Notes: (a) Calculated from equation 10.1

(b) Calculated from equation 10.2

(c) After reference 40

(d) Calculated from bulk fracture energy results from reference 40 together with σ_{yt} and E data from this work.

Since the G_{Ic}-bond thickness relationship is maintained throughout the joint width range studied, it is again of interest to compare computed values of $2r_{y2}$ and t_m. This data is shown in Table 10.4. As indicated, reasonable agreement exists suggesting conformity with the plastic zone restriction-adhesive layer constraint model.

TABLE 10.4

Comparison of adhesive bond thickness, t_m, and plane-strain and plane-stress plastic zone diameters, $2r_{y1}$ and $2r_{y2}$. Variable joint width.

Temperature (°C)	$\log_{10}\dot{\gamma}$ (ms^{-1})	Joint Width (mm)	t_m (mm)	$2r_{y1}$(a) (mm)	$2r_{y2}$(b) (mm)
20	-4.78	3	0.85	0.23(c)	0.80(c)
20	-4.78	6	0.65	0.18	0.62
20	-4.78	12	0.80	0.18	0.62
20	-4.78	25	0.90	0.17	0.59
20	-4.78	49	0.80	0.15	0.51

Notes: (a) Calculated from equation 10.1
(b) Calculated from equation 10.2
(c) Calculated from bulk fracture toughness results interpolated from Figure 7.14, Chapter 7.

The variation of both G_{Icm} and t_m with joint width is shown in Figure 10.7, which shows G_{Icm} increasing significantly with joint width, whilst t_m remains essentially constant. Furthermore, at $t>>t_m$ G_{Ic} joint $\approx G_{Ic}$ bulk for all the joint widths investigated. Thus for wide joints, where G_{Icm} is high, the drop in G_{Ic} at $t>t_m$ becomes extremely severe. These interesting observations can be explained in terms of the restriction-constraint model.

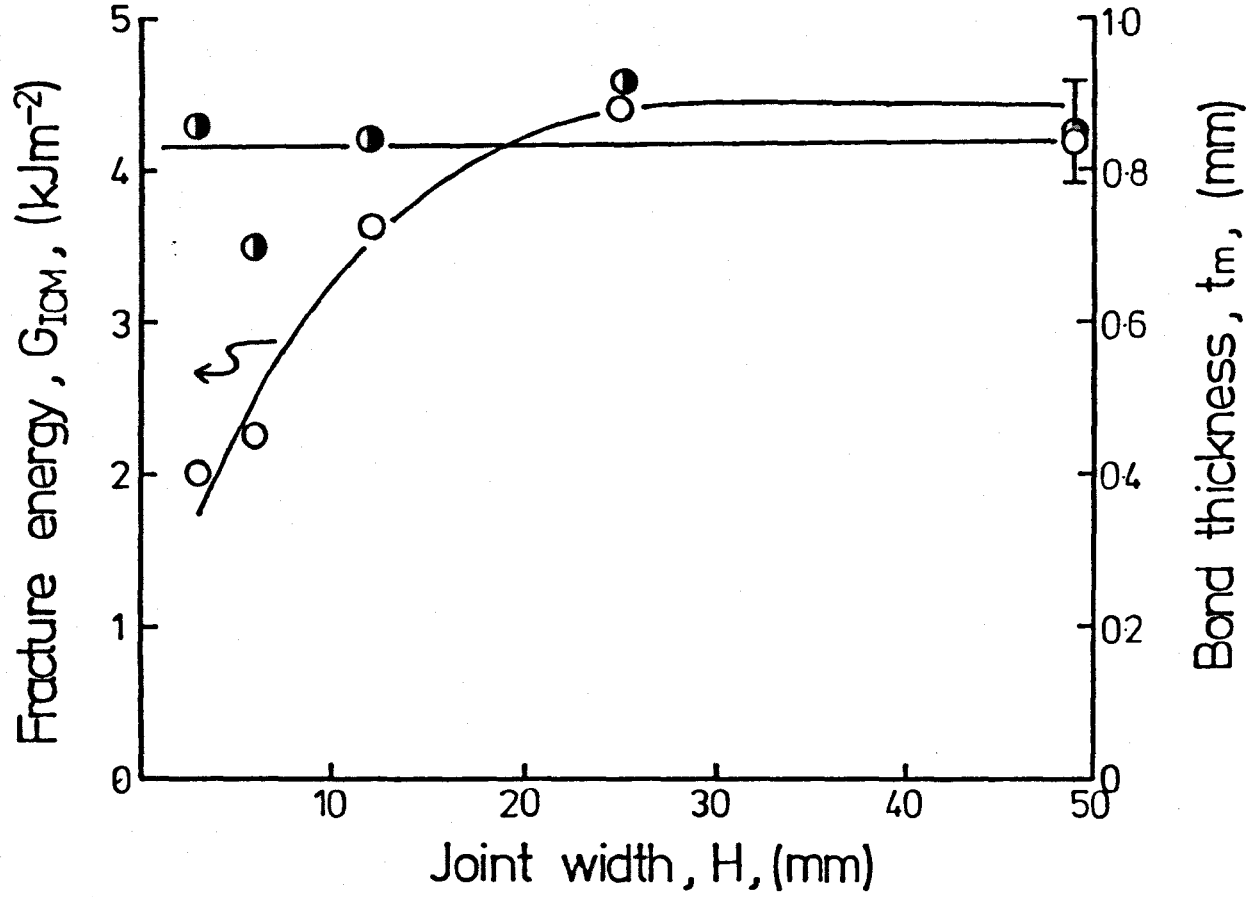

Figure 10.7 Adhesive fracture energy maximum, G_{IOM}, and corresponding bond thickness, t_m, versus joint width. Rate: 1mm min^{-1}

Now the agreement between t_m and $2r_{y2}$ shown in Table 10.4 clearly supports the plastic zone restriction part of the model. However it fails to explain both the substantial increase in G_{Icm} which occurs with increasing width and the rapid decline in G_{Ic} which inevitably occurs at $t>t_m$. As discussed earlier, Wang and co-workers (18) found during their finite-element analyses of cantilever beams that increased constraint on the adhesive layer, brought about by higher E_s/E_a ratios and reductions in bond thickness, increased the distance over which the σ_{11} stress level acted. Increased joint width can be considered as imparting a similar effect on adhesive layer constraint and thus would have the effect indicated previously in Figure 10.2 for increasing constraint on the σ_{11} stress level. Consequently G_{Icm} would be expected to increase significantly with increasing width and this would inevitably produce a sharp reduction in G_{Ic} at $t>t_m$, as G_{Ic} joint $\rightarrow$ G_{Ic} bulk. A brief study of the G_{Ic}-bond thickness curves at 3 and 49 mm width (Figure 8.9, Chapter 8) shows general agreement with this proposal. For example, the 3 mm wide joints would experience substantially less constraint than the 49 mm wide joints. Thus, G_{Icm} would be similar to G_{Ic} (bulk) and thus the decline in G_{Ic} at $t>t_m$ would be less than that found with the 49 mm joints.

One question remains to be answered. Why should a plastic zone based upon plane-stress assumptions influence the bond thickness effect? In Chapter 9 a toughening mechanism was proposed based upon two basic deformation processes, namely rubber particle cavitation and plastic shear flow of the matrix. It was suggested that cavitation within the particles reduces triaxiality within the crack tip region, producing a state of stress probably having more plane stress character than plane strain. Thus from this theory, a G_{Ic}-bond thickness relationship controlled partly by a plane stress, as opposed to a plane strain plastic zone, is reasonable.

10.5 Failure Criteria

In Chapter 9 a failure criterion based upon the concept of crack tip blunting was proposed for both the unmodified and rubber-modified epoxies. In both cases it was shown that failure was governed by the need to achieve a critical stress acting over a certain distance ahead of the crack tip. Recent work has indicated that this type of failure criterion can also be applied to adhesive joint configurations comprising unmodified epoxy adhesives and that the critical values of stress and distance are similar to those obtained for corresponding bulk systems (54). However, its application to the failure of joints employing the rubber-modified adhesive will be severely complicated by the joint geometry effects discussed in this chapter. However the similarities in G_{Ic}(joint) and G_{Ic}(bulk) and crack growth characteristics, at $t>>t_m$ under all the conditions studied implies that a critical stress - critical distance criterion could be operative at $t>>t_m$.

At $t<t_m$, joint geometry problems arise. It would appear that in this case the concept of combining the critical stress and distance criterion with an analysis of the stress-field in the adhesive layer as a function of joint geometry could be a promising approach.

10.6 Comparison Between Bulk and Joint Fracture.

As discussed above, the complex fracture behaviour of the adhesive joints compared to the bulk rubber-modified epoxy, is caused by the constraints imposed upon the adhesive layer by the high modulus substrates.

Similarities in G_{Ic}(joint) and G_{Ic}(bulk) only occurred at $t>t_m$. G_{Ic}(joint) was, in some cases, substantially greater than G_{Ic}(bulk) over certain ranges of bond thickness. This effect is illustrated in Figure 10.8. Both types of specimen ie adhesive joint and bulk are

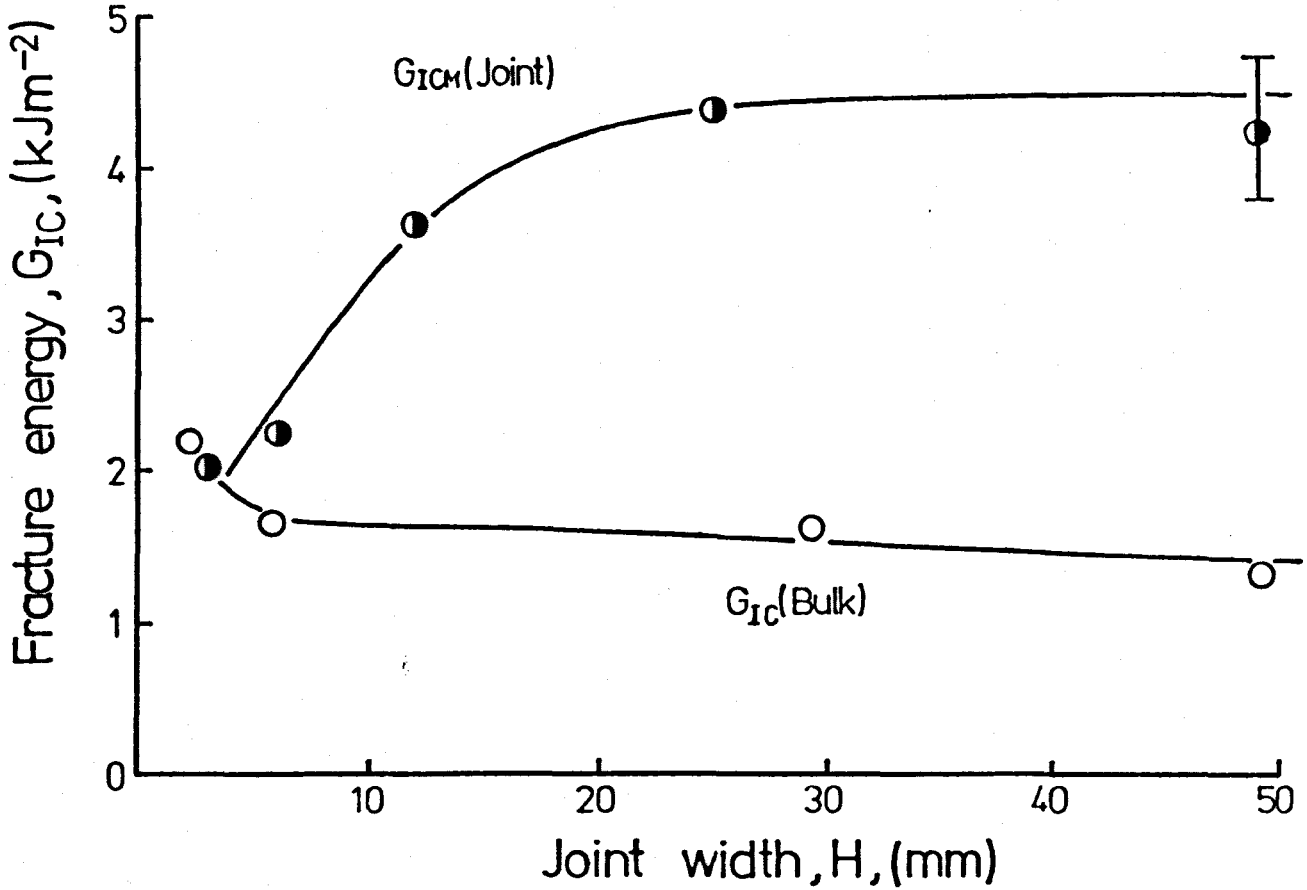

Figure 10.8 Fracture energy, G_{ICM} (joint), and G_{IC} (bulk) versus joint width, H. Rate: 1mm min^{-1}. 20°C.

depicted in this figure. As shown, G_{Ic} bulk decreases slightly with increasing specimen thickness (see section 7.4.2, Chapter 7). G_{Icm} however increases significantly so that at joint widths greater than approximately 3 mm, G_{Icm} and consequently G_{Ic}(joint) over certain ranges of bond thickness, are greater than G_{Ic}(bulk). A similar observation is recorded in Figure 10.9 from the work of Bascom and co-workers (40). At temperatures below approximately 30 °C, G_{Ic}(joint) is higher than G_{Ic}(bulk). At higher temperatures the bulk material exhibits a ductile tearing mode of fracture which is not observed in the adhesive layer due to the constraint imposed by the high-modulus substrates. Hence G_{Ic} bulk becomes greater than G_{Icm}.

These interesting effects can be explained using the plastic zone restriction-adhesive layer constraint model developed in this chapter. The degree of constraint on the adhesive layer, as explained previously, will be a function of joint width. An increase in width will increase the degree of constraint on the adhesive layer and thus increase G_{Icm} relative to G_{Ic}(bulk).

Similarity in crack growth behaviour between bulk and adhesive joint specimens was observed when $t>t_m$ in the latter, with unstable propagation coninciding with similar values of G_{Ic}(joint) and G_{Ic}(bulk). The major difference was at $t<t_m$ where the adhesive joints exhibited stable propagation which was not observed to any significant extent with bulk specimens at 20 °C. This behaviour has been previously discussed (section 10.2.3) in terms of plastic zone-substrate surface interaction and thus would be specific to adhesive joints.

10.7 Summary

(i) The G_{Ic}-bond thickness relationship, where G_{Ic} passes through a maximum, G_{Icm}, at a particular bond thickness, t_m, has been discussed in terms of a plastic zone

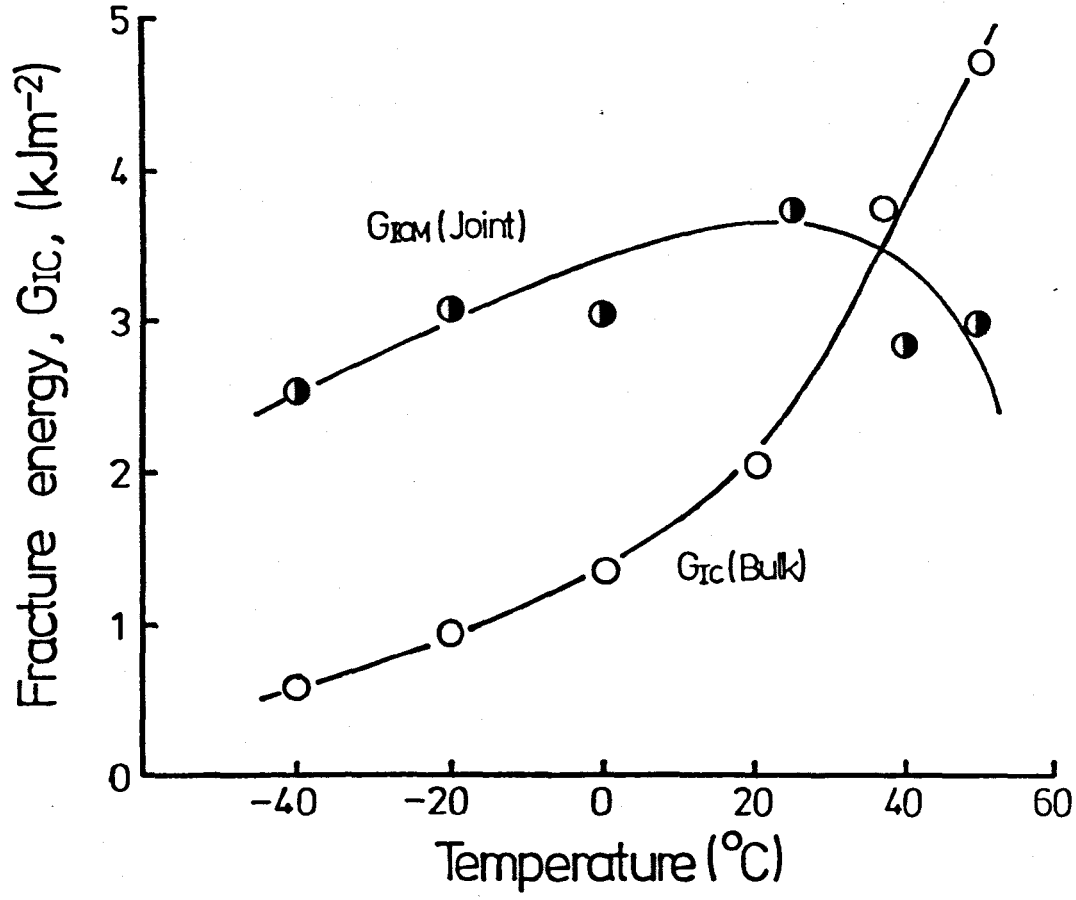

Figure 10.9 Fracture energy, G_{ICM} (joint) and G_{IC}(bulk) versus temperature. Rate: $2{\cdot}2\times10^{-5}ms^{-1}$.

restriction-adhesive layer constraint model.

(ii) Similarities between t_m and plane stress plastic zone diameter, $2r_{y2}$, have been demonstrated. This suggests that the plane stress plastic zone influences the G_{Ic} - bond thickness relationship at $t<t_m$.

(iii) Constraint on the adhesive layer, brought about by the presence of the high modulus substrates, has also been proposed as having a significant influence on the G_{Ic}-bond thickness relationship.

(iv) The effects of displacement rate, joint width, temperature and differences between G_{Ic}(joint) and G_{Ic}(bulk) have been explained using the plastic zone restriction-adhesive layer constraint model.

CHAPTER ELEVEN

SUMMARY OF CONCLUSIONS

11.1 General

1. The preparation and curing conditions employed for the rubber-modified system produces a two-phase microstructure with rubber particles, approximately 2-5 μm diameter, dispersed in a crosslinked epoxy matrix. Dynamic mechanical studies indicate a minimal presence of rubber in the matrix.

2. Under virtually all test rates and temperatures the rubber-modified epoxy exhibits a substantially greater fracture toughness than its unmodified counterpart. This is achieved without major reductions in modulus and glass transition temperature.

3. A toughening mechanism is proposed which suggests that the greater toughness exhibited by the rubber-modified epoxy arises from a greater degree of energy dissipating deformations occurring in the vicinity of the crack tip. Two basic deformation processes are proposed: (i) rubber particle cavitation and (ii) plastic shear yielding in the matrix. These two processes interact to magnify the degree of shear yielding in the matrix. This results in a pronounced increase in plastic zone size and thus increased toughness.

11.2 Bulk Behaviour

1. Three main types of crack growth have been identified with both the unmodified and rubber-modified epoxy systems. They are (i) brittle stable, (type C), (ii) brittle unstable (type B), and (iii) ductile stable, (type A). The type of crack growth obtained is dependent upon both test temperature and rate.

2. For both systems the fracture toughness is dependent upon the test temperature and rate: increasing the temperature or decreasing the rate generally increases the fracture toughness and vice-versa. The rubber-modified epoxy exhibits the greater dependence.

3. With both systems the crack opening displacement increases with increasing temperature and decreasing rate. There is little evidence to demonstrate a constant value even at low temperatures. Thus a constant crack opening displacement does not provide a unique failure criterion.

4. Both the unmodified and rubber-modified epoxies obey a failure criterion dependent upon the attainment of a critical stress over a particular distance ahead of the crack tip.

5. The unmodified epoxy exhibits an extremely pronounced tough/brittle transition. The three variables studied (rate, temperature and specimen thickness) all exert a strong influence on this transition. A plane stress/plane strain transition is proposed to account for this behaviour.

6. The rubber-modified epoxy does not exhibit a sharp tough/brittle transition. This is due to a substantial change in the crack tip stress field brought about by the presence of the rubber particles. This inhibits the typical plane stress/plane strain transition.

11.3 Adhesive Joint Behaviour

1. Previous investigations have shown similarities in the fracture behaviour of bulk and adhesive joint specimens employing unmodified epoxies. This study indicates clearly that this is not true, under the majority of conditions, for a rubber-modified epoxy.

2. With the rubber-modified epoxy, variations in the bond thickness have a pronounced effect upon the adhesive fracture energy, G_{Ic}. A maximum, G_{Icm}, occurs at a particular bond thickness, t_m. Values of

G_{Ic}(joint) and G_{Ic}(bulk) are only similar when the bond thickness is substantially greater than t_m. This bond thickness effect has been attributed to two main influences. Firstly, the substrates can restrict the development of the crack tip plastic zone in the bond thickness direction and thus reduce G_{Ic}. Secondly, constraint on the adhesive layer, imparted by the presence of high modulus substrates, has a significant influence on both the shape and volume of the plastic zone. Both of these effects combine to produce the complex G_{Ic}-bond thickness relationship.

3. The value of t_m at which G_{Icm} occurs has a similar value to the plane stress plastic zone diameter, $2r_{y2}$, calculated from bulk fracture toughness values. This correlation allows the prediction of t_m for adhesive joints from bulk mechanical properties.

4. The application of a failure criterion for adhesive joints employing the rubber-modified epoxy adhesive, based upon a critical stress - critical distance concept, is severely complicated by joint geometry effects.

CHAPTER TWELVE

SUGGESTIONS FOR FURTHER WORK

The results obtained from this investigation indicate several topics on which further research could be conducted:

1. The sharp tough/brittle transitions observed with the unmodified epoxy appear unique. No other unmodified formulation so far studied is reported to behave in such a manner. Thus it would be of interest to determine the reason(s) for this apparent difference. One potential cause requiring consideration concerns the range of temperatures and rates employed in previous investigations. In a minority of cases the investigations were too limited to observe a tough/brittle transition. Thus further more extensive studies with these systems would be beneficial. However it is clear that with most of the previously studied systems, sharp tough/brittle transitions do not occur, thus indicating a significant difference in fracture behaviour to that obtained for the present unmodified epoxy system. The data currently available for both the present and previously studied unmodified systems does not provide any indications of potential causes. Thus, as an initial exercise, it would be of interest to investigate differences in various factors such as microstructural characteristics (eg nodular morphology), yield behaviour and dynamic mechanical behaviour in an attempt to isolate major differences which may indicate reasons for the different fracture behaviour.

2. It has been concluded that the tough/brittle transitions obtained with the unmodified epoxy are associated with transitions from plane stress to plane strain behaviour. In particular a critical specimen thickness/plane stress plastic zone size, H/r_{y2}, criterion has been proposed. However it was not possible to isolate a precise value for

this ratio. Any future attempt at doing so would need to consider in some detail the three major points discussed in section 9.4.3 of Chapter 9, regarding the thickness dependent tough/brittle transitional behaviour shown in Figure 7.13. They are, (a) the statistical significance of the minor decline in K_{Ic} between 2.3 and 49 mm thickness, (b) the magnitude and effects of the temperature increase resulting from an exotherm, on mechanical properties and (c) a critical study of the validity of the bimodal analysis employed in Chapter 9.

3. The toughening mechanism developed in this thesis was based upon two basic deformation mechanisms, namely rubber particle cavitation and plastic shear yielding of the matrix. Although no explicit morphology dependence was incorporated in the model, it is likely that the precise morphology would play an important role in the toughening process. Thus it would be of interest to study the morphology dependent behaviour of rubber-toughened epoxy systems. Variations in morphology can be produced by several approaches. For example, changes in the nature and concentrations of both the rubber and curing agent can produce major changes in morphology. However it is suggested that the best approach would be to keep formulation variables constant and vary morphology by changes in cure conditions. Such an approach would allow a clearer understanding of the relationships between fracture behaviour and morphology. Complicating factors such as for example, changes in epoxy matrix structure brought about by the use of different curing agents, would be kept to a minimum.

4. The failure criterion proposed in Chapter 9 was based upon a quantitative expression (equation 9.8), derived from crack blunting principles, which was found to fit the fracture data over wide ranges of rate and temperature. Two parameters were obtained which provided a unique failure criterion for both the epoxy formulations.

Although these parameters are simply curve-fitting constants, it was suggested that they represent a failure criterion based upon the need to attain a critical stress over a critical distance ahead of the crack tip. The values of critical stress obtained point to the existence of a constrained yield stress. However, the physical significance of the critical distance parameter remains obscure. The fractographic studies conducted in this investigation failed to locate any fracture surface features of similar dimensions to the critical distance values. Thus further studies are required to understand the physical significance of the critical distance term.

5. Previous investigations have shown that the critical stress-critical distance failure criterion can be applied to both bulk and adhesive joint specimens when unmodified epoxies are employed. However this study has clearly demonstrated the complications which can arise when a rubber-modified epoxy is used, due to substantial joint geometry effects. Thus the application of a critical stress and distance criterion to an adhesive joint comprising a rubber-modified epoxy, would need to consider also the pronounced changes in the crack tip stress field which occur as a result of joint geometry changes. This is clearly, therefore, an area worthy of further study.

REFERENCES

1. Bucknall C B., Toughened Plastics, Applied Science Publishers Ltd, London, 1977.

2. Ostromislensky I I., U.S. Pat 1, 613, 673; 1927.

3. Amos J L., McCurdy J L and McIntire O R., U.S. Pat 2, 694, 692; 1954.

4. Cizek E.P., U.S. Pat 3, 383, 435; 1968.

5. McGarry F J and Willner A M., Toughening of an Epoxy Resin by an Elastomeric Second Phase, Res. Rept. R68-8, M.I.T., 1968.

6. Sultan J N and McGarry F J., Microstructural Characteristics of Toughened Thermoset Polymers, Res. Rept R69-59, M.I.T., 1969.

7. Rowe E H., Siebert A R and Drake R S., Mod. Plast., 49, 110,(1970)

8. Drake R S., Rowe E H., Siebert A R and Riew C K., Reinforced Plastics, Feb/March, 38, (1971).

9. Riew C K., Rowe E H and Siebert A R., ACS, Div. Org. Coat. Chem., 34 (2), 353, (1974).

10. Riew C K., Rowe E H and Siebert A R., Rubber Toughened Thermosets, Advances in Chemistry Series, No 154, 326, 1976.

11. Griffith A A., Phil. Trans. Roy. Soc., A221, 163, (1920).

12. Orowan E., Repts. Prog. Phys., 12, 185, (1948).

13. Irwin G R., Appl. Mats. Res., 3, 65, (1964)

14. Berry J P., J. Polym. Sci., 50, 107, (1961).

15. Berry J P., J. Polym. Sci., 50, 313, (1961).

16. Westergaard H M., J.Appl. Mech., A, 46, June 1939.

17. Trantina G G., J. Composite Mat., 6, 192, (1972).

18. Wang S S., Mandell J F and McGarry F J., Int. J. Fract., 14, 39, (1978).

19. Broek D., Elementary Engineering Fracture Mechanics, Sijthoff and Noordhoff, p105, 1978.

20. Irwin G R and Paris P C., Fracture - An Advanced Treatise, Vol 3, Ed by H Liebowitz, Academic Press, New York, p1, 1971.

21. Hahn G T and Rosenfield A R., ASM Trans., 59, 909, (1966)

22. Broutman L J and McGarry F J., J. Appl. Polym. Sci., 9, 609, (1965).

23. Mostovoy S and Ripling E J., J. Appl. Polym. Sci., 10, 1351,(1966)

24. Diggwa A D S., Polymer 15, 101, (1974).

25. Meeks A C., Polymer 15, 675, (1974)

26. Selby K and Miller L E., J. Mats. Sci., 10, 12, 1975.

27. Griffiths R and Holloway D G., J. Mats. Sci., 5, 302, 1970.

28. Bascom W D., Cottington R L., Jones R L and Peyser P., J. Appl. Polym. Sci., 19, 2545, (1975).

29. Mostovoy S and Ripling E J., J. Appl. Polym. Sci., 15, 641,(1971)

30. Phillips D C., Scott J M and Jones M., J. Mats. Sci., 13, 311 (1978).

31. Yamini S and Young R J., J. Mats. Sci. 14., 1609, (1979).

32. Mijovic J and Koutsky J A., Polymer 20, 1095, (1979)

33. Laible R C and McGarry F J., Polym. Plast. Tech. Eng. 7 (1), 27, (1976).

34. Lee H and Neville K., Handbook of Epoxy Resins, McGraw-Hill, New York, 1967.

35. Potter W G., Epoxy Resins, Iliffe, London, 1970

36. Young R J and Beaumont P W R., J. Mats. Sci., 11, 779, (1976)

37. Yamini S and Young R J., Polymer., 18, 1075, (1977)

38. Gledhill R A., Kinloch A J., Yamini S and Young R J., Polymer, 19, 574, (1978)

39. Cherry B W and Thomson K W., J. Mats. Sci., 16, 1925 (1981)

40. Bascom W D and Cottington R L., J. Adhesion, 7, 333, (1976)

41. Rushford J L., Bitner J L and Hunston D L., Coatings and Plastics Prep., American Chemical Society, 41, 379 (1979).

42. Mai Y W and Atkins A G., J. Mats. Sci., 10, 2003, (1975).

43. Mai Y W., Atkins A G and Caddell R M., Int. J. Fract., 11, 939, (1975).

44. Beaumont P W R and Young R J., J. Mats. Sci., 10, 1334, (1975)

45. Young R J and Beaumont P W R., Polymer, 17, 717, (1976)

46. Williams J G and Marshall G P., Polymer, 15, 251, (1974)

47. Mostovoy S and Ripling E J ., J. Appl. Polym. Sci., 15, 661,(1971)

48. Mostovoy S ., Ripling E J and Bersch C F., J.Adhesion, 3, 125, (1971)

49. Mostovoy S and Ripling E J., Appl. Polym. Symp. 19, 395, (1972)

50. Scott J M., Wells G M and Phillips D C., J. Mats. Sci., 15, 1436 (1980).

51. Kinloch A J and Young R J., Fracture Behaviour of Polymers, Applied Science, 1983.

52. Knott J F., Fundamentals of Fracture Mechanics, Butterworths, London, p132, 1973.

53. ASTM-E 399-78. Plane-Strain Fracture Toughness of Metallic Materials.

54. Kinloch A J and Shaw S J., Developments in Adhesives -2, Ed by A J Kinloch, Applied Science, London, p83, 1981.

55. Mostovoy S and Ripling E J., J. Appl. Polym. Sci., 13,1083 (1969)

56. Mai Y W., J. Adhesion, 7, 141 (1975)

57. Gledhill R A and Kinloch A J., J. Mats. Sci., 10, 1261 (1975)

58. Gledhill R A and Kinloch A J., Polymer, 17, 727, 1976.

59. Bascom W D., Cottington R L and Timmons C O., Appl. Polym. Symp., 32, 165 (1977).

60. Gledhill R A., Kinloch A J and Shaw S J., J. Mats. Sci., 14, 1769 (1979)

61. Mostovoy S., Crosley P B and Ripling E J., J. Mats., 2, 661 (1967)

62. Ripling E J., Mostovoy S and Corten H T., J. Adhesion, 3, 107, (1971).

63. ASTM Standard D790-71. 1973.

64. ASTM Standard D695-69, 1973.

65. Bowden P B., The Physics of Glassy Polymers, Ed by R N Haward, Applied Science, London, p279, 1973.

66. Robertson R E., J. Appl. Polym. Sci., 7, 443 (1963)

67. Roetling J A., Polymer. 6, 311 (1965)

68. Holt D L., J. Appl. Polym. Sci., 12, 1653, (1968)

69. Bauwens-Crowet C., Bauwens J C and Homes G., J. Polym. Sci., A2, 7, 735, (1969)

70. Bauwens-Crowet C., Ots, J M and Bauwens J C., J. Mats. Sci., 1, 1197 (1974).

71. Yoshii T., Structure-Property Relationships in Rubber-Modified Epoxy Resins, Ph.D Thesis, Cranfield Institute of Technology, 1975.

72. Bitner J L., Rushford J L., Rose W S., Hunston D L and Riew C K Adhesion and Adhesives: Science, Technology and Applications, Conf., Durham, Plastics Rubb. Inst., London, p14. 1, 1980.

73. Bowerman, H H and McCarthy W J., High Strain-Rate Testing of CTBN Modified Epoxy Resins, 28th Annual Tech. Conf., Reinforced Plastics/Composites Inst., SPE, 1973.

74. Kline D E., J. Polym. Sci., 47, 237, (1960).

75. May C W and Weir F E., SPE Trans. 2, 3 (1962).

76. Dammont F R and Kwei T K., J. Polym. Sci., 5, 761, (1967)

77. Van Hoorn H., J. Appl. Polym. Sci., 13, 871 (1968)

78. Delatycki O., Shaw J C and Williams J G., J. Polym. Sci., 7, 753, (1969)

79. Hirai T and Kline D E., J. Appl. Polym. Sci., 16, 3145, (1972)

80. Arridge R G C and Speake J H., Polymer, 13, 443 (1972)

81. Hirai T and Kline D E., J. Appl. Polym, Sci., 17, 31 (1973)

82. Williams J G., J. Appl. Polym. Sci., 23, 3433 (1979)

83. Manzione L T., Gillham J K and McPherson C A., J. Appl. Polym. Sci., 26, 889, (1981)

84. Shaw S J., Unpublished Results.

85. Vincent P I., Polymer, 15, 111, (1974)

86. Kisbenyi M., Birch M W., Hodgkinson J M and Williams J G., Polymer, 20, 1289 (1979)

87. Andrews E H., Fracture in Polymers, Oliver and Boyd, London 1968.

88. Racich J L and Koutsky J A., J. Appl. Polym. Sci, 20, 2111, (1976).

89. Dušek K., Plešťil J., Ledricky F and Lunak S., Polymer, 19, 393, (1978)

90. Uhlmann D R., Farad. Disc., 68, 87, (1979)

91. Matyi R J., Uhlmann D R and Koutsky J A., J.Polym. Sci., Polym. Phys. Ed., 18, 1053 (1980).

92. Merz E H., Claver G C and Baer M., J. Polym. Sci., 22, 325(1956)

93. Kunz-Douglas S., Beaumont P W R and Ashby M F., J. Mats. Sci., 15, 1109 (1980).

94. Bascom W D and Hunston D L., Proc. Int. Conf. on Toughening of Plastics, Plastics and Rubber Inst., London, p22, 1. (1978).

95. Gent A N., Science and Technology of Rubber Ed. by F R Eirich, Academic Press, New York, P419, 1978.

96. Bucknall C B and Smith R R., Polymer, 6, 437, (1965)

97. Van der Boogart A., Physical Basis of Yield in Glassy Polymers, Ed. by R N Haward, Institute of Physics, London, 1966.

98. Lilley J and Holloway D G., Phil. Mag., 28, 215, (1973)

99. Donald A M and Kramer E J., J. Mats, Sci., 17, 1871 (1982).

100. Newman S and Strella S., J. Appl. Polym. Sci., 9, 2297, (1965)

101. Bucknall C B., Clayton D and Keast W E., J.Mats. Sci., 7, 1443, (1972).

102. Sultan J N and McGarry F J., Polym. Engng. Sci., 13, 29 (1973)

103. Bucknall C B and Yoshii T., Brit. Polym. J., 10, 53 (1978)

104. Goodier J N., J. Appl. Mech., 55, 39 (1933)

105. Bucknall C B., 5th European Conf. on Plastics and Rubbers, Paris, pD8, 1978.

106. Lange F F and Radford K C., J. Mats. Sci., 6, 1197 (1971)

107. Mallick P K and Broutman L J., Mat. Sci. Eng., 18, 63 (1975)

108. Broutman L J and Sahu S., Mat. Sci. Eng., 8, 98 (1971)

109. Hammond J C and Quayle P V., 2nd Intern. Conf. on Yield, Deformation and Fracture, Churchill College, Cambridge, Plastics Rubb. Inst., London, p11, 1973.

110. Young R J and Beaumont P W R., J. Mats. Sci. 12, 684 (1977)

111. Lange F F., Phil. Mag., 22, 983, (1970)

112. Evans A G., Phil. Mag., 26, 1327, (1972)

113. Evans A G., J. Mats. Sci., 9, 1145, (1974)

114. Phillips D C and Harris B., Polymer Engineering Composites, Ed by M.O.W Richardson, Applied Science, London, p45, 1977.

115. Dugdale D S., J Mech. Phys. Solids, 8, 100, (1960)

116. Wronski A S and Pick M., J. Mats. Sci., 12, 28, (1977)

117. Adams R D, Coppendale J and Peppiatt N A., Adhesion-2, Ed by K W Allen, Applied Science, London, p105, 1978.

118. Yamini S and Young R J., J. Mats. Sci., 15, 1823, (1980)

119. Kinloch A J and Williams J G., J. Mats. Sci., 15, 987,(1980)

120. McMeeking R M., J. Mech. Phys. Solids, 25, 357, (1977)

121. Rice J R and Rosengren G F., J. Mech. Phys. Solids, 16, 1, (1968).

122. Rice J R and Johnson M A., Inelastic Behaviour of Solids, Ed by M F Kanninen., W Alder., A Rosenfield and R Jaffe, McGraw Hill, New York, p641, 1970.

123. Ritchie R O., Knott J F and Rice J R., J. Mech. Phys. Solids, 21, 395 (1973).

124. Curry D A and Knott J F., Metal Science, 13, 341, (1979)

125. Berry J P., Fracture - An Advanced Treatise, Vol 7, Academic Press, New York, p37, 1972.

126. Hulse G., Physics of Plastics, Ed by P D Ritchie, Iliffe, p120, 1965.

127. Parvin M and Williams J G., Int. Journ. of Fracture, 11, 963, (1975).

128. Irwin G R., J. Appl. Mechs., 29, 651, (1962).

129. Parvin M and Williams J G., J. Mats. Sci., 10, 1883 (1975)

130. Fraser R A and Ward I M., Polymer, 19, 220, (1978)

131. Hobbs S Y and Bopp R C., Polymer, 21, 559, (1980).

132. Pitman G L and Ward I M., Polymer, 20, 895, (1979)

133. Gledhill R A and Kinloch A J., Propellants and Explosives, 4, 73, (1979).

134. Yap O F, Mai Y W and Cotterell B., J. Mats.Sci., 18, 657, (1983)

135. Gledhill R A., Private communication.

136. Hunston D L., Bitner J L., Rushford J L and Oroshnik J., J. Elast. Plastics, 12, 133, (1980).

CORRECTIONS

1. Page 14, line 22: 'rpocess' should read 'process'
2. Page 23, line 14: 'poissons' should read 'Poisson's'
3. Page 29, line 9: 'von mises' should read 'von Mises'
4. Page 29, line 15: 'betwwen' should read 'between'
5. Page 35, line 15: 'appropraite' should read 'appropriate'
6. Page 40, line 7: 'consdierably' should read 'considerably'
7. Page 53, line 25: 'Mostoroy' should read 'Mostovoy'
8. Page 66, line 3: 'resons' should read 'reasons'
9. Page 66, line 15: 'were' should read 'where'
10. Page 70, line 14: 'wich' should read 'which'
11. Page 74, line 11: 'unaxial' should read 'uniaxial'
12. Page 147, line 26: 'istropic' should read 'isotropic'
13. Page 150, lines 22 and 27 : 'pining' should read 'pinning'
14. Page 151, lines 4 and 10: 'inpenetrable' should read 'impenetrable'
15. Page 151, line 17: 'inpenetrability' should read 'impenetrability'
16. Page 151, lines 18, 20 and 27: 'pining' should read 'pinning'
17. Page 172, line 4: 'respecitively' should read 'respectively'
18. Page 174, line 11: 'respecitively' should read 'respectively'.
19. Page 174, line 12: 'intensificiation' should read 'intensification'.
20. Page 184, line 24: 'or' should read 'of'
21. Page 209, line 20: 'coinciding' should read 'coinciding'